

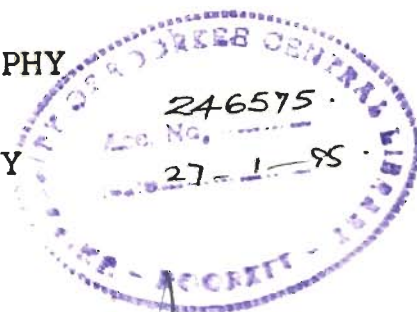
METAMORPHIC EVOLUTION OF THE HIGHER HIMALAYAN CRYSTALLINE, ZANSKAR, JAMMU AND KASHMIR

A THESIS

submitted in fulfilment of the
requirements for the award of the degree

of
DOCTOR OF PHILOSOPHY

in
APPLIED GEOLOGY



By

A. ASOKAN

AK Jain
13-5-92

Professor and Head
Department of Earth Sciences
University of Roorkee
ROORKEE



DEPARTMENT OF EARTH SCIENCES
UNIVERSITY OF ROORKEE
ROORKEE-247667 (INDIA)

MAY, 1992



TO MY LOVING SISTERS

- ***AKKA, THEN, ARUL & GOWRI***



CANDIDATE'S DECLARATION

I hereby certify that the work, which is being presented in the thesis entitled "METAMORPHIC EVOLUTION OF THE HIGHER HIMALAYAN CRYSTALLINE, ZANSKAR, JAMMU AND KASHMIR" in fulfilment of the requirement for the award of the Degree of DOCTOR OF PHILOSOPHY, submitted in the Department of Earth Sciences of the University, is an authentic record of my own work carried out during a period from April, 1988 to May, 1992 under the supervision of Dr. RM. Manickavasagam, Prof. A. K. Jain and Prof. V. K. S. Dave.

The matter embodied in this thesis has not been submitted by me for the award of any other Degree.

A. Asokan
A. ASOKAN

Candidate's Signature

This is to certify that the above statement made by the candidate is correct to the best of our knowledge.

Signature of Supervisors

DR. RM. MANICKAVASAGAM
Reader in Geology
Department of Earth Sciences
University of Roorkee
ROORKEE - 247 667

V.K.S. Dave

PROF. V.K.S. DAVE
Professor of Geology
Department of Earth Sciences
University of Roorkee
ROORKEE -247 667

A.K. Jain

PROF. A.K. JAIN
Professor of Geology
Department of Earth Sciences
University of Roorkee
ROORKEE - 247 667

The Ph.D. Viva-Voce examination of Mr. A. Asokan, Research Scholar was held on 21-10-93.

Signature of Guides

Signature of External Examiner

ACKNOWLEDGEMENTS

First and foremost I convey my deep indebtedness to my supervisors Dr. RM. Manickavasagam, Prof. A. K. Jain and Prof. V. K. S. Dave, Department of Earth Sciences, University of Roorkee, Roorkee. I am gratified to them for their stimulating discussions, erudite guidance and perpetual encouragement throughout my research.

I am thankful to Prof. B. B. S. Singhal, ex-Head and Prof. R. K. Goel, Head, Department of Earth Sciences, University of Roorkee, Roorkee for providing me all the possible research facilities.

I express my boundless reverence to Prof. Kailash Chandra, Director, University Science Instrumentation Centre (USIC) who in fact fostered my interest in microprobe analysis. Besides, I am thankful to Mrs. Amita Khare, Mr. Jagdish Saini and Dr. Arun Kumar, USIC for their affectionable help.

The present work was carried out under the DST sponsored research project "Evolution of Metamorphic Belts in Phanerozoic Collision Boundary in the Himalaya", in which the Electron Probe Micro Analyser (EPMA) Laboratory was established. I am very grateful to DST for providing generous funds for the field work and the probe facilities.

The tireless and selfless efforts in developing computer

programs for P-T calculations by SriRam and Nachi deserve a special mention.

The facilities and timely help provided by Dr. M. S. Pandian, O.C. computer, Department of Earth Sciences is highly appreciated.

I express my heartfelt appreciation to my friends Pankaj, Ramesh, Sandeep, Bidyut, Lalan and Manoj for their cheerful and affectionate company during the strenuous field work with moral and physical support.

Pankaj, Dinesh, Anurag, Alok, Jairam, Krishna, Tamal, Ravindra, Manoj, Vineet and Mukundhan spontaneously and generously devoted their time in the preparation of the thesis for which I am indeed grateful.

My profound and sincere thanks are due to all my colleagues and friends particularly Jagat, Arvind, Kush, Rajeev, Ujjwala, Meena, Neeti, Suresh, Sakthivel, Anns, Mohan, Venkat and Babu for their constant moral boosting throughout the research work.

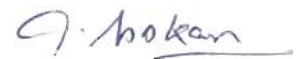
I am thankful to Kamesh Gupta for constant and friendly company during the fieldwork and neat drafting which has added a sense of perfectness to the work. Help extended by R.C. Punj, Ram Dal and Amar Singh in preparation of thin sections, Sri S.D. Sharma in the reproduction of photographs and Om Prakash for neat xeroxing the manuscripts is highly appreciated.

I am grateful to Dicky and Ram Karan for their assistance

during field work.

In the end, the immutable encouragement received from my parents for constantly inspiring me to fulfill my ambition for higher studies bounds no words.

The assistance of all individuals who have in any way been associated with the completion of this work but not have been mentioned so far, is sincerely acknowledged.


(A. ASOKAN)

ABSTRACT

The Himalaya is a composite mountain belt of the Trans-Himalayan batholith in north, followed successively in the south by the Indus-Tsangpo Suture Zone (ITSZ), Tethyan Sedimentary Zone (TSZ), Higher Himalayan Crystalline (HHC), Lesser Himalayan Proterozoic Foreland and Sub-Himalayan Tertiary belt with variable geological characters. However, metamorphic rocks occur mainly in the Higher Himalaya as a continuous belt and discontinuously in the Lesser Himalaya. The Higher Himalayan Crystalline (HHC) belt is deformed and metamorphosed due to intracontinental collision and crustal shortening in Cenozoic period.

Detailed work on metamorphism and deformation has been carried along two sections of the HHC in Jammu and Kashmir, NW-Himalaya. These include i) Chenab-Bhot Nala cross section from Thatri, Chhatru, Kishtwar, Atholi, Bhujaz and Mulung Tokpo, and ii) Suru-Doda Valleys section along the northern margin of the HHC from Sankoo, Panikhar, Parkachik, Ringdom, Pensila and Padam.

Thick pile of Salkhala Group metamorphics of the Higher Himalayan Crystalline is thrust over the Lesser Himalayan Proterozoic Foreland of the Kishtwar Window along the Main Central Thrust (MCT). Towards southwest and west, it constitutes a part of Kashmir Nappe, which is overlain by the fossiliferous Paleozoic-Mesozoic succession of Kashmir-Bhadarwah Basin. On the other hand, the Zaskar Shear Zone (ZSZ) marks the northeastern

margin of the HHC with the Tethyan Sedimentary Zone along the Suru - Doda Valleys.

Chenab-Bhot Nala sections through the Lesser and Higher Himalayan tectonic units reveal a polyphase Barrovian - type regional metamorphism. Low grade rocks viz, metavolcanics, carbonaceous phyllite, mica schist and quartzite with granitic intrusives are exposed in the Lesser Himalayan Foreland. The HHC comprises mainly different varieties of mica schist, sillimanite gneiss, mica gneiss, calc-silicate, amphibolite and granitoids.

In HHC, metamorphism increases from garnet grade at its base along the Main Central Thrust (MCT) to sillimanite-K-feldspar grade towards higher topographic and structural levels. The peak of metamorphism is accompanied by extensive anatexis, migmatization and formation of leucogranite. Further NE towards Tethyan Sedimentary Zone, garnet to sillimanite-muscovite grades are truncated by the Zaskar Shear Zone along the Suru - Doda Valleys.

Detailed petrographic work only on pelites reveal different mineral assemblages in metamorphic grades (a) garnet: garnet-biotite-muscovite-quartz±K-feldspar±plagioclase±chlorite, (b) staurolite-kyanite: garnet-biotite-muscovite-quartz±staurolite-kyanite±K-feldspar±plagioclase, (c) sillimanite-muscovite: sillimanite/kyanite-garnet-biotite-muscovite-quartz-K-feldspar-plagioclase, and (d) sillimanite-K-feldspar: sillimanite-garnet-biotite-quartz-K-feldspar-plagioclase±cordierite.

Final and textural relations indicate that mica, garnet, staurolite, kyanite, sillimanite etc. are grown syntectonically to most pervasive D_2 deformation. This deformation produces a most pervasive axial planar foliation (S_2), NE plunging reclined folds (F_2) and a consistent co-axial lineation (L_2). The growth of these minerals with respect to D_2 deformation is indicated by helicitic growth with concordant internal Si fabric to external Se during main metamorphism M_2 .

Garnet has grown in at least two distinguishable stages of metamorphism M_2 which is documented by inclusion-rich, syntectonic (G-I) and inclusion-free post-tectonic (G-II) garnet. In a few samples, garnet has a pre-tectonic core of metamorphism M_1 which is almost devoid of inclusions (G-0), syntectonic inner rim with prominent spiral inclusions like G-I and inclusion-free outer rim of G-II. In higher grades, garnet shows dissolution and corroded margins that is more prevalent in migmatite zone.

Staurolite is found only in a few samples with kyanite and mica. Kyanite predominantly occurs as blades and is restricted only to staurolite-kyanite grade. Sillimanite occurs as prisms and fibrolite. Sillimanite is found in association with feldspar, garnet, quartz and cordierite in higher grades and also as polymorphic transformation of kyanite in sillimanite-muscovite grade rocks. Fibrolite is commonly observed as epitaxial growth in biotite, feldspar and sometimes even in garnet. Cordierite is of very limited occurrence and is seen only in migmatite.

Retrogression is less in the area of investigation, excepting in Doda Valley and close to tectonic boundaries. Chloritisation of garnet, biotite and staurolite and sericitisation of feldspar are common in the rocks of this area.

Mineralogical and textural studies suggest the growth of garnet, staurolite, kyanite, sillimanite etc. in different grades due to several continuous and discontinuous metamorphic reactions.

Fe/Fe+Mg of coexisting garnet and biotite increases with metamorphic grade, except in garnet grade, which shows more Fe enrichment than staurolite-kyanite grade. Muscovite is poorer in paragonite component, while approaching from lower to higher metamorphic grades. Plagioclase is more albitic with anorthite reaching a maximum of 35% in a few samples and revealing no variation in anorthite content with respect to metamorphic grade. Staurolite shows Mg rich core and Fe rich rim showing evidence of zoning. Ilmenite is almost pure but sometimes, reveal Fe depletion.

Garnet from all the metamorphic grades reveal the presence of zoning. Growth zoning is very common in the garnet to staurolite-kyanite grade rocks and is inferred to be because of prograde metamorphism. However, sillimanite-muscovite and sillimanite-k-feldspar grade rocks reveal reverse zoning with Mg rich and Mn poor core and Fe/Fe+Mg and Mn rich rim. The later phenomenon is due to thermal relaxation and volume diffusion after peak metamorphism.

AFM topology of coexisting mineral phases indicate equilibrium condition. However, in the low to medium grade rocks crossing of tie lines are observed implying the non-ideal conditions of the participating phases.

P-T condition of metamorphism are determined using suitable geothermobarometers for the relevant mineral assemblages. The garnet-biotite exchange thermometer is used to obtain temperature, applying various calibrations. Pressure is estimated with garnet- Al_2SiO_5 -quartz-plagioclase and for garnet-muscovite-biotite-plagioclase assemblages using different calibrations. Error estimation for temperature and pressure is calculated following standard methods. The inferences made from the P-T data along the Chenab - Bhot Nala section and Suru-Doda Valleys are summarised below:

- 1) In topmost portion of the Himalayan footwall near the MCT, rims of garnet-I show temperature of 500-560°C and pressure of 7.00-9.60 kbar for garnet grade. The rocks occurring above MCT at the base of HHC on the SW side also show more or less the same P-T condition.

- 2) The HHC rocks, occurring within 1 km and above the MCT on the NE side of the Kishtwar Window in staurolite-kyanite grade, record the core and rim temperatures of 500-570°C and 550-650°C and rim pressure of 7.50-9.00 kbar. P-T values of subidioblastic garnet-II are exactly similar to the rim data obtained from garnet-I.

3) Further moving up NE in higher structural level, garnet-I of sillimanite-muscovite grade gives core temperature of 700-740°C and rim P-T of 610-650°C and 6.00-8.50 kbar. Sillimanite-K-feldspar grade rocks give core temperature and pressure of about 780°C and 9.00-11.00 kbar. However, the rim P-T show 600-665°C and 4.50-6.50 kbar. A few samples show substantial reduction in core and rim P-T from the above mentioned values, but these values are noteworthy in the zone of migmatite.

4) While moving further NE towards ZSZ in sillimanite-muscovite grade, garnet rim and subidioblastic garnet-II grains give temperature and pressure of about 675°C and 7.75 kbar, whereas staurolite-kyanite grade rocks show 600°C and 6.00 kbar from rims of garnet-I.

5) In the Suru Valley, along the main cross-section from Panikhar to Ringdom, the staurolite-kyanite grade rocks record core P-T of 450°C and 5.25 kbar, while rim gives 560-650°C and 6.75-9.75 kbar.

p-T data, obtained staurolite-kyanite grade, suggest that these rocks have been developed during prograde metamorphic condition. The normal growth zoning and increasing temperature towards garnet rim support their heating during late stage of metamorphism M₂. Presence of kyanite, rarity of staurolite and increasing Fe/Fe+Mg ratio towards garnet rim in some samples is interpreted to have been formed in near isobaric and increased temperature conditions. About 10-18 km from the MCT towards higher structural level, garnet-I core temperature is increased

by about 170°C with pressure remaining constant from that of staurolite-kyanite grade. On the other hand, the rim temperature remains more or less constant, but pressure is reduced by 2.00-3.00 kbar from staurolite-kyanite grade. Still up in the topographic level and up to about 23 km in sillimanite-K-feldspar grade, garnet-I core records an increase of about 40-80°C from sillimanite-muscovite grade with a slight increase in pressure. For the same grade, P-T condition for garnet rim or subidioblastic grains is reduced to about 150°C and 2.50-3.50 kbar from core. The rim pressure, however, is reduced by another about 1.5-2.00 kbar than the sillimanite-muscovite grade without much change in rim temperature. The only supporting evidence for prograde metamorphism in the higher grades is from garnet, which shows reverse zoning with high Mg/Fe ratio and lower Mn at the core. The temperature and pressure reduction is evidenced by epitaxial growth of fibrolite in biotite, and an increase in Fe/Fe+Mg ratio and Mn at garnet rim. At the highest topographic level between 23 and 40 km from window, the rocks are extensively migmatized in the sillimanite-K-feldspar grade. Garnet is partially reequilibrated and show grain-size reduction, and therefore, does not give peak metamorphic P-T condition.

Detailed study on texture, petrography and P-T data establishes the presence of inverted metamorphism in HHC of Jammu and Kashmir like in Garhwal, Kumaon and Nepal-Bhutan-Sikkim Himalaya. Many models have been proposed to explain inverted metamorphism in the Himalaya. The data obtained in this study have been compared with all the models of inverted metamorphism

to understand their applicability for this region.

The P-T values indicate that metamorphism has been initiated at depth because of subsidence of the Indian Plate during the onset of collision with Eurasian Plate. Further, collision has caused intense ductile shearing during main deformation and metamorphism at depth of about 25-35 km. Southward ductile shearing has probably displaced higher grade rocks over lower grade and caused inverted metamorphism. This seems to have resulted in the cooling of the higher grade and heating of the lower grade rocks giving an apparent isothermal uplift. Also, the pressure release during fast uplift of the higher structural levels in comparison to the lower level or basal part of the HHC, probably resulted in the thermal relaxation and equilibration in the whole of HHC. Therefore, it is possible that the inverted metamorphism observed in this part of the HHC may be due to ductile shearing and uplift after an initial subsidence.

C O N T E N T S

	PAGE
ACKNOWLEDGEMENTS	
ABSTRACT	i-viii
1. INTRODUCTION	
1.1 BACKGROUND	1
1.2 HIGHER HIMALAYAN CRYSTALLINE	2
1.3 LESSER HIMALAYAN PROTEROZOIC FORELAND	5
1.4 INVERTED METAMORPHISM	7
1.5 SELECTION OF THE AREA	9
1.6 SCOPE OF THE WORK	9
1.7 METHODOLOGY	11
2. GEOLOGICAL FRAMEWORK	
2.1 INTRODUCTION	12
2.2 GEOLOGY OF PADAR AREA	14
2.3 GEOLOGY OF HIGHER HIMALAYAN CRYSTALLINE	14
2.3.1 KISHTWAR-PADAR SECTION	14
2.3.2 SURU-DODA VALLEYS SECTION	15
2.4 DESCRIPTION OF ROCK TYPES	17
2.4.1 LESSER HIMALAYAN SEDIMENTARY FORELAND	17
2.4.2 HIGHER HIMALAYAN CRYSTALLINE (HHC)	19
3. DEFORMATION AND METAMORPHISM	
3.1 INTRODUCTION	27
3.2 DEFORMATIONAL PHASES	28
3.2.1 LITHOLOGICAL LAYERING/BANDING (So)	28

3.2.2	FIRST DEFORMATIONAL PHASE (D ₁)	28
3.2.3	SECOND DEFORMATIONAL PHASE (D ₂)	30
3.2.4	THIRD DEFORMATIONAL PHASE (D ₃)	32
3.2.5	D _{LATE} DEFORMATIONAL PHASE	35
3.6	MAJOR STRUCTURES	35
3.6.1	FOLDS	35
3.6.2	THRUSTS AND SHEAR ZONES	38
3.7	METAMORPHIC EPISODES	41
3.7.1	M ₁ METAMORPHIC EPISODE	42
3.7.2	M ₂ METAMORPHIC EPISODE	43
3.7.3	M ₃ METAMORPHIC EPISODE	52
3.7.4	POST-M ₃ METAMORPHISM	54
4.	METAMORPHISM AND MINERAL CHEMISTRY	
4.1	REGIONAL METAMORPHISM	55
4.2	METAMORPHISM	56
4.2.1	CHENAB-BHOT NALA SECTION	56
4.2.2	SURU AND DODA VALLEYS SECTION	57
4.3	MINERAL ASSEMBLAGES	57
4.3.1	BIOTITE GRADE	58
4.3.2	GARNET GRADE	58
4.3.3	STAUROLITE-KYANITE GRADE	59
4.3.4	SILLIMANITE-MUSCOVITE/SILLIMANITE-K-FELDSPAR GRADE	60
4.4	METAMORPHIC REACTIONS AND ISOGRADS	60
4.4.1	GARNET ZONE	61
4.4.2	STAUROLITE-KYANITE ZONE	61
4.4.3	SILLIMANITE-MUSCOVITE ZONE	63

4.4.4 SILLIMANITE-K-FELDSPAR ZONE	64
4.5 MINERAL CHEMISTRY	65
4.5.1 PROBE ANALYSIS	65
4.5.2 GARNET	67
4.5.3 BIOTITE	69
4.5.4 MUSCOVITE	69
4.5.5 PLAGIOCLASE	70
4.5.6 STAUROLITE	70
4.5.7 ILMENITE	70
4.5.8 RUTILE	71
4.6 AFM DIAGRAMS	71
4.7 GARNET ZONING	72
4.8 DISCUSSION	77
5. GEOTHERMOMETRY AND GEOBAROMETRY	
5.1 INTRODUCTION	81
5.2 THERMOMETRY	81
5.3 BAROMETRY	82
5.4 THERMODYNAMIC BASIS	83
5.5 APPLICATION OF GEOTHERMOBAROMETRY	84
5.5.1 GARNET-BIOTITE GEOTHERMOMETER (GB)	85
5.5.2 GEOBAROMETRY	86
5.6 PROCEDURE FOR GEOTHERMOBAROMETRY	88
5.7 GEOTHERMOBAROMETRIC RESULTS	89
5.7.1 CHENAB-BHOT NALA SECTION	90
5.7.2 LADAKH-ZAANSKAR SECTION	92
5.8 DISCUSSION	94

6. SUMMARY AND CONCLUSION

6.1 INTRODUCTION	98
6.2 GEOLOGY OF THE AREA	98
6.3 DEFORMATION AND RELATED METAMORPHISM	99
6.4 REGIONAL METAMORPHIC FRAMEWORK	101
6.5 TEXTURES OF METAMORPHIC ROCKS	103
6.6 METAMORPHIC PARAGENESIS AND MINERAL REACTIONS	104
6.7 THERMOBAROMETRIC RESULTS	106
6.8 MODEL FOR INVERTED METAMORPHISM	112
REFERENCES	117
APPENDIX-I (MICROPROBE ANALYSIS OF GARNET)	i
APPENDIX-II (MICROPROBE ANALYSIS OF CHLORITE)	xiii
APPENDIX-III (MICROPROBE ANALYSIS OF BIOTITE)	xiv
APPENDIX-IV (MICROPROBE ANALYSIS OF MUSCOVITE)	xx
APPENDIX-V (MICROPROBE ANALYSIS OF PLAGIOCLASE)	xxv
APPENDIX-VI (MICROPROBE ANALYSIS OF K-FELDSPAR)	xxx
APPENDIX-VII (MICROPROBE ANALYSIS OF STAUROLITE)	xxxi
APPENDIX-VIII (MICROPROBE ANALYSIS OF ILMENITE)	xxxii
APPENDIX-IX (MICROPROBE ANALYSIS OF RUTILE)	xxxiv

CHAPTER - 1

I N T R O D U C T I O N

1.1 BACKGROUND

The Himalaya provides an opportunity to study the processes of deformation and metamorphism as well as the thermal regimes of continental crust during thrusting and uplift. The evolution of the Himalayan Arc has been described as a classical example of large-scale continental convergence along the Indus-Tsangpo Suture Zone. The Tethyan Oceanic Crust of the Indian Plate is believed to have been subducted beneath the Eurasian Plate along the Indus-Tsangpo Suture Zone in the Cenozoic period ($\approx 50 - 45$ Ma) (Gansser, 1964; Dewey and Bird, 1970; Dewey and Burke, 1973; Le Fort, 1975, 1986; Mattauer, 1986; Thakur, 1987; Searle et al., 1988).

After the closure of Tethys Ocean, the crustal shortening has taken place along the southerly migrating major thrusts such as the Main Central Thrust (MCT), the Main Boundary Thrust (MBT), the Main Frontal Thrust (MFT) as well as along large-scale strike-slip faults in Tibet (Molnar and Tapponnier, 1975; Toksoz and Bird, 1977; Bouchez, 1978; Valdiya, 1980; Bouchez and Pecher, 1981; Le Fort, 1986; Mattauer, 1986; Thakur, 1987). It is estimated that approximately 2000 km of continental crust has been shortened in the last 40 Ma (Windley, 1988). As a result, the Tibetan crust has attained a thickness of about 70 km (Narian, 1973).

A composite belt of crystalline rocks having different

tectonometamorphic history is observed all along the Himalayan chain to the south of the Indus-Tsangpo Suture Zone in the Higher Himalaya and to a limited extent in the Lesser Himalaya. Southerly-verging MCT separates the Higher Himalayan metamorphic rocks from the Lesser Himalayan Sedimentary Foreland and, thus, is viewed as a major intracontinental shear zone (Toksoz and Bird, 1977; Bouchez, 1978; Bouchez and Pecher, 1981). The Higher Himalaya represents a zone of immense crustal shortening of the Indian lithosphere. Therefore, thick pile of the Higher Himalayan metamorphics seems to have played a very significant role during intracontinental collision. The most appropriate area in Higher Himalaya to study metamorphism, deformation and to decipher the thermal regime in collision tectonics is, therefore, a segment of NW-Himalaya in Jammu and Kashmir, where a composite belt of crystalline rocks of different tectonometamorphic units is well exposed.

1.2 HIGHER HIMALAYAN CRYSTALLINE

The backbone of the Great Himalayan Range and the base of the Tethyan Sedimentary Zone is the Higher Himalayan Crystalline (HHC). It forms a continuous belt from Kashmir in the west to Arunachal Pradesh in the east. The width of this belt is variable ranging from 10-30 km in Kumaon, western and central Nepal and more than 100 km wide in Kashmir, eastern Nepal, Sikkim and Bhutan (Pecher and Le Fort, 1986). The metamorphic and igneous rocks of this zone are described as the Vaikrita Group in Spiti, Bushehar and Rupshu area by Hayden (1904) and as

Crystalline Series, Central Gneiss and older crystalline rocks in the Kumaon Himalaya by Heim and Gansser (1939). Besides the general nomenclature for these crystalline rocks, various other names have been given in different parts of the Himalaya such as Darjeeling gneiss in Darjeeling and Sikkim (Ray, 1947), Tibetan Slab or Dalle du Tibet in Nepal (Lombard, 1958; Bordet, 1961), Takhtsang Group in Bhutan (Jangpangi, 1974), Siang Group in Arunachal Himalaya (Jain et al., 1974), Kishtwar Group in Kishtwar area (Wakhaloo and Dhar, 1971) and Suru Formation (Nanda and Singh, 1977) and Giambal Gneissic Complex (Srikantia et al., 1978) in the Zaskar area of Ladakh.

The Higher Himalayan Crystalline, hereafter referred to as the HHC, has been investigated by various workers and is characterised by the following features:

- i) Metamorphic rocks of the HHC occur both as a continuous belt roughly coinciding with the physiographic Greater Himalaya and klippen or half-klippen extending into the physiographic Lesser Himalaya (Le Fort, 1975).
- ii) The HHC is a continuous litho-tectonic unit in the NW-Himalaya and can be traced from the Zaskar range of Kashmir in the west through Himachal, Garhwal and Kumaon towards east (Thakur, 1980).
- iii) This unit is constituting a large geanticline (Wadia, 1931; Saxena, 1971), which probably forms a barrier between the fossiliferous Tethyan sediments in the north and the largely

non-fossiliferous Lesser Himalayan sediments in the south (Thakur, 1980).

iv) The HHC is bounded by the MCT in the south (Jhingran et al., 1976) and the Tethyan Sedimentary Zone in the north. This sedimentary zone is separated from HHC by a shear zone known as Zaskar Shear Zone (ZSZ) (Herren, 1987).

v) The metamorphic pile of the HHC is characterised by progressive regional metamorphism of the Barrovian-type ranging from lower greenschist to upper amphibolite facies. Gansser (1964) pointed out that the HHC reveals a normal metamorphic pattern and is thrust over the Lesser Himalaya sedimentary zone. However, other workers have described more complex metamorphism in the HHC (Pecher, 1975; Thakur, 1977; Le Fort, 1986; Hodges et al., 1988; Searle and Rex, 1989; Pognante et al., 1990). Pecher (1989) observed two main episodes of metamorphism: an older Barrovian-type metamorphism, superimposed by a younger lower pressure and/or higher temperature metamorphism. This phenomenon has resulted due to quasi-adiabatic uplift of the Tibetan slab by transport along the MCT and also due to thermal refraction effects along the contact zone between the gneiss and the sedimentary cover (also see, Barnicoat and Treloar, 1989).

vi) P-T conditions of the Greater Himalayan sequence in the Central Himalaya covering eastern Garhwal, west-central

Nepal, east-central Nepal, the Everest region and the Makalu region show a complicated Tertiary thermal history. Several of these areas exhibit an early medium to high-pressure and medium temperature thermal event, followed by a later low- to medium pressure and high-temperature event (Hodges et al., 1988).

vii) The HHC is associated with highly deformed granitoids of Proterozoic (2000 Ma), early Paleozoic (500 Ma) and late Tertiary (25-10 Ma) tourmaline-bearing leucogranite (e.g., Manaslu Granite, Gangotri and Badrinath Granite etc.).

viii) Two metamorphic episodes M_1 - M_2 and three main deformational episodes D_1 - D_3 have been identified on the regional scale in the HHC (Jhingran et al., 1976; Singh et al., 1980; Thakur, 1980; Das, 1979). However, four main deformations have been worked out in NW-Garhwal (Jain and Anand, 1988) and Zaskar (Patel, 1991). Of these, folds generated during main Himalayan deformation (D_2) are isoclinal reclined and plunge towards NE or SW. These are superposed by NW or SE plunging recumbent to inclined folds (F_3).

1.3 LESSER HIMALAYAN PROTEROZOIC FORELAND

The Lesser Himalaya is bounded to the north by the Main Central Thrust (MCT) and to the south by the Main Boundary Thrust (MBT). It consists of weakly metamorphosed late Proterozoic (Riphean - Vendian) and early Paleozoic sediments, which have been overridden by thrust nappes of high grade gneiss derived

from the HHC (Stocklin, 1980; Valdiya, 1981; Sinha Roy, 1981). The sediments are predominantly carbonate with Riphean stromatolites, slate, phyllite, quartzite and metavolcanics. The rocks have been transported southwards in several thrust slices (e.g. the Krol and Chail nappes). The nappe sequence consists primarily of low-grade metasedimentary rocks with metavolcanics but structurally, the upper most portion of some sections contain amphibolite facies assemblages (Le Fort, 1975; Valdiya, 1980).

The base of the Lesser Himalayan Zone is nowhere exposed hence it is highly conjectural to postulate the basement of largely Proterozoic sedimentary sequence of this belt. However, the southern margin of this zone is defined by Main Boundary Thrust (MBT) zone having a series of N-dipping faults with a cumulative displacement of demonstrably tens (Heim and Gansser, 1939; Stocklin, 1980) or probably hundreds of kilometres (Powell and Conaghan, 1973). The Miocene - Pleistocene Siwalik molasse (Gansser, 1964), which constitutes the bulk of the Sub-Himalayan Zone, forms the footwall of the MBT.

The autochthonous units of the Proterozoic sediments of Lesser Himalaya are mainly exposed in the vast tectonic windows (e.g., Damtha and Tejam Groups of Garhwal-Kumaon Himalaya; Valdiya, 1980) where the sediments are tightly folded and exhibit low-grade metamorphism. Fuchs (1975) correlated the tectonic windows of the Lesser Himalayan sedimentary rocks with lithologies of the Chail Formation. In a few tectonic windows,

the Lesser Himalayan units are surrounded by the overthrust Higher Himalayan metamorphics e.g., the Kishtwar Window, consisting of slate, schist, quartzite, metavolcanics and various granitoids (Staubli, 1989).

1.4 INVERTED METAMORPHISM

One of the most controversial problem of the Himalaya is the inverted metamorphism, observed across the crystalline parts of the orogen (Gansser, 1964). In many areas, this phenomenon is spatially related to the MCT (Le Fort, 1975; Pecher, 1978; Searle and Fryer, 1986; Brunel and Kienast, 1986). Near the base of the hanging wall close to the MCT, kyanite grade pelitic assemblages are common (Hodges and Silverberg, 1988; Staubli, 1989; Pognante et al., 1990). Towards structurally higher levels in the hanging wall, metamorphic grade appears to increase systematically and sometimes reaches sillimanite-K-feldspar grade several kilometres above the MCT. This pattern is interpreted as inverted metamorphism. The inverted metamorphism is well displayed in some sections of the HHC and Lesser Himalaya mainly in Darjeeling - Sikkim (Jangpangi, 1972; Mukherjee, 1979; Bhattacharya and Das, 1983; Mohan et al., 1989), Nepal (Le Fort, 1975, 1986; Pecher, 1978; Brunel and Kienast; 1986), Garhwal (Heim and Gansser, 1939; Hodges and Silverberg, 1988), Simla (Naha and Ray, 1970), Zaskar (Searle et al., 1988; Pognante and Lombardo, 1989; Staubli, 1989), Kashmir (Searle and Fryer, 1986) and Pakistan (Treloar et al., 1989a, b).

In the Higher Himalayan Crystalline (HHC) of SE Jammu and

Kashmir, grade of metamorphism increases from garnet grade at its base, demarcated by the MCT, to sillimanite-K-feldspar grade gneiss, migmatite and the Late Oligocene - Miocene leucogranite towards highest topographic and structural levels. Searle et al. (1988) suggested that the metamorphic isograds became inverted by post- metamorphic SW-verging recumbent folding and thrusting along the base of the High Himalayan Slab. Along the top of the slab, isograds become normal but are telescoped by normal faulting along the Zaskar Shear Zone (ZSZ) (Herren, 1987). Pognante and Lombardo (1989) explained in SE Zaskar, the inverted metamorphism by thrusting of the HHC over the lower grade Lesser Himalayan rocks. They concluded that the inversion could have been produced by thermal conductivity and the cooling of the upper and lower parts of the HHC. Staubli (1989) concluded that the spatial inverse metamorphism exposed within the Lesser Himalaya of the Kishtwar Window is regarded as a product of polyphase metamorphism combined with ongoing thrusting and shearing and is reflected by condensed M_2 isograds around the Kishtwar Window.

Many models to explain inverted metamorphism in the Himalaya include: (i) conductive heating of the Lesser Himalaya and concomitant cooling of the basal Higher Himalaya as a result of 'hot-over-cold' thrusting (Le Fort, 1975, 1986; Brunel and Kienast, 1986), (ii) shear heating along the MCT (Searle and Fryer, 1986), (iii) thermal heating due to leucogranite magmatism (Searle and Rex, 1989) and (iv) recumbent folding and/or thrust

imbrication of pre-existing 'normal' metamorphic sequences (Searle et al., 1988; Treloar et al., 1989a, b). The proposed models were based on regional mapping, distribution of isograds, geothermobarometric constraints and with a few P-T path analysis. Among these models, the hot-over-cold and recumbent models could explain the inverted metamorphism in Nepal and in parts of Kulu Valley in Himachal Pradesh. However, these models do not satisfactorily explain the mechanism of inverted metamorphism and the heat source in other areas.

1.5 SELECTION OF THE AREA

In view of the above controversies, an area along the Chenab - Bhot Nala section and Suru - Doda Valleys of Zaskar, Jammu and Kashmir, NW- Himalaya has been selected. The study area lies between latitudes $33^{\circ}0'$ and $34^{\circ}20'$ and longitudes $75^{\circ}30'$ and $77^{\circ}0'$. Field work covering numerous traverses along accessible tracks was undertaken during summers of 1987, 1988 and 1989. It is to be kept in mind that large part of area lies above 3000 meters and largely inhospitable with limited accessibility. The terrain is extremely rugged, covered by glaciers, moraines, talus, turbulent rivers with poor transportation facilities (Fig. 1.1).

1.6 SCOPE OF THE WORK

The present investigation aims to analyse the Higher Himalayan metamorphism. P-T path and its relation to deformation during the Collision Tectonics of the Indian and Eurasian Plates. Further, it is desired to study the applicability of the proposed

models of inverted metamorphism in collision zone. The scope of this work, in terms of geological, metamorphic and deformational aspects are highlighted below:

- a) Geological mapping, structure and metamorphism of the Higher Himalayan Crystalline (HHC) and Lesser Himalayan Proterozoic Foreland in parts of Jammu and Kashmir, NW-Himalaya.
- b) Textural relationship between metamorphism and deformation.
- c) Study of detailed mineralogical assemblages and paragenesis in different metamorphic grades, with emphasis mostly on the pelitic rock.
- d) Microprobe analysis of the individual minerals of pelitic rocks for variation in chemical composition with metamorphic grades and to characterise the mineralogical reactions and delineating the reaction isograds.
- e) Study of zoning in garnet and its relation to deformation and tectonics.
- f) Microprobe analysis of suitable mineral pairs or coexisting mineral assemblages to determine P-T condition using suitable geothermobarometeries.
- g) Correlation of the already proposed models of inverted metamorphism for the study area with textural, deformational and P-T data.

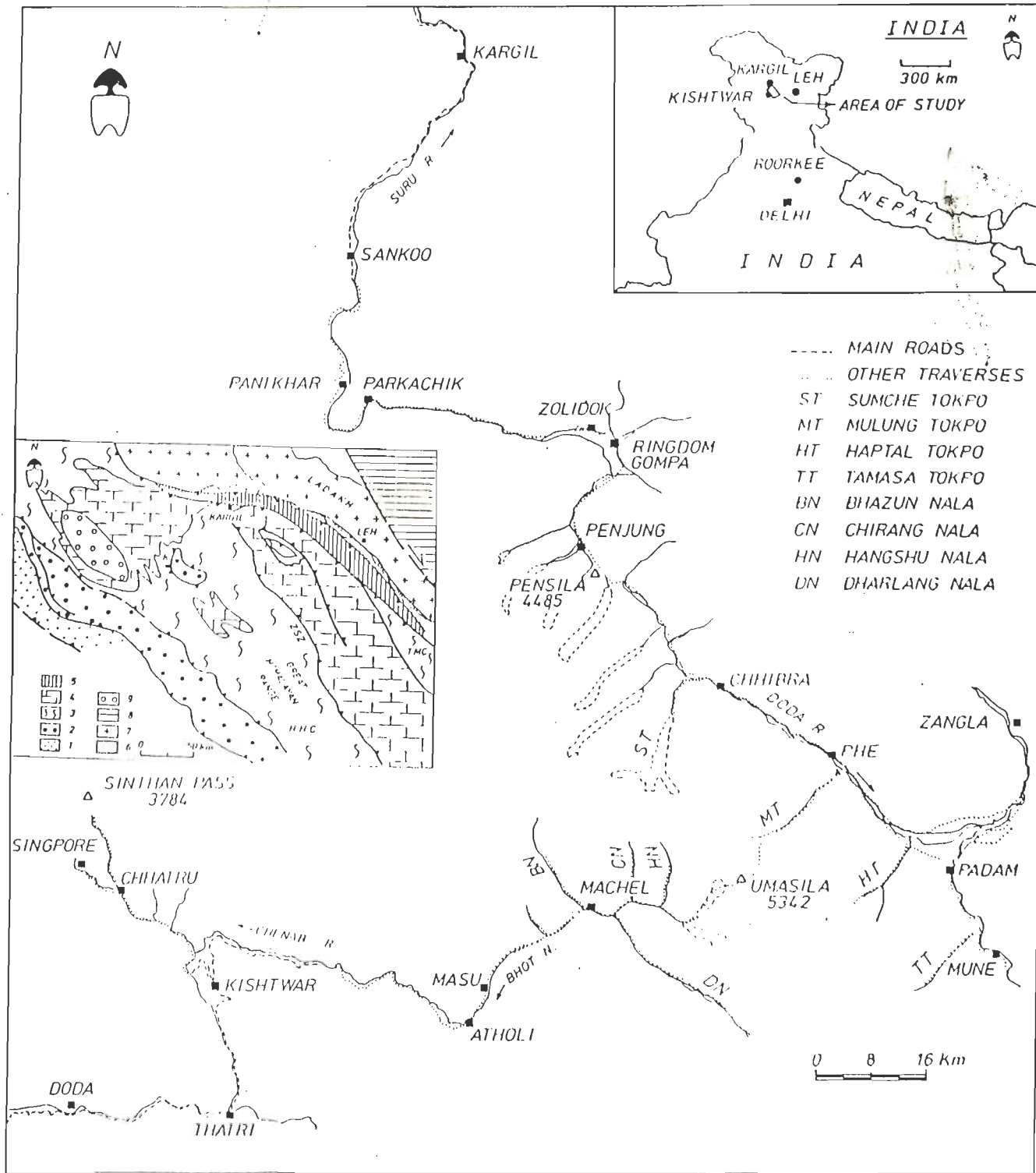


FIGURE 1.1 : Location map of the investigated area with main road and other traverses undertaken. Inset shows simplified geological framework of Jammu and Kashmir. 1 - Sub-Himalaya. 2 - Lesser Himalaya. 3 - Higher Himalayan metamorphic (HHC) and Tso-Morari Crystalline (TMC). 4 - Tethyan Sedimentary Zone of Kashmir, Chamba and Zaskar. 5 - Indus Suture Zone. 6 - Kargil Molasse Basin. 7 - Ladakh Batholith Complex. 8 - Shyok Suture Zone and Karakoram Batholith Complex. 10 - Karewa of Kashmir Basin. MCT - Main Central Thrust. ZSZ - Zaskar Shear Zone. K - Kishtwar.

1.7 METHODOLOGY

The following methods have been adopted to fulfil the above mentioned objectives:

- Systematic geological mapping on 1:50,000 scale using Survey of India, toposheets No. 43N/15, 43N/16, 43O/10, 43O/11, 43O/15, 43O/16, 52B/4, 52B/7, 52B/8, 52C/3, 52C/5, 52C/6, 52C/7, 52C/10, 52C/14 and 52C/15.
- Detailed sampling of various rock types in different metamorphic grades and preparation of isograd map on the basis of mega- and microscopic studies.
- Textural analysis mainly of pelitic rock for different metamorphic grades.
- Mineral paragenesis and determination of suitable mineral reactions.
- Microprobe analysis of individual minerals and coexisting mineral assemblages of metamorphic grades.
- P-T calculations using suitable mineral assemblages and different geothermo-barometric calibrations.
- Study of zoning in garnet.

CHAPTER - 2

GEOLOGICAL FRAMEWORK

2.1 INTRODUCTION

This chapter incorporates the results of geological investigations along Chenab, Suru and Doda Rivers and their tributaries in parts of Padar and Zanskar regions of Jammu and Kashmir, NW Himalaya. The main objective of the present chapter is to establish geological and tectonic relationships between different lithological units.

The term Higher Himalayan Crystallines (HHC) is used for medium to high grade polymetamorphic rocks. The terms like Higher Himalaya and Lesser Himalaya are used only in the physiographic sense.

Observations by different investigators from the Department of Earth Sciences, University of Roorkee, Roorkee, during the project "Evolution of Metamorphic Belts in the Phanerozoic Collision Zones, NW-Himalaya", funded by Department of Science and Technology (DST), are invaluable in bridging the gaps of our knowledge about the Higher Himalayan Crystalline and Lesser Himalayan Proterozoic Foreland.

The Kishtwar area has been earlier studied by number of workers e.g., Wakhaloo and Dhar (1971), Das (1973), Srivastava (1976), Staubli (1989) etc. and their classification of rock units are given in Table 2.1. The Kishtwar region is located to the southeast of Kashmir Valley across the Saribal Range which

offshoots from Pir Panjal and joins the Great Himalayan Range. The area encompasses the main lithotectonic units of the Higher Himalayan Crystalline (HHC) and Lesser Himalayan Proterozoic Foreland. Vast metamorphic terrain constituting the HHC is exposed around Kishtwar towards north and northeast and is thrust on the Lesser Himalayan Proterozoic Foreland of the Kishtwar Window along the MCT (Staubli, 1989). Towards northwest and west, it constitutes a part of Kashmir nappe, which is overlain by the fossiliferous Paleozoic-Mesozoic succession of Kashmir-Bhadarwah Basin (Fig. 2.1)

Lydekker (1878) described the rocks of Kishtwar area into two categories, namely the 'Pangi slates' of Silurian age and granite gneiss of older age. Middlemiss (1910) revised a part of Lydekker's map in Lidar valley of Kashmir. Nanda (1959) and Mehrotra (1959-60) classified Kishtwar area into a the Salkhala Formation of Archean age. Wakhaloo and Dhar (1971) divided the rocks of this area into two groups namely, the Kishtwar Group and the Sinthan Group. They considered the entire rock sequence overlying the Salkhala Formation and underlying the Panjal trap as Agglomeratic slate. They found two thrusts in this area namely : (i) the Kishtwar Thrust lying between the Shalimar quartzites and other members of Kishtwar Group and (ii) the Chhatru Thrust between Kishtwar Group and Sinthan Group.

Srivastava (1976) modified litho-stratigraphic classification of Kishtwar region and did not indicate any thrust contacts. Singh et al. (1980) divided the rocks mainly into

TABLE 2.1 CLASSIFICATION OF ROCK UNITS OF KISHTWAR AREA

Wakhaloo and Dhar, 1971		Das, 1973	Srivastava, 1976		Present Study	Age
S	Panjal Trap		S	Panjal Trap		Permo-Triassic
I G	A		I G	Agglomeratic Slate		Upper Carboni -ferous
N R	g l s		N R	Fenestella Shale		Middle Carboni -ferous
T O	o l	Shaly phyllite	T O	Syringothyris Limestone	T E T H Y A N	Lower Carboni -ferous
H U	e t	Slaty quartzite	H U	MUTH QUARTZITE	S E D I M E N T A R Y	Devonian Silurian
A P	a t		A P	RAMSU FORMATION		Ordovician
N	i c	Pebbly phyllite	N		Z O N E	Cambrian
---- Chhatru Thrust ----		-- Chhatru Thrust --			----- ZSZ -----	
	POST SALKHALA INTRUSIVE GRANITE	POST SALKHALA (granite and gneiss)	K	CHAMALWAS FORMATION	K	
			I		I G	
			S		S R	WOIL FORMATION
			H	Piparan Member	H O	A
			T S P		T U	r
			W A O		W P	
			A L R	Woil Member	A	c
			R K M		R	DUL FORMATION
			H A	Dul Member		h
			G A T		----- MCT -----	
			R L I		S	e
			O A O	Sirthal Member	A G	
			U N		L R	SIRTHAL FORMATION
			P		K O	(schist, gneiss, granitic gneiss)
					H U	
					A P	
					L	
					A	
	SALKHALA FORMATION (schist and Dul Quartzite)	SALKHALA FORMATION (schist, phyllite and quartzite)				a
						n

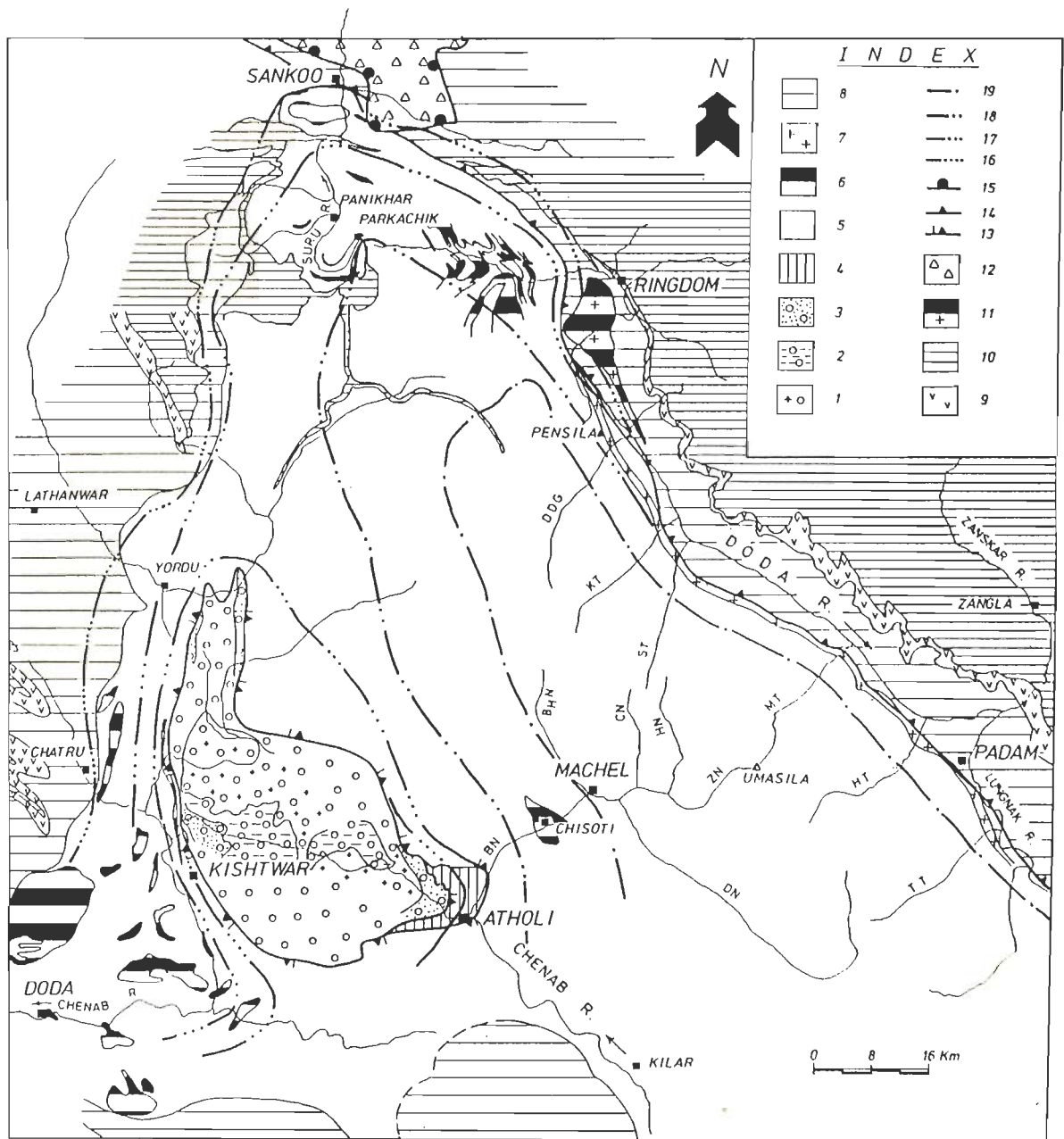


FIGURE 2.1 : Simplified geological map of SE Jammu and Kashmir showing major tectonic units and regional metamorphic isograds. Lesser Himalayan Proterozoic Foreland (Autochthon - Kishtwar Window) - Kishtwar Group : Woil Formation : 1 - Granite gneiss, 2 - Phyllite schist. Dul Formation : 3 - Quartzite - metavolcanics, 4 - Carbonaceous phyllite. Higher Himalayan Crystalline (Allochthonous) : 5 - Schist, gneiss, migmatite, 6 - Granitoid intrusives, 7 - Leucogranite. Tethyan Sedimentary Zone : 8 - Haimanta Group, 9 - Phe Volcanics, 10 - Lilang Group, 11 - Granite. Indus Suture Zone : 12 - Dras Volcanics. 13 - Main Central Thrust. 14 - Zanskar Shear Zone. 15 - Dras Thrust. Metamorphic isograd boundaries : 16 - Garnet, 17 - Kyanite - staurolite, 18 - Sillimanite - muscovite, 19 - Sillimanite - K-feldspar. BN - Bhot Nala, BHN - Bhazun Nala. CN - Chirang Nala, HN - Hangshu Nala, ZN - Zanskari Nala, DN - Dharlang Nala, TT - Temasa Tokpo, HT - Haptal Tokpo, MT - Mulung Tokpo, ST - Sumche Tokpo, KT - Kange Tokpo, DDG - Durung Drung Glacier. Modified after Srivastava (1976), Honegger et al. (1982), Staubli (1989).

two units : (i) Unit-A -a part of Salkhalas, consisting predominantly of metapelite, metacalcareous sediments, paragneiss, migmatite, orthogneiss and amphibolite and (ii) Unit-B -mainly of quartzite and green schist. Units-A and B are separated by Duldhar Thrust (Kaul et al., 1970) or Kishtwar Thrust (Wakhaloo and Dhar, 1971).

2.2 GEOLOGY OF PADAR AREA

This area lies to the south of the Great Himalayan Range and north of Chenab river along Bhot Nala. Parimoo and Raina (1970), observed phyllite interbedded with quartzite, mica-schist, gneiss, granulite, marble, amphibolite, tremolite-actinolite schist, granite gneiss, migmatite and pegmatite veins. Tewari (1981) has given a general tectonic set up of the Padar area along Kudi Nala west of Sumcham.

2.3 GEOLOGY OF HIGHER HIMALAYAN CRYSTALLINE

2.3.1 KISHTWAR - PADAR SECTION

The Higher Himalayan Crystalline is exposed on all sides of the Kishtwar Window. These extend towards Chhatru in west, Thatri in south and beyond Masu along the Bhot Nala towards Zanskar. The rocks exposed in Kishtwar and Thatri areas include garnetiferous mica schist, staurolite-kyanite schist, granitic gneiss with mylonitised gneiss, amphibolite and calc-silicates (Fig. 2.2).

Along the Bhot Nala section, the HHC is separated from the Lesser Himalayan Kishtwar Window by the Main Central Thrust. Garnetiferous schist, staurolite-kyanite schist/gneiss,

sillimanite-muscovite schist/gneiss and sillimanite-K-feldspar schist/gneiss, marble and calc-silicate, amphibolite and granite intrusives occur in this section. The granitic gneiss is found in Chisoti and Bhuzun domes. Migmatite and two mica garnetiferous leucogranite are seen frequently associated with higher grade metamorphic rocks of sillimanite-muscovite and sillimanite-K-feldspar gneiss (Fig. 2.1).

The Lesser Himalayan rocks, exposed in Kishtwar Window, consist mainly of black carbonaceous phyllite, schist, yellowish-white quartzite, green sericitic schist, augen gneiss and granitic gneiss.

2.3.2 SURU - DODA VALLEYS SECTION

Rocks along northern margin of the HHC in Suru and Doda Valleys have been classified into the Suru Group (Srikantia et al., 1976; Vohra et al., 1976; Nanda and Singh, 1977; Ganesan et al., 1981; Honegger et al., 1982; Fuchs, 1987; Thakur et al., 1990).

Nanda and Singh (1977) studied the metamorphic rocks, migmatite and granitoids along the Suru Valley and named these as the Suru Formation. They subdivided it into Tangul, Padam, Penjung and Darcha members on the basis of grade of metamorphism. Srikantia et al. (1978) carried out extensive work in Zaskar and named the metamorphics as the Giambal Group after the Giambal Valley. The Giambal Group is exposed all along the southwestern part of Zaskar from Tsarap Lingti Chu to Pensi La and along the Suru Valley upto Sankoo. They have correlated it

with the Rohtang Gneissic Complex of Lahaul - Spiti. Its contact with the Tethyan sediments is described as concordant and gradational. The Giambal Group is subdivided into lower unit of high grade rocks and upper unit of metasedimentary rocks. Later, Ganesan et al. (1981) modified this name as the Giambal Gneissic Complex. Thakur (1981) has designated it as the Zaskar Crystalline Complex and correlated with the Central Crystalline Complex of Himachal, Garhwal and Kumaon. Searle (1983, 1986) has considered this as Precambrian basement and designated as the Higher Himalayan Central Crystalline Complex metamorphosed during the peak of Himalayan Orogeny.

Honegger et al. (1982) in their geological map of western Ladakh have shown the infolded Mesozoic Tethyan rocks within Zaskar Crystalline in southern parts of Zaskar. Fuchs (1987) has described the high grade metamorphic rocks under Central Crystalline and included the uppermost Darcha member of the Suru Formation (cf., Nanda and Singh, 1977) in the Tethyan Sedimentary Zone. Recently, Thakur et al. (1990) have classified the Suru Valley metamorphics into the Suru crystalline group, incorporating Parkachik, Sangra and Sankoo Formations.

It is, therefore, appropriate to name this part of HHC as the Suru Group, which is best exposed between Sankoo and Pensi La. The Suru Group has been traced all along the southwestern parts of Zaskar from Mune to Pensi La (Fig. 2.1). Towards north, these rocks are separated from the Tethyan Sedimentary Zone by the Zaskar Shear Zone (Fig. 2.1). The proposed

tectonostratigraphic succession along Chenab, Suru and Doda Valleys from south to north is given in Table 2.2. The Suru Group is predominantly made up of pelite and psammite, ranging from upper greenschist to upper almandine - amphibolite facies with numerous granitoids. Greenschist facies rocks are exposed near the villages of Sankoo, Shamakarpo and Zolidok Gompa. The different rock types include garnetiferous mica schist, quartz schist and calc-schist, sillimanite-K-feldspar gneiss, sillimanite-muscovite gneiss, staurolite-kyanite schist, amphibolite, intrusive granitoid, leucogranite, aplite, pegmatite and mylonite.

2.4 DESCRIPTION OF ROCK TYPES

2.4.1 LESSER HIMALAYAN SEDIMENTARY FORELAND

2.4.1.a KISHTWAR GROUP

(i) DUL FORMATION:

A thick sequence of predominantly white to brownish pale quartzite with bands of chlorite schist and metavolcanics, ranging in thickness from less than a meter to 100 metres, occurs east of Kishtwar around Dul. This formation extends northwards upto Ikhale and beyond and attains a maximum thickness of about 1000 metres southeast of Kishtwar. The quartzite around Dul forms an antiform whose western limb has been cut off by MCT (Kishtwar Thrust). The quartzite is again exposed on the eastern flank of the Kishtwar Window near Atholi on subthrust side of the MCT.

The Dul quartzite shows granoblastic to schistose texture

TABLE 2.2 TECTONOSTRATIGRAPHIC SUCCESSION ALONG CHENAB, SURU AND DODA VALLEYS IN PARTS OF ZANSKAR REGION OF JAMMU AND KASHMIR, NW-HIMALAYA, FROM SOUTH TO NORTH

TETHYAN SEDIMENTARY ZONE			Late Proterozoic to Lower Eocene	
Z S Z				
C H R I Y M S A T L A L Y L I N E	SURU GROUP		Garnetiferous mica schist, staurolite-kyanite schist, sillimanite-muscovite gneiss/schist, sillimanite-K-feldspar gneiss/schist, amphibolite, mylonite, intrusive granite bodies	
	SALKHALA GROUP SIRTHAL FORMATION		Garnetiferous mica schist, staurolite-kyanite schist, migmatite, granitic gneiss	
	M C T			
	K I G S R H O T U W P A R	DUL FORMATION		Quartzite, metavolcanics, carbonaceous phyllite.
		WOIL FORMATION		Muscovite-biotite schist, phyllite and slate, augen gneiss, granitic gneiss.
	M C T			

and consists of irregular but nearly equidimensional quartz grains. The other constituents are biotite, feldspar, muscovite, chlorite and sericite. The flaky minerals show preferred orientation. Irregularly distributed carbonaceous material, magnetite, apatite, zircon, detrital tourmaline and occasional sphene are present as accessories.

Carbonaceous phyllite is found between Gulabgarh and Masu along Bhot Nala section and contains thin sheared limestone bands. This phyllite sequence physically overlies the Dul quartzite with a sharp tectonic boundary. It separates the Lesser Himalayan sediments and the Higher Himalayan Crystalline and is observed along the right bank of Chenab River, west of Atholi.

(ii) WOIL FORMATION:

Conformably overlying the Dul Member, the Woil Formation comprises muscovite - biotite schist, phyllite and slate with interbedded limestone. In Woil-Galhar area, sericite - chlorite - quartz schist and biotite - muscovite - quartz schist are the most common varieties. At places, the schist is graphitic in nature.

The phyllite and slate are light grey to greenish grey in colour, thinly bedded and foliated. With increase in arenaceous content, the phyllite grades into quartz phyllite and schistose quartzite showing sub-schistose structure. Quartz, muscovite, chlorite and sericite are important constituents, while

magnetite, hematite and ilmenite occur as accessory minerals.

Crystalline limestone ranging in thickness from less than a metre to about 50 m is interbedded within the Woil Formation. It is generally dark grey in colour with thin argillaceous partings. It often grades into argillaceous limestone.

The Woil Formation is intruded by sills and dykes of basic and granite bodies. Field observations indicate that these basic intrusives are older than granite bodies and metamorphosed to amphibolite and greenschist. The largest two-mica granite intrusive at Shasho is fine grained and gneissic with numerous xenoliths of biotite schist.

2.4.2. HIGHER HIMALAYAN CRYSTALLINES (HHC)

The HHC is classified into the Salkhala Group of Kishtwar area and Suru Group of Bhot Nala - Suru - Doda Valleys.

2.4.2.a SALKHALA GROUP:

The Salkhala Group rocks are found mostly around Sirthal and towards east of Chhatru in the Kishtwar area. Based on the present investigations, only the Sirthal member described by Srivastava (1976), is included in the Salkhala Group. Other three members of his classification are included in the Kishtwar Group of the Lesser Himalayan Proterozoic Foreland (Table 2.1).

The Sirthal Formation consists of kyanite - staurolite schist, garnet - biotite - muscovite schist, migmatite and paragneiss. Numerous two-mica granite gneiss bodies having

porphyritic and augen varieties and sometimes mylonitised occur between Chhatru and Thatri (Fig. 2.2).

2.4.2.b SURU GROUP (Along Bhot Nala - Zanskari Nala):

The different rock types of the HHC along Bhot Nala - Zanskari Nala are garnetiferous mica schist, kyanite - staurolite schist, sillimanite - muscovite gneiss/schist, sillimanite - K-feldspar gneiss/schist, granitic gneiss and amphibolite. The brief description of these rock types is given below:

Garnetiferous mica schist: The garnetiferous mica schist is exposed around Atholi and Masu villages, NE of Kishtwar Window. These schists are grey to steel grey and greyish brown in colour and medium to fine grained. The foliation planes are characterised by uniform orientation of mica flakes interspersed with quartz. Garnet porphyroblasts occur in a matrix of quartz, biotite, muscovite and plagioclase.

Kyanite - staurolite schist: This schist is found near Masu and upto Kundel along Bhot Nala. These rocks are well foliated, grey coloured and medium to coarse grained. Kyanite blades are arranged parallel to mica lineation and plunge gently towards NE or SW on the main foliation. Other important minerals include biotite, muscovite, quartz, staurolite, garnet and plagioclase (oligoclase - andesine).

Sillimanite - muscovite gneiss/schist: These are exposed from Kundel to near Machel along the Bhot Nala. These rocks are medium to coarse grained mainly with sillimanite/fibrolite, biotite,

muscovite, garnet, plagioclase and quartz. Biotite, muscovite and fibrolite form the main foliation. The fibrolite aggregates are fibrous and acicular.

Sillimanite - K-feldspar gneiss/schist: These rocks are exposed continuously from Machel to the Great Himalayan Range towards Zanskar along the Bhazun Nala, Dharlang Nala, Chirang Nala and Hagshu Nala. These rocks are compact and hard consisting of sillimanite, biotite, garnet, plagioclase, K-feldspar and quartz. The foliation planes are defined by alternating dark and white bands of biotite and quartz/feldspar with well developed sillimanite needles. These rocks are coarse grained and made up mostly of plagioclase and K-feldspar.

Partial melting of gneiss and generation of migmatite and the tourmaline bearing leucogranite is common in this region.

Granite gneiss: Granite gneiss is exposed within the HHC in Chisoti and Bhuzun domes of Bhot Nala section. It is granitic-granodioritic in composition with local migmatized contacts. The gneiss has alternating bands of light and dark coloured minerals of biotite-muscovite and feldspars-quartz. The minerals in the gneiss include quartz, plagioclase, K-feldspar, biotite, muscovite and garnet with minor amount of tourmaline.

Amphibolite: Amphibolite bands occur at various places as concordant bodies within HHC, having sharp contact with the country rock. The amphibolite, in general, is compact and greenish colour. Hornblende and biotite are oriented along the

foliation. Amphibolite contains hornblende, biotite, plagioclase, garnet, epidote and sphene. Opaques are present in minor amounts.

2.4.2.c SURU GROUP (Along Suru - Doda Valleys):

Various rock types along the Suru - Doda Valleys are sillimanite-K-feldspar schist/gneiss, sillimanite-muscovite gneiss/schist, kyanite-staurolite schist, garnetiferous mica schist, amphibolite, granitic gneiss, augen gneiss, mylonite gneiss and quartz-muscovite-biotite (psammitic) gneiss. The brief description of these rocks is follows:

Garnetiferous mica schist: The garnetiferous mica schist is exposed near Sankoo and along Ringdom - Parkachik section near Shamakarpo. On the basis of relative content of quartz, biotite and muscovite, these rocks may be further classified into: (i) biotite-muscovite-quartz-garnet schist and gneiss and (ii) quartz-muscovite-biotite-garnet schist and gneiss. Out of these, biotite-muscovite-quartz-garnet schist and gneiss are more abundant, while northernmost part of the HHC near Sankoo is characterised by quartz rich muscovite- biotite-garnet schist and gneiss.

Kyanite - staurolite schist: These rocks are exposed around Parkachik and Panikhar along Sankoo-Ringdom section, near Pensi La and along the Doda Valley, close to ZSZ . These rocks are well foliated, grey in colour and medium to coarse grained. Large-size kyanite blades are abundant in some pegmatitic veins intruding these rocks.

Sillimanite - muscovite gneiss/schist: Sillimanite - muscovite gneiss and intercalated schist are exposed around Tangol - Parkachick region and along many tributaries from Mune to Pensi La. This gneiss is well foliated and contains quartz, muscovite, biotite, sillimanite and plagioclase minerals.

Sillimanite - K-feldspar gneiss/schist: Sillimanite - K-feldspar gneiss and schist are the highest grade metamorphic rocks exposed in interior parts of the Suru Group. These rocks are observed along the Mulung Tokpo, Temsa Tokpo, Haptal Tokpo and Sumche Tokpo. These rocks are hard, compact, foliated and consist of medium grained K-feldspar, plagioclase, sillimanite, biotite, garnet and quartz.

Granite gneiss: Granite gneiss is exposed within the HHC along the right bank of the Doda River and numerous mappable bodies between Parkachik and Zolidok. Hard, compact, light coloured and well foliated granite gneiss is interbanded within high - grade psammites and trends NW - SE with dip towards NE. Foliation plane is demarcated by alternating bands of dark and light coloured minerals. Near the ZSZ, muscovite is more predominant instead of biotite. Further SW, the gneissosity is poorly defined by coarse grained quartz and feldspar augen.

Mylonite gneiss: Mylonite gneiss associated with mica schist and augen gneiss shows various degree of mylonitisation at different localities. In this region, mylonite bands are mainly confined along the Zanskar Shear Zone. The width of mylonite band is

variable at different localities and ranges from one meter to several hundred meters occurring between HHC and Tethyan Sedimentary Zone.

This rock is fine grained and dark greyish to greyish in colour. The essential minerals in the mylonite are quartz, feldspar, biotite, muscovite, garnet etc. Quartz and feldspar augen are present with their curved tapering ends which give evidence of sense of shearing.

Quartz-muscovite-biotite gneiss: Psammitic gneiss within the HHC along Mulung Tokpo and at some other localities along Parkachik - Ringdom section are comprised of 100 to 200 m thick quartz, biotite, muscovite, feldspar-rich rocks. These are interbedded with kyanite-staurolite gneiss along Parkachik - Ringdom section and also with sillimanite-muscovite gneiss in Mulung Tokpo section. Along the foliation planes, intrusive quartz veins are segregated into boudinage.

Amphibolite: Amphibolite occurs as concordant sporadic lenses and thin bands within the HHC. Amphibolite is found mainly in Ringdom - Parkachik - Sankoo section and range in thickness from 1 to 5 m, except a good mappable outcrop near Sankoo. These amphibolite bands have sharp contact with the other metasediments. Main foliation usually trends in NW-SE and dips towards NE.

Granitoids in the HHC: Within the HHC, several granitoid bodies appear to have been emplaced at different periods. These

include tourmaline bearing leucogranite, porphyritic granite and biotite granite.

Tourmaline bearing leucogranite is exposed all along the Zanskar Shear Zone on the right bank of the Doda River. This granite contains quartz, K-feldspar, plagioclase, biotite, muscovite, tourmaline and minor amount of garnet. It is medium to coarse grained and is well foliated. Due to shearing along the Zanskar Shear Zone, this rock is also deformed and mylonitised.

The other variety biotite-leucogranite is medium to coarse grained and exposed within the HHC. It consists quartz, feldspar and fine grained muscovite with little tourmaline and biotite. It is deformed and found associated with migmatite and mica gneiss. This biotite bearing granite is considered to have been generated by partial melting of metamorphic gneiss during main ductile phase of deformation in the HHC. The partial melting is observed in high grade metamorphic rocks i.e. sillimanite - muscovite and sillimanite - K-feldspar grade. Near the contact with gneiss, granite is fine grained having the segregation of biotite. Away from the gneissic contact it becomes coarser with reduction in biotite. As a result different granite zones of different composition and colour are observed. Mineralogically, it consists of quartz, feldspar, biotite and garnet.

Sankoo granite: A huge dome-shaped granitic body emplaced within the HHC has been mapped south of Sankoo. It is 2 to 3 km in

width and extends towards west for many kilometers. The northern contact with garnetiferous quartz mica schist is sharp and very well exposed near Sankoo. The metasediments show the development of spotted biotite, producing hornfels. Within the Sankoo granite, discordant basic dykes, now metamorphosed to greenschist, are commonly seen and appear to be the feeder dykes to the overlying Phe Volcanics. Within the Sankoo granite, main foliation is very well developed and prominently marked by biotite-muscovite lineation. These foliations trend WNW-ESE and dip moderately to steeply towards NE along the northern margin. It appears that the Sankoo granite has intruded prior to the main phase of deformation (D_2) in this region (Patel, 1991) and subsequently deformed to large dome to isoclinally folded bodies.

Mineralogically, this granite consists of quartz, K - feldspar, plagioclase, muscovite and biotite. Foliation planes are defined by alternate mica-rich and quartzo-feldspathic layers where biotite and muscovite are preferly oriented. Near the contact with metamorphics, granite is fine grained and contains less amount of biotite and muscovite. Moving away from contact, the granite becomes coarser with an increase in muscovite.

CHAPTER - 3

DEFORMATION AND METAMORPHISM

3.1 INTRODUCTION

Structural analysis of deformed rocks has established many criteria for interpretation of folds and their relationship with foliation, lineation and other fabric elements (Turner and Weiss, 1963; Ramsay, 1967). It is possible to decipher whether superposed deformation belongs to a single period or all together different orogenies (Ramsay, 1967). The following criteria are useful in identifying different phases of deformation:

- a) Overprinting and cross-cutting structures of different episodes. Such outcrops are useful in identifying style and orientation of structures of different generations.
- b) As each deformational phase takes place at a particular P/T condition and strain rate, structures of each phase is characterised by distinct geometric styles.
- c) Growth of metamorphic minerals is related to a particular deformational phase. Hence, minerals grown during various deformational phases are preferably oriented and overprinted. Such studies help in correlating metamorphic fabric with deformational events.

Main lithotectonic units of polymetamorphosed and deformed rocks of the HHC and Kishtwar Window have been described in Chapter-2. The present chapter incorporates deformational and

metamorphic history of the these rocks.

- a) Identification and description of structural elements.
- b) Large-scale structures.
- c) Relationship of deformation with metamorphic episodes.

3.2 DEFORMATIONAL PHASES

Traverses across the HHC and Lesser Himalayan Sedimentary Foreland indicate the presence of numerous deformational phases. These are recognised on the basis of character, style, shape, orientation and structural relationship with each other.

3.2.1 LITHOLOGICAL LAYERING/BANDING (So):

Lithological layering/metamorphic banding or gneissic layering is a structure of unknown origin and phase in the HHC and Kishtwar Window. This is deformed by subsequent phases. However, there is no evidence of widespread transposition of lithological layering/metamorphic banding So (e.g., rootless hinges, extreme limb attenuation, dislocation of layering parallel to schistosity) (cf., Willis, 1984; Patel, 1991). Lithological layering (So) is defined by psammitic layers of different thickness having sharp contacts with pelitic rocks in most of medium and high grade rocks. This structure generally trends NW-SE and dips towards NE at moderate angles.

3.2.2 FIRST DEFORMATIONAL PHASE (D₁):

The earliest structures of first deformational phase (D₁) are rarely observed. Lithological layering (So) has been deformed

into isoclinal/tight F_1 folds having axial planar metamorphic banding/foliation S_1 (Fig. 3.1a). Quartz veins and granite layers, parallel to the S_0 , have also been deformed by D_1 . These structures are found on the scale of hand specimens and small outcrops.

F_1 folds: During this phase of deformation, F_1 folds, axial plane foliation (S_1) and lineation are developed. At a few localities along Parkachik - Ringdom section, these folds are rootless with 'flame type' hinges (Fig. 3.1a). These folds are highly asymmetric, tight to isoclinal, reclined in nature and show invariably thickened hinges and thinned limbs with variable wavelengths (Fig. 3.1b).

S_1 foliation: The term " S_1 foliation" is used here for the first recognizable, penetrative and oldest deformational lithological banding/layering surface. No primary sedimentary structures have been observed, both in Kishtwar Group (Dul Quartzite and phyllite/schist of the Woil Formation) and the HHC. It is, therefore, presumed that lithological banding/layering is the earliest planar structure in this region. S_1 is defined by metamorphic segregation foliation of alternating quartzo-feldspathic and mica bands of preferably oriented phyllosilicates (Fig. 3.1b). This foliation parallels the axial surfaces of F_1 folds and cuts across the hinge zones (Fig. 3.1b).

L_1 lineation: Despite the presence of a few F_1 folds, there is an almost absence of L_1 lineation. Curved, SW plunging L_1 lineation,

FIGURE 3.1 : Deformational structures from the HHC of D_1 and D_2 phases.

- a. Rootless "flame-type" tight F_1 folds with S_1 axial plane foliation/banding parallel to lithological layering (S_0). Loc. Parkachik. Lens cap - 55 mm diameter.
- b. Earliest recognisable lithological/metamorphic layering (S_0) defined by psammatic layers of different thickness has been folded into tight F_1 folds. Prominent metamorphic foliation S_1 is axial planar to F_1 folds. These F_1 folds show invariably thickened hinges and thin limbs. Loc. Parkachik. Pen length - 14 cm.
- c. In sillimanite-muscovite gneiss, quartz-feldspathic layers have been folded into isoclinal F_2 folds having rounded hinges. S_2 axial plane foliation is oblique to the S_1 foliation planes in hinge zone and parallels the S_1 foliation on the limbs. S_1 foliation wraps around the F_2 fold hinges. Loc. Yogmarchhahpochi near Parkachik. Pen length - 14 cm.
- d. Sub-parallel S-C fabric in biotite gneiss in which 'S' surface is defined by alternating quartzo-feldspathic and fine grained biotite-rich bands. S surfaces undergo small displacements towards top-to-SW due to sub-horizontal 'C' shear surfaces. Loc. Near Parkachik. Length of arrows - 3 cm.

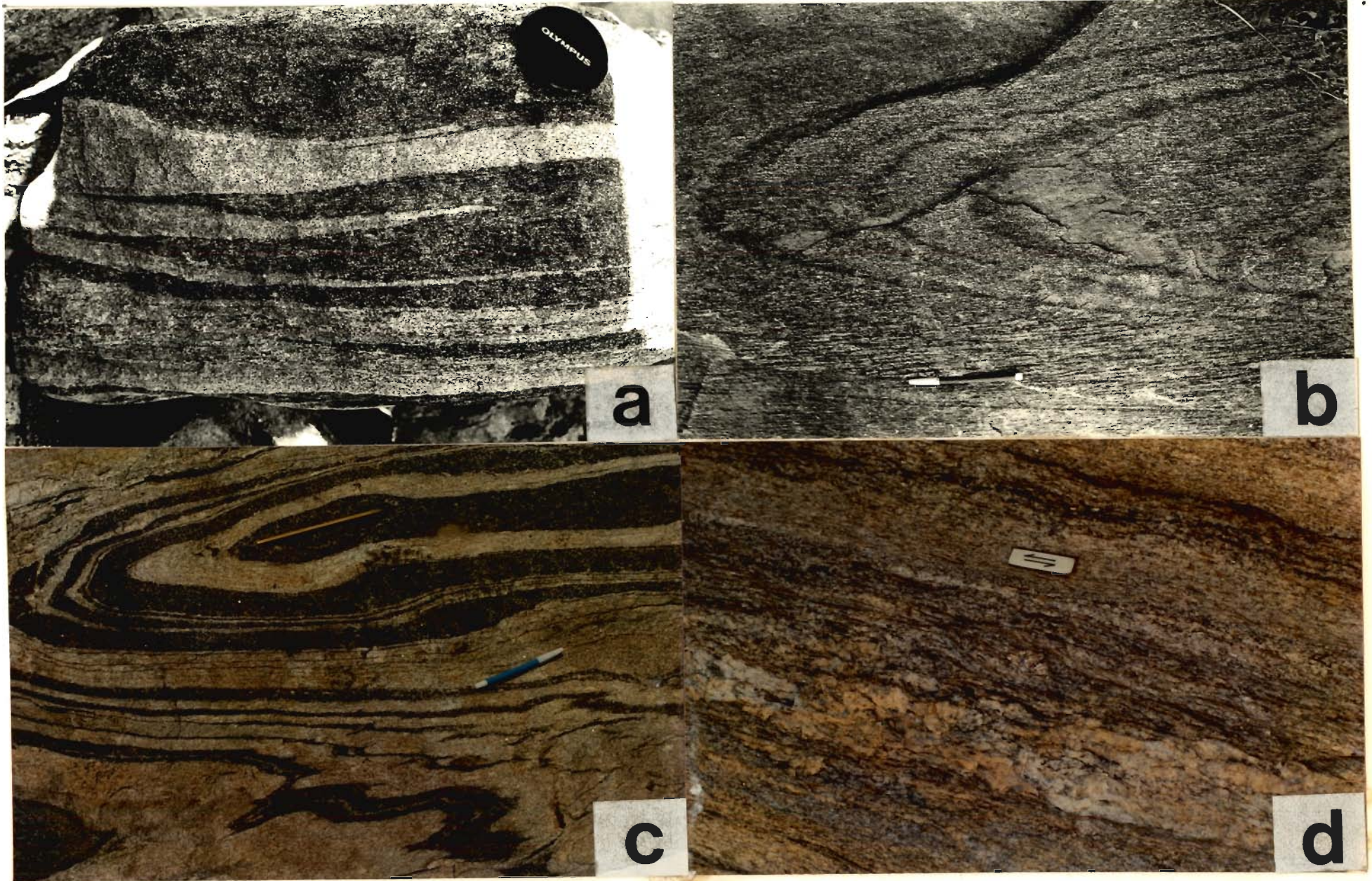


FIGURE 3.1

defined by biotite and muscovite in the hinge zone of later F_2 folds, is clearly observed at a few localities.

3.2.3 SECOND DEFORMATIONAL PHASE (D_2):

Second generation structures can be identified by their superposed relationship, consistent style and orientation.

F_2 folds: Both S_0 and S_1 surfaces are deformed during D_2 . Folds associated with this deformation are tight to isoclinal. Most of the F_2 folds are of reclined-type with down-the-dip plunging hinges on their axial surfaces (Fig. 3.1c). Interlimb angles of the folds vary from 0° to 60° . In some cases, both the limbs of a fold are eliminated leaving only acute isolated disconnected hinges. F_2 folds plunge between $20-45^\circ$ towards NE and lie on S_2 plane. F_2 folds are strongly oriented subparallel to L_2 lineation in most of the area. Along Kishtwar-Thattri region, F_2 folds plunge $40-50^\circ$ towards SW, while these plunge NE along Bhot Nala and Suru-Doda Valleys.

S_2 Axial plane foliation: This foliation parallels the F_2 axial surfaces of F_2 folds and is most penetrative planar structure. This foliation is parallel to the S_1 foliation on limbs of the F_2 folds, except in their hinge zones (Figs. 3.1c). S_2 is characterised by alternating quartzo-feldspathic and mica-rich bands in granite gneiss. In amphibolite, S_2 is defined by quartzo-feldspathic layers and biotite, hornblende-rich layers. In all cases, S_2 foliation is parallel to axial surfaces of F_2 folds and completely overprint the S_1 surfaces. Isoclinal

nature, tight stretched limbs of folds and large-scale transposition are mainly responsible for obliteration of S_1 foliation, except in the hinge zones of F_2 folds. S_2 surface regionally trends $N320^\circ$ - $N330^\circ$ and dips 25 - 45° towards NE.

From the field study, polished and thin sections of the samples, it has been observed that S_2 surface is a S-C composite planar foliation and is developed due to the D_2 deformation (also see section 3.7.2-f). This relationship is noticeable throughout the HHC and along numerous shear zones affecting the HHC. One of these surfaces is the 'C' (cisaillement) shear surface, defined by alternating feldspathic and fine grained biotite ribbons. The other is S (foliation) surface, which undergoes gradual rotation due to small displacement along C-surfaces (Figs. 3.1d; cf., Berthe et al., 1979). S-C fabric reveals top-to-SW sense of ductile shearing during D_2 deformation and is associated with numerous other shear criteria showing same sense of displacement (Jain et al., 1992).

Linear structures (L_2): Linear structures are extensively developed in the HHC and Kishtwar Window rocks and include mineral lineation, stretching lineation, rodding and boudinage.

Mineral lineation is developed due to preferred orientation of prismatic and tabular minerals in all lithologies of the HHC. In medium to high grade metamorphic rocks, kyanite, staurolite, biotite and sillimanite are found to be oriented parallel to F_2 fold hinges (Fig. 3.2a). Mineral lineations due to arrays of

biotite or muscovite minerals in mica schist/gneiss are more prominent. In amphibolite, acicular or long prismatic crystals of actinolite and hornblende form the mineral lineation. In garnetiferous mica schist, pressure shadows around garnet crystals are prominently seen on S_2 foliation and parallel the F_2 folds. In gneiss, augen of quartz and feldspar are stretched on the main foliation planes and parallel the L_2 lineation. L_2 lineation plunges $35-45^\circ$ towards NE, but in Kishtwar-Thatri region, it plunges towards S and SW.

In rocks along the Zanskar Shear Zone, penetrative NE-plunging stretched mineral lineation of tourmaline, quartz and feldspar on S_2 surfaces parallels the F_2 fold axes.

3.2.4 THRID DEFORMATIONAL PHASE (D_3):

Structures associated with D_3 deformational phase are developed on S_0 , S_1 and S_2 surfaces. Structures of this deformational phase are separated into two subphases: an early D_{3a} deformation superposed by D_{3b} phase.

3.2.4-a Early D_{3a} deformational phase:

i) F_{3a} folds: F_{3a} folds are developed on quartzo-feldspathic and foliated layers of earlier generations in gneiss and schist (Fig. 3.2b). These folds are close to isoclinal, plunging 10° to 30° towards ESE/E or NW/W. These folds are developed on all scales including some of the most spectacular large kilometer-scale folds around Tangol (see section 3.6). Axial surfaces are subhorizontal to moderately inclined (Fig. 3.2b).

FIGURE 3.2 : Deformational structures of D_2 and D_3 phases in the HHC.

- a. Mineral lineation (L_2) due to preferred orientation of kyanite and biotite in kyanite-biotite gneiss. Loc. Near Kundel. Scale - 5 cm. .
- b. Close to isoclinal F_{3A} folds with S_{3A} axial plane foliation developed in biotite schist and calc-schist and foliated layers of earlier generation. In the core and hinge of the folds, the rocks show crenulation foliation subparallel to the S_{3A} axial surfaces. S_{3A} surfaces parallel to S_2 surfaces on limbs. Loc. Near Atholi. Length of arrows - 3 cm.
- c. Earlier L_2 lineation are folded by open F_{3B} fold. Angle between L_2 lineation and F_{3B} fold axis is very high. Hammer parallels the F_{3B} fold hinge. Rock type: Sillimanite-muscovite gneiss. Loc. Near Chisoti.
- d. Close to isoclinal F_{3A} folds with co-axial open to close asymmetric F_{3B} folds are developed in quartzo-feldspathic sillimanite gneiss. F_{3B} folds are asymmetric and have rounded to angular hinges. Loc. Near Dangel. Photo frame about 15 cm in length.

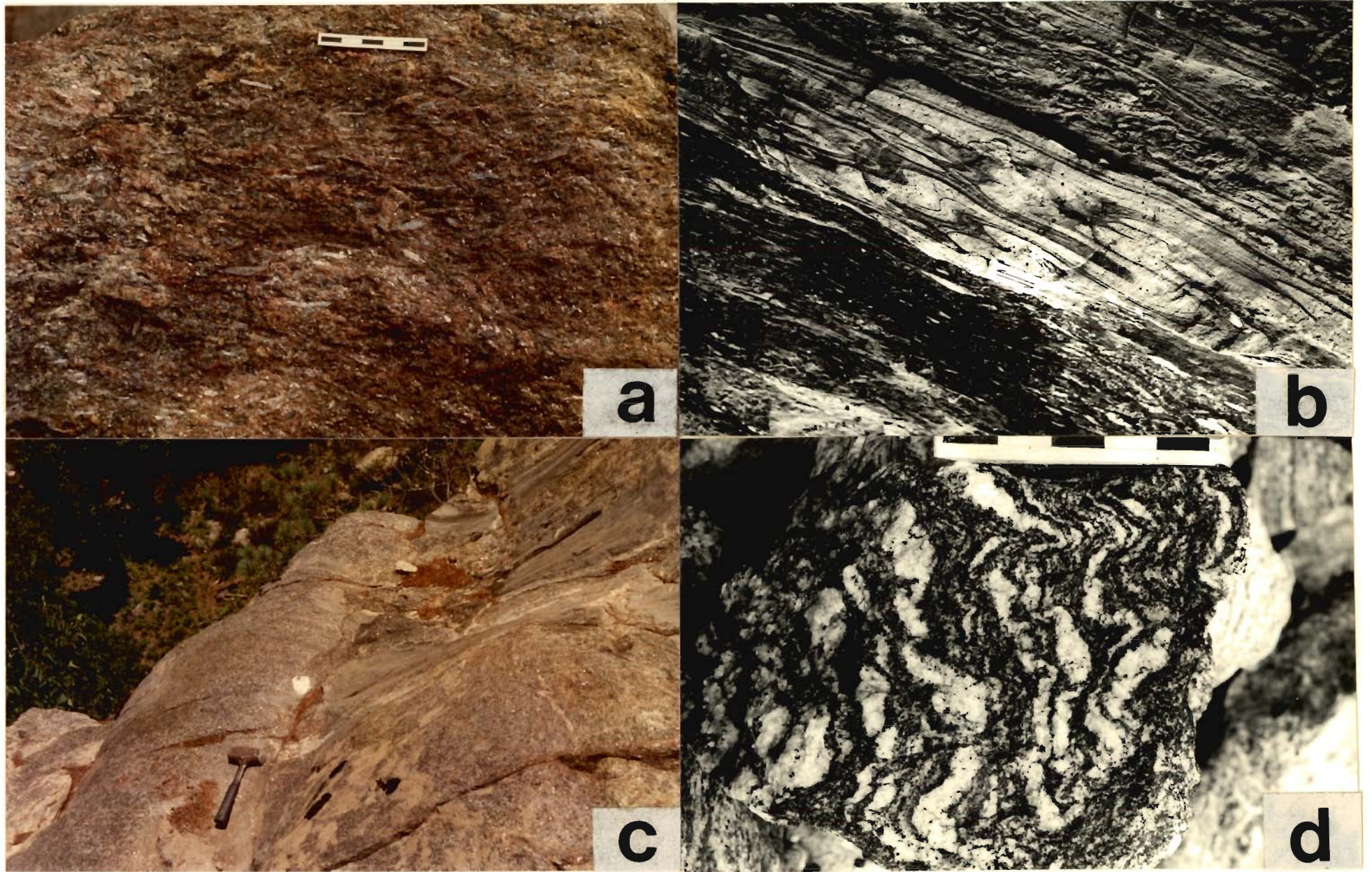


FIGURE 3.2

ii) S_{3a} axial plane foliation: S_{3a} foliations are developed parallel to axial surfaces of F_{3a} folds and are defined by quartz-feldspar and muscovite-biotite rich layers (Figs. 3.2b). The angle between S_2 and S_{3a} surfaces is very low. The overprinting of S_1 , S_2 and S_{3a} surfaces generate composite planar foliation which defines the main foliation S_m in this region. In the core and hinge of the F_{3a} folds, the pelitic rocks develop crenulation foliation subparallel to the S_{3a} axial surfaces (Fig. 3.2b). F_{3a} folds are isoclinal with S_{3a} parallel to S_2 foliation on limbs, hence it is not easy to distinguish S_2 and S_{3a} surfaces except in the hinge zones of S_{3a} folds (Fig. 3.2b). S_{3a} foliation trends $N300^\circ$ - $N315^\circ$ and dips 20 - 25° towards NE. In Kishtwar-Thattri region, S_{3a} foliation trends almost N-S and steeply dips towards W.

iii) L_{3a} lineation: This lineation parallels the F_{3a} fold hinges and is poorly preserved in this area. Mineral lineations of biotite and muscovite flakes paralleling the to F_{3a} folds are observed at a few localities and are highly oblique to L_2 lineation.

3.2.4-b Late D_{3b} Deformational Phase:

i) F_{3b} folds: F_{3b} folds, generated on S_{3a} surfaces and earlier surfaces, are ubiquitously developed in all lithologies. These folds are open to close in nature and plunge gently to moderately towards SE or NW (Figs. 3.2c, d). Folds are asymmetric with rounded (Fig. 3.2d) to angular hinges. S_{3b} hinges are wider than

all earlier folds. Long limbs of F_{3B} folds dip gently towards NE, while short limbs dip steeply causing SW vergence of folds. The angle between L_2 lineation and F_{3B} fold is very high (Fig. 3.2a).

ii) S_{3B} crenulation foliation: In psammite, pelite and quartzofeldspathic-rich layers, F_{3B} axial plane foliations are faintly developed. Crenulation foliation S_{3B} is very well seen in pelitic and gneissose units on axial plane foliation of early folds on mesoscopic and microscopic scales (Fig. 3.2d). Development of crenulation foliation generally involves formation of new structures that overprint existing cleavages or foliations (cf., Hatcher, 1990).

Development of crenulation is associated with the F_{3B} asymmetric folding. In the HHC and Kishtwar Window rocks, alternating mica and quartz-rich layers are generated due to crenulation with mica-rich layers coinciding with alternate limbs of asymmetrical crenulation.

iii) L_{3B} lineation: Due to development of crenulation foliation, strong intersection lines and small-scale F_{3B} crenulation folds define L_{3B} lineation associated with late D_{3B} deformational phase. The angle between the early lineation L_2 and L_{3B} lineation is very high i.e., about 70° to 80° . In mica-rich rocks, these lineations are characterised by alignment of mica flakes parallel to the axes of the crenulation.

Since both early and late stages of D_3 deformation produce

parallel or sub-parallel coaxial folds (Fig. 3.2d), it becomes difficult to distinguish lineations related to F_{3a} and F_{3b} folds.

3.2.5 D_{late} DEFORMATIONAL PHASE:

The associated structures of the D_L deformational phase overprinting all earlier structures are well developed shear planes (extensional crenulation cleavage), foliation boudinage, pull-apart structures, slickenside on extensional crenulation cleavage and small-scale kink bands in micaceous rocks etc.

3.6 MAJOR STRUCTURES

Different lithotectonic units of the Higher Himalayan Crystalline and the Lesser Himalayan Sedimentary Foreland have been deformed during various deformational phases resulting into major folds and thrust zones in this region of southern parts of Zaskar. Some of the major structures observed during the field investigations are described below.

3.6.1 FOLDS:

No major fold structures related to D_1 deformational phase have been identified in the HHC and Kishtwar Window from this part of the NW - Himalaya. Nevertheless, a few of these folds are developed on metamorphic/lithological banding. During the Himalayan Orogeny, these folds are superposed by structures of various deformational phases which appear to obliterate older structures. In this region, large folds of D_2 deformational phase are also not observed, though these are profusely developed on small scale. This has been considered here as the earliest

phase of the Himalayan Orogeny, because stretching/mineral lineation marked by growth of sillimanite, kyanite and other minerals and F_2 fold axes are sub-parallel to tectonic transport direction. Therefore, large-scale folds influencing the mappable lithounits and their outcrop patterns mainly belong to D_3 and younger deformational phases. Some of the folds developed in this region are described below.

(i) **Chisoti Dome:** A large, open, NW and SE doubly plunging Chisoti antiform occurs around Chisoti (Chisoti Dome; Kundig, 1989) and trends NW-SE. This dome consists of granitic gneiss with migmatite and is overlain by dark coloured metamorphics. The contact between the granite gneiss and overlying metamorphics is sharp and concordant. At a few places towards northeast of the dome, the overlying metamorphics are cut by discordant granitic veins. A few amphibolite bands are also found towards northern contact of this dome. The dip of S_2 foliation in adjacent semipelites is 50° /SW on the Masu side and 40° /NE on the Macheal side. The mica-bearing migmatite of the Chisoti dome show evidences of ductile shearing and development of F_{3b} crenulations.

(ii) **Sankoo - Karpokhar:** Some large folds are developed on both steep valley slopes of the Suru River between Sankoo bridge and Karpokhar, where the leucocratic Sankoo granite emplaced in the Higher Himalayan Crystalline is folded into large gently double plunging folds. This fold extends westward and trends almost

E - W. It appears to be a large doubly plunging dome of the Sankoo granite exposed in its core where it is enveloped by garnetiferous mica schist. The Sankoo dome probably tapers off across the river into isoclinally folded and ENE - plunging antiform where the granitic gneiss is again exposed in its core. The Sankoo dome is a large F_{3a} fold affecting the structures of D_2 deformational phase.

(iii) Tangol: Some of the largest F_{3a} folds are developed looking up Tangol village on left bank of the Suru River in frontal parts of Nun - Kun peaks. Two major fold structures with rounded hinges and gentle opposite-dipping limbs characterise the region. Large-scale folds plunge gently almost due E and affect the granitic gneiss and schist of the HHC.

(iv) Suru Dome: A huge open antiform has been mapped between Thangbu - Panikhar - Tangol - Parkachik - Kangriz Glacier almost all along the sinuous river course of Suru. The Suru dome is the largest fold observed in the area and affects all the structures generated before D_{3b} deformational phase. It is therefore interpreted as a fold developed during D_{3b} deformation and is later refolded during post D_3 cross - folding. Geometry of the Suru Dome becomes indistinct due the presence of numerous mappable granite gneiss intercalations.

(v) F_{3a} Folds around Ryalmothungos: Mountain slopes on left bank of the Suru Valley between Kangriz Glacier and Latafsafarka

Nala are characterised by numerous granite gneiss bodies occurring as concordant sheets between sillimanite - muscovite and staurolite - kyanite schist/gneiss (see also Honegger et al., 1982; Thakur et al., 1990). It appears that granite gneiss occupies higher tectonic levels like the Sankoo granite; however it is uncertain if these belong to a single concordant sheet or represent numerous bodies of granite gneiss.

3.6.2 THRUSTS AND SHEAR ZONES:

Like folds, thrust and shear zones have also definite pattern of dislocation affecting the HHC and Kishtwar Window. The following major zones have been identified in this region.

- i) Main Central Thrust separating the HHC from Lesser Himalayan Sedimentary Foreland of Kishtwar Window.
- ii) Zaskar Shear Zone separating the HHC from the TSZ.

3.6.2-a Main Central Thrust (MCT): The term Main Central Thrust was coined by Heim and Gansser (1939) to designate the surface along which the HHC is thrust southwestward over the Lesser Himalayan metasediments in parts of Kumaon Himalaya. This nomenclature has been followed by a number of subsequent workers (Gansser, 1964; Mehdi et al., 1972; Agarwal and Kumar, 1973; Bordet, 1973; Crawford, 1974; Valdiya, 1978; Thakur, 1981; Pati and Rao, 1981; Brunel, 1986; Staubli, 1986, 1989). All these authors identify the MCT between the metamorphics of almandine-amphibolite facies belonging to the HHC and the Lesser Himalayan metasediments of the greenschist facies. Valdiya (1978) has,

however, redesignated this tectonic boundary as the Maunsari Thrust and postulated that the MCT is located further northwards throughout the Higher Himalaya. In Central Nepal, Le Fort (1975), Pecher (1978) and Caby et al. (1983) mapped the MCT approximately along the kyanite-isograd. Searle and Rex (1989) defined the MCT in the Kishtwar area as a major ductile shear zone containing several zones of high strain.

The MCT is considered as a gently-dipping thick shear zone resulting from the southwards emplacement of a deep rooted Central Crystallines of the basement (Bouchez and Pecher, 1981). Locally, the MCT borders the Kishtwar Window as a steeply dipping zone parallel to the S_2 schistosity (30° - 60° ; Staubli, 1989), whereas in Nepal, the MCT is considered rather as a flat-lying thrust zone, gently dipping to the north (15° - 30° ; Brunel, 1986).

In the present work, the original status and position of the MCT has been retained. During detailed geological investigations along Chenab - Bhot Nala, it has been observed that the MCT is not a simple tectonic boundary between the HHC and the Lesser Himalayan Sedimentary Foreland, as has been worked out. The following characters are noteworthy along the MCT in this area.

- (i) Along the thrust, metasediments of the Kishtwar Group comprising quartzite, carbonaceous phyllite and quartz-chlorite-sericite schist and garnetiferous schist of greenschist facies are overlain predominantly by gneiss and schist of amphibolite facies belonging to the Salkhala and

Suru Groups (Chapter-2).

- (ii) Evidences of ductile shearing in carbonaceous phyllite of Kishtwar Group are numerous so that each foliation surface appears to have behaved as a ductile thrust surface.
- (iii) Development of bands of phyllonite, mylonite and mylonitised augen gneiss in the ductile shear zone coinciding with the surface trace of the MCT.
- (iv) Near the MCT, P-T estimation on the HHC shows no evidence of any effect of the MCT in this area (also see Chapter-5).

Nature of the MCT depicts as a ductile intracrustal shear zone, probably in the basement from which the thrust has developed into a southward moving major thrust that juxtaposed the HHC zone over the metasediments of Lesser Himalaya along a zone of imbrication. Pile of the HHC rocks has been deformed into a ductile zone due to which S_2 foliation and a constant NE-plunging stretching lineation has developed on the S_2 foliation surface during D_2 deformational phase. The imbricate nature of the MCT is very well documented by the presence of imbricate zone within the Kishtwar Group within HHC.

3.6.2-b Zanskar Shear Zone (ZSZ): The Zanskar Shear Zone extends from Mune in SE to Sankoo in NW separating the HHC from the rocks of the Tethyan Sedimentary Zone (Fig. 2.1; cf., Jain et al., 1992). This major shear zone can be mapped on the basis of morphological depression and by presence of sheared rocks. Shear zone can be approximately located on the basis of colour and topographic variations and its width changes from about 0.5 to

2 km. Best continuous exposures of rocks along ZSZ have been observed along the Mulung Tokpo, where kyanite-staurolite schist is exposed immediately beneath the Tethyan Sedimentary Zone (Fig. 2.1). The Zanskar Shear Zone regionally trends NW - SE and dips 25° to 40° towards NE (Jain et al., 1992). Foliation planes developed along the Zanskar Shear Zone are parallel to axial plane foliation associated with F₂ folds. Further, the ZSZ is characterised by stretching lineation, mylonitization and other different shear structures such as asymmetric augen, pressure shadow, non-cylindrical folds, tectonic lenses, foliation boundinage, extensional crenulation cleavage, brittle and brittle ductile normal faults. Different metamorphic isograds truncate against the ZSZ around Penjung and Pensi La so that garnet zone rocks are not seen along the Doda Valley. Along the Doda Valley, the isograds are approximately subparallel to the ZSZ. Jain et al. (1992) have concluded from critical evaluation of shear criteria that the ZSZ represents a complex deformational history.

3.7 METAMORPHIC EPISODES

Various metamorphic minerals have developed in different lithotectonic units of the Lesser Himalayan Sedimentary Foreland and HHC along Chenab, Suru and Doda Valleys (section 3.2). The present section correlates deformational phases with metamorphic episodes for mineral paragenesis on the basis of textural relationships.

3.7.1 M₁ METAMORPHIC EPISODE:

Although evidences of earliest M₁ metamorphism have largely been superposed and obliterated by later events, recrystallisation of mica, quartz, feldspars approximately parallel to the metamorphic segregation layering. This type of layering formation was syntectonic to M₁ event and coeval with the F₁ folds. In such folds tiny mica flakes trend uniformly across the hinge and parallel the lithological layering. It is observed in quartz-sericite schist or folded aplite veins.

In the low grade rocks, F₁ microfolds are defined by fine opaques and thin bands of equigranular quartz where syn-kinematic felt of fine chlorite and sericite occurs at high angle near the hinges but fans out and becomes quasi-parallel on the limbs.

S₁ foliation "sensu stricto" has been observed in the hinge zones of rootless intrafolial F₂ folds indicating intense transposition of the earlier planar structure. Fold profiles reveal that the earliest detectable recrystallisation occurred during the development of folds of first generation and is, therefore, related to the D₁ phase of deformation. Due to this textural control early generation of mica flakes and quartz are preferably oriented along the axial plane foliation S₁. Early lepidoblastic mica flakes are oriented at high angles in hinge zone of F₂ folds, but subsequently crystallised mica are parallel to the limbs.

Feldspars-I occurring along the S₁ foliation is folded later

on by F_2 folds. In the hinge zones, K-feldspar-I reveals irregular grain boundaries with many quartz, biotite and muscovite inclusions and grown synkinematically along the S_1 foliation during the D_1 deformational phase.

M_1 metamorphism is evident from the core of garnet porphyroblasts (G-0), overgrown by the later generations of garnet (G-I; Fig.3.3a). In such garnet, the core contains rarely discordant inclusions of minute quartz and opaques. It is overgrown by garnet (G-I) where inclusions are concordant with the external F_2 fabric (Fig.3.3a). The contact between garnets G-0 and G-I is marked by coarse quartz inclusion. These M_1 garnets are present in many grades indicating the D-I growth (Fig. 3.3a).

The presence of quartz-sericite-chlorite-biotite-feldspar-I-garnet-opaque assemblage suggests a greenschist facies metamorphism. Superposition of high grade metamorphism and intense D_2 deformation has probably obliterated the textures and minerals of the M_1 metamorphism in most of the cases.

3.7.2 M_2 METAMORPHIC EPISODE:

M_2 metamorphism is the most important episode during which the metamorphism reached its peak with crystallisation of porphyroblastic index minerals in the HHC. As a result of strong penetrative deformation (flattening and ductile shearing), S_2 foliation is defined by mica-I, quartz-I and feldspar porphyroblasts indicating their syn- to late-tectonic growth. In most of the F_2 fold profiles, an older generation of mica, quartz

FIGURE 3.3 : Garnet texture in Suru Group of the HHC.

- a. Pre-tectonic garnet core (G-0) showing discordant Si inclusions of quartz, is overgrown by syn-tectonic garnet (G-I) with circular bigger Si quartz inclusions. Post-tectonic garnet (G-II) grown over the edges of Garnet-I is also seen. Line chemical analysis of this grain was carried out along nearly horizontal traverse through the centre of the grain (Fig. 4.33). Rock type: Sillimanite-muscovite schist (MP5). Loc. Padam. PL, 20X

- b. Coalesce embryonic garnet-I oriented parallel to the S_2 foliation. Right centre shows bowing out-like structure of foliation around skeletal garnet oriented perpendicular to the S_2 foliation. Left corner shows slightly rotated skeletal garnet growth. Rock type: Garnet-biotite-schist (PL8/99). Loc. Lago La. PL, 20X

- c. Augen-shaped S_2 foliation deflected around growing skeletal garnet with biotite inclusion. Such garnet grains used for garnet-biotite inclusion thermometers. Rock type: Staurolite-kyanite-schist (32A/89). Loc. Parkachik, PL, 20X

- d. Straight garnet-I stringers in centres with strong curvature towards tails showing shear component having top-to-left sense of rotational movement. Rock type: actinolite-garnet-schist (P54/197). Loc. Parkachik. PL, 20X

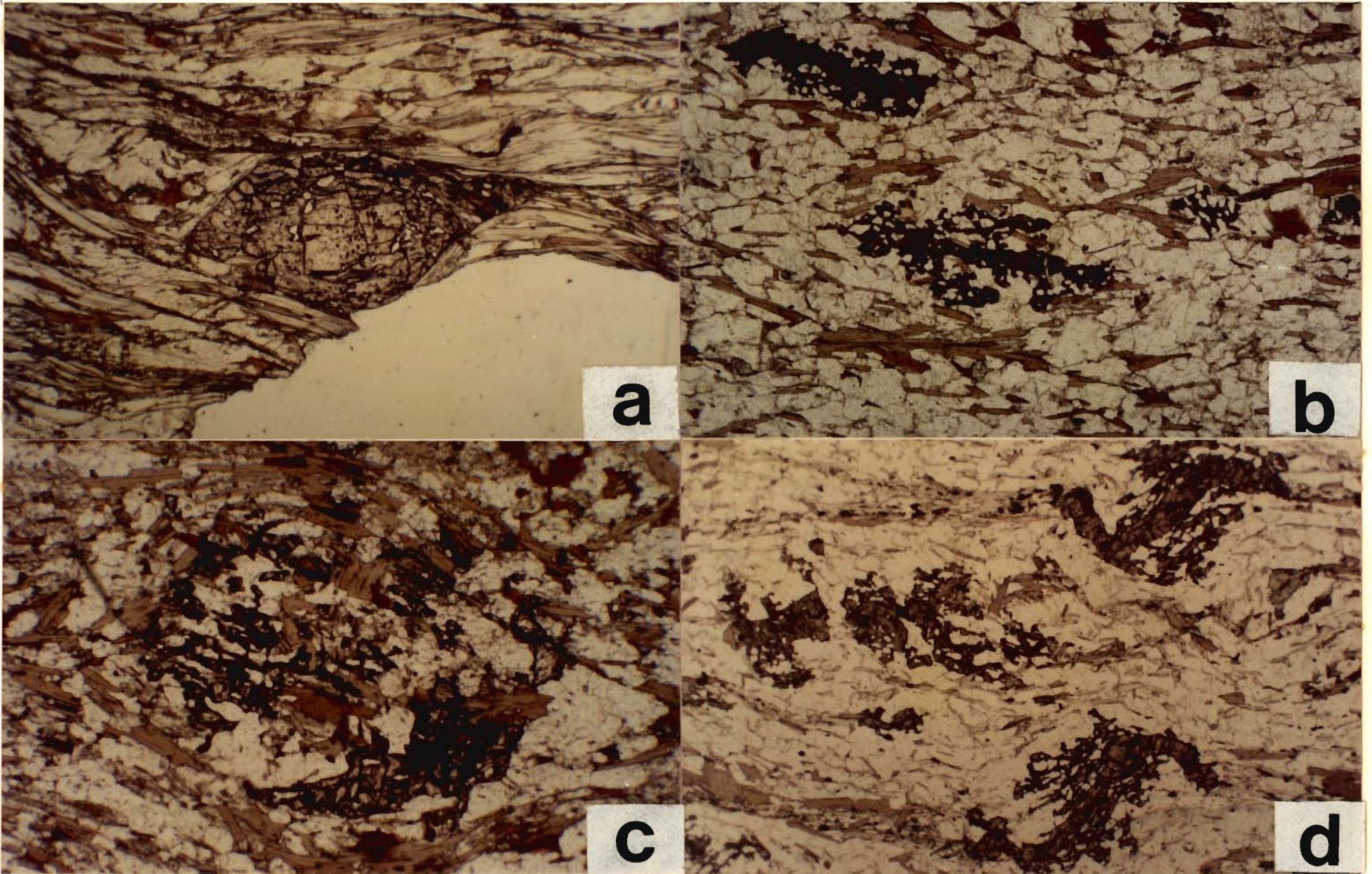


FIGURE 3.3

and feldspar define the S_1 foliation which is isoclinally folded with S_2 as the axial plane foliation. Biotite-I, muscovite-I and quartz-I do not texturally differ from early mica and quartz, except in their elongate shape. Orientation of early mica and quartz varies according to their location within the F_2 fold profile and is usually at high angles in the hinges in immediate vicinity of psammitic layers, but is subparallel to the mica orientation of second generation on the limbs or in hinge zones of pelitic layers.

Porphyroblastic garnet, feldspar, staurolite, kyanite, sillimanite etc. are significant in understanding the textures and are elaborated below.

3.7.2-a Garnet: All stages of garnet growth such as embryonic or skeletal, snowball and subhedral garnet-I (G-I) are observed in the HHC. Embryonic garnet-I is developed as stringers, which are thick or slender, widely spaced or coalesce together (Fig. 3.3b). In most cases, garnet stringers approximately are either parallel to main foliation S_2 (Fig. 3.3b) or display bowing out-like structures at almost normal to the foliation (Fig. 3.3b; cf., Misch, 1971). Some of the examples show augen-like relationship with S_2 foliation which is deflected around the garnet stringers (Fig. 3.3c). All these commonly observed patterns, which show nearly parallel relationship with S_2 foliation, are cut off or attenuated at the extremity of stringers (Fig. 3.3d). Above observations suggest an incipient stage of garnet growth in

FIGURE 3.4 : Garnet textures in Suru Group of the HHC and Lesser Himalayan Proterozoic Foreland.

- a. Syntectonic xenoblastic garnet-I (G-I) with S-shaped, spiral Si inclusions of quartz and opaques overgrown by post-tectonic inclusion free rim of garnet-II (G-II). Rock type: Garnet-biotite gneiss (KC21/23). Loc. Chhatru. PL, 20X
- b. Field photograph showing large syntectonic rotational snowball garnet-I with Si || Se relations along the margins and top-to-SW sense of ductile shearing. Rock type: Garnet-biotite-schist. Loc. Shamrakarpó. Arrow - 5 cm.
- c. Syntectonic garnet-I containing straight Si inclusions of quartz parallel to S₂ foliation is overgrown by post-tectonic subidioblastic garnet-II. Note inclusions in garnet are mostly parallel to S fabric which is sheared by horizontal C-planes marked mostly by mica and quartz. Rock type: Garnet-mica schist (A45/50). Loc. south of Masu on the footwall side of the MCT. PL, 20X
- d. Post-tectonic garnet-II gas rimmed the syntectonic garnet-I having quartz, biotite and sillimanite inclusions which are used for garnet-inclusion geothermobarometry. Rock type: Sillimanite-muscovite gneiss (A53/62B). Loc. Chisoti. PL, 65X

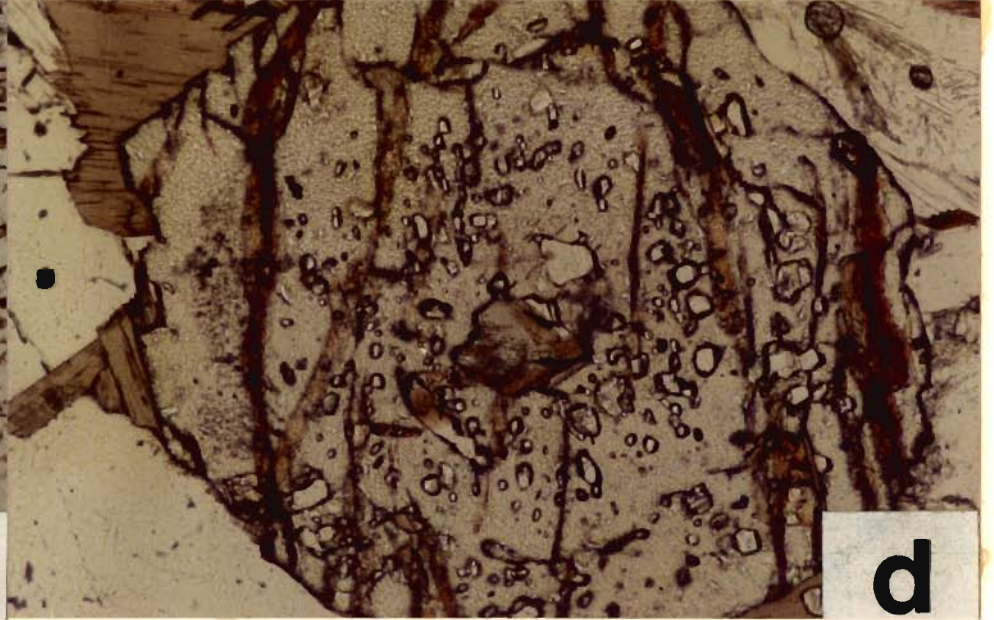
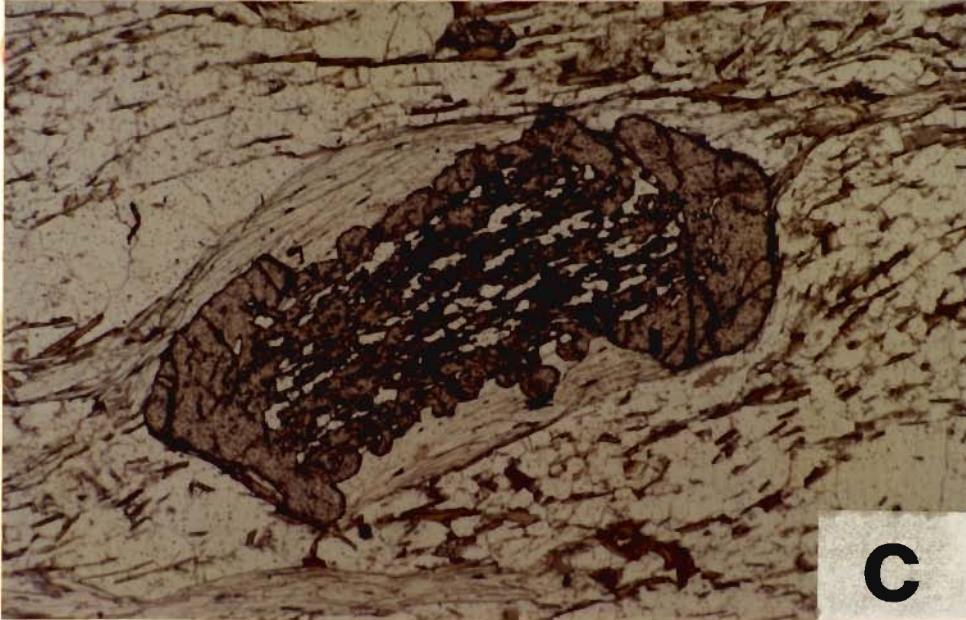
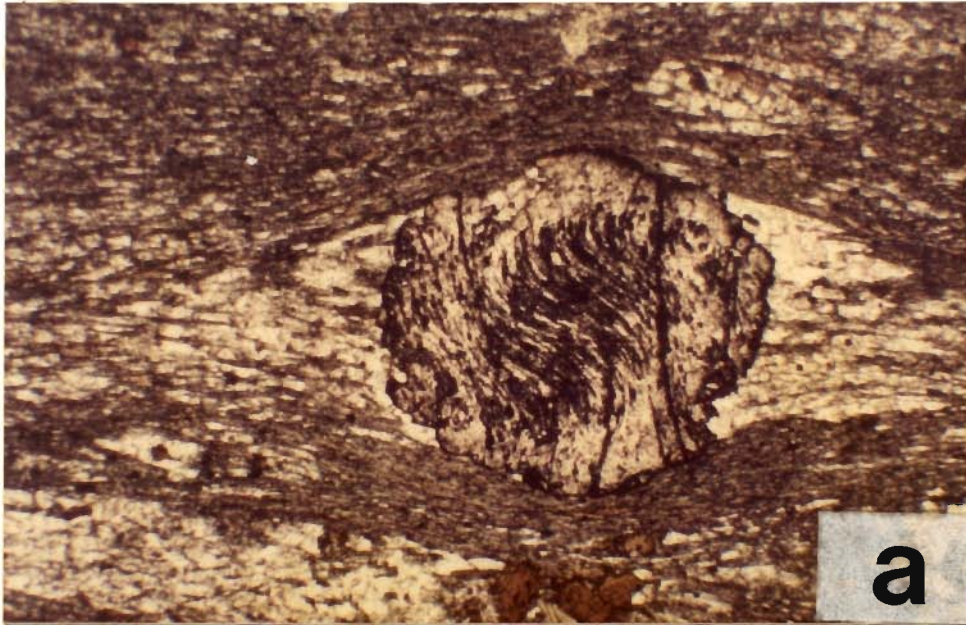


FIGURE 3.4

the form of stringers during the early period of D_2 deformational phase.

In the advanced stage during D_2 deformation, syntectonic xenoblastic garnet is noticed with the development of S-shaped spiral or rotational S_1 inclusions of small quartz, mica and opaque minerals (Figs. 3.4a, b). Internal fabric S_1 is rotated, but is continuous with the external foliation S_2 in snowball garnet (Fig. 3.4b). Sometimes, continuity is maintained at one end, but is disturbed at the other. It has been observed that S_1 and S_2 maintain their continuity upto 90° rotation or slightly more (Fig. 3.4b; Zwart, 1963).

A number of samples show that garnet-0 is overgrown by garnet-I during M_2 metamorphism (Fig. 3.3a), where garnet G-0 with straight inclusions has a rim of syntectonically grown garnet G-I having curved inclusions. Moulding effects of the growing porphyroblasts on the matrix is clearly seen in Figures 3.4a, d).

During late to post D_2 deformational phase and metamorphism M_2 , idioblastic to subidioblastic garnet (G-II), containing a very few inclusions of opaques or quartz has crystallised (Fig. 3.4c). This garnet (G-II) is fractured along planes running both along and across the S_2 foliation (Figs. 3.4c, d).

In most of the samples, garnet G-I is often overgrown by subidioblastic, inclusion-free post-tectonic garnet (G-II - Figs. 3.5a-d). In a few cases, all the three stages (pre-, syn-

and post-kinematic) of garnet growth are observed (Fig. 3.3a). These are described by garnet cores with straight S_1 (inferred to have grown in the absence of rotation during D_1 -G-0), intermediate zones with curved S_1 (inferred to have grown during rotation in D_2 -G-I) and outer zones with no inclusions (inferred to have grown statically during post- D_2 -G-II) (cf., Sturt and Harris, 1961; Johnson, 1963).

S_1 and S_2 relationships of a snowball garnet in pelitic schist is significant in interpreting mineral growth and rotation in a matrix undergoing layer-parallel shearing (Figs. 3.4b, 3.5d) or flattening (Fig. 3.4a) across the foliation.

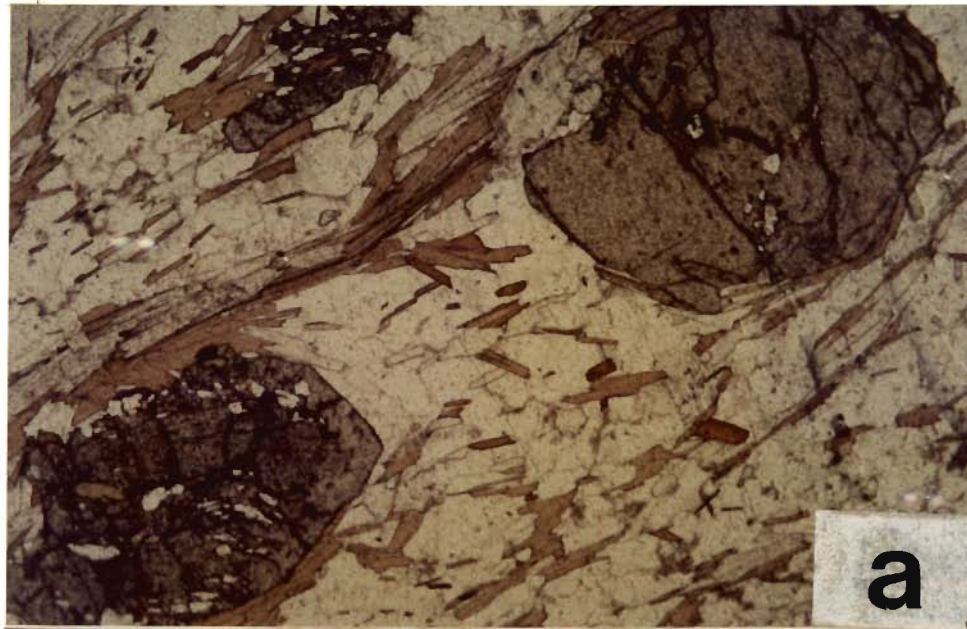
According to Zwart (1963), low angle rotational stringers are formed in the initial stages due to flattening of the matrix, while the crystals remains stationary. However, high angle rotational patterns are found during which the crystal rotates more or less as a ball between the two walls. Such relations have been observed within a single thin section from the HHC and represent heterogeneous rotation in different parts of the sample.

Ramsay (1962) considered that garnet remains essentially stationary in syntectonic growth and grew over the schistosity, which is itself rotating due to homogeneous irrotational strain.

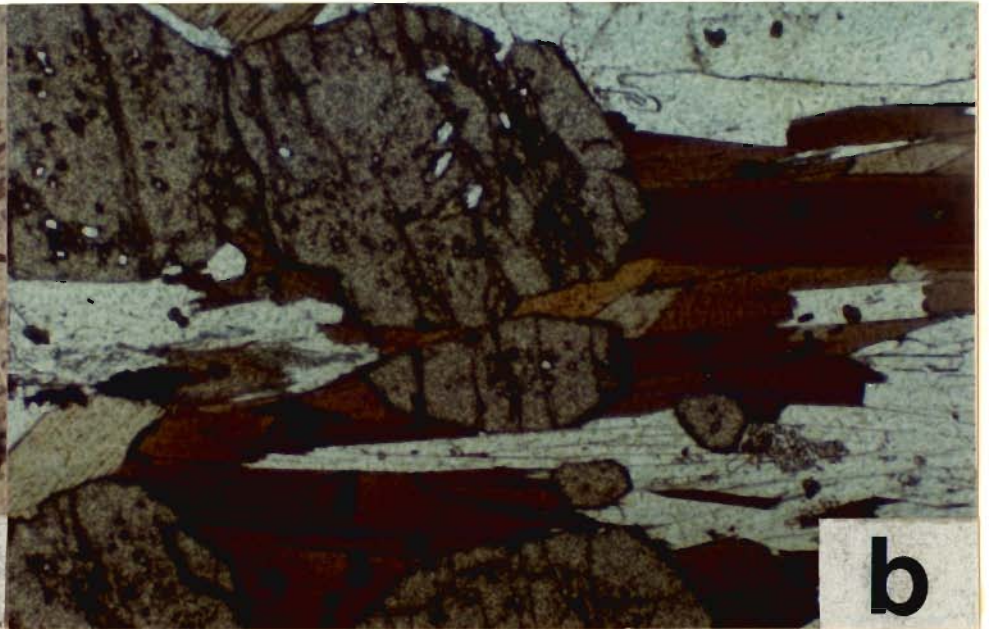
On the other hand, Spry (1963) laid emphasis on rotation of the crystal itself. According to him, the trails of inclusions are doubly-curved cylindrical surfaces. Powell and Treagus

FIGURE 3.5 : Different garnet textures in the rocks of Suru Group, HHC.

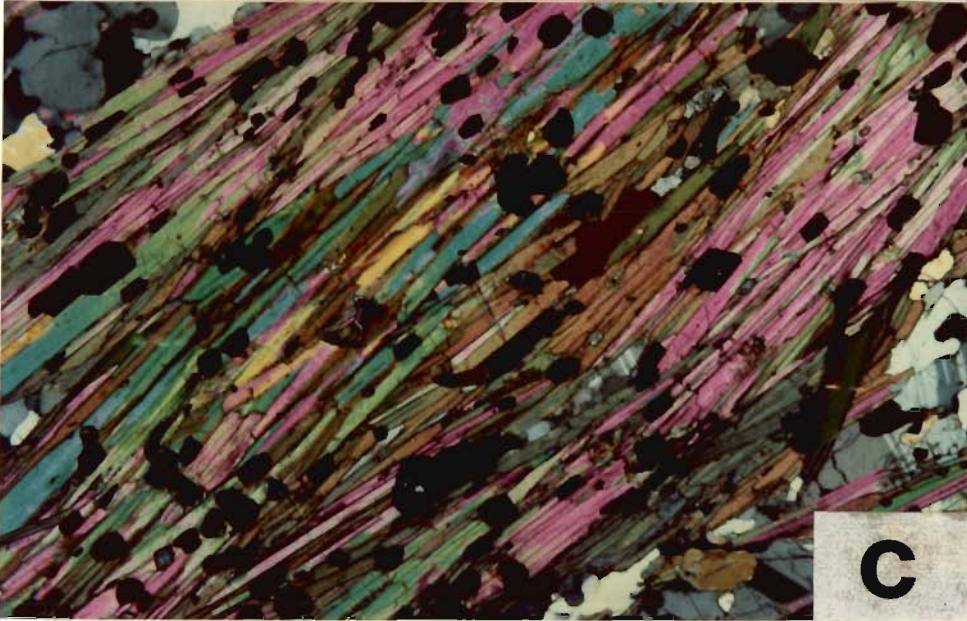
- a. Syntectonic garnet-I is overgrown by post-tectonic subidioblastic garnet-II. Rock type: Staurolite-kyanite schist (PR6/81). Loc. Parkachik. PL. 20X
- b. Fractured Post-tectonic garnet-II grown over syntectonic garnet-I having curved inclusions. Rock type: Sillimanite-muscovite-gneiss (A53/62B). PL, 20X
- c. Idioblastic post-tectonic garnet-II superposed upon the S_2 foliation characterised by muscovite-biotite flakes. Rock type: Staurolite-kyanite schist. Loc. 2 Km north of Masu. PL, 13X
- d. Syntectonic rotational snowball garnet-I with Sillimanite relations along the margins. Post-tectonic tourmaline and biotite grown upon S_2 foliation. Note S-C composite character of S_2 foliation with mica growing along both the surfaces. Rock type: Staurolite-kyanite schist (PC29/24). Loc. Near Shamrakarpo. PL, 13X



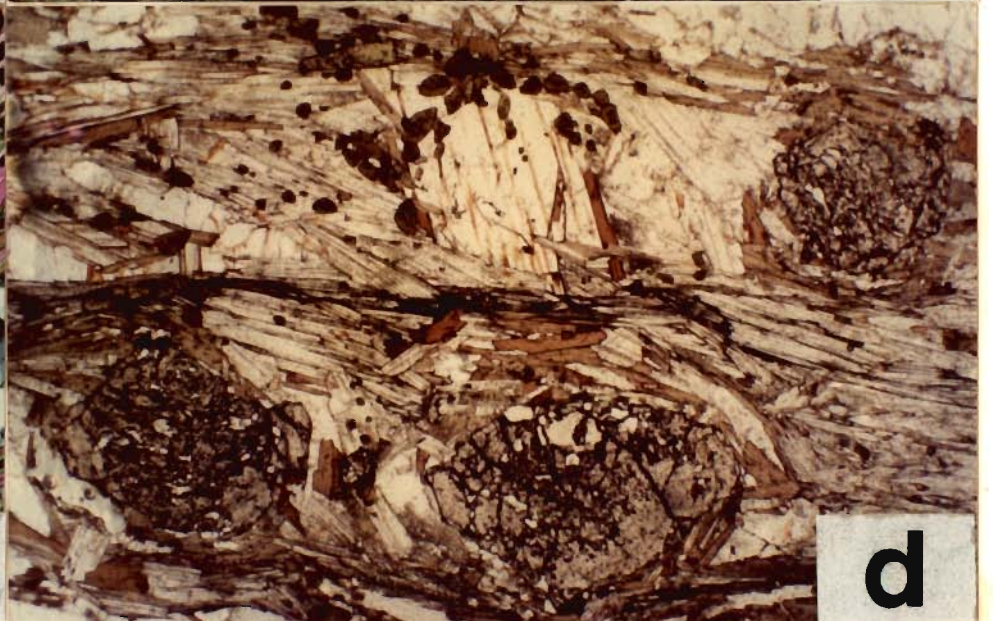
a



b



c



d

FIGURE 3.5

(1967, 1970) postulated that the crystal does not rotate, but grows at a constant rate, while the matrix is rotating at an uniform velocity. At different stages of growth, the rotated matrix is incorporated within the growing crystal which results into a S-shape inclusions.

Vernon (1978) and Borradaile et al. (1982) described various criteria for distinguishing syntectonic growth of porphyroblast as (i) each porphyroblast contains only one S_1 sigmoid which is symmetrical about the centre of the porphyroblast, (ii) S_1 sigmoid in adjacent porphyroblasts indicate the same sense of rotation and (iii) spiral of quartz inclusions and spiral of other matrix minerals intersect with the same geometrical relationship as described by Schoneveld (1977).

More recent contributions have been made by Bell and Rubenach (1980, 1983), Ward (1984), Bell (1985), Bell et al. (1986), Jamieson and Vernon (1987) and Vernon (1989) on the interpretation of porphyroblast-matrix microstructural relationships. The truncation of S_1 in the garnet is inferred to be the result of dissolution during the cleavage development (Bell and Rubenach, 1983). Vernon (1989) suggested that the curved inclusion trails may be used to relate metamorphic reactions to deformation, especially with regard to generations and stages of crenulation development.

The present study of garnet-I of embryonic and snowball varieties suggests synkinematic growth of both of these

FIGURE 3.6 : Characteristics of staurolite in staurolite-kyanite schist of Suru Group, HHC.

- a. Syntectonic staurolite along S_2 foliation containing inclusions of lenticular quartz, mica and opaques which are parallel to S_e . Note absence of any rotational fabric. Rock type: Staurolite-kyanite schist (PC16D/83). Loc. Pensi La. PL, 13X
- b. Porphyroblastic staurolite containing inclusions of quartz, mica and opaques which are parallel to S_2 foliation showing mild rotation. Rock type: Staurolite-kyanite schist (P9/49). Loc. Along Mulung Tokpo below Zanskar Shear Zone. PL, 13X
- c. Syntectonic staurolite with growth of spiral Si inclusions showing top-to-left rotation. Rock type: Staurolite-kyanite schist (PC16/83). Loc. Pensi La. PL, 13X
- d. Syntectonic staurolite porphyroblast containing sigmoidal Si inclusions showing top-to-left rotation. Note the inclusions of garnet porphyroblasts within the staurolite. Also noteworthy is the crystallisation of small staurolite crystal along C- shear surface. Rock type: Staurolite-kyanite schist. Loc. Mugalmaidan along Chhatru Nala. PL, 13X

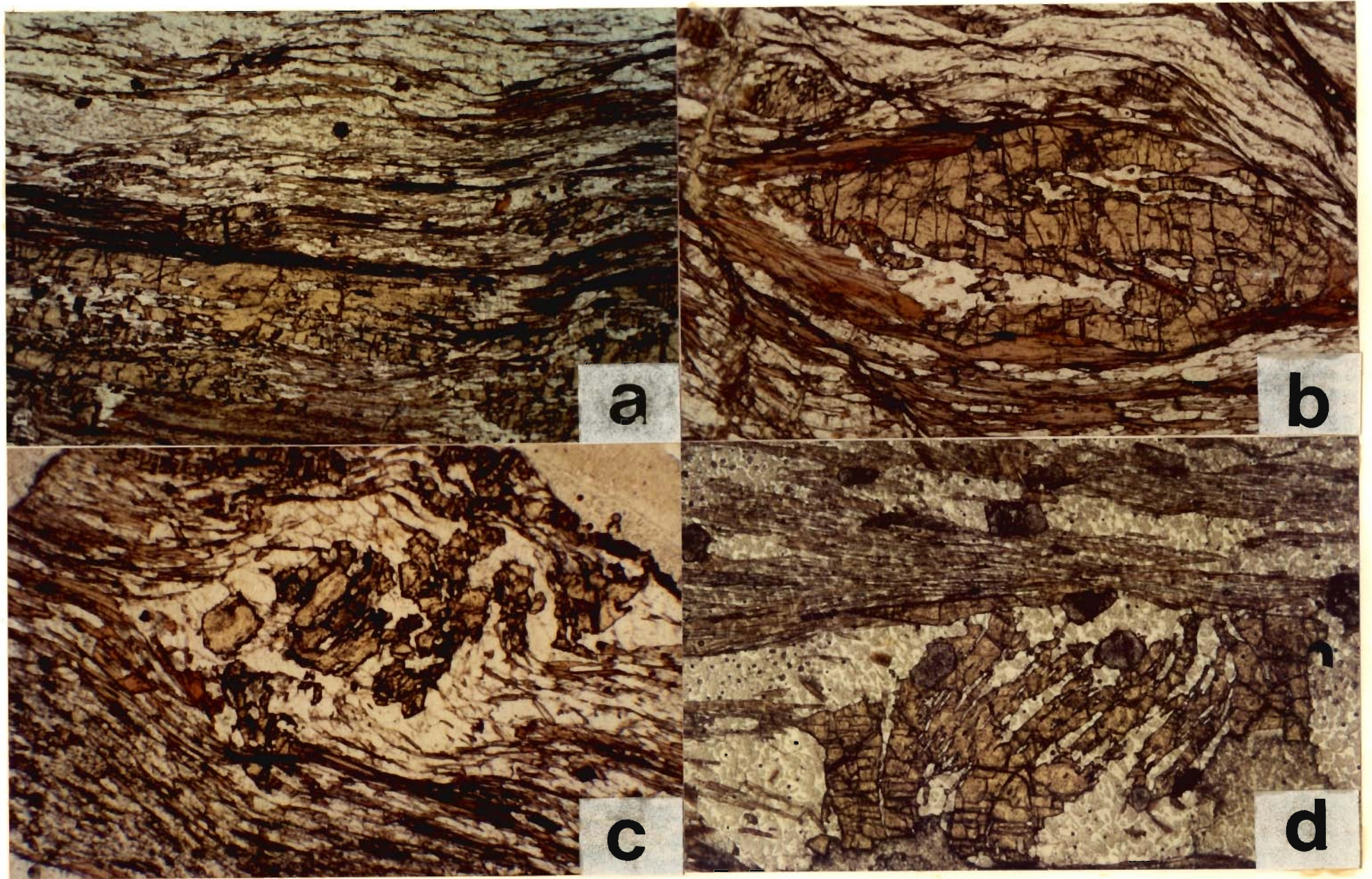


FIGURE 3.6

varieties. Skeletal garnet grows without any effect on the S_2 foliation, while bowing-out of foliation in the matrix mark snowball garnet of second generation. Misch (1971) interpreted 'bowing-out' of foliation as unequivocal proof of mechanical displacement due to crystal growth (also, Harris, 1977). Nevertheless, other interpretations include (i) flattening of schist during or subsequent to growth of porphyroblast (Shelley, 1972), (ii) diffusion of material and reduction of volume immediately around the growth site (Shelley, 1972) and (iii) development of foliation during F_2 followed by post-tectonic growth of porphyroblast.

3.7.2-b Staurolite: Large and faintly pleochroic staurolite porphyroblasts are commonly sieved, where external S_2 fabric of quartz, mica and opaque continues undisturbed S_1 (Figs. 3.6a, b). However, these inclusions are occasionally arranged in a sigmoidal pattern indicating syntectonic rotation and growth during D_2 deformational phase (Figs. 3.6c, d). A few subidioblastic staurolite crystals are almost inclusion-free and fractured (Fig. 3.7a). The crystals are elongated across the S_2 foliation and a few grow over it. Therefore, staurolite crystallisation is essentially syn- to late-kinematic to the D_2 deformation.

3.7.2-c Kyanite: Kyanite blades are mostly aligned parallel to the S_2 foliation (Fig. 3.7b), but a few also show discordant relationships (Fig. 3.7c). Kyanite reveals $S_1 \parallel S_2$ relationship with ilmenite, biotite specks and quartz inclusions merging into

FIGURE 3.7 : Microphotographs of different porphyroblastic textures within HHC.

- a. Subidioblastic staurolite with a few fine inclusions of quartz and opaque inclined to S_2 foliation. Rock type: Staurolite-kyanite schist (15B1/71). Loc. Pensi La. PL, 13X
- b. Kyanite blades (dark blue) paralleling the S_2 foliation and showing prograde change to sillimanite over it. Rock type: Sillimanite-kyanite schist (14/103). Loc. Tangol. Crossed, 13X
- c. Growth of kyanite and staurolite porphyroblasts across the main S_2 foliation containing inclusions of quartz, biotite and opaques paralleling S_2 . Note the alteration of staurolite and kyanite to sericite along their margins. Rock type: Staurolite-kyanite schist (KC26/28). Loc. Mugalmaidan along Chhatru Nala. PL, 13X
- d. Kyanite blades along S_2 foliation are folded by F_{3B} fold. Post- F_{3B} muscovite growth acrosses S_2 foliation and hinge zone of F_{3B} fold. Note distinct time relations of later generation stumpy muscovite across kyanite-flaky muscovite along the S_2 foliation in centre of photo. Rock type: Staurolite-kyanite schist (U96/114B). Loc. Masu. Crossed, 56X

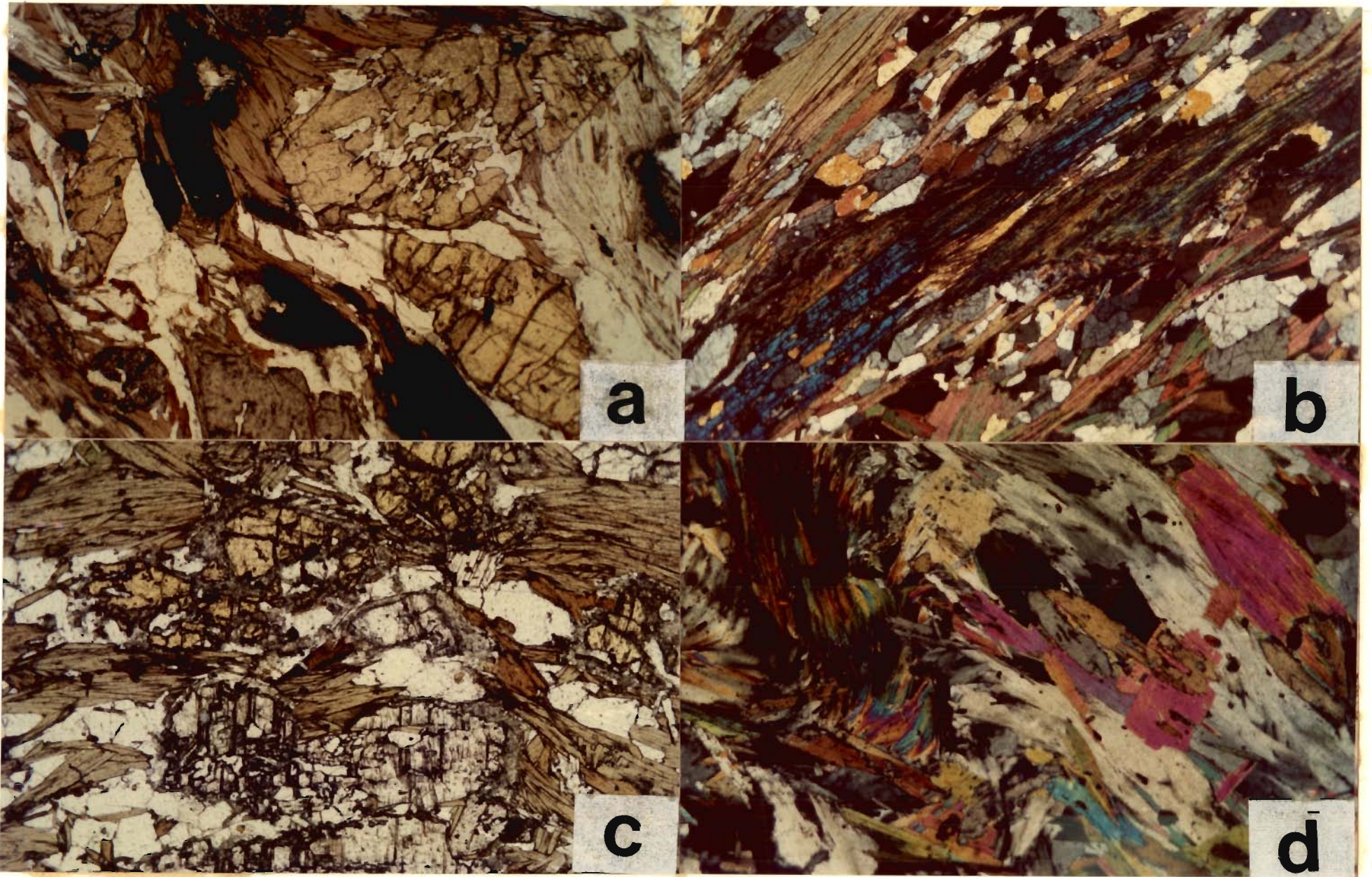


FIGURE 3.7

the S_2 foliation (Figs. 3.7c, d) indicating syntectonic growth with the D_2 deformation. Such blades are occasionally folded by D_3 deformation along with the external fabric (Fig. 3.7d). It appears that kyanite has grown simultaneously with the development of S_2 foliation and outlasted this fabric during late phase of D_2 deformation.

3.7.2-d Sillimanite: Sillimanite occurs mostly as elongate prisms (Fig. 3.8a) as well as in needles of fibrolite (Fig. 3.8b). Fibrolite occurs as epitaxial growth in biotite (Fig. 3.8a) and muscovite (Fig. 3.8c), breakdown product of garnet and polymorphic transformation of kyanite (Fig. 3.7b). In a few cases, truncation of the fibrolite by later biotite and folding of fibrolite by D_3 deformation are clearly observed (Fig. 3.8b). Elsewhere, intrafolial folds within sillimanite along the S_2 foliation and its crystallisation both along S and C composite planar fabric (Fig. 3.8a) reveal intense ductile deformation and shearing during the D_2 deformation. Therefore, fibrolite crystallisation is essentially late-kinematic to D_2 deformation, while sillimanite has grown synkinematically to this phase of deformation.

3.7.2-e Feldspar: Large porphyroblasts of K-feldspar-II, mainly microperthite patches, contain inclusions of quartz, sericite and, in places, subhedral plagioclase-I. Rarely the elongated kyanite crystals, which lie parallel to S_2 , are also found as inclusions within K-feldspar-II and plagioclase-II. It has been

FIGURE 3.8 : Characteristics of sillimanite/fibrolite within sillimanite gneiss of HHC.

- a. Growth of prismatic sillimanite along S-C fabric. Rock type: Sillimanite-K-feldspar gneiss (A65/78). Loc. Dangel. PL, 16X
- b. Fibrolite needles along S_2 foliation are isoclinally folded by F_{3a} fold. Note that biotite changing to fibrolite. Rock type: Sillimanite-muscovite gneiss (P54/191). Loc. Takkar. PL, 65X
- c. Growth of sillimanite needles over muscovite and replacing it. Note the association of garnet, biotite and sillimanite. Rock type: Sillimanite-muscovite gneiss (A53/62B). Loc. Chisoti. PL, 16X
- d. S-C relation in sillimanite-muscovite schist with sinistral sigmoid of S-surface becoming parallel to C-surface. Note that sillimanite replaces muscovite and biotite. Rock type: Sillimanite-muscovite gneiss. Loc. Near Bardan Gompa. Crossed, 13X

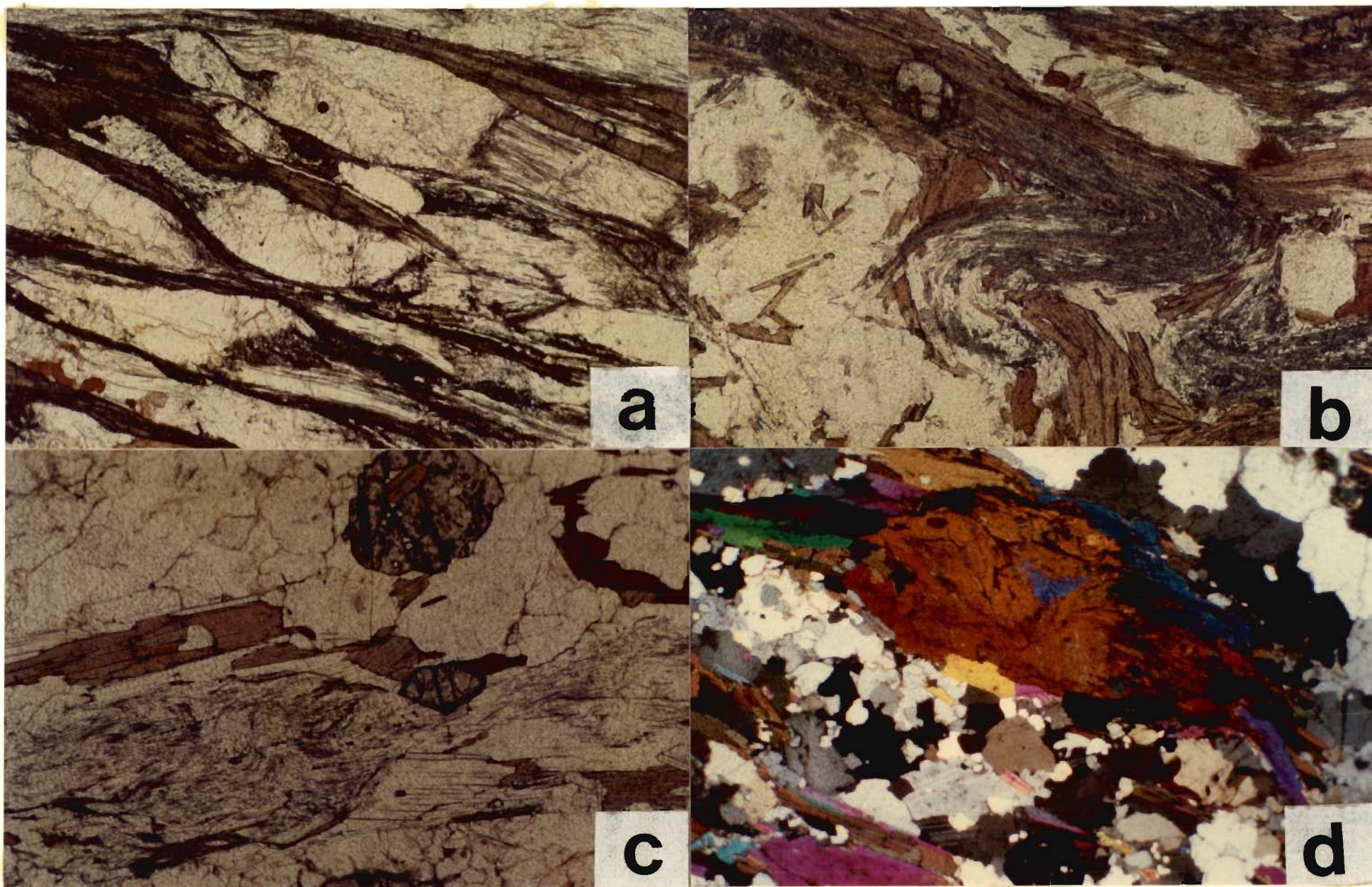


FIGURE 3.8

noticed that wherever myrmekitic intergrowth has taken place, feldspar is perthitic in character.

Formation of discontinuous rims of albite (sodic plagioclase-II) around K-feldspar-II in gneiss could be explained due to later phase of development of sodic plagioclase. Large porphyroblasts of plagioclase-II are mostly untwinned or faintly twinned, cloudy in appearance and sericitised. Both K-feldspar-II and plagioclase-II porphyroblasts developed syn-kinematically along the S_2 foliation and contain many mica and quartz inclusions with S_1 || S_2 relationship. However, in a few instances, inclusions are arranged in a sigmoid pattern suggesting simultaneous development of porphyroblasts and rotation during the D_2 deformation.

3.7.2-f Other rotational criteria: Besides rotational evidences in embryonic, sigmoidal and snowball garnet in the shear regime of the M_2 metamorphism, other useful features, observed both in the Lesser Himalayan Sedimentary rocks and the HHC, are given below.

(i) **S and C composite planar fabric:** In the XZ sections cut parallel to the lineation a composite planar fabric producing two foliation configuration marks the S_2 foliation in the schistose and gneissic rocks throughout the region irrespective to the location of the major tectonic boundaries (Fig. 3.8d). Berthe et al. (1979) studied the progressive development of two sets of planar anisotropies and described these as primary 'C' and 'S'



surfaces. 'C' surfaces refer to cisaillement shear and 'S' surfaces have been identified as schistosity (foliation).

In parts of the HHC marked by low shear train, C-surfaces are aligned parallel to main shear boundary and S-surfaces are oriented at about 40° - 50° . With increasing strain magnitude in the ductile shear zone, coinciding, at places, with the dislocation surfaces of the MCT and ZSZ, S-surfaces turn progressively into parallelism with C-surfaces in mylonitic and prograde metamorphic rocks. The sense of displacement is given by the general foliation trajectory pattern i.e., S-surfaces oblique to the C-surfaces curve into C-surfaces so that angular relationship between two surfaces define sense of shear. The movement along C-surfaces within gneisses is always compatible with general sense of shear zone. In all the gneissic rocks it is of overthrust type with top-to-SW sense of displacement.

Microstructural studies indicate that major shearing and rotational movements are associated with this phase of deformation particularly in the XZ sections. Texturally, sigmoidal mica and quartz-II produce lozen/almond-shaped domain from quartz-I having an angular relation of about 30° in the schistose quartzite. This mica and quartz-II contain evidences of shear (Eisbacher, 1970; Burg and Laurent, 1978) and clearly indicate overthrusting sense of movement. Identical features characterise the MCT zone in the Nepal Himalaya (Pecher, 1977; Bouchez and Pecher, 1981), the MCT zone in the Garhwal Himalaya (Anand, 1986) and in the Zaskar Shear Zone (Patel, 1991).

Berthe et al. (1979) envisaged exact parallelism between main foliation and local orientation XY plane of finite strain ellipsoid and suggested that both C- and S-surfaces are synchronous due to same mineral assemblages on these planes. During D_2 deformational phase, minerals like garnet, staurolite, kyanite and sillimanite (Figs. 3.8a, 3.9a) are grown synkinematically along S-C composite planar fabric defining the S_2 foliation.

(ii) **Asymmetric pressure shadows:** Asymmetric pressure shadows are frequently observed in the XZ sections of rocks from the HHC. The feldspar porphyroblasts with asymmetric pressure shadow wings indicate top-to-Sw overthrust sense of movement. The same feldspar megacrysts in these gneissic rocks are broken and displaced antithetically into fragmental trails, which are later filled in with recrystallised quartz. This can be explained by development of the ductile shear indicated by asymmetric shadow with slip taken place along initial cracks in the opposite sense like stacks of cards (Etchecopar, 1974).

3.7.3 M_3 METAMORPHIC EPISODE: Metamorphic minerals of the M_2 metamorphic episode are later affected by the D_3 deformation. M_3 metamorphism is manifested in these rocks as post-kinematic crystallisation of quartz, muscovite and greenish biotite along the S_{3a} foliations in the hinge zones of F_{3a} folds (Fig. 3.9b). It is noteworthy that quartz-II grains, though attained their grain boundaries orientation and incorporated numerous helicitic tiny mica flakes during late D_2 deformational phase, probably

FIGURE 3.9 : Photomicrograph showing different textures within HHC and Lesser Himalayan Proterozoic Foreland.

- a. Growth of kyanite, garnet and mica along S-C composite planar fabric having top-to-right sense of rotation. Rock type: Stauroilite-kyanite schist (T10/17B). Loc. Near Thatri. Crossed, 20X
- b. Growth of biotite and quartz along sub-horizontal S_{3a} foliation in hinge zone of F_{3a} fold. Note sillimanite-biotite-rich S_2 foliation wrapping the F_{3a} fold hinge. Rock type: Sillimanite-garnet gneiss (P11/57). Loc. Mulung Tokpo. PL, 13X
- c. Differentiated crenulation foliation S_{3b} with sharp planar discontinuities and sigmoidal bending of mica of S_2 foliation in Lesser Himalayan Proterozoic Foreland. Rock type: Chlorite-sericite-quartz schist (A4/2). Loc. Near Dul. PL, 65X
- d. Coarse mica flakes and garnet along S_2 foliations are kinked and affected by F_{3b} folds with overlapped mica flakes in hinge zone. Rock type: Stauroilite-kyanite schist (A49/59). Loc. Masu. Crossed, 16X

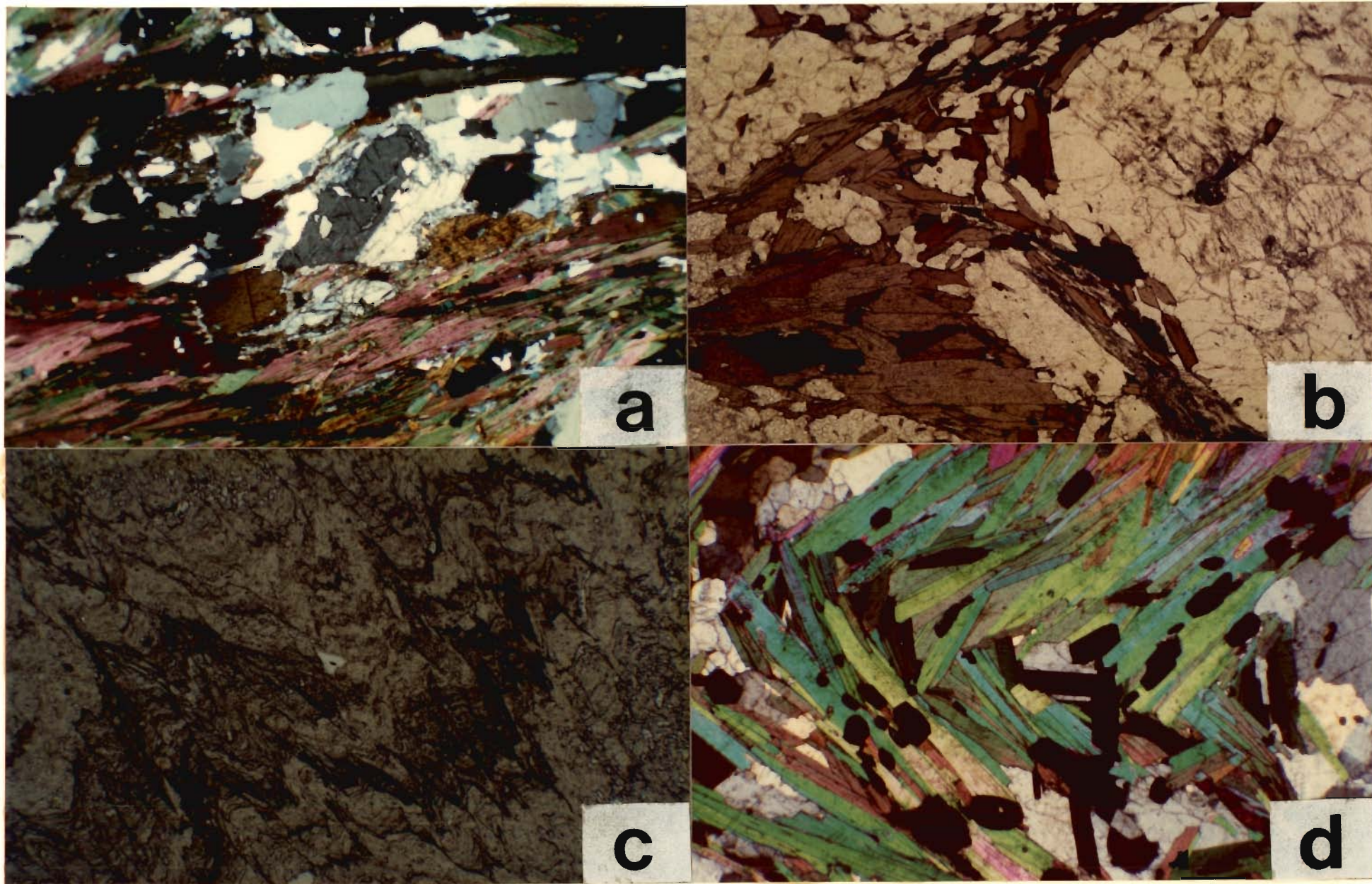


FIGURE 3.9

attained their strain-free straight extinction sometime after prior to the D_{3B} deformational phase, which produced the F_{3B} crenulation folds.

Along the S_{3B} foliation, preferably oriented newly crystallised mica flakes are parallel to the axial traces of F_{3B} folds and at high angle with earlier muscovite-I and biotite-I in the pelitic schist (Fig. 3.9c). In more advanced development, discrete crenulation foliation planes S_{3B} are characterised by sigmoidally folded muscovite-I and biotite-I with sharp planar discontinuities changing into gradational boundaries (Fig. 3.9c). In higher grade rocks, F_{3B} folds kink coarse mica flakes and produce overlapped crystallised mica flakes as well as affect garnet-rich S_{3A} foliation (Fig. 3.9d).

Extensive retrograde metamorphism probably has taken place during the later part of the D_{3B} deformational phase (Figs. 3.10a, b). As a result, chlorite either interleaves with biotite-I along the foliation or pseudomorphs both after biotite and garnet (Fig. 3.10a). Close association of iron ores in chlorite flakes indicate that chlorite is developed due to retrogression of biotite. Later bending and crenulation of chlorite and biotite along with folded opaque inclusions clearly indicate its post- D_2 development unrelated to the transposition of earlier foliation in the whole area.

Different stages in the progressive degeneration of garnet have also been observed. In the first stage, garnet of different

FIGURE 3.10 :

- a. Chloritised biotite and porphyroblastic garnet along S-C composite planar fabrics in immediate vicinity of the MCT. Partial chlorite pseudomorph after garnet on left hand seen. Rock type: Garnet-biotite schist of the HHC (T3/5). Loc. Kishtwar. PL, 13X
- b. Chloritised garnet-I (G-I): syntectonic snowball straight chlorite and biotite rich boundary on extreme right indicate growth of post-tectonic garnet-II. Note completely chloritised outer margin of garnet-I containing numerous quartz inclusions. Rock type: Garnet-biotite schist of the HHC. Loc. E of Parkachik. PL, 13X
- c. Growth of post-S_{3B} stumpy randomly oriented helicitic biotite containing numerous opaque inclusions upon S_{3B} crenulations. Rock type: Mica schist (KC18/18). Loc. SE of Chhatru along Chhatru Nala. PL. 56X
- d. Growth of post-D_{3B} biotite superimposed on S_{3B} foliation in hinge zone of a F_{3B} fold without any deflection of S_{3A} foliation. Rock type: Sillimanite-K-feldspar gneiss (A57/68). Loc. Machel. PL. 13X

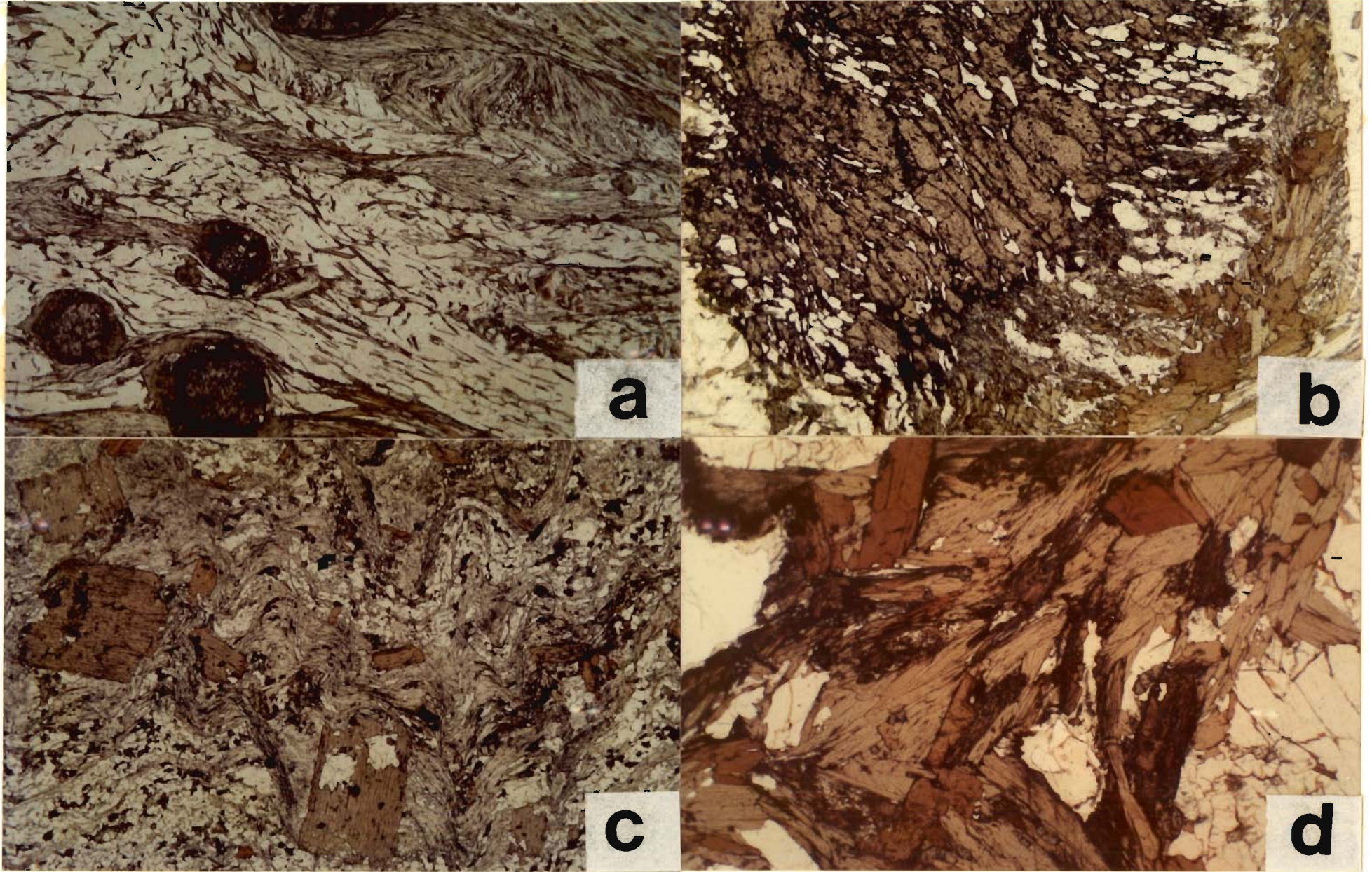


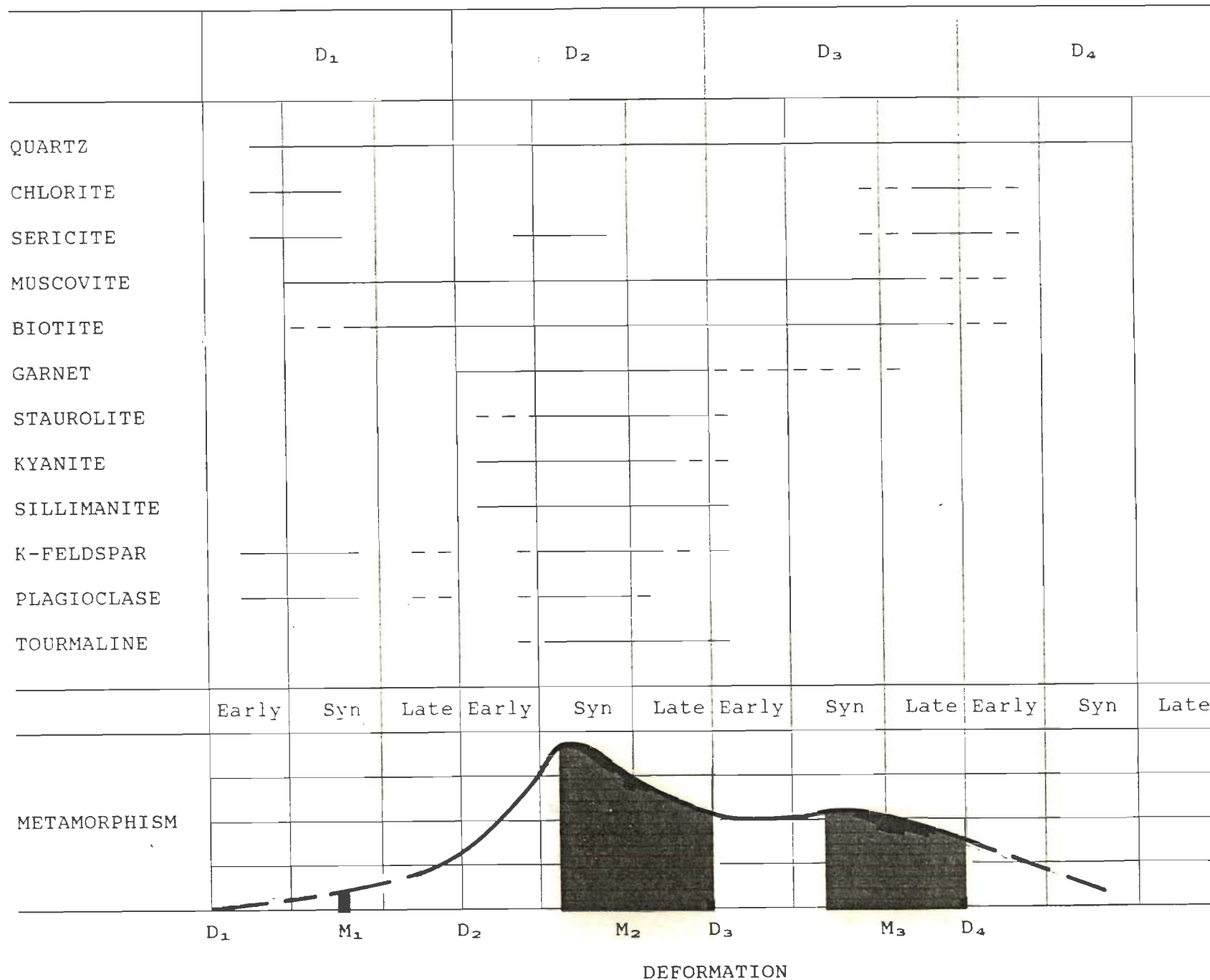
FIGURE 3 .10

generations loses its outlines and chlorite is formed around them (Fig. 3.10b). Chlorite develops along fractures and during the final stages, relicts of garnet are left in an aggregate of chlorite, biotite and opaque near the vicinity of the thrust zone (Fig. 3.10a). Sericitisation of kyanite and staurolite has taken place during this retrogression (Fig. 3.7c).

3.7.4 POST-M₃ METAMORPHISM: A weak prograde metamorphism during D₄ deformational phase is intimately associated with the growth of stumpy muscovite and biotite porphyroblasts (Figs. 3.10c, d). Stumpy biotite is greenish brown in contrast to yellowish brown biotite of earlier events and, at places, is superimposed on F_{3B} hinge without any post-crystalline rotation (Fig. 3.10d). These contain numerous helicitic opaque inclusions even of kyanite (Fig. 3.7d) in muscovite and chloritised biotite (Fig. 3.10c). More commonly, biotite-II and muscovite-II are randomly oriented and superimposed upon the earlier composite S-C planar fabric.

Table 3.1 summarises the mineral paragenesis mainly of the Higher Himalayan Crystallines in relation to the distinct phases of metamorphism and deformation.

TABLE 3.1 RELATIONSHIP BETWEEN DEFORMATION AND METAMORPHISM FROM HIGHER HIMALAYAN CRYSTALLINE



DEFORMATION

CHAPTER - 4

METAMORPHISM AND MINERAL CHEMISTRY

4.1 REGIONAL METAMORPHISM

The Lesser and Higher Himalayan tectonic units of the study area have undergone a polyphase Barrovian-type metamorphism. In general, metamorphism in Lesser Himalayan Kishtwar Window mostly remains within greenschist facies condition, whereas metamorphism in HHC varies from upper greenschist to almandine-amphibolite facies condition (Wakhaloo and Dhar, 1971; Das, 1978, 1987; Honeggar et al., 1982; Thakur, 1980; Sandhu, 1985; Searle and Rex, 1989; Staubli, 1989). Most of the workers have derived the P-T condition of metamorphism based on a few samples from this region (Honeggar et al., 1982; Staubli, 1989). However, detail work on (i) mineral paragenesis to decipher the metamorphic reactions and to delineate the reaction isograds and ii) the change in chemistry of minerals with respect to change in P-T condition, are very limited. Detailed work has been done in this study for mineral paragenesis in conjunction with texture and chemistry of individual minerals from all the metamorphic grades to characterise the isograds and the variation in mineral chemistry. The metamorphic texture is described in Chapter-3 and the techniques of mineral analysis by EPMA is described in this chapter. For the sake of convenience, the area has been divided into two parts viz., i) Chenab-Bhot Nala section covering Chhatru-Thatri towards SW and Atholi-Bhujaz-Mulung Tokpo in the

NE of the Kishtwar Window and ii) the section extending from Sankoo-Ringdom-Pensila-Padam covering Suru and Doda Valleys for the metamorphic study.

4.2 METAMORPHISM

4.2.1 Chenab-Bhot Nala Section

The Lesser and Higher Himalayan units are separated by MCT. The Lesser Himalayan rocks occur mainly in Kishtwar Window. The Higher Himalayan rocks occur on both sides of the window extending on the southwestern side towards Chhatru and Thatri and on the northeastern side towards Umasila and upto Zanskar Shear Zone (Fig. 2.1). The window zone is made up of phyllite, mica schist and quartzite which are intruded by granite. The window zone rocks are metamorphosed from chlorite to garnet grade of greenschist facies. To the south of the Kishtwar Window along Chhatru and Thatri road sections in Kishtwar area, the grade of metamorphism reached upto staurolite - kyanite grade of amphibolite facies. At the northeastern margin of Kishtwar Window, the grade of metamorphism remain in staurolite-kyanite close to MCT, and increases towards the Zanskar region of Bhot Nala section. The peak metamorphism is attained towards the centre of Great Himalayan Range reaching upto sillimanite-K-feldspar grade condition. The peak condition is accompanied by extensive anatexis, migmatisation and formation of leucogranite. Further moving in the northeast, the metamorphism gradually reduces and reaches to staurolite - kyanite grade condition (Fig. 2.2).

4.2.2 Suru and Doda Valleys Section

Along the Suru Valley in the Zaskar region, the metamorphism is varying from lower greenschist to amphibolite facies condition. The biotite grade rocks occur in and around Sankoo and Ringdom and the sillimanite-muscovite grade rocks occur east of Parkachik (Honeggar et al., 1982; Thakur, 1980). In this zone, the rocks are migmatized to a greater extent and cut by numerous pegmatite veins. Approaching from Ringdom towards Pensila the metamorphism gradually increases and reaches upto staurolite-kyanite grade (Fig. 2.1).

In Doda Valley, the Higher Himalayan Crystalline rocks are exposed from Pensila to Padam and this marks the northeastern margin of the Crystalline belt. The HHC rocks are separated from Paleozoic Tethyan sedimentaries by Zaskar Shear Zone (Herren, 1987; Patel, 1991; Jain et al., 1992; Pognante et al., 1990). The grade of metamorphism mostly remain in staurolite-kyanite to sillimanite-K-feldspar grade condition of amphibolite facies (Fig. 2.1).

4.3 MINERAL ASSEMBLAGES

For the purpose of texture and petrographic work, about 400 thin sections of metamorphic rocks, covering the Chenab-Bhot Nala section and the Suru-Doda Valleys were prepared. All the thin sections were studied in detail for the mineral assemblages. The sample locations are given in (Fig. 4.1) and the data for selected rocks are presented in Tables 4.1 and 4.2. The detailed mineral assemblages and the possible reactions are described for

individual metamorphic grade in the forthcoming section.

4.3.1 Biotite grade

Biotite grade rocks occur only near Sankoo in the Suru Valley and consist mostly of phyllite and chlorite schist with little intercalations of greenschist and calcareous rocks. These rocks are fine grained and have well marked foliation defined by the orientation of chlorite, muscovite and actinolite. The mineral assemblages in pelitic and basic rocks are:

PELITIC : Biotite - Muscovite/Phengite - Chlorite - Quartz ±
Plagioclase (Ab) ± Opaque (Carbonaceous)

BASIC : Actinolite - Zoisite - Quartz ± Epidote ± Plagioclase
± Chlorite ± Biotite ± Opaque.

4.3.2 Garnet grade

Garnet grade rocks are found in Sankoo - Panikhar section of Suru Valley and also on the southwestern side of Kishtwar Window, just above the MCT, towards Thatri in the Chenab-Bhot Nala section. In both the areas, the rocks are mainly pelites and sometimes, quartzite and metabasics are associated as thin bands. However, the metabasic association is found only in Suru Valley. The assemblages found in different rock types include:

PELITIC : Biotite - Muscovite - Garnet - Plagioclase - Quartz -
K-feldspar ± Chlorite.

BASIC : Actinolite - Epidote/Zoisite - Albite - Quartz ±
Opaque ± Chlorite.

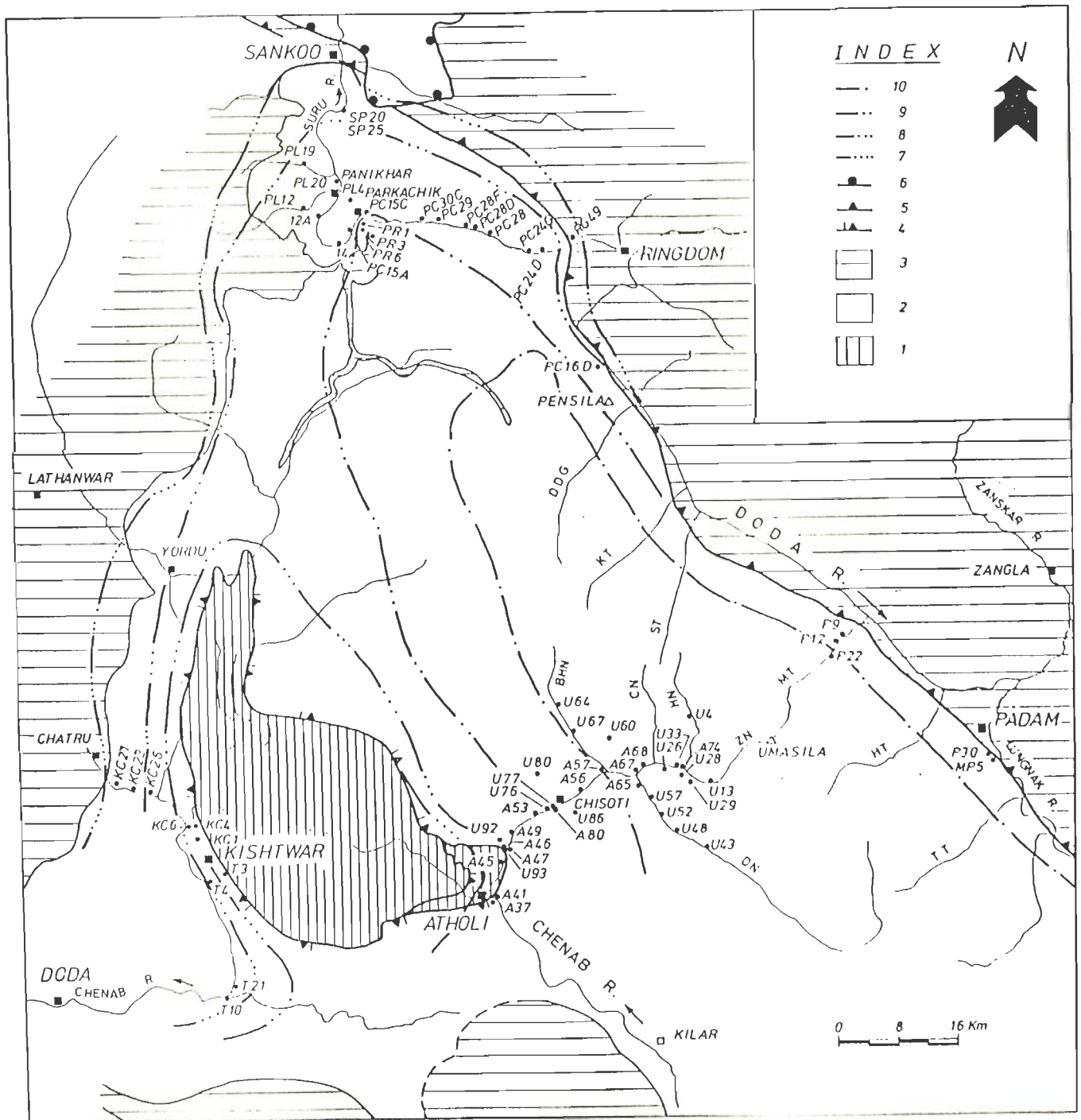


FIGURE 4.1 : Sample location map of the investigated area. (Probe analysed samples are only given). 1 - Lesser Himalayan Sediment. 2 - Higher Himalayan metamorphic (HHC). 3 - Tethyan Sedimentary Zone. 4 - Dras Volcanics. 5 - Main Central Thrust. 6 - Zaskar Shear Zone. 7 - Dras Thrust. Metamorphic isograd boundaries : 8 - Garnet, 9 - Kyanite-staurolite, 10 - Sillimanite-muscovite, 11 - Sillimanite-K-feldspar. BN - Bhot Nala, BHN - Bhazun Nala. CN - Chirang Nala, HN - Hangshu Nala, ZN - Zanskari Nala, DN - Dharlang Nala, TT - Temasa Tokpo, HT - Haptal Tokpo, MT - Mulung Tokpo, ST - Sumche Tokpo, KT - Kange Tokpo.

TABLE 4.1 MINERAL ASSEMBLAGE FOR BHOT NALA SAMPLES

S.NO.	SAMPLE NO.	CHLORITE	BIOTITE	MUSCOVITE	GARNET	STAUROLITE	KYANITE	SILLIMANITE	K-FELDSPAR	PLAGIOCLASE	QUARTZ
1	KC21/23	X	X	X	X				X	X	X
2	KC23/26	X	X	X	X				X	X	X
3	T3/5	X	X	X	X				X	X	X
4	KC26/28		X	X	X	X	X				X
5	T4/6		X	X	X	X					X
6	KC6/7		X	X	X				X	X	X
7	KC4/5		X	X	X					X	X
8	KC1/1		X	X	X					X	X
9	T21/28		X	X	X		X	X		X	X
10	T10/16		X	X	X		X			X	X
11	A45/50	X	X	X	X					X	X
12	A37/43		X	X	X				X	X	X
13	A41/48		X	X	X		X			X	X
14	A46/51		X	X	X					X	X
15	A47/54		X	X	X		X		X	X	X
16	A47/55		X	X	X				X	X	X
17	A47/56		X	X	X	X	X			X	X
18	U92/110		X	X	X					X	X
19	U93/111A		X	X	X					X	X
20	U93/111B		X	X	X					X	X

TABLE 4.1 - continued

S.NO.	SAMPLE NO.	CHLORITE	BIOTITE	MUSCOVITE	GARNET	STAUROLITE	KYANITE	SILLIMANITE	K-FELDSPAR	PLAGIOCLASE	QUARTZ
21	U93/111C		X	X	X					X	X
22	U93/112B		X		X					X	X
23	A49/59		X	X	X		X		X	X	X
24	A53/62B		X	X	X			X	X	X	X
25	U76/85		X	X	X			X		X	X
26	U77/90		X	X	X			X		X	X
27	U86/103		X	X	X			X		X	X
28	U80/95		X	X	X			X	X	X	X
29	U80/96		X	X	X			X	X	X	X
30	A56/66		X	X	X			X		X	X
31	A80/111		X	X	X				X	X	X
32	A57/68		X		X			X	X	X	X
33	U64/67		X	X	X			X	X	X	X
34	U67/70		X	X	X			X	X	X	X
35	U60/63		X		X			X	X	X	X
36	A65/78		X		X			X	X	X	X
37	A67/86		X		X			X	X	X	X
38	U57/60		X		X			X	X	X	X
39	U26/28		X		X			X	X	X	X
40	U33/35		X		X			X	X	X	X

TABLE 4.1 - continued

S.NO.	SAMPLE NO.	CHLORITE	BIOTITE	MUSCOVITE	GARNET	STAUROLITE	KYANITE	SILLIMANITE	K-FELDSPAR	PLAGIOCLASE	QUARTZ
41	U52/55		X		X			X	X	X	X
42	A74/97		X		X			X			X
43	U28/30		X		X			X	X	X	X
44	U29/31		X		X			X	X	X	X
45	U48/51		X		X			X	X	X	X
46	U13/13		X		X			X	X	X	X
47	U43/47		X		X			X	X	X	X
48	U4/4		X		X			X	X	X	X
49	P22/86		X		X			X	X	X	X
50	P12/20		X	X	X			X		X	X
51	P9/50		X	X	X				X	X	X
52	P9/46		X	X	X	X				X	X

TABLE 4.2 MINERAL ASSEMBLAGE FOR SURU - DODA VALLEYS SAMPLES

S.NO.	SAMPLE NO.	CHLORITE	BIOTITE	MUSCOVITE	GARNET	STAUROLITE	KYANITE	SILLIMANITE	K-FELDSPAR	PLAGIOCLASE	QUARTZ
1	SP20		X	X	X				X	X	X
2	SP25		X	X	X				X	X	X
3	PL19/123		X	X	X				X	X	X
4	PL20/125		X	X	X		X			X	X
5	PL12/113		X	X	X		X			X	X
6	12A/126		X	X	X					X	X
7	14/103		X	X	X		X	X		X	X
8	PC15A/1		X	X	X	X	X	X	X	X	X
9	PR3/76		X	X	X					X	X
10	PR6/81		X	X	X		X			X	X
11	PR1/73		X	X	X					X	X
12	PL4/93		X	X	X					X	X
13	PC15C/22		X	X	X					X	X
14	PC30C/5		X	X	X		X	X		X	X
15	PC29/24		X	X	X					X	X
16	PC28F/40		X	X	X					X	X
17	PC28D/30		X	X	X	X		X			X
18	PC28/42		X	X	X					X	X
19	PC24G/61		X	X	X					X	X
20	PC24D/66		X	X	X						X

TABLE 4.2 - continued

S.NO.	SAMPLE NO.	CHLORITE	BIOTITE	MUSCOVITE	GARNET	STAUROLITE	KYANITE	SILLIMANITE	K-FELDSPAR	PLAGIOCLASE	QUARTZ
21	RG49		X	X	X					X	X
22	PC16D/83		X	X	X	X				X	X
23	P30/120		X	X	X					X	X
24	MP5		X	X	X			X	X	X	X

In Bhot Nala samples, chlorite is found in association with muscovite and biotite. However, coexistence of chlorite and garnet is rarely found in these rocks. Near Sankoo the pelitic rocks show contact metamorphic effect close to Paleozoic granitic intrusion. Undeformed euhedral garnet and biotite, showing hornfelsic texture, are developed in pelites. In the associated metabasic rocks, rounded epidote clusters and radiating actinolite are observed.

4.3.3 Staurolite-kyanite grade

Medium grade rocks are found in both the sections and are medium to coarse grained. Pelitic rocks have the growth of porphyroblastic garnet, staurolite and kyanite. In Bhot Nala section above the MCT, kyanite is invariably present in substantial quantities, whereas staurolite is restricted in occurrence. Away from the MCT towards Chhatru and Thatri, both staurolite and kyanite occur substantially. In Suru Valley, staurolite is found in Panikhar-Parkachik region with very limited occurrence of kyanite. However, in Doda Valley both these minerals are common. Biotite and muscovite vary sympathetically. Plagioclase is also variable in amount, being more in some samples and negligible in few others. Chlorite is mostly of retrograde nature and found in Doda Valley and Bhot-Nala samples. The following mineral assemblages are found in pelitic rocks:

PELITIC : Biotite - Muscovite - Garnet - Kyanite - Quartz -
Plagioclase - K-feldspar ± Staurolite

4.3.4 Sillimanite-muscovite/sillimanite-K-feldspar grade

The high grade sillimanite-muscovite and sillimanite-K-feldspar pelites with calc-silicate rocks are found only along Bhot Nala section of the HHC. In the Suru-Doda Valleys, only sillimanite-muscovite grade rocks are observed. These rocks are mostly gneissose and medium to coarse grained. Calc-silicate rocks are more granular and coarse grained. The mineral assemblages for both the metamorphic grades include:

PELITIC : Garnet - Biotite - Muscovite - Sillimanite
± Plagioclase - K-feldspar - Quartz.

Garnet - Biotite - Sillimanite - K-feldspar -
Plagioclase - Quartz ± Cordierite.

Epitaxial growth of sillimanite in biotite and muscovite are observed in many samples. In sillimanite-K-feldspar grade second generation muscovite is observed in few samples. Garnet show corroded margins in most of the samples. The presence of cordierite is observed in few samples.

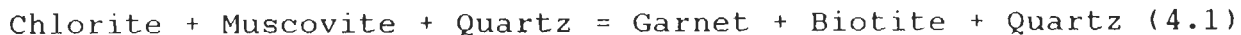
4.4 METAMORPHIC REACTIONS AND ISOGRADS

Metamorphic reactions and delineation of metamorphic isograds have been done based on texture, modal variation, mineral paragenesis, discontinuity in AFM topology and also from changes observed in mineral composition (Thompson, 1976, 1982; Winkler, 1979; Turner, 1981; Yardley, 1989). As there is not much variation in the mineralogical assemblage, from both the sections of the study area and in individual metamorphic grades, the

metamorphic reactions and delineation of isograds are considered together.

4.4.1 Garnet Zone:

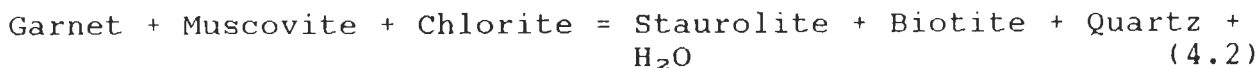
In this zone, the mineral assemblage includes garnet, biotite, chlorite, muscovite, albite and quartz (section 4.3.2). The texture, mineral assemblage and the modal variation suggest the following reaction for the formation of garnet:



This is a continuous reaction and the product and reactant minerals can occur over a temperature range. In the three phase association chlorite-biotite-garnet, chlorite is relatively Fe-rich in the initial stages. As the reaction proceeds with increase in temperature, the garnet-biotite phases are relatively enriched in Fe/Fe+Mg than chlorite (Thompson, 1976). This is consistent with the chemical data on garnet and biotite which indicate an enrichment of Fe in garnet rim and in biotite.

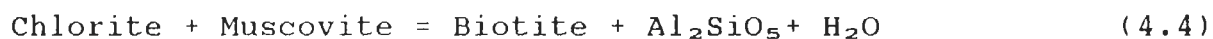
4.4.2 Staurolite-kyanite Zone:

In this zone, besides other common minerals, staurolite and kyanite are present. However, as mentioned earlier, staurolite is of limited occurrence than kyanite (section 4.3.3). Although staurolite can be produced by number of reactions (Winkler, 1979), the possible reactions for the formation of staurolite seem to be:

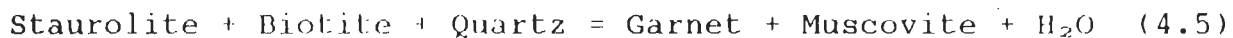




Reaction (4.2) takes place at a fixed temperature for any given pressure, as it is a discontinuous reaction and proceeds until garnet is consumed. The texture does not indicate any evidence of garnet consumption in the assemblage and, therefore, this reaction may not explain the formation of staurolite. However, texture and modal increase in biotite and staurolite suggest that appearance of staurolite and biotite is likely to be in Fe-rich rocks through continuous reaction (4.3) (Thompson, 1976; Yardley, 1989). The formation of kyanite in the assemblage could be due to continuous reaction:

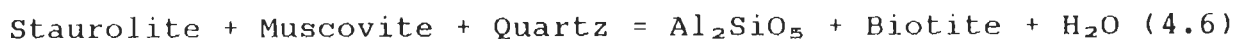


The disappearance of staurolite at increasing temperature condition may be by continuous reaction:



This reaction results in the growth of garnet due to progressive shifting of three phase field of staurolite-biotite-garnet towards higher X_{Mg} side in the AFM projection (Thompson, 1976). It thus explains the crystallisation of garnet and biotite commonly observed in the pelitic schists of the staurolite - kyanite zone. The staurolite inclusions in the peripheral region of garnet observed in a few thin sections (e.g. PC15A/1) presumably have formed due this reaction. Increase in kyanite and decrease in staurolite and muscovite in the

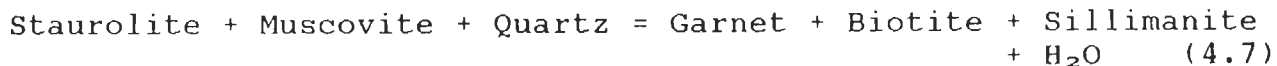
assemblage may be explained by continuous reaction at increased temperature condition (Thompson, 1976; Yardley, 1989):



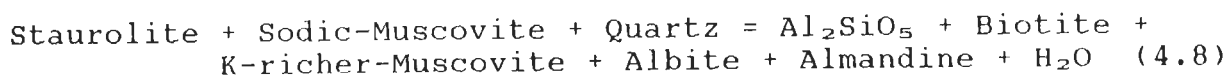
Due to this reaction, three phase field of staurolite - biotite - kyanite shifts to lower X_{Mg} side of the AFM projection. As the reaction progresses, biotite - kyanite field is enlarged in the AFM diagram (Thompson, 1976). The shift in three phase field is explained by compositional change in staurolite with higher X_{Fe} in the rim compared to the core and the enrichment of X_{Fe} in biotite.

4.4.3 Sillimanite-muscovite Zone:

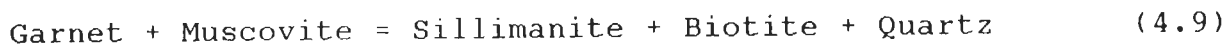
In this zone, kyanite decreases substantially in modal percentage with the development of sillimanite. Some garnet porphyroblasts show resorption and replacement of fibrolite. Epitaxial growth of sillimanite in muscovite is common in these samples. Staurolite is totally lacking in this zone. The formation of sillimanite could be due polymorphic transformation of kyanite either in reduced pressure and increasing temperature or at constant pressure and increasing temperature conditions (Holdaway, 1971). However, formation of sillimanite, biotite and garnet can possibly be explained by discontinuous reaction:



This causes staurolite to disappear from the AFM diagram at higher temperature and may reduce the modal muscovite from the assemblage. It is not common to find that muscovite is modally reduced at this grade. However, a more complex and realistic reaction for garnet and sillimanite formation has been inferred from petrographic studies by Guidotti (1970):



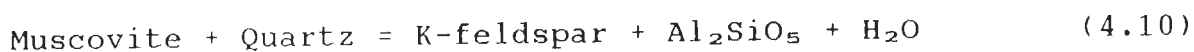
Garnet resorption and fibrolite replacement in the assemblage may be due to the reaction (Thompson, 1976):



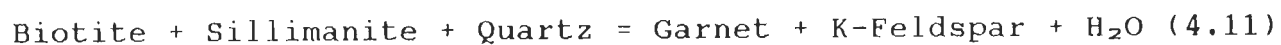
Reverse growth zoning in garnet is explained by this reaction with higher X_{Fe} in garnet rim (section 4.7) and corresponding higher X_{Mg} of the product phases. The resorption of garnet may be due to the shift in two phase field towards lower X_{Mg} side of the AFM projection.

4.4.4 Sillimanite-K-feldspar Zone:

In this grade, sillimanite has developed at the expense of biotite and, sometimes, in plagioclase as epitaxial growth. Muscovite is totally lacking in this zone. Garnet often shows corroded margins indicating resorption. The disappearance of muscovite and appearance of K-feldspar and sillimanite in this grade suggest the reaction:



This reaction may be in addition to the reaction (4.8) mentioned earlier in sillimanite-muscovite grade condition. The formation of garnet in the assemblage may be due to the reaction:



4.5 MINERAL CHEMISTRY

4.5.1 PROBE ANALYSIS

Analytical Procedure

Analyses were performed using an automated JEOL JXA-8600M Electron Probe X-Ray Microanalyser, operated at an accelerating voltage of 15 kV and a sample current of 2×10^{-8} ampere, having beam size between 1 μm (for garnet, staurolite, ilmenite and rutile) and 10 μm (for biotite, muscovite, chlorite, K-feldspar and plagioclase). For quantitative and qualitative analyses, three channel Wavelength Dispersive Spectrometers (WDS) were used. The samples were well polished and then coated with carbon to a thickness of about 100 Å. Natural mineral standards (SPI Standard, Canada) such as almandine and pyrope garnets, biotite, chlorite, plagioclase, sanidine, hematite and rutile and wherever necessary, multi-mineral standards were used in the analysis. ZAF correction for X-ray absorption, X-ray fluorescence, atomic number effect, back scatter and ionization-penetration losses was applied to the data, using the software programme supplied by JEOL through DEC LSI-11/23 and 11/73 computers.

Total of 2616 points in 980 grains, which include 161 garnet, 307 biotite, 165 muscovite, 2 chlorite, 199 plagioclase,

28 K-feldspar, 7 staurolite, 104 ilmenite and 7 rutile grains, were analysed in 80 samples, to evaluate the P-T condition and chemical variation in different metamorphic grades of the study area. The details of EPMA analysis is given in Fig. 4.2. Except for the zoned minerals, composition close to the rim of the coexisting minerals have been analysed and used in the calculation. For garnets, rim and core compositions and in some cases, intermediate points also have been analysed to calculate the P-T condition of metamorphism. Analyses have also been carried out along two lines in different directions at regular intervals to infer the compositional zoning. The rim, intermediate and core analyses were grouped and averaged on the basis of chemical similarity upto second decimal in the mole fraction. Plagioclase, K-feldspar, biotite and muscovite analyses were averaged out from 3 to 4 points in each grain. However, plagioclase analyses were carried out very close to the contact of garnet or muscovite to avoid the effect of zoning in plagioclase. Staurolite was analysed both at rim and core in each sample. Inclusions such as rutile, ilmenite, biotite, plagioclase etc. within garnet and other phases were also analysed, as and when these occur in the main phases. The microprobe analyses of garnet, chlorite, biotite, muscovite, plagioclase, K-feldspar, staurolite and ilmenite and rutile are tabulated in Appendices (I-IX). The mole fractions for garnet, biotite, muscovite and plagioclase are tabulated for the Bhot Nala and for Suru-Doda Valleys samples in Tables (4.3 - 4.4) and (4.5 - 4.6) respectively.

EPMA

DETAILS OF ANALYSIS

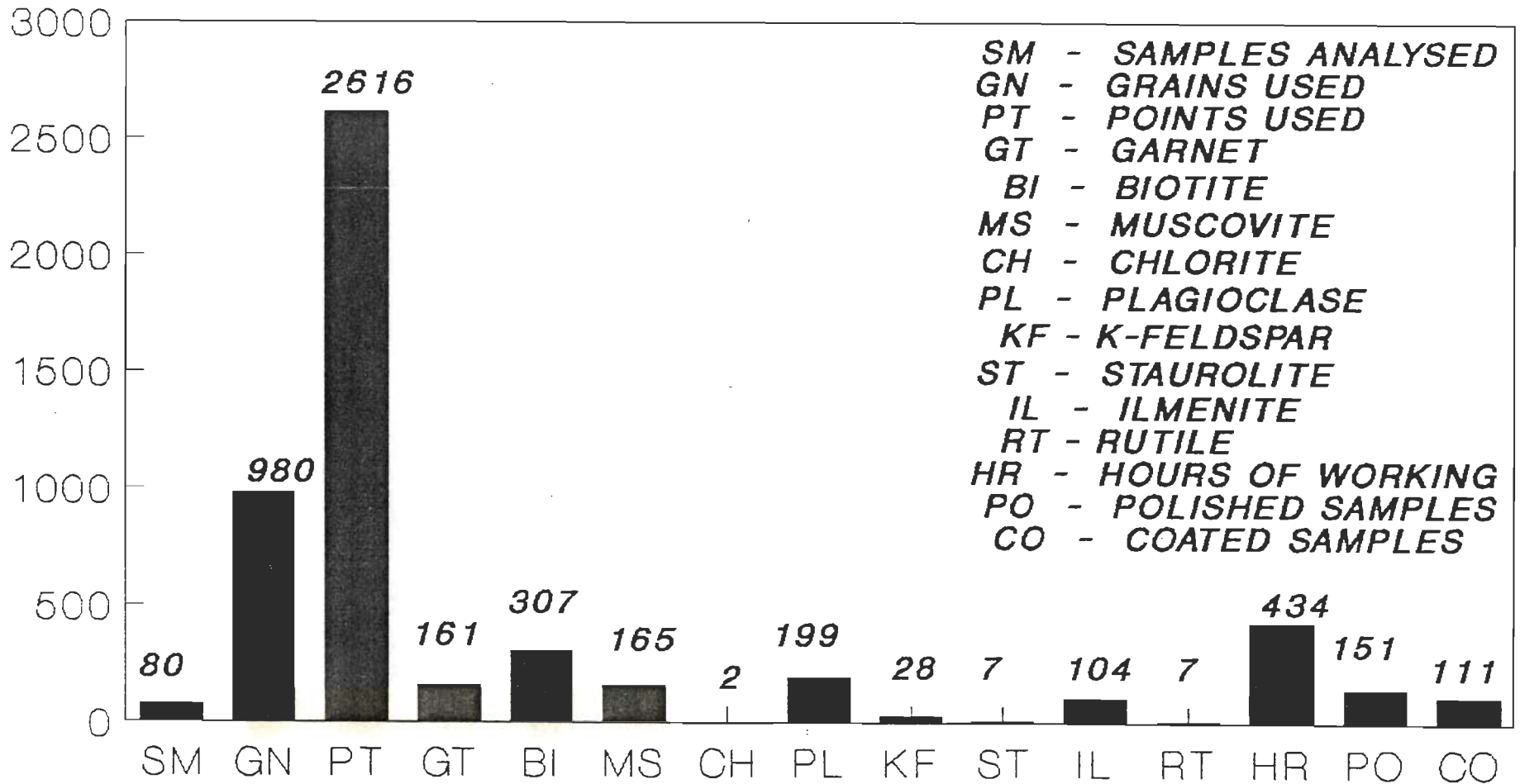


FIGURE 4.2 : Details of Electron Probe X-Ray Microanalyser (EPMA) analysis.

TABLE 4.3 MOLEFRACTION DATA OF GARNET FROM CHENAB VALLEY

S. Sample No. No.	GARNET-I					GARNET-II									
	CORE					RIM									
	X_{Fe}	X_{Mg}	X_{Mn}	X_{Ca}	$\frac{Fe}{Fe+Mg}$	X_{Fe}	X_{Mg}	X_{Mn}	X_{Ca}	$\frac{Fe}{Fe+Mg}$	X_{Fe}	X_{Mg}	X_{Mn}	X_{Ca}	$\frac{Fe}{Fe+Mg}$
1. KC21/23	.521	.025	.237	.222	.954	.849	.074	.022	.055	.920	-	-	-	-	-
2. KC23/26	.567	.031	.156	.246	.948	.690	.047	.081	.182	.936	-	-	-	-	-
3. T3/5	.743	.076	.125	.056	.907	.789	.100	.037	.074	.888	-	-	-	-	-
4. KC26/28	.664	.134	.098	.104	.832	.686	.143	.083	.088	.828	-	-	-	-	-
5. T4/6	.781	.158	.038	.023	.832	.779	.134	.035	.052	.853	.760	.166	.017	.057	.821
6. KC6/7	.662	.044	.237	.057	.938	.633	.033	.269	.064	.950	-	-	-	-	-
7. KC4/5	.773	.159	.024	.044	.829	.748	.146	.029	.077	.837	-	-	-	-	-
8. KC1/1	.697	.149	.035	.119	.824	.671	.139	.031	.160	.829	-	-	-	-	-
9. T21/28	.702	.118	.128	.060	.856	.702	.109	.131	.058	.865	-	-	-	-	-
10. T10/16	.740	.121	.089	.051	.859	.761	.126	.085	.029	.858	-	-	-	-	-
11. A45/50	.730	.063	.058	.150	.921	.823	.108	.016	.054	.884	-	-	-	-	-
12. A37/43	.644	.044	.074	.237	.936	.763	.073	.051	.114	.913	.757	.069	.073	.102	.916
13. A41/48	.677	.089	.056	.178	.884	.695	.150	.026	.129	.823	.658	.141	.028	.174	.824
14. A46/51	.719	.151	.048	.083	.826	.730	.128	.056	.085	.851	.728	.135	.051	.086	.844
15. A47/54	.584	.223	.029	.164	.724	.582	.202	.030	.187	.742	.593	.237	.033	.137	.714
16. A47/55	.721	.149	.040	.090	.829	.719	.157	.040	.085	.821	.704	.157	.038	.101	.818
17. A47/56	.731	.193	.018	.058	.791	.745	.171	.019	.065	.814	.744	.184	.019	.054	.802
18. U92/110	-	-	-	-	-	.656	.053	.098	.192	.925	-	-	-	-	-
19. U93/111A	.673	.111	.098	.110	.858	.628	.090	.157	.125	.874	-	-	-	-	-
20. U93/111B	.657	.101	.116	.126	.867	.617	.076	.174	.133	.891	-	-	-	-	-
21. U93/111c	-	-	-	-	-	.648	.102	.110	.140	.864	-	-	-	-	-
22. U93/112B	-	-	-	-	-	.558	.108	.065	.270	.838	-	-	-	-	-

TABLE 4.3 - continued

S. Sample No. No.	GARNET-I										GARNET-II				
	CORE					RIM					X _{Fe}	X _{Mg}	X _{Mn}	X _{Ca}	Fe
	X _{Fe}	X _{Mg}	X _{Mn}	X _{Ca}	Fe	X _{Fe}	X _{Mg}	X _{Mn}	X _{Ca}	Fe					
23. A49/59	-	-	-	-	-	-	-	-	-	-	.725	.148	.037	.091	.831
24. A53/62B	.795	.100	.078	.027	.888	.824	.087	.064	.025	.905	-	-	-	-	-
25. 076/85	-	-	-	-	-	-	-	-	-	-	.683	.126	.137	.053	.844
26. 077/90	-	-	-	-	-	-	-	-	-	-	.803	.094	.028	.075	.895
27. 086/103	.797	.086	.084	.032	.903	.796	.086	.089	.030	.902	.793	.086	.084	.032	.903
28. 080/95	-	-	-	-	-	-	-	-	-	-	.763	.070	.130	.038	.916
29. 080/96	.733	.072	.123	.073	.911	.754	.066	.128	.051	.920	-	-	-	-	-
30. A56/66	-	-	-	-	-	-	-	-	-	-	.858	.063	.050	.029	.932
31. A80/111	.758	.100	.019	.124	.883	.725	.143	.035	.097	.835	.697	.176	.028	.011	.798
32. A57/68	.783	.117	.062	.038	.870	.719	.078	.144	.058	.902	-	-	-	-	-
33. 064/67	-	-	-	-	-	.696	.113	.153	.037	.860	-	-	-	-	-
34. 067/70	-	-	-	-	-	-	-	-	-	-	.771	.067	.134	.027	.920
35. 060/63	.785	.129	.047	.039	.859	.753	.074	.136	.037	.9111	-	-	-	-	-
36. A65/78	.736	.133	.068	.063	.847	.725	.098	.121	.056	.881	-	-	-	-	-
37. A67/86	.702	.188	.025	.086	.789	.701	.117	.123	.059	.857	-	-	-	-	-
38. 057/60	-	-	-	-	-	-	-	-	-	-	.630	.145	.177	.048	.813
39. 026/28	-	-	-	-	-	-	-	-	-	-	.656	.157	.150	.037	.807
40. 033/35	.780	.114	.073	.034	.872	.765	.072	.122	.041	.914	-	-	-	-	-
41. 052/55	.766	.104	.095	.036		.714	.068	.178	.040	.913	-	-	-	-	-
42. A74/97	.787	.107	.080	.026	.880	-	-	-	-	-	.795	.111	.076	.019	.877
43. 028/30	.782	.115	.057	.046	.872	.775	.075	.113	.036	.912	-	-	-	-	-
44. 029/31	.778	.118	.070	.035	.868	.772	.081	.114	.033	.905	-	-	-	-	-

TABLE 4.3 - continued

S. Sample No. No.	GARNET-I					GARNET-II									
	CORE					RIM									
	X _{Fe}	X _{Mg}	X _{Mn}	X _{Ca}	Pe	X _{Fe}	X _{Mg}	X _{Mn}	X _{Ca}	Pe	X _{Fe}	X _{Mg}	X _{Mn}	X _{Ca}	Pe
Pe+Mg					Pe+Mg					Pe+Mg					
45. U48/51	.761	.124	.079	.036	.860	.722	.083	.169	.026	.897	-	-	-	-	-
46. U13/13	.797	.109	.069	.026	.880	.741	.058	.177	.024	.927	-	-	-	-	-
47. U43/47	.802	.073	.068	.056	.917	.811	.044	.110	.035	.949	-	-	-	-	-
48. U4/4	.774	.104	.085	.037	.882	.787	.099	.088	.026	.888	-	-	-	-	-
49. P22/86	.799	.098	.078	.026	.891	.755	.077	.139	.029	.907	.782	.081	.110	.086	.906
50. P12/20	.818	.101	.057	.024	.890	.756	.064	.156	.024	.922	-	-	-	-	-
51. P9/50	.720	.096	.096	.087	.882	.693	.089	.111	.107	.886	-	-	-	-	-
52. P9/46	-	-	-	-	-	-	-	-	-	-	.714	.096	.126	.063	.881

TABLE 4.4 - continued

S. Sample No. No.	BIOTITE					MUSCOVITE		PLAGIOCLASE						
	MATRIX			INCLUSION		X _{Mu}	X _{Pa}	X _{An}	X _{An}					
	X _{Fe}	X _{Mg}	X _{Ti}	X _{Al^{VI}}	Fe					Fe				
				Fe+Mg	Fe+Mg									
23. A49/59	.335	.458	.046	.161	.422	-	-	-	-	.306	-			
24. A53/62B	.535	.270	.052	.141	.665	-	-	-	-	.760	.078	.153	-	
25. U76/85	.412	.394	.050	.140	.511	-	-	-	-	.731	.155	.260	-	
26. U77/90	.493	.301	.056	.150	.621	-	-	-	-	.761	.120	.366	-	
27. U86/103	.540	.272	.076	.108	.665	.451	.338	.048	.162	.638	.731	.111	.200	-
28. U80/95	.519	.234	.090	.150	.689	-	-	-	-	-	-	.152	-	
29. U80/96	.564	.227	.020	.182	.713	-	-	-	-	-	.763	.054	.161	-
30. A56/66	.540	.251	.063	.145	.683	-	-	-	-	-	.745	.118	.176	-
31. A80/111	.398	.399	.038	.163	.499	-	-	-	-	-	.695	.086	.252	-
32. A57/68	.497	.279	.068	.150	.640	.503	.286	.017	.192	.640	.755	.068	.194	.206
33. U64/67	.440	.339	.076	.137	.565	-	-	-	-	-	.737	.051	.260	-
34. U67/70	.533	.243	.070	.151	.687	-	-	-	-	-	.800	.051	.192	-
35. U60/63	.525	.231	.080	.158	.694	-	-	-	-	-	.804	.057	.199	-
36. A65/78	.481	.294	.077	.145	.621	.466	.296	.062	.173	.612	.773	.056	.278	.285
37. A67/86	.427	.346	.045	.179	.552	.418	.353	.054	.173	.552	-	-	.239	.265
38. U57/60	.379	.407	.049	.157	.482	-	-	-	-	-	-	-	.335	-
39. U26/28	.351	.439	.030	.177	.444	-	-	-	-	-	.828	.037	.316	-
40. U33/35	.493	.266	.051	.187	.650	.486	.272	.022	.217	.641	.786	.065	.246	-
41. U52/55	.507	.257	.070	.157	.664	.494	.288	.039	.171	.632	.789	.069	.244	-
42. A74/97	.481	.295	.042	.180	.620	.454	.330	.043	.172	.579	-	-	.285	-
43. U28/30	.483	.304	.055	.155	.614	.514	.277	.073	.135	.650	-	-	-	-
44. U29/31	.504	.257	.080	.155	.662	.455	.314	.104	.127	.592	-	-	.191	-

TABLE 4.4 - continued

S. Sample No. No.	BIOTITE										MUSCOVITE	PLAGIOCLASE		
	MATRIX					INCLUSION						MAT.	INC.	
	X_{Fe}	X_{Mg}	X_{Ti}	X_{Al}^{VI}	Fe	X_{Fe}	X_{Mg}	X_{Ti}	X_{Al}^{VI}	Fe	X_{MUS}	X_{Pa}	X_{An}	X_{An}
					$\overline{Fe+Mg}$									
45. U48/51	.482	.288	.070	.154	.626	.461	.318	.073	.147	.542	.764	.079	.112	-
46. U13/13	.502	.268	.056	.169	.652	.492	.274	.051	.178	.642	.765	.090	.177	-
47. U43/47	.530	.220	.030	.216	.707	-	-	-	-	-	.777	.064	.155	-
48. U4/4	.498	.262	.087	.150	.655	-	-	-	-	-	-	-	.206	-
49. P22/86	.507	.242	.071	.173	.677	-	-	-	-	-	-	-	.177	-
50. P12/20	.571	.210	.048	.162	.731	-	-	-	-	-	.778	.057	.117	-
51. P9/50	.426	.372	.034	.163	.534	-	-	-	-	-	.735	.126	.245	-
52. P9/46	.434	.343	.045	.175	.559	.438	.353	.049	.157	.554	.721	.153	.252	-

TABLE 4.5 MOLEFRACTION DATA OF GARNET FROM SURU AND DODA VALLEYS

S. Sample No. No.	GARNET-I										GARNET-II				
	CORE					RIM									
	X_{Fe}	X_{Mg}	X_{Mn}	X_{Ca}	$\frac{Fe}{Fe+Mg}$	X_{Fe}	X_{Mg}	X_{Mn}	X_{Ca}	$\frac{Fe}{Fe+Mg}$	X_{Fe}	X_{Mg}	X_{Mn}	X_{Ca}	$\frac{Fe}{Fe+Mg}$
1. SP20	.669	.131	.051	.148	.836	.697	.116	.068	.119	.857	.743	.108	.020	.129	.873
2. SP25	-	-	-	-	-	-	-	-	-	-	.562	.044	.142	.252	.927
3. PL19/123	.685	.108	.064	.143	.846	.708	.145	.029	.117	.830	-	-	-	-	-
4. PL20/125	.720	.140	.063	.077	.837	.779	.137	.035	.049	.850	-	-	-	-	-
5. PL12/113	.728	.180	.048	.045	.802	.793	.155	.063	.043	.827	-	-	-	-	-
6. 12A/126	.734	.133	.035	.098	.847	.743	.140	.047	.070	.841	-	-	-	-	-
7. 14/103	.690	.153	.080	.077	.819	.695	.141	.092	.072	.831	-	-	-	-	-
8. PC15A/1	.742	.182	.033	.043	.803	.753	.138	.068	.042	.845	-	-	-	-	-
9. PR3/76	.755	.087	.083	.075	.897	.741	.071	.107	.081	.913	-	-	-	-	-
10. PR6/81	-	-	-	-	-	.735	.149	.066	.050	.831	-	-	-	-	-
11. PR1/73	.659	.086	.100	.155	.885	.697	.147	.085	.072	.826	-	-	-	-	-
12. PL4/93	.608	.124	.077	.191	.831						-	-	-	-	-
13. PC15C/22	.558	.079	.183	.180	.876						.632	.079	.103	.186	.889
14. PC30C/5	.639	.086	.116	.159	.882	.696	.154	.062	.089	.819	.673	.151	.117	.059	.817
15. PC29/24	.689	.075	.093	.144	.902						.714	.095	.034	.157	.883
16. PC28F/40	.781	.155	.028	.036	.834	.767	.131	.029	.072	.854	-	-	-	-	-
17. PC28D/30	.784	.176	.023	.016	.817	.758	.148	.027	.067	.837	-	-	-	-	-
18. P28/42	-	-	-	-	-	.810	.061	.024	.105	.930	-	-	-	-	-
19. PC24G/61	.689	.081	.133	.096	.895	.689	.073	.172	.066	.904	.701	.071	.149	.078	.908
20. PC24D/66	.743	.124	.060	.073	.857	.750	.110	.060	.080	.872	-	-	-	-	-
21. RG49	-	-	-	-	-	.653	.034	.027	.285	.951	-	-	-	-	-
22. PC16D/83	.760	.142	.047	.050	.843	.766	.127	.060	.046	.835	.762	.118	.082	.038	.866
23. P30/120	.713	.130	.109	.048	.846	.668	.099	.177	.055	.871	-	-	-	-	-
24. MP5	.723	.146	.109	.023	.832	.791	.119	.048	.042	.869	.779	.126	.046	.049	.858

TABLE 4.6 MOLEFRACTION DATA OF BIOTITE, MUSCOVITE AND PLAGIOCLASE FROM SURU AND DODA VALLEYS

S. Sample No. No.	BIOTITE										MUSCOVITE	PLAGIOCLASE		
	MATRIX					INCLUSION						MAT.	INC.	
	X_{Fe}	X_{Mg}	X_{Ti}	X_{Al}^{VI}	Fe	X_{Fe}	X_{Mg}	X_{Ti}	X_{Al}^{VI}	Fe	X_{MUS}	X_{Pa}	X_{An}	X_{An}
					Fe+Mg									
1. SP20	.444	.363	.064	.124	.550	-	-	-	-	-	.728	.073	.315	-
2. SP25	.416	.400	.041	.143	.510	-	-	-	-	-	.672	.051	.205	-
3. PL19/123	.438	.385	.038	.135	.532	-	-	-	-	-	.645	.165	.113	-
4. PL20/125	.397	.414	.038	.151	.490	-	-	-	-	-	.653	.203	.102	-
5. PL12/113	.392	.415	.041	.150	.486	-	-	-	-	-	.649	.214	.132	-
6. 12A/126	.388	.406	.040	.165	.489	-	-	-	-	-	.641	.228	.105	-
7. 14/103	.375	.430	.042	.150	.466	.370	.436	.033	.159	.459	.686	.143	.215	-
8. PC15A/1	.427	.379	.054	.139	.530	-	-	-	-	-	.680	.159	.140	-
9. PR3/76	.541	.260	.064	.133	.675	-	-	-	-	-	.769	.073	.203	-
10. PR6/81	.388	.402	.059	.148	.491	-	-	-	-	-	.695	.153	.111	-
11. PR1/73	.423	.389	.050	.131	.521	-	-	-	-	-	.577	.080	.186	-
12. PL4/93	.400	.407	.048	.142	.496	-	-	-	-	-	.746	.085	.349	-
13. PC15C/22	.428	.382	.052	.134	.528	-	-	-	-	-	.742	.081	.198	-
14. PC30C/5	.381	.409	.057	.151	.482	.370	.433	.039	.156	.461	.716	.134	.201	.265
15. PC29/24	.481	.310	.055	.149	.608	-	-	-	-	-	.751	.073	.201	-
16. PC28F/40	.437	.360	.058	.145	.548	-	-	-	-	-	-	-	-	-
17. PC28D/30	.415	.377	.038	.169	.524	-	-	-	-	-	.637	.215	.089	-
18. P28/42	.533	.215	.069	.159	.720	-	-	-	-	-	.712	.050	.105	-
19. PC24G/61	.516	.267	.067	.142	.659	.479	.267	.071	.176	.642	.717	.064	.114	-
20. PC24D/66	.457	.324	.045	.170	.585	-	-	-	-	-	.717	.067	.092	-
21. RG49	.514	.338	.056	.088	.603	-	-	-	-	-	-	-	.244	-
22. PC16D/83	.428	.372	.027	.171	.535	-	-	-	-	-	.620	.254	.088	-
23. P30/120	.454	.342	.029	.167	.570	.476	.333	.026	.159	.588	.707	.108	.167	-
24. MP5	.477	.320	.044	.157	.598	-	-	-	-	-	.675	.123	.143	-

Out of 400 thin sections studied, about 80 samples of pelites having equilibrium mineral assemblage were selected and analysed through microprobe. Samples were selected from all metamorphic grades ranging from greenschist to upper amphibolite facies, covering Kishtwar - Zaskar and Suru - Padam sections and also along the number of tributaries in these sections (Fig. 2.1).

The chemistry of individual minerals are analysed to characterise the compositional variation in all metamorphic grades. The minerals analysed include biotite, muscovite, staurolite, garnet, plagioclase, K-feldspar, rutile and ilmenite. Quantitative line analysis has been done only for garnet, as it shows invariably zoning. Though zoning of plagioclase and staurolite are reported in the literature (e.g., Tracy, 1982), only rim analyses were carried for these minerals, as the main emphasis was given on the P-T calculation. Likewise, rutile and ilmenite occur mostly as inclusions in garnet rather than in the matrix and only inclusions are analysed. The analyses are reported in Appendices (I-IX) and mole fraction of end member components for individual minerals, except for ilmenite and rutile, is given in Tables 4.3-4.6. Ilmenite and rutile analyses are not utilised for interpretation in this study.

4.5.2 Garnet:

Garnet from different metamorphic grades is characterised by almandine-rich composition with varying spessartine, pyrope and grossular contents (Tables 4.3 and 4.5). The core Fe/Fe+Mg ratio

ranges from 0.80 to 0.95 and 0.80 to 0.90 moles along Bhot Nala and Suru Valley respectively. However, Fe is enriched more than Mg in garnet grade in the Bhot Nala section than in higher grades (Fig. 4.3). In the Suru Valley, there is not much variation in the ratio with respect to metamorphic grade (Fig. 4.4). Core X_{Mn} , from both the sections, do not show much variation in regard to metamorphic grades (Figs. 4.5 and 4.6). It remains <0.1 moles in all the metamorphic grades, except for a few samples from garnet grade where it is >0.1 moles (Fig. 4.5). X_{Ca} is less than 0.05 moles in sillimanite-muscovite and sillimanite-K-feldspar grades than the other lower metamorphic grades and this is observed only along Bhot Nala (Fig. 4.7). However, X_{Ca} is <0.15 moles and shows a random distribution with respect to metamorphic grade in Suru Valley (Fig. 4.8).

In Bhot Nala and Suru - Doda Valleys, Fe/Fe+Mg of garnet rim ranges from 0.82 to 0.95 moles, from garnet to sillimanite-K-feldspar grade. Generally Fe is enriched in higher grades, except in garnet grade where it is relatively more than the staurolite-kyanite grade (Figs. 4.9 and 4.10). X_{Mg} show a clear reversal from lower grade to higher grade ranging from 0.17 to 0.03 moles, except in garnet grade, and this feature is observed in both the sections (Figs. 4.9 and 4.10). X_{Mn} is less than 0.1 moles in lower grades, whereas it is more than 0.1 moles in higher grades (Figs. 4.11 and 4.12). X_{Ca} does not show a clear distribution with grade, however it is observed that X_{Ca} is significantly less in higher grades than in the lower grade samples (Figs. 4.13 and 4.14).

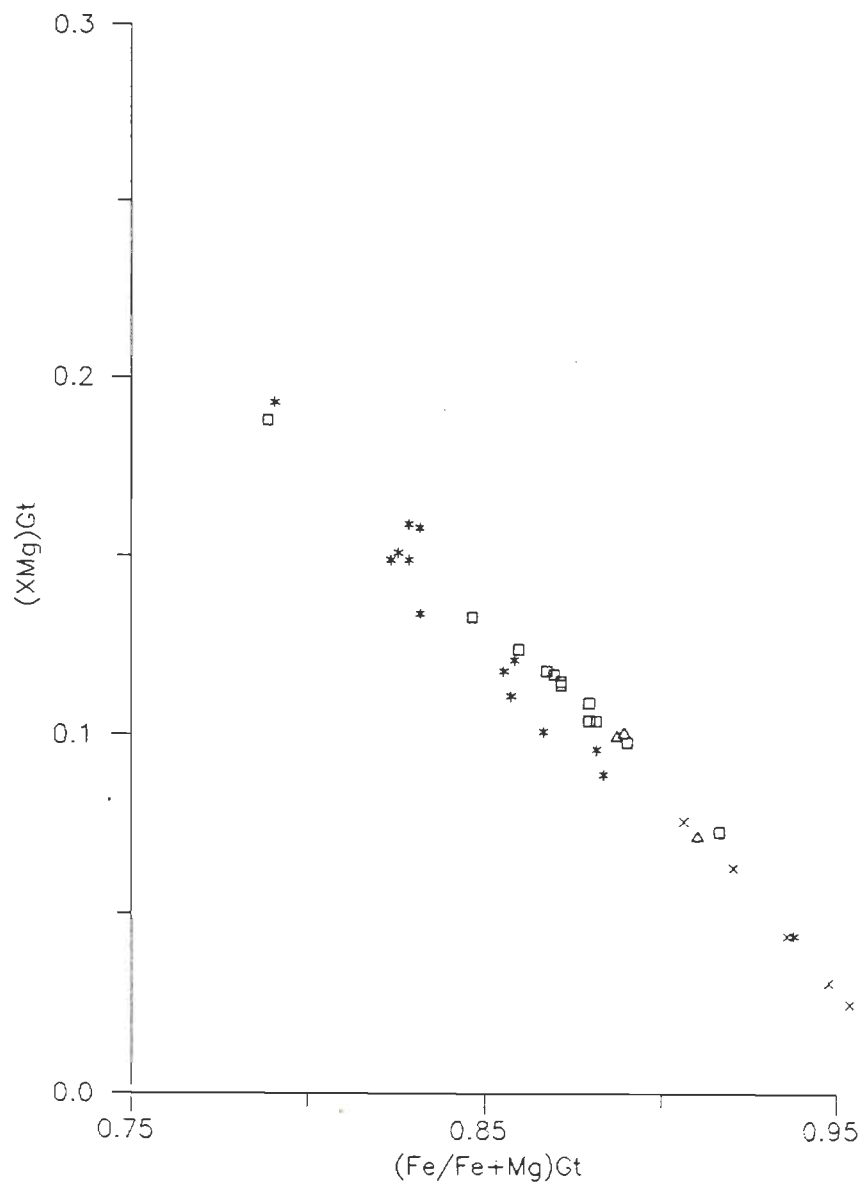


FIGURE 4.3: Plot showing XMg vs Fe/Fe+Mg for garnet core in different metamorphic grades of the HHC - Bhot Nala section. x - Garnet grade; * - Staurolite-kyanite grade; Δ - Sillimanite-muscovite grade; □ - Sillimanite-K-feldspar grade

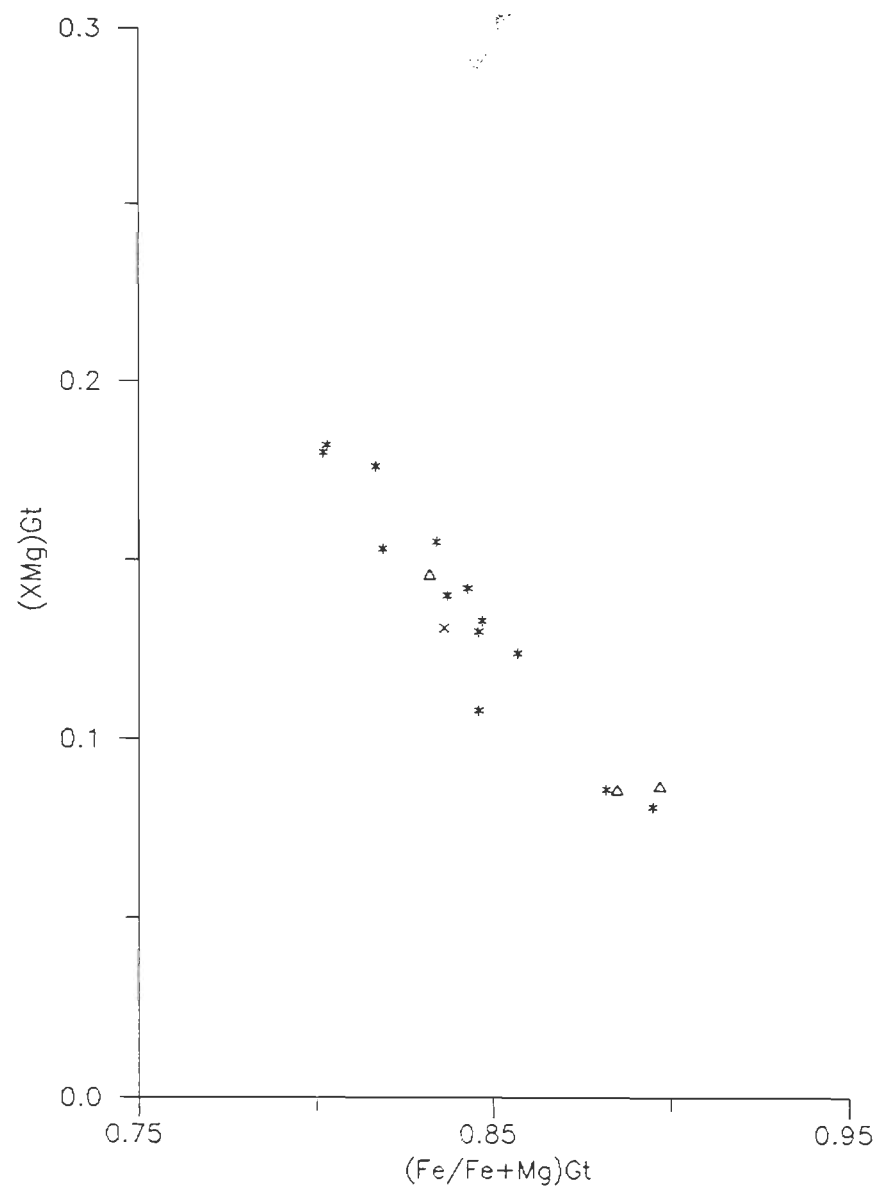


FIGURE 4.4: Plot showing XMg vs Fe/Fe+Mg for garnet core in different metamorphic grades of the HHC - Suru-Doda Valleys section. Symbols as in Fig. 4.3.

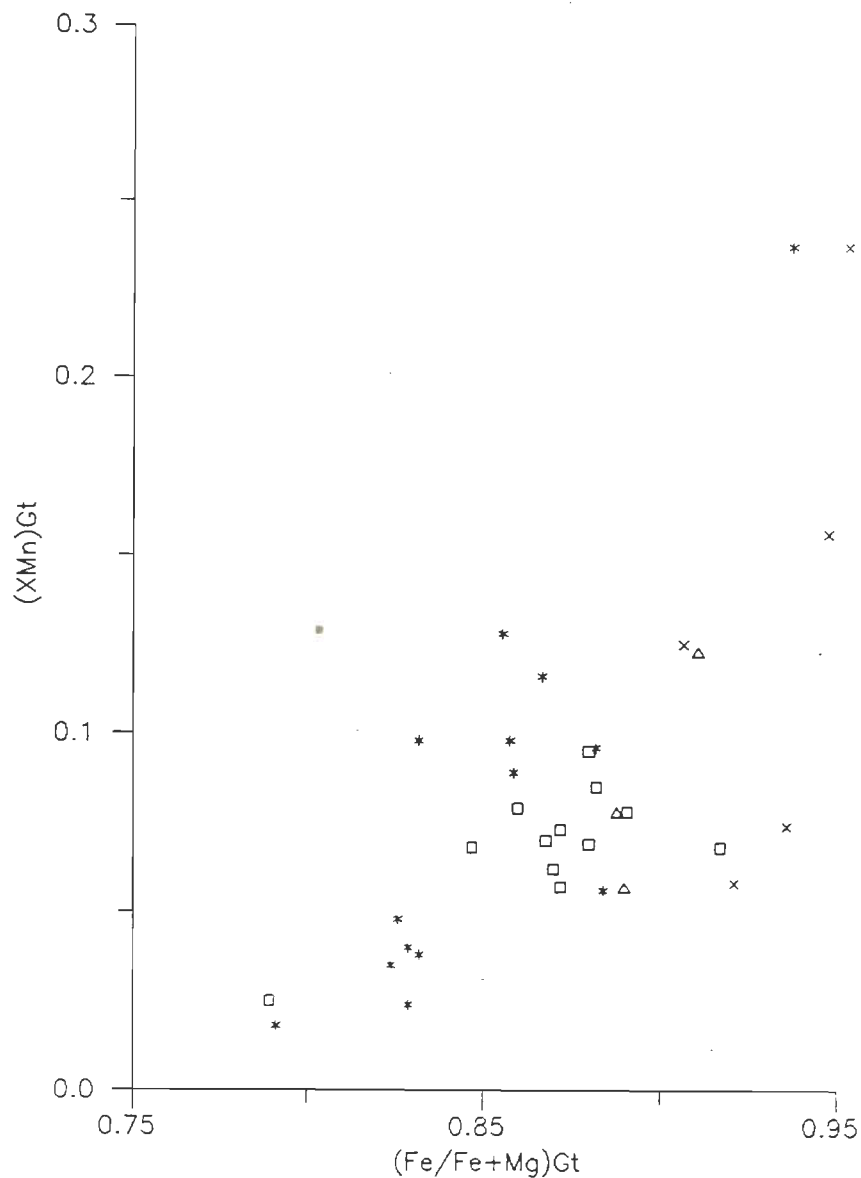


FIGURE 4.5: Plot showing XMn vs Fe/Fe+Mg for garnet core in different metamorphic grades of the HHC - Bhot Nala section. Symbols as in Fig. 4.3.

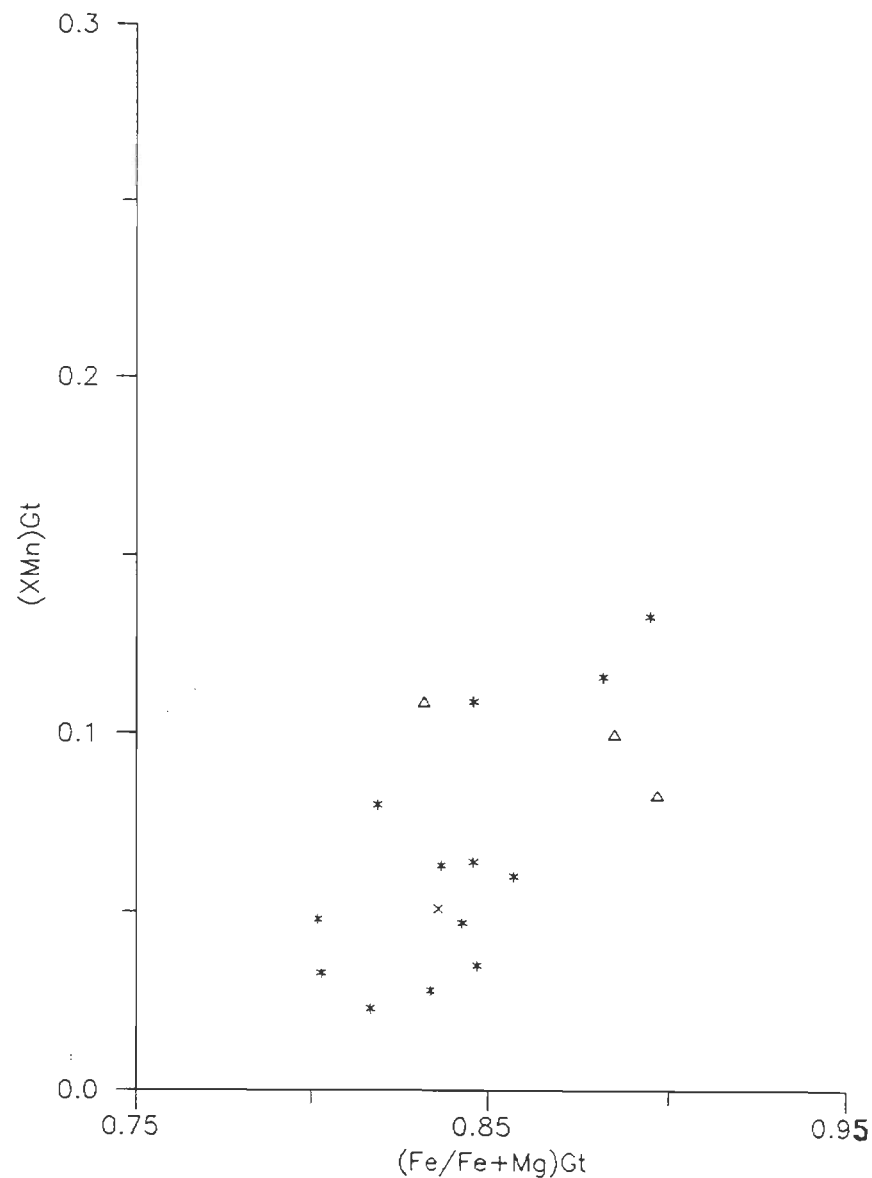


FIGURE 4.6: Plot showing XMn vs Fe/Fe+Mg for garnet core in different metamorphic grades of the HHC - Suru-Doda Valleys section. Symbols as in Fig. 4.3.

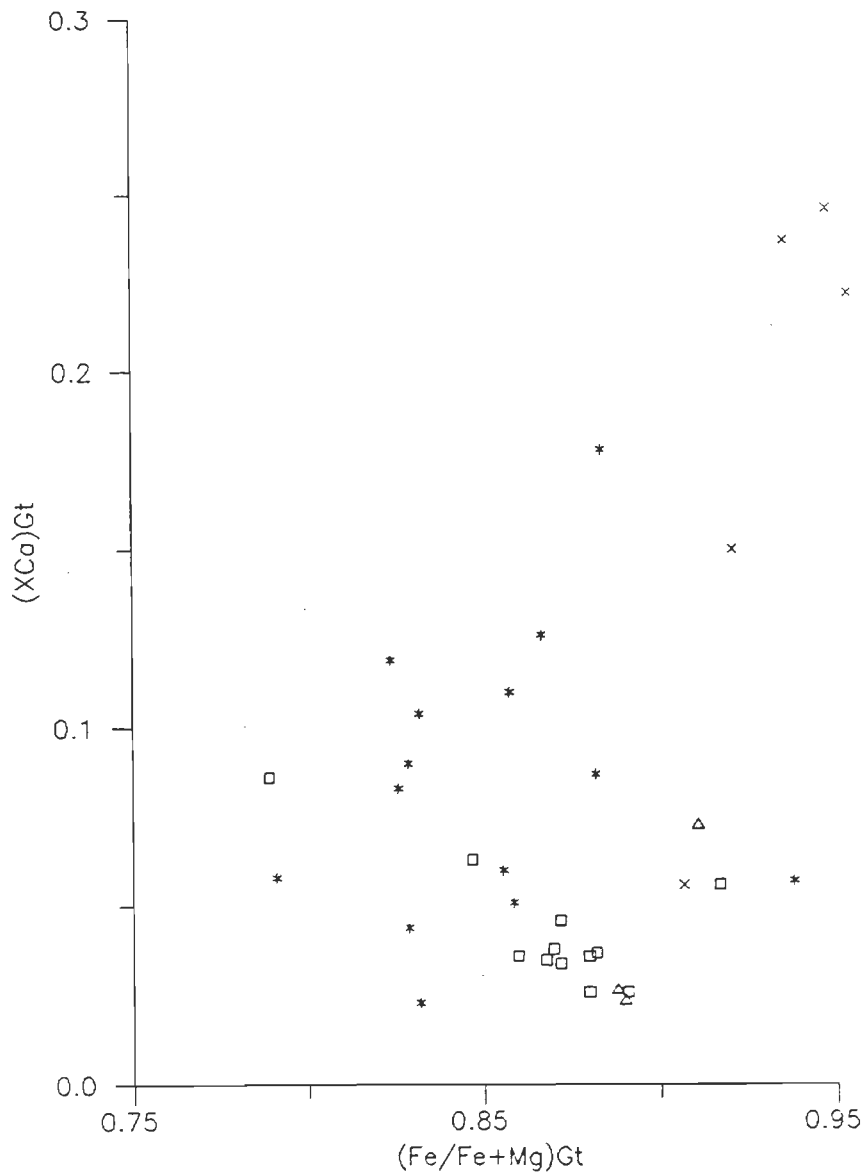


FIGURE 4.7: Plot showing X_{Ca} vs $Fe/Fe+Mg$ for garnet core in different metamorphic grades of the HHC - Bhot Nala section. Symbols as in Fig. 4.3.

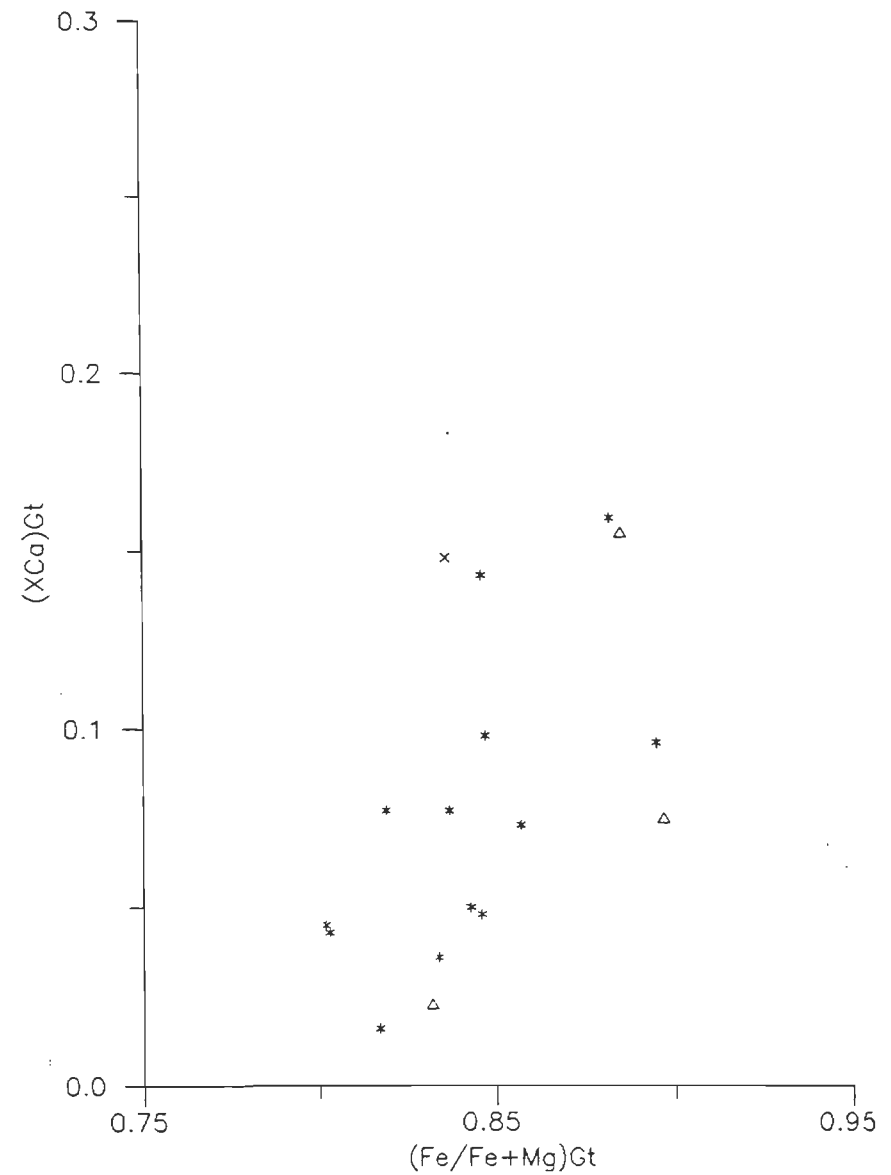


FIGURE 4.8: Plot showing X_{Ca} vs $Fe/Fe+Mg$ for garnet core in different metamorphic grades of the HHC - Suru-Doda Valleys section. Symbols as in Fig. 4.3.

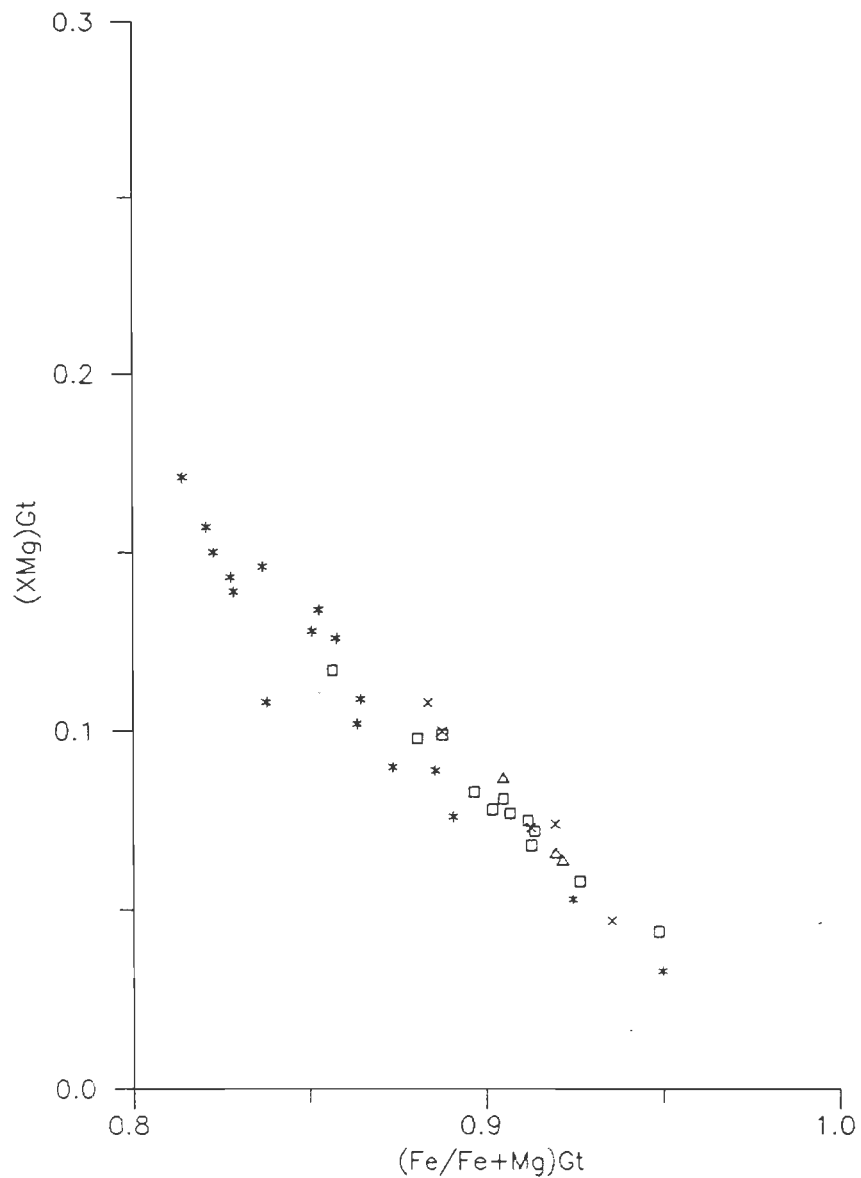


FIGURE 4.9: Plot showing XMg vs Fe/Fe+Mg for garnet rim in different metamorphic grades of the HHC - Bhot Nala section. Symbols as in Fig. 4.3.

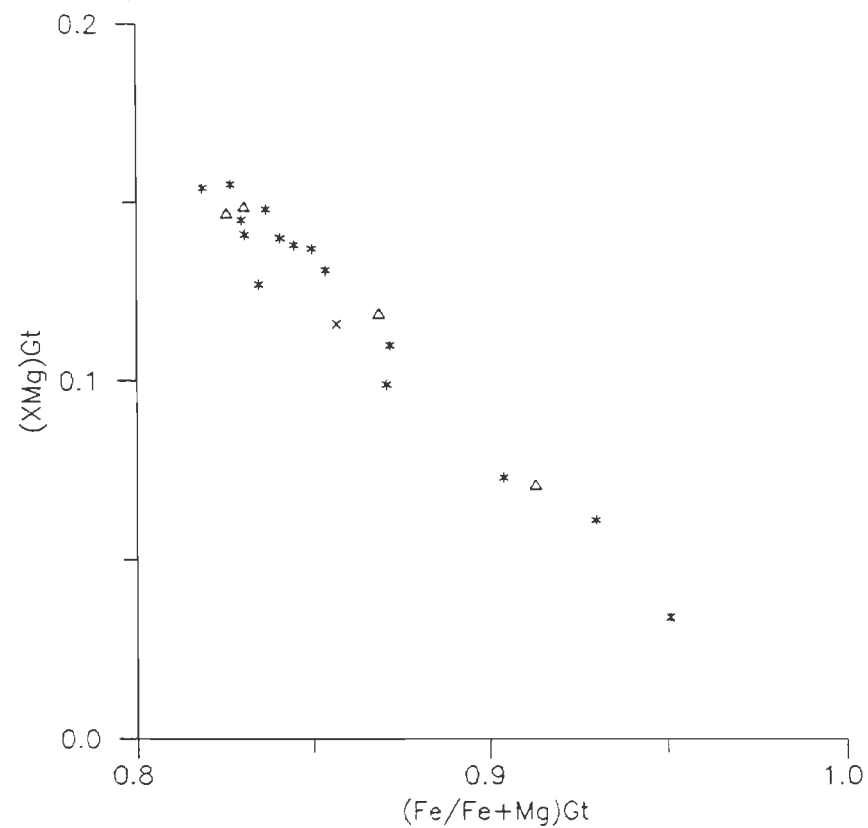


FIGURE 4.10: Plot showing XMg vs Fe/Fe+Mg for garnet rim in different metamorphic grades of the HHC - Suru-Doda Valleys section. Symbols as in Fig. 4.3.

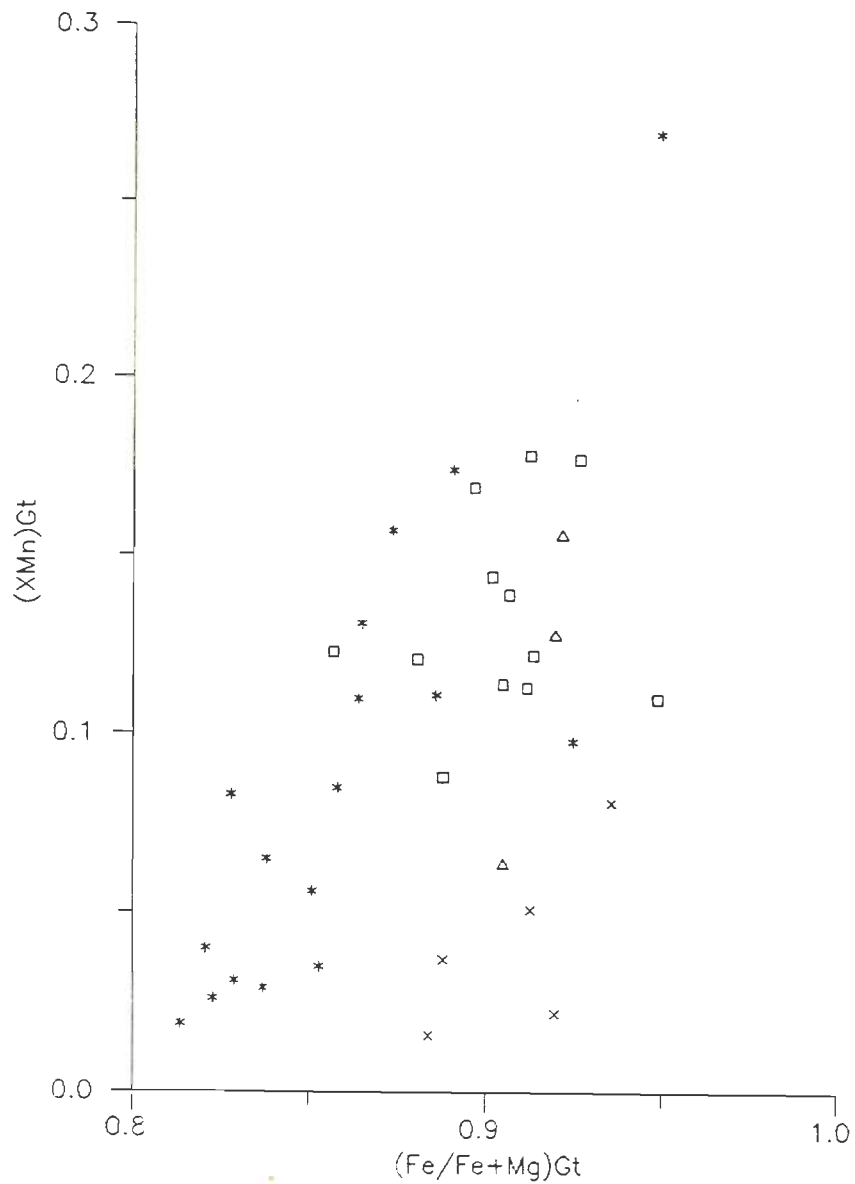


FIGURE 4.11: Plot showing XMn vs Fe/Fe+Mg for garnet rim in different metamorphic grades of the HHC - Bhot Nala section. Symbols as in Fig. 4.3.

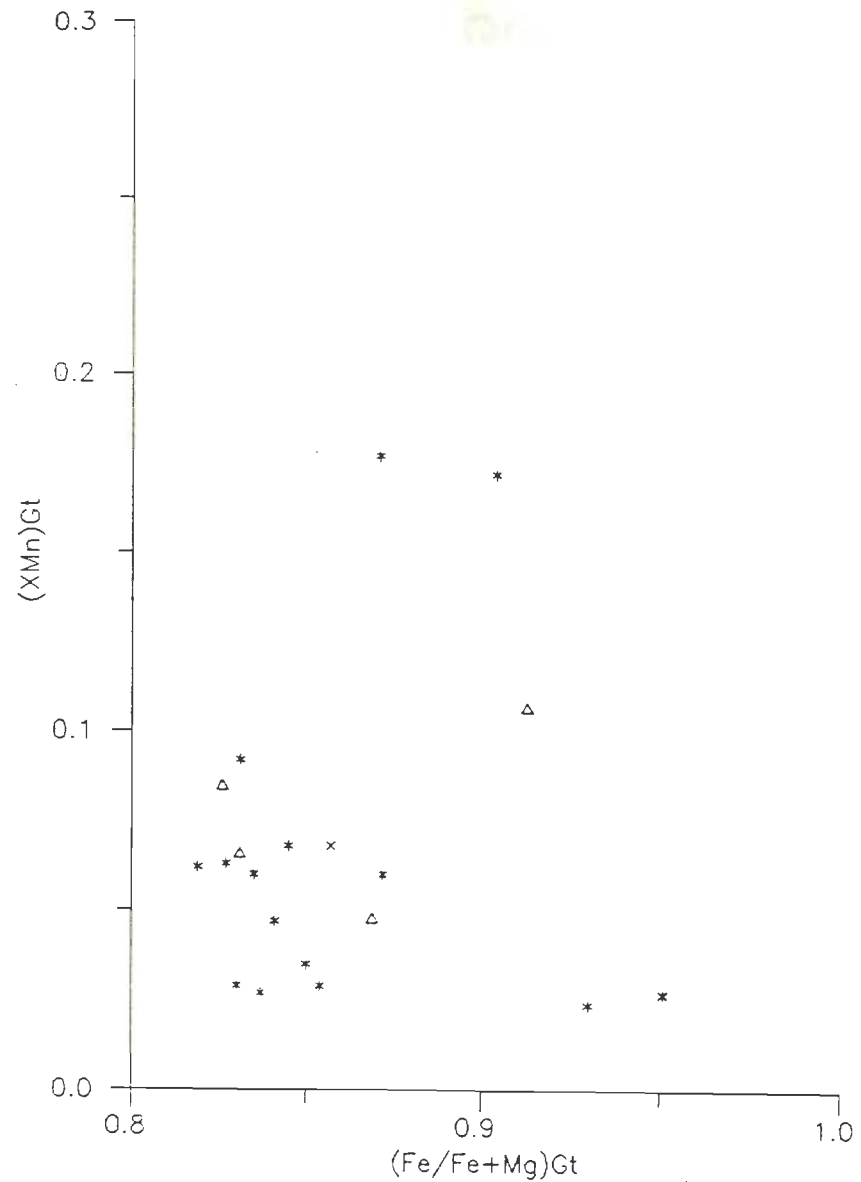


FIGURE 4.12: Plot showing XMn vs Fe/Fe+Mg for garnet rim in different metamorphic grades of the HHC - Suru-Doda Valleys section. Symbols as in Fig. 4.3.

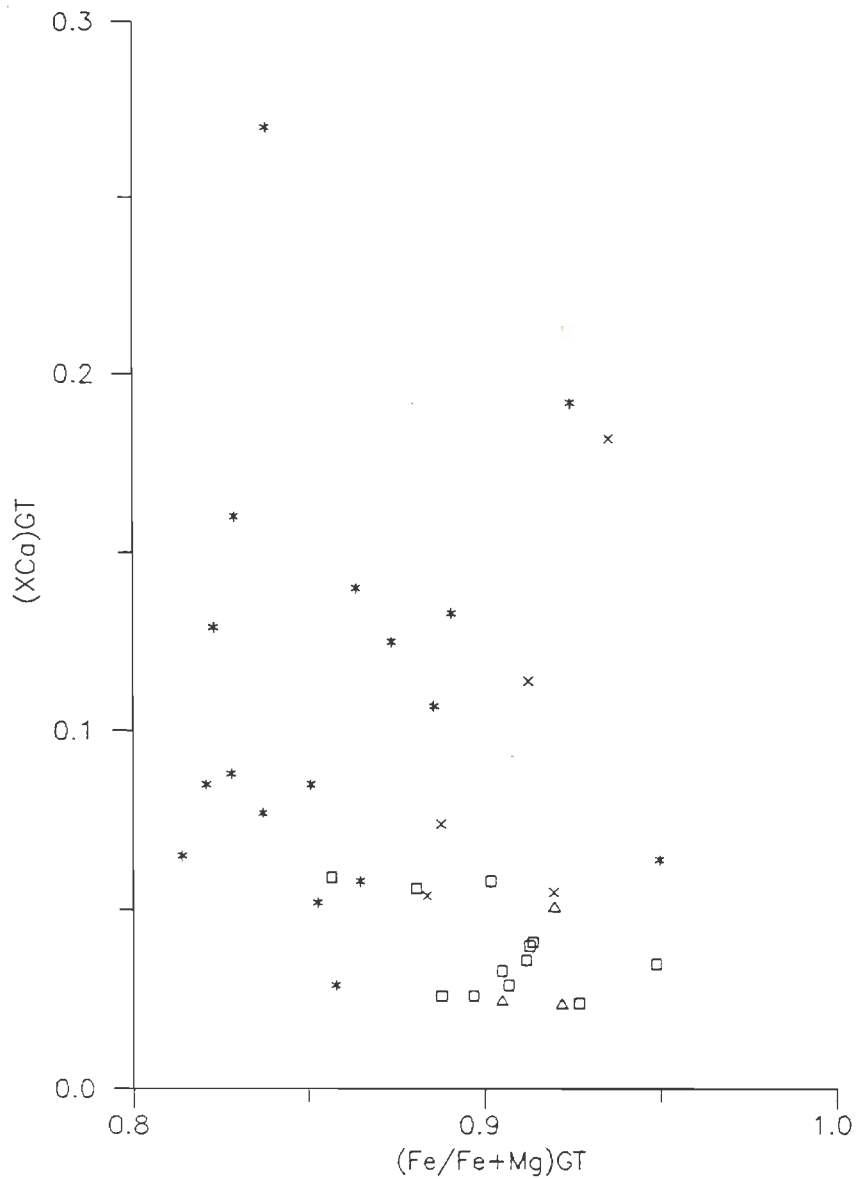


FIGURE 4.13: Plot showing X_{Ca} vs $Fe/Fe+Mg$ for garnet rim in different metamorphic grades of the HHC - Bhot Nala section. Symbols as in Fig. 4.3.

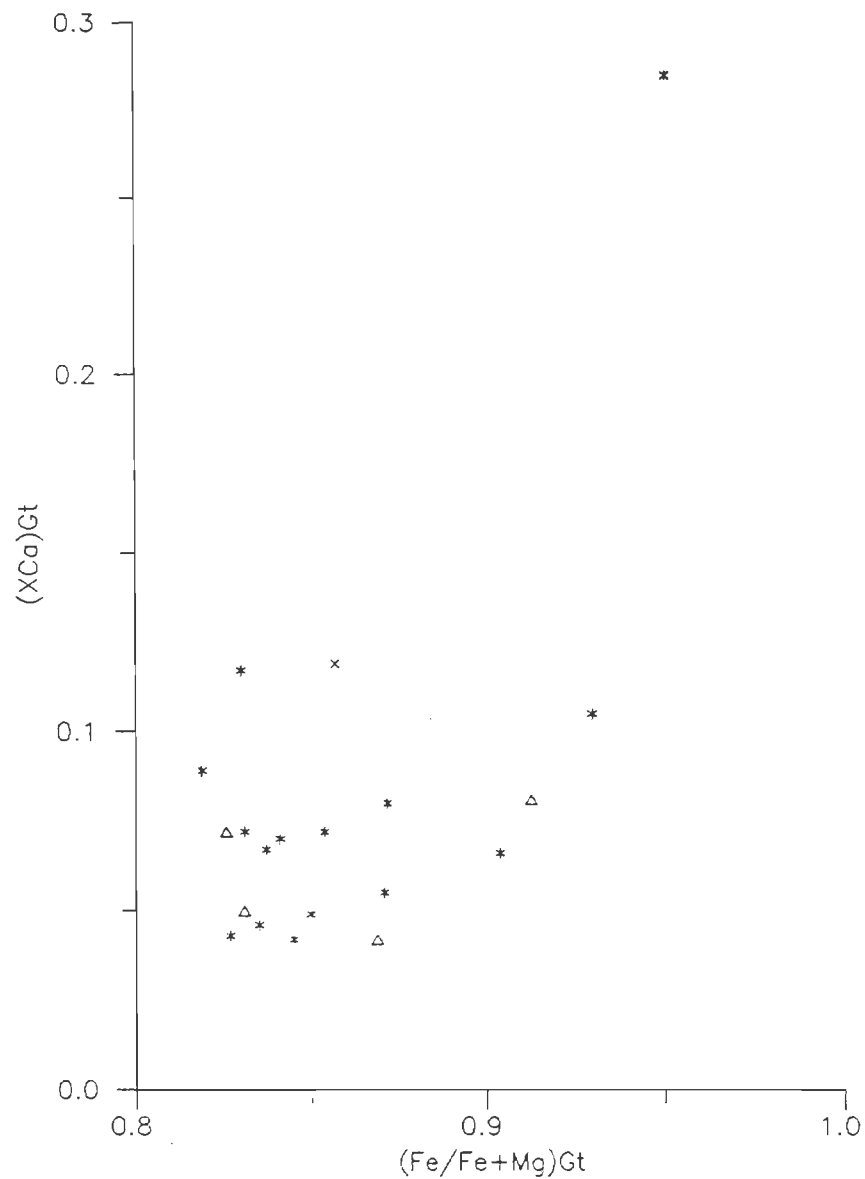


FIGURE 4.14: Plot showing X_{Ca} vs $Fe/Fe+Mg$ for garnet rim in different metamorphic grades of the HHC - Suru-Doda Valleys section. Symbols as in Fig. 4.3.

4.5.3 Biotite:

Matrix biotite from both the sections are relatively enriched in Fe and the Fe/Fe+Mg ratio ranges from 0.45 to 0.76 moles. This ratio remain <0.6 moles in staurolite-kyanite grade whereas the higher grade samples show >0.6 moles, except the garnet grade samples (Figs. 4.15 and 4.16). In the higher grades, Fe and Mg show a clear antipathic relationship. Al^{VI} and Ti do not show much variation with grade of metamorphism (Figs. 4.17, 4.18, 4.19 and 4.20). Fe/Fe+Mg ratio of biotite inclusions in garnet from different metamorphic grades ranges from 0.4 to 0.65 moles. This ratio is significantly <0.5 moles in staurolite-kyanite grade and the higher grades show 0.55 to 0.65 moles (Fig. 4.21). Al^{VI} and Ti do not show any significant variation with grade of metamorphism (Fig. 4.22 and 4.23) and they remain more or less in the same limits as observed in matrix biotites (Figs. 4.17, 4.18, 4.19, 4.20, 4.22, and 4.23).

4.5.4 Muscovite:

Muscovite shows a little variation in Al^{VI} from garnet to sillimanite-muscovite grades and range between 0.85-0.93. In garnet grade, X_{Muss} and X_{Pa} range between 0.68-0.69 and 0.09-0.17 moles respectively in Bhot Nala. However, there is sudden decrease of X_{Pa} and increase of X_{Muss} in staurolite-kyanite and sillimanite-muscovite grades. In Suru - Doda Valleys, muscovite does not show any variation in Al^{VI} in all the metamorphic grades. In garnet grade, muscovite has more X_{Muss} (0.67-0.73) and much less X_{Pa} (0.05-0.07). However, X_{Pa} shows an increase (0.06-

0.25) in staurolite-kyanite grade and again reduces in higher grades.

4.5.5 Plagioclase:

Plagioclase is more albitic ($X_{An} = 0.12-0.29$), but a few samples show an enrichment in anorthite component (SP20 = 0.32 and PL4/93 = 0.35). As far as the rim is concerned, plagioclase does not show any compositional variation with the grade of metamorphism in the Bhot Nala and Suru - Doda Valleys.

4.5.6 Staurolite:

The chemical composition of staurolite shows that Mn and Ti are ranging from 0.02-0.10 and 0.15-0.20 moles. ZnO shows no consistent pattern and varies between 0.161 and 1.261 wt%. In Kishtwar area, ZnO ranges from 0.82 to 0.93 wt% (KC26/28 and T4/6) and in Suru Valley from 1.16-1.26 wt% (PC15A/1). However, it is reduced to 0.16 - 0.18 wt% in Pensi La (PC16D/83) and 0.31-0.38 wt% (P9/43) along Doda Valley samples. All samples give high Fe/Fe+Mg values ranging from 0.80 to 0.85 (Appendix-V). Core analysis of staurolite indicates slightly higher X_{Mg} . Generally, ZnO in core is lesser by 0.1 wt% from rim except in samples P9/46 and PC16D/83.

4.5.7 Ilmenite:

Fe, Ti, V, Al and Cr are analysed in ilmenite. On the basis of 6 oxygen basis, Fe ranges from 1.85 to 2.01 atom % and Ti ranges from 1.94 to 2.05 atom %. In one sample (PL4/93) from Suru Valley, more Ti-rich ilmenite having 2.28 atom % with Fe reduced to 1.41 atom % is also detected. V is more or less constant in

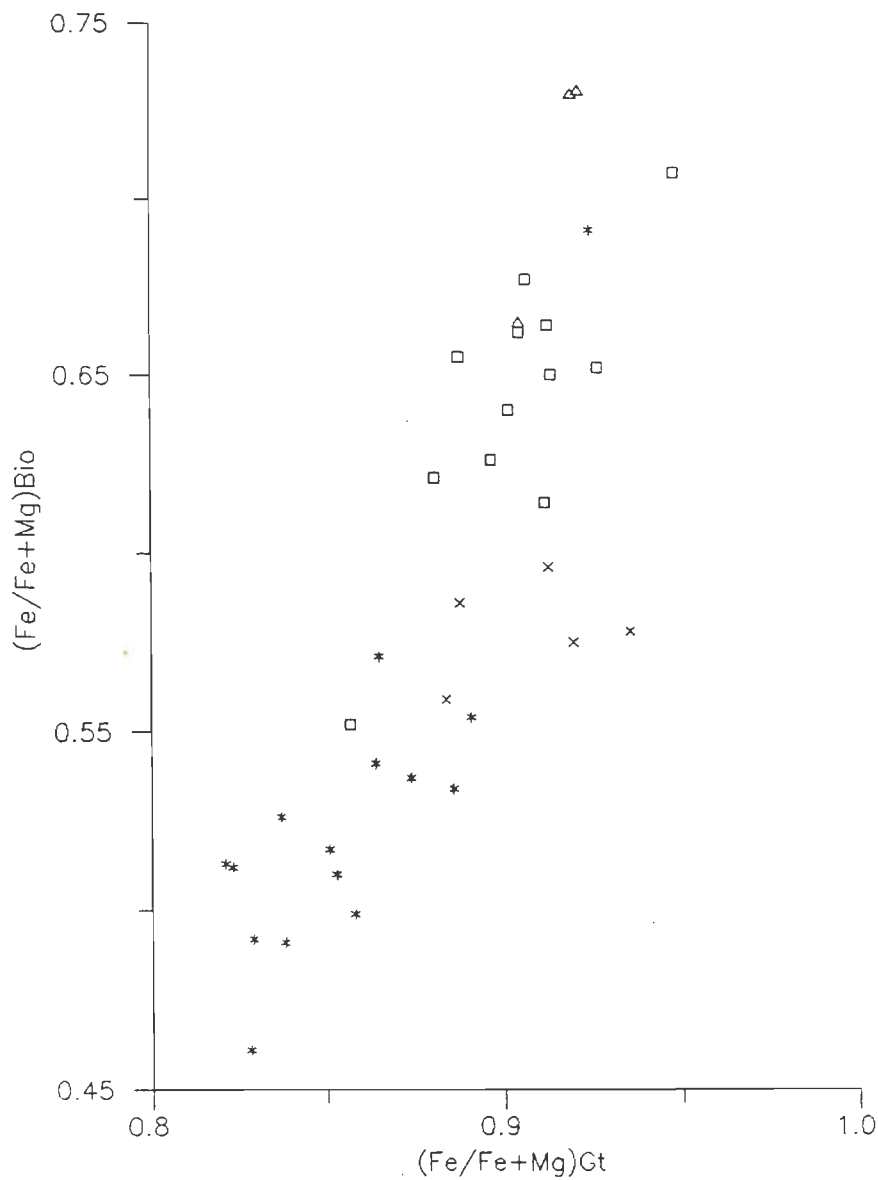


FIGURE 4.15: Plot showing Fe/Fe+Mg of matrix of biotite vs Fe/Fe+Mg of garnet rim in different metamorphic grades of the HHC - Bhot Nala section. Symbols as in Fig. 4.3.

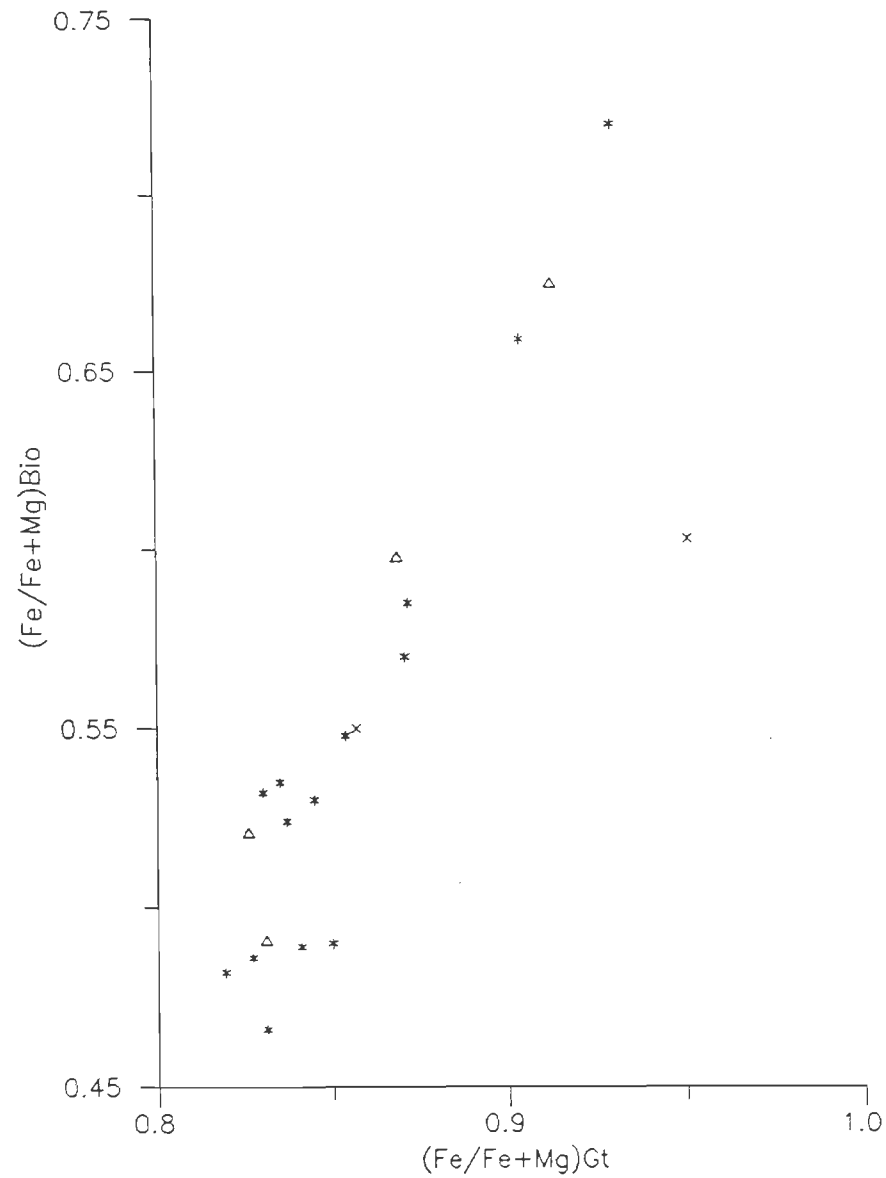


FIGURE 4.16: Plot showing Fe/Fe+Mg of matrix of biotite vs Fe/Fe+Mg of garnet rim in different metamorphic grades of the HHC - Surudoda Valleys section. Symbols as in Fig. 4.3.

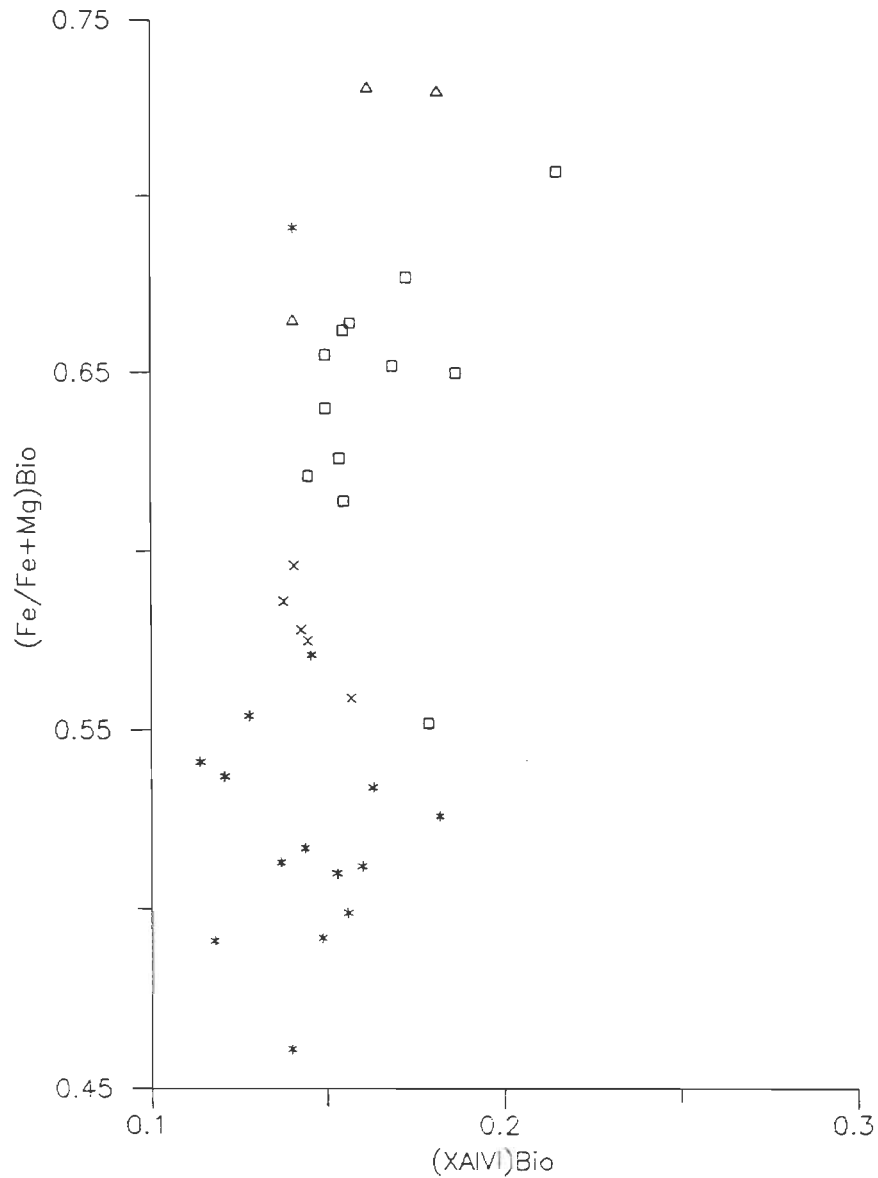


FIGURE 4.17: Plot showing Fe/Fe+Mg vs XAlVI for matrix biotite in different metamorphic grades of the HHC - Bhot Nala section. Symbols as in Fig. 4.3.

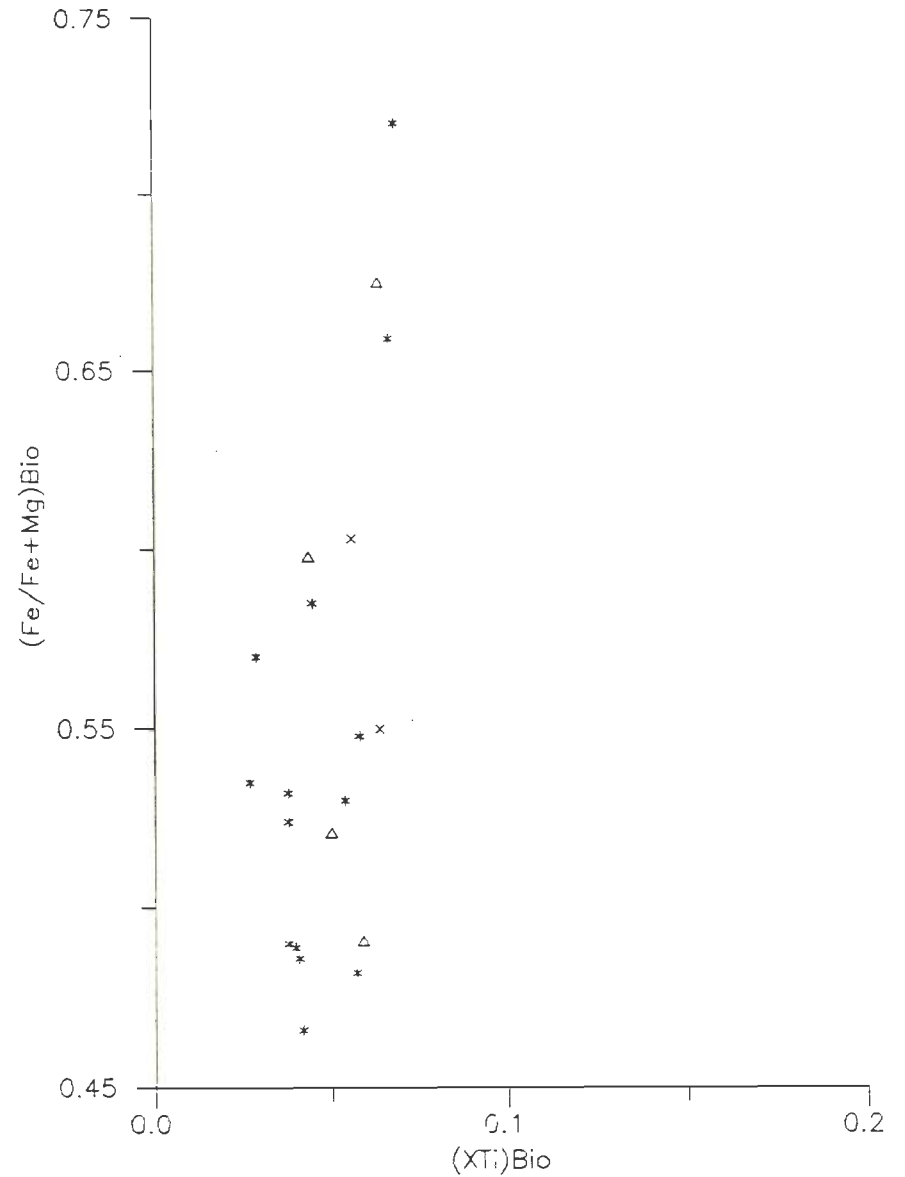


FIGURE 4.18: Plot showing Fe/Fe+Mg vs XAlVI for matrix biotite in different metamorphic grades of the HHC - Suru-Doda Valleys section. Symbols as in Fig. 4.3.

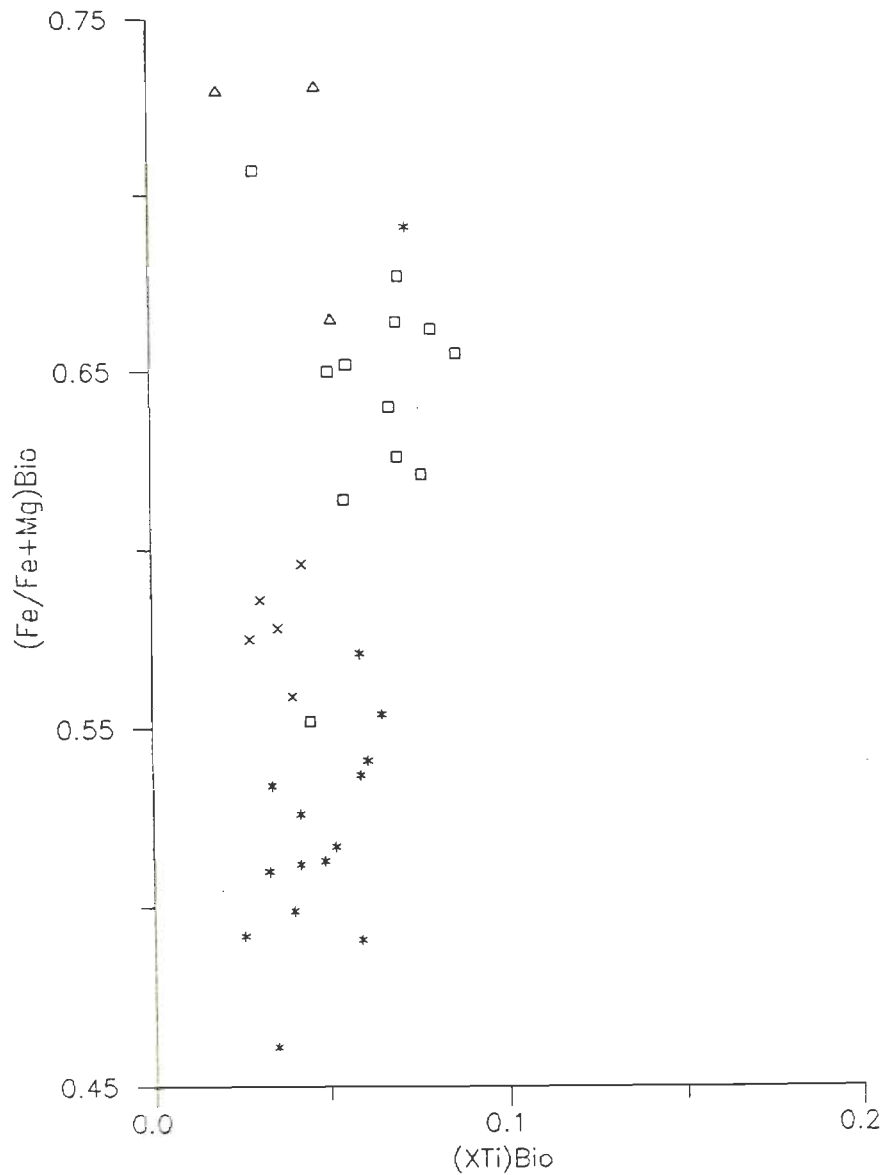


FIGURE 4.19: Plot showing $Fe/Fe+Mg$ vs XTi for matrix biotite in different metamorphic grades of the HHC - Bhot Nala section. Symbols as in Fig. 4.3.

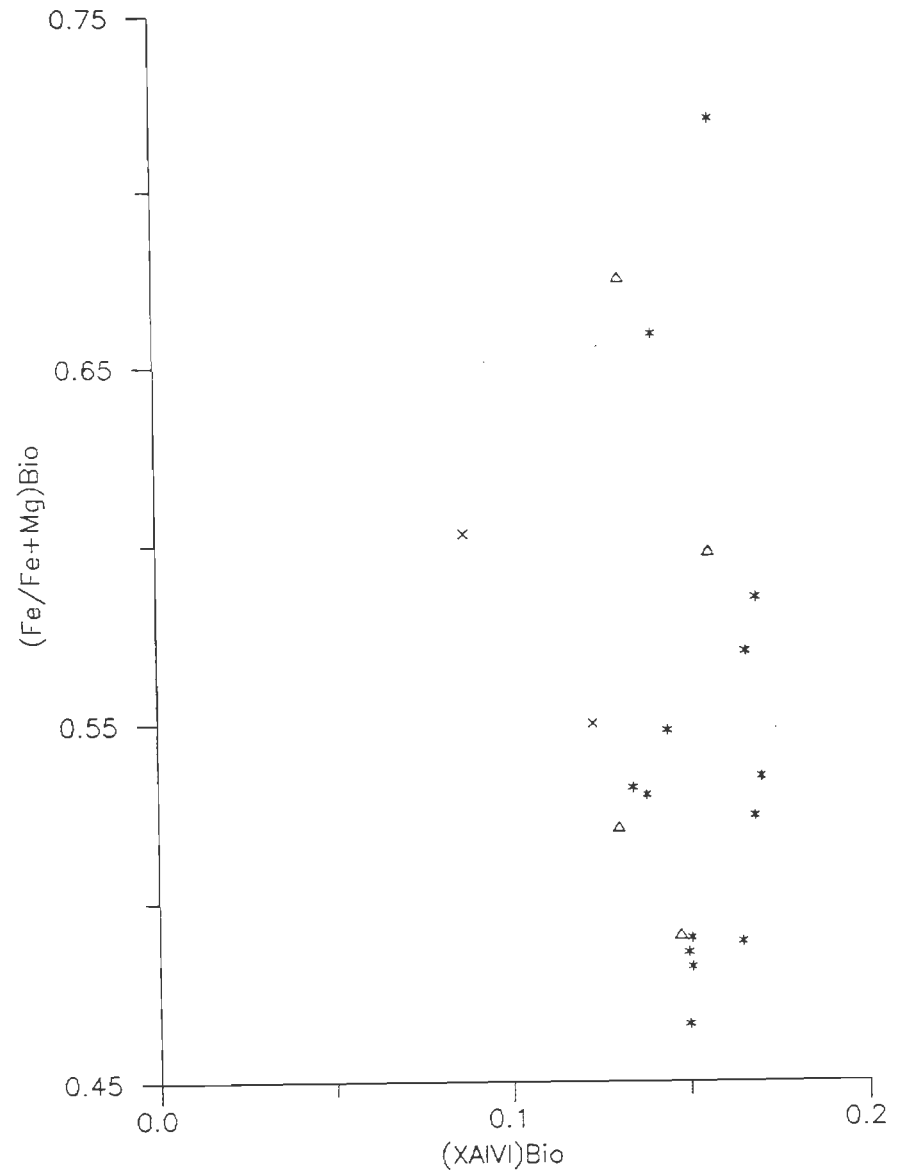


FIGURE 4.20: Plot showing $Fe/Fe+Mg$ vs XTi for matrix biotite in different metamorphic grades of the HHC - Suru-Doda Valleys section. Symbols as in Fig. 4.3.

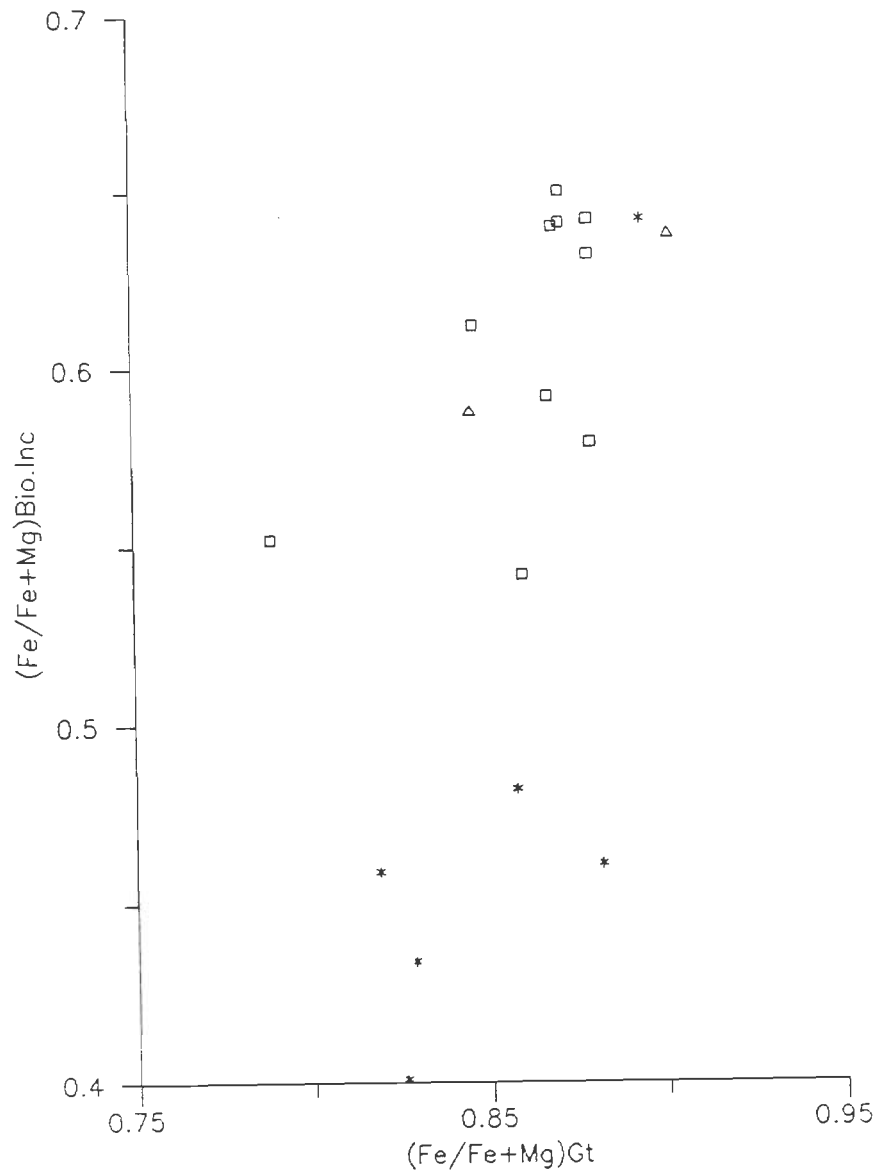


FIGURE 4.21: Plot showing Fe/Fe+Mg of biotite inclusion vs Fe/Fe+Mg of garnet core in different metamorphic grades of the HHC - Bhot Nala section. Symbols as in Fig. 4.3.

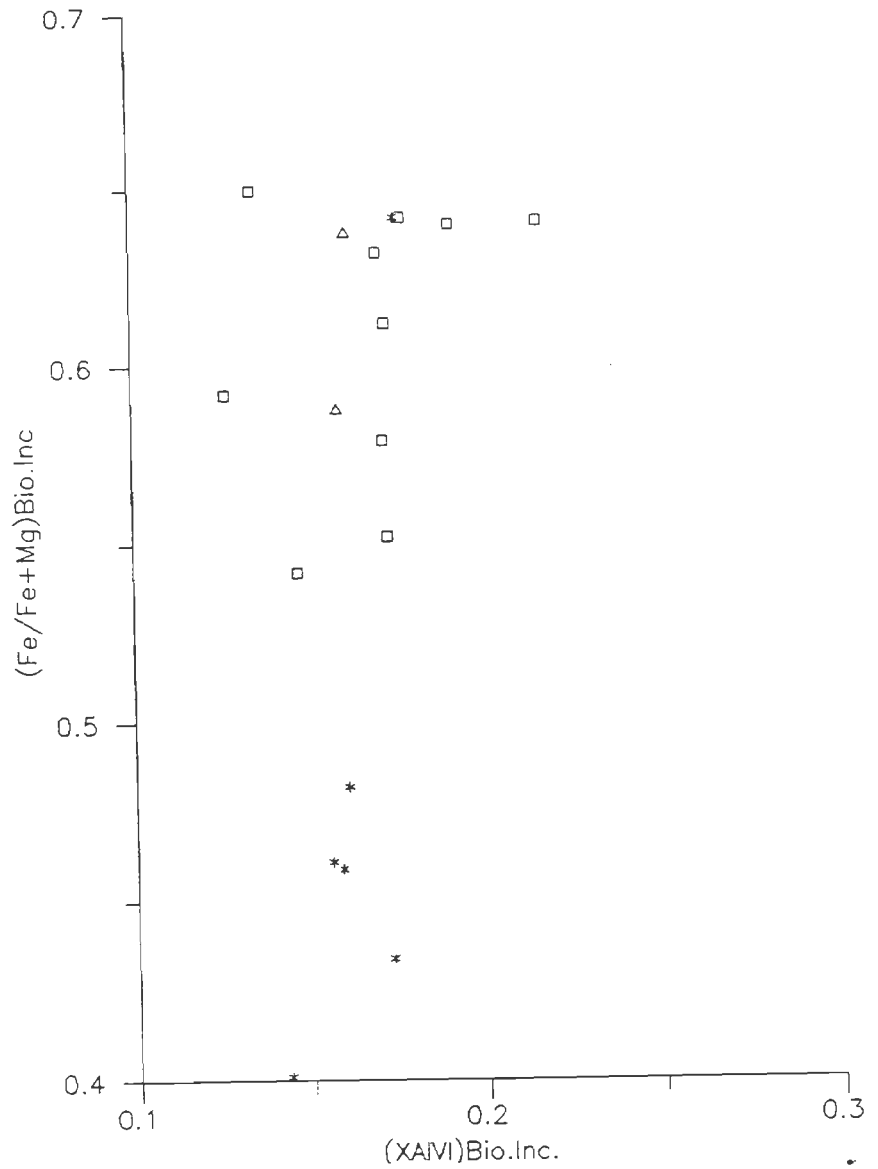


FIGURE 4.22: Plot showing Fe/Fe+Mg vs XAlVI for biotite inclusion in different metamorphic grades of the HHC - Bhot Nala and Suru-Doda Valleys section. Symbols as in Fig. 4.3.

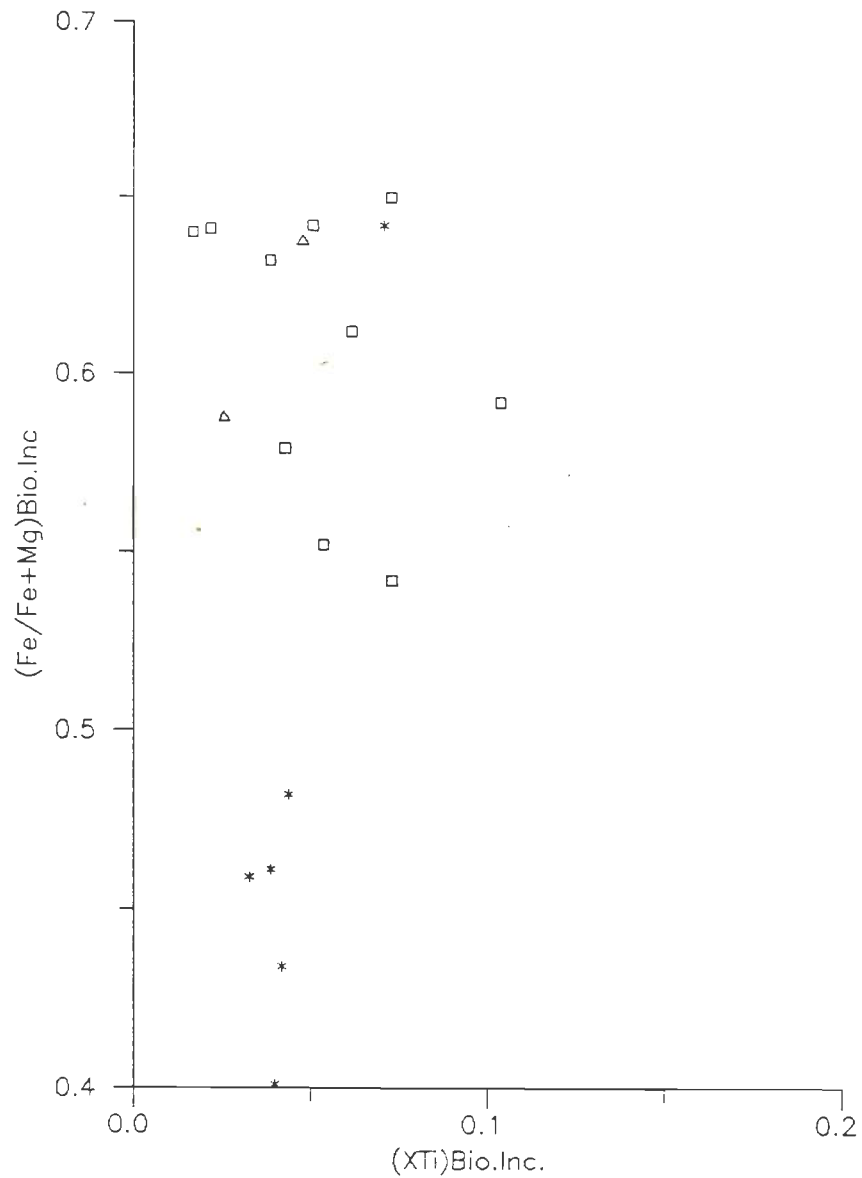


FIGURE 4.23: Plot showing $\text{Fe}/\text{Fe}+\text{Mg}$ vs XTi for biotite inclusion in different metamorphic grades of the HHC - Bhot Nala and Suru-Doda Valleys section. Symbols as in Fig. 4.3.

ilmenite from all the grades. Al and Cr occur in negligible amount in a few ilmenite grains.

4.5.8 Rutile:

Almost pure rutile is found mostly in staurolite-kyanite grade rocks. However, nearly about 1 wt % is made up of other oxides like FeO, V₂O₃, Al₂O₃, Cr₂O₃ etc. Rutile does not show any compositional variation.

4.6 AFM DIAGRAMS

AFM projections, based on equilibrium mineral paragenesis and chemistry of coexisting minerals, are presented for individual metamorphic grades (Thompson, 1957). Only rim analysis is considered for plotting the phase compositions. All the components in the system (such as KMnFMASH, NaKFMASH) are not considered at present to comprehend and construct the petrogenetic grid to understand the effect of minor elements. AFM plotting has been done to infer the shift in three/two phase compositional field with respect to metamorphic grade. The samples for individual metamorphic grade from both the sections are plotted together.

Compositions of coexisting garnet-biotite from garnet grade samples are shown in the Fig. 4.24. As chlorite is not in association with garnet-biotite in many of these samples, chlorite is not represented in the diagram. Within this zone, garnet-biotite show compositional co-linearity, except for sample RG49, indicating equilibrium conditions. The AFM topology of staurolite-kyanite grade is represented in Fig.4.25. Three phase

field of staurolite-garnet-biotite shows compositional co-linearities in most of the samples, except in one sample where tie line crossing suggests that this sample possibly has undergone post-metamorphic reequilibration. Also, garnet and biotite show relative enrichment in Mg than that of garnet grade samples (Fig. 4.25). In sillimanite-muscovite grade, garnet and biotite show relative enrichment in Fe than Mg (Fig. 4.26) in three phase field of garnet-biotite-sillimanite. This trend continues in sillimanite-K-feldspar grade (Fig. 4.27). Fe/Fe+Mg ratio of garnet rim and matrix biotite increases with grade of metamorphism. This is clearly observable from Bhot Nala and Suru - Doda Valleys samples (Figs. 4.15 and 4.16). However, biotite inclusions within garnet core show an increase in Fe/Fe+Mg ratio with metamorphic grade, but garnet core shows no clear trend (Fig. 4.21). The Mg/Mg+Fe ratio decreases in Bio>St>Gt order. Mn/Mn+Fe+Mg ratio decrease in Gt>St>Bio order in coexisting minerals is in agreement with Thompson (1976).

4.7 GARNET ZONING

Mineral zoning provides an opportunity to understand the growth and/or diffusion processes with respect to changing P- T conditions and kinetics of metamorphic processes. It is also useful to infer P-T-t path during tectonic evolution (e.g., Tracy, 1982; Loomis, 1983; Spear and Selverstone, 1983; Thompson and England, 1984). Among various minerals that show zoning, garnet invariably retains the zoning after its growth because of its refractory nature (e.g., Tracy, 1982). The other minerals equilibrate and become homogeneous within the regional

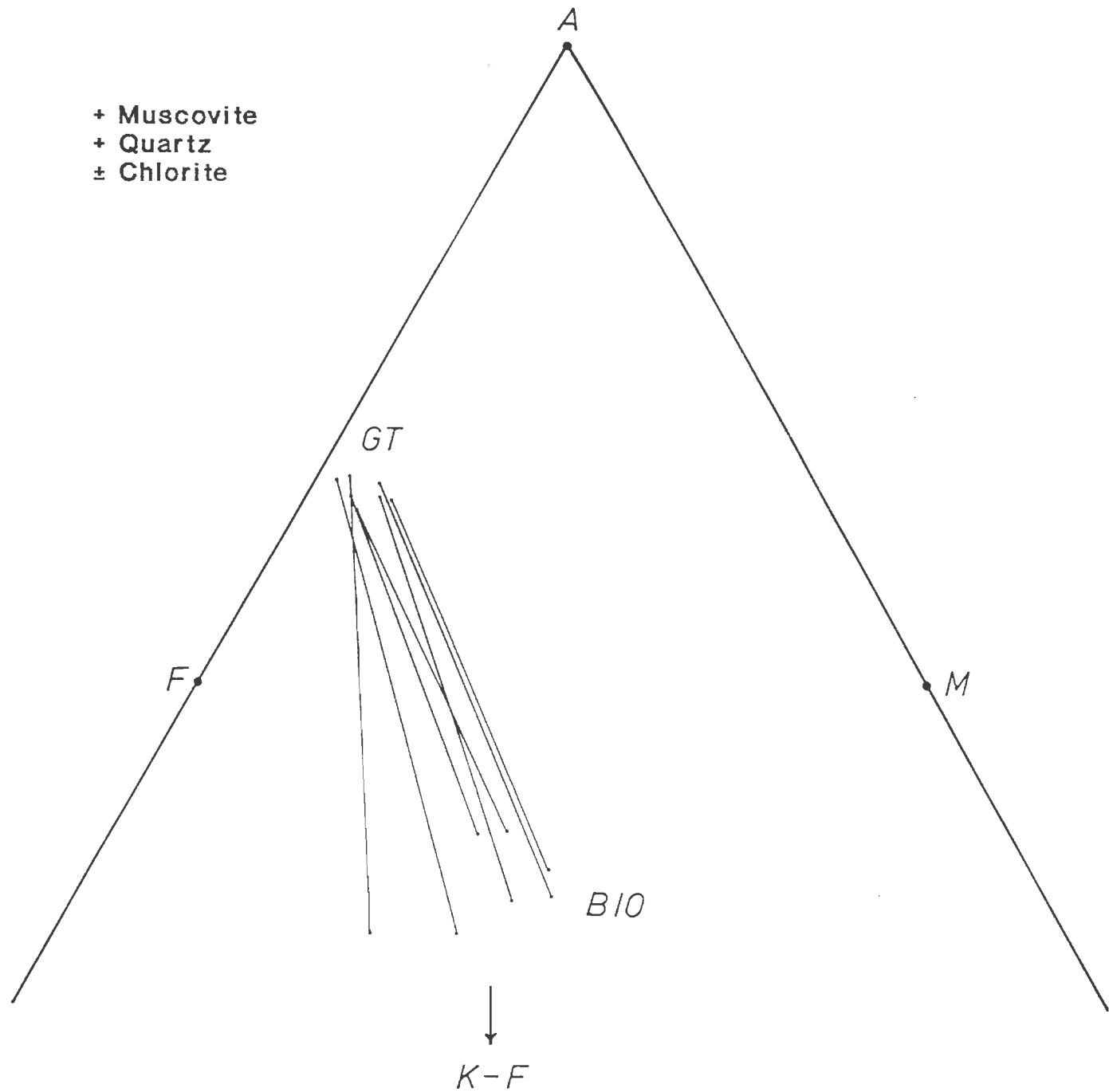


FIGURE 4.24 : AFM projection for garnet grade.

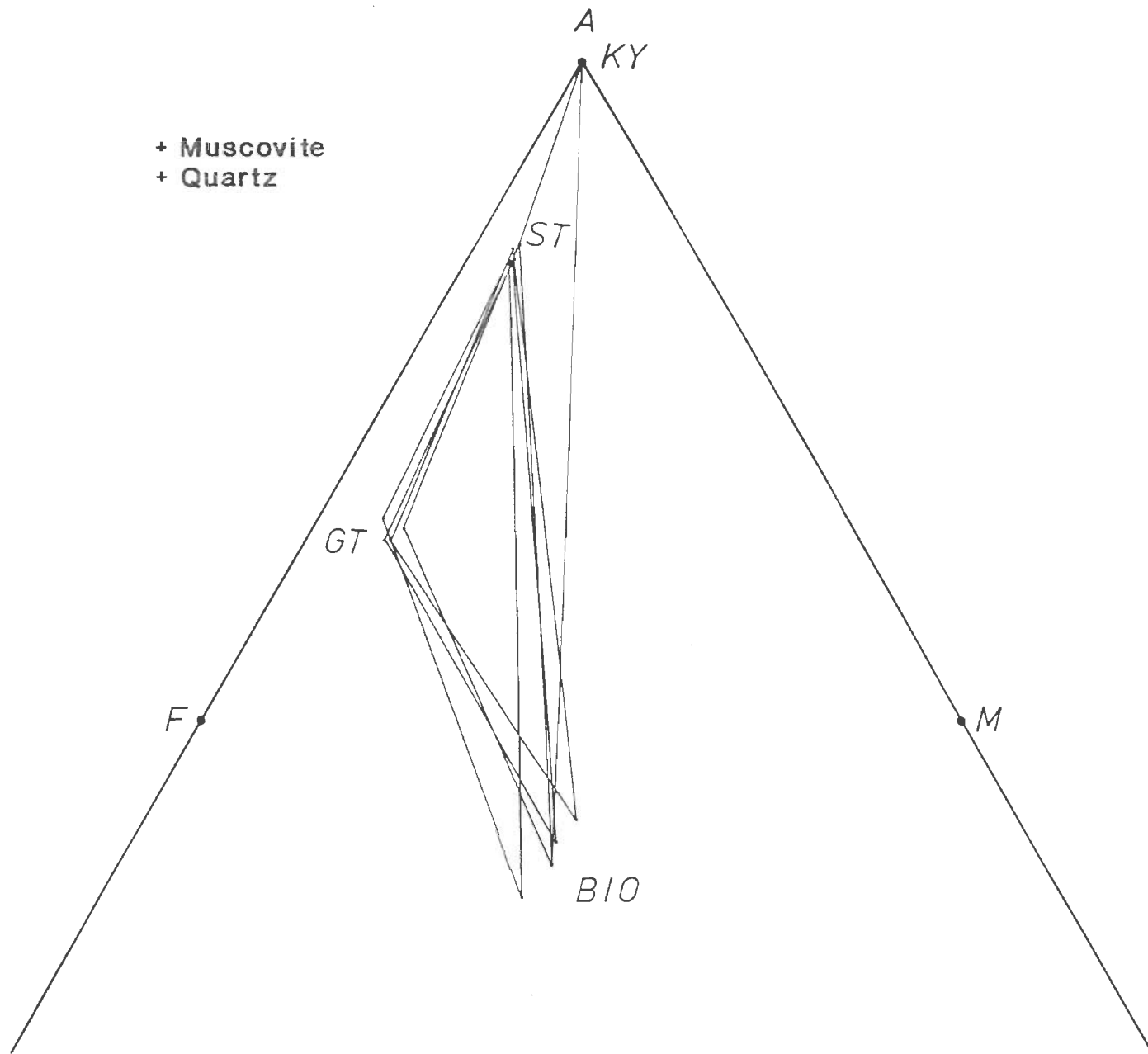


FIGURE 4.25 : AFM projection for staurolite-kyanite grade.

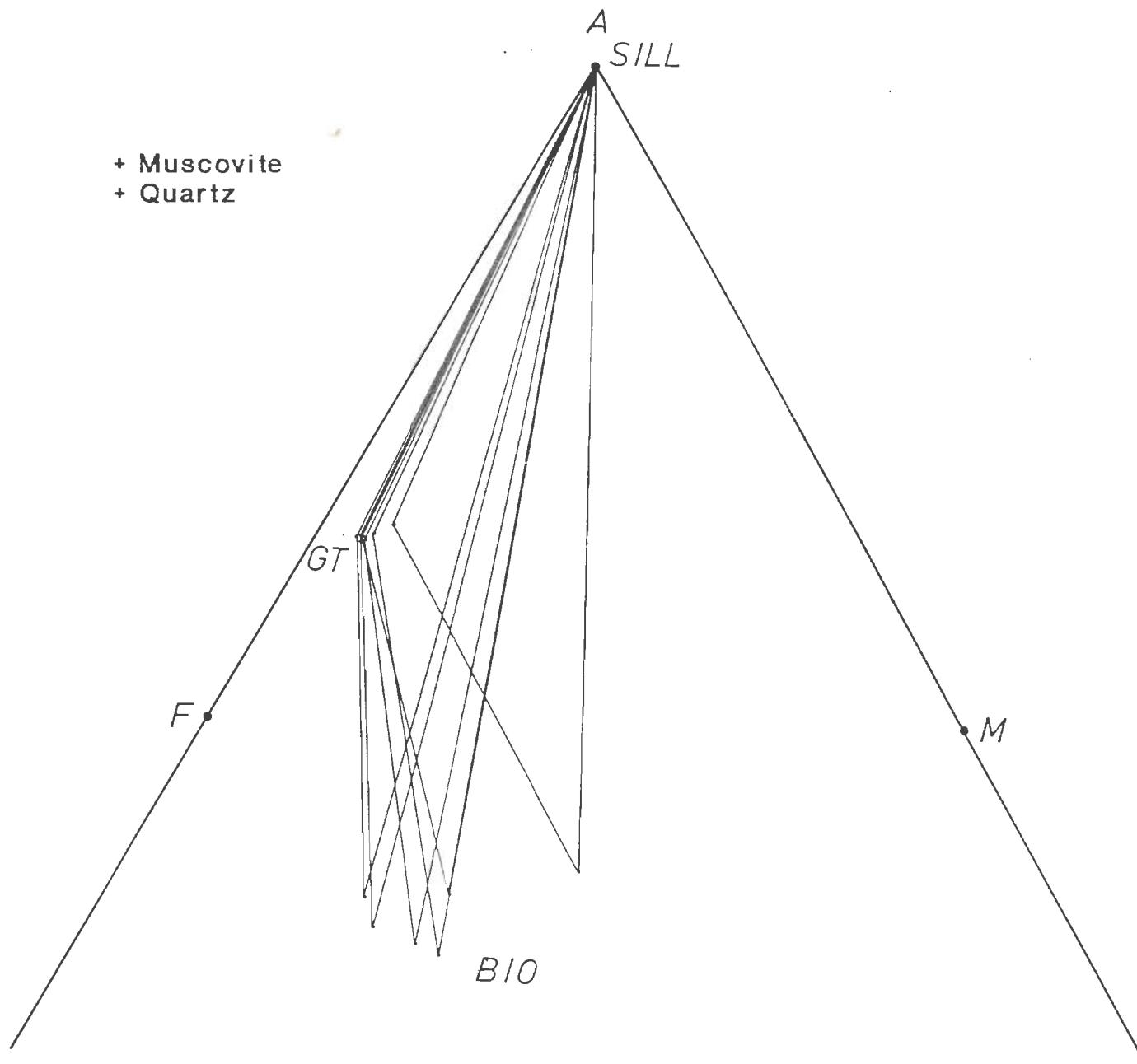


FIGURE 4.26 : AFM projection for sillimanite-muscovite grade.

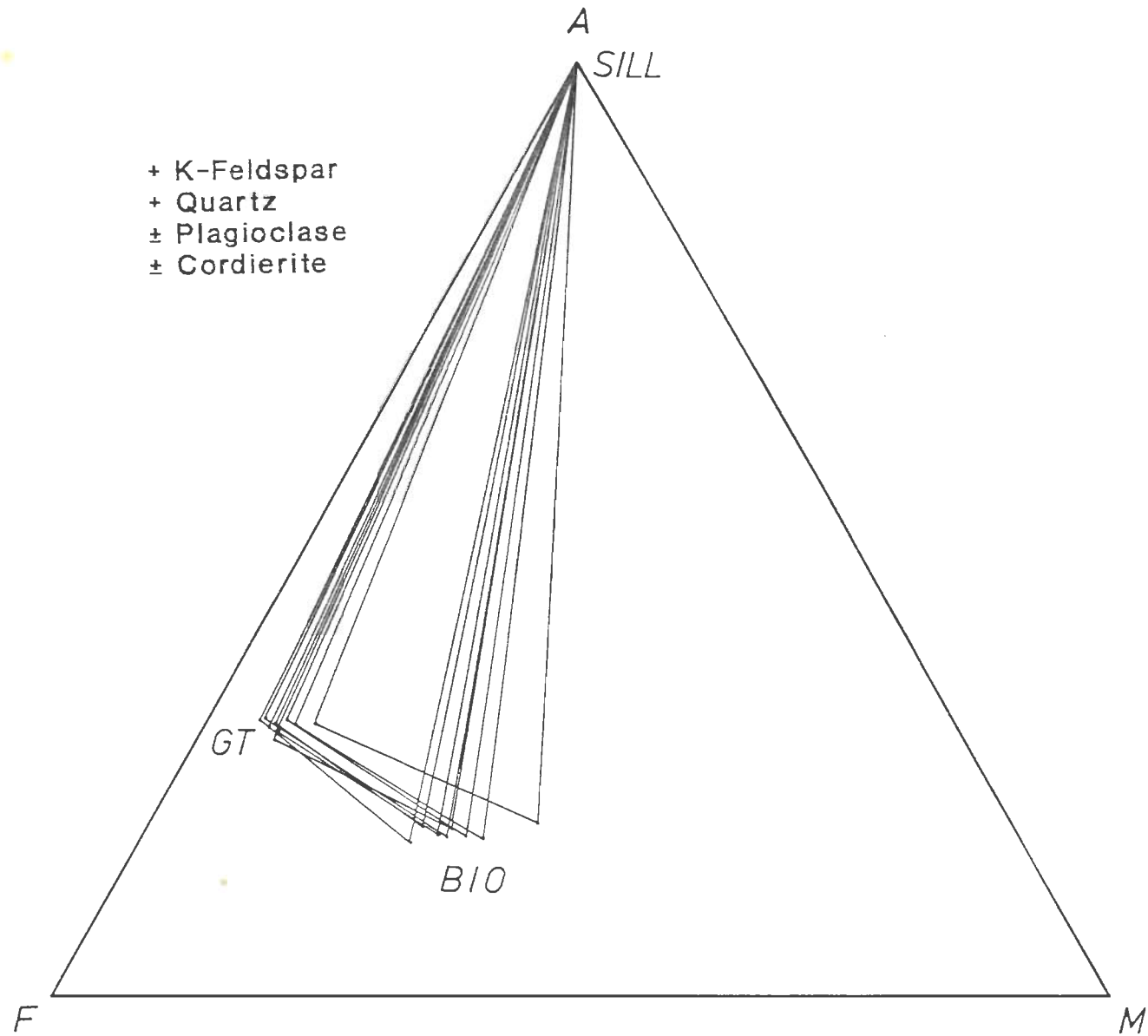


FIGURE 4.27 : AFM projection for the sillimanite-K-feldspar grade.

metamorphic time frame and does show very little zoning. Therefore, emphasis has been given mainly on garnet zoning as this is a very common mineral in pelitic rocks of all metamorphic grades.

In general, normal zoning in garnet is described as continuous or discontinuous fractionation processes operated during garnet growth with changing pressure and temperature conditions. Such growth zoning with low volume diffusion is observed mostly upto staurolite-kyanite grade rocks (Tracy, 1982; Spear, 1988). This type of growth zoning reveals bell-shaped profile of Mn and/or Ca and an enrichment of Fe and Mg towards rim. However, growth zoning is modified by intracrystalline volume diffusion in sillimanite grade rocks (Tracy, 1982). Calculated diffusion models on garnet growth and homogenisation suggest that garnet >1mm size can preserve growth zoning even at upper amphibolite facies condition. However, garnet of <1mm size undergoes intragranular diffusion and experiences complete homogenisation (Spear, 1988; Jiang and Lasaga, 1990; Florence and Spear, 1991). Similarly, it is observed that garnet of >0.4 mm preserve growth zoning in staurolite isograd and is not affected by diffusional homogenisation at this temperature condition (Florence and Spear, 1991).

To evaluate both growth and diffusional zoning in garnet from pelitic rocks, garnet grains mainly of syntectonic (garnet-I) and a few post-tectonic (garnet-II) origin were analysed from all metamorphic grades. In each grade, one or two samples were

selected for this purpose .In each sample, quantitative line analyses were performed by microprobe to decipher garnet zoning for end-member components. The analyses were carried out along garnet diameters parallel and perpendicular to the main schistosity. This is done mainly to obtain information regarding the exchange of major components with other coexisting phases as well as the effect of temperature and pressure on growth and diffusion processes. In general, garnet-I reveals zoning, whereas garnet-II is homogeneous in composition from core to rim. Therefore, garnet-I zoning is used to decipher the effects of particularly temperature and mineral assemblage on the growth and diffusional processes.

Garnet-I from garnet grade (KC21/23), occurring on the western side of Kishtwar Window near Chhatru, shows typical bell-shaped profile for Mn and Ca and enrichment of Fe and Mg ratios towards the rim (Fig.4.28) indicating normal growth zoning and reaction partitioning with biotite (Trzcienski, 1977). In staurolite-kyanite grade (KC26/28), garnet shows more or less similar zoning pattern as observed in garnet grade, but there is a relaxation in the profile. Towards the edges, garnet shows reversal in Mg and Mn zoning (Fig.4.29). The relaxed trend in the growth zoning indicates that growth has been partially modified due to elevated temperature condition. The reversal in zoning at the rim may be either due to post-metamorphic growth and/or by the breakdown of Mn-rich chlorite (Kretz, 1973). In the same grade, sample from Suru Valley (PC30C/5) shows more or less similar relaxed zoning pattern, except for Fe. In this

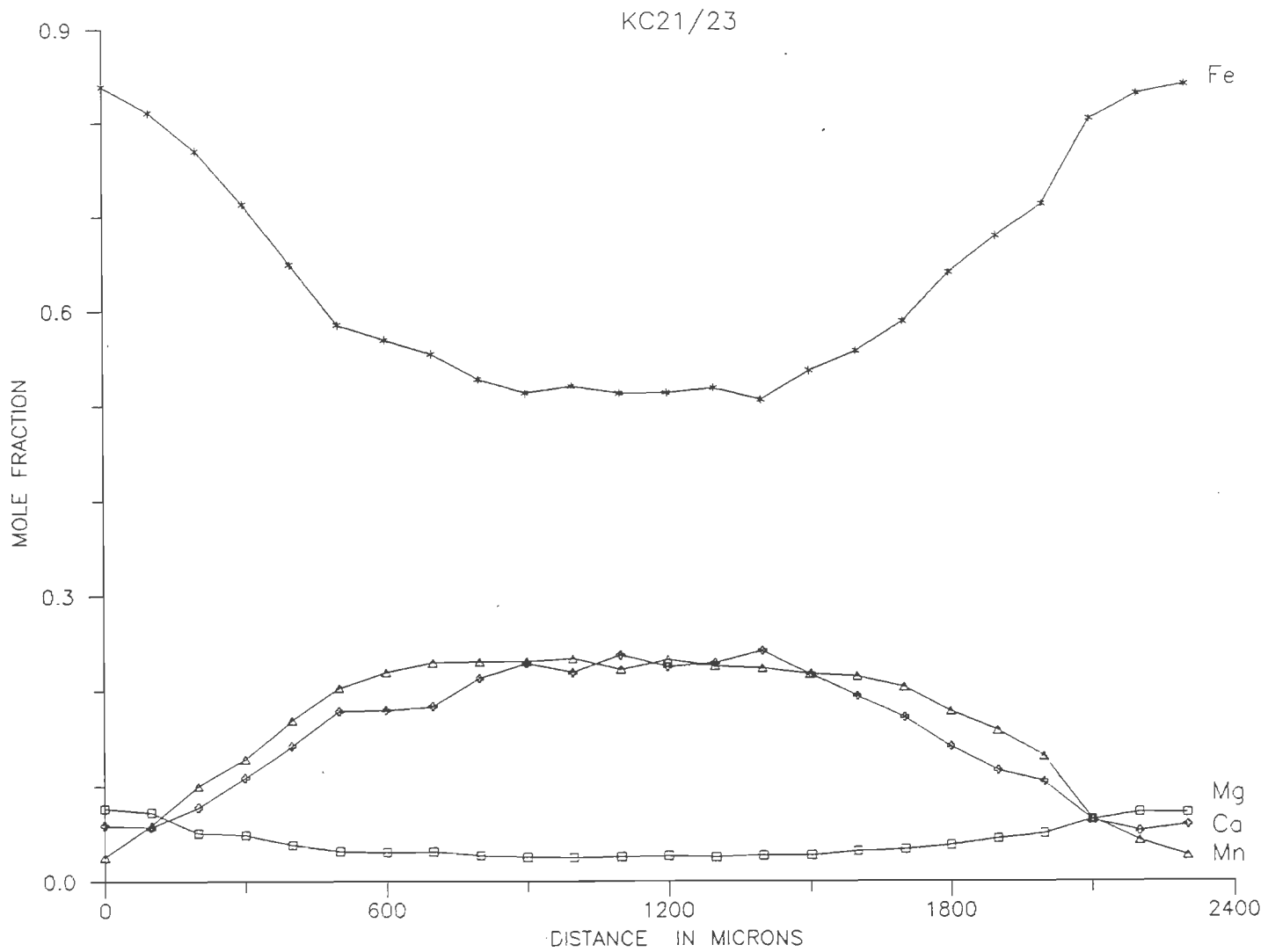


FIGURE 4.28 : Garnet zoning profile (Rim-Core-Rim) for garnet grade. Sample KC21/23.

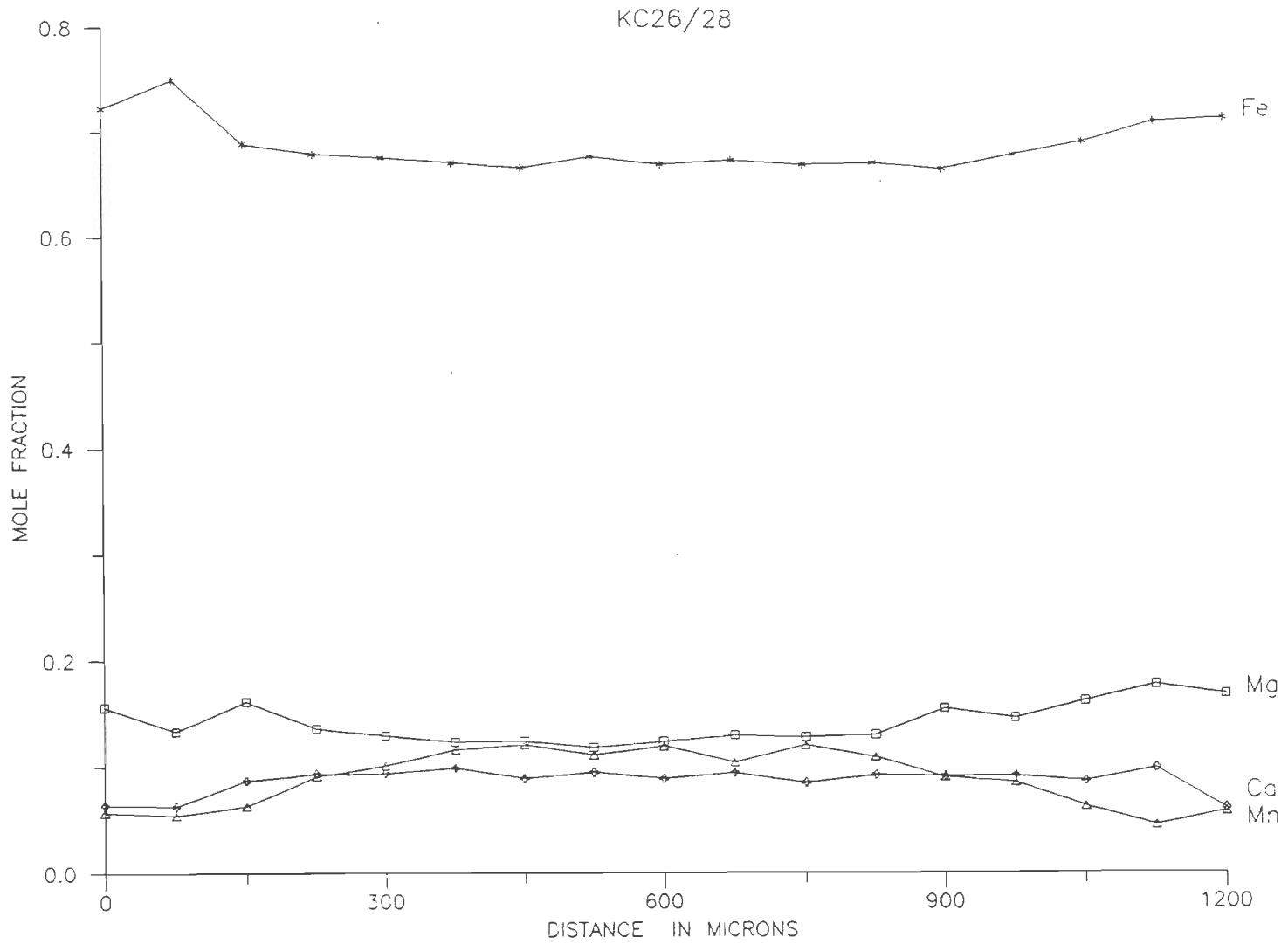


FIGURE 4.29 : Garnet zoning profile (Rim-Core-Rim) for staurolite- kyanite grade. Sample KC26/28.

sample, Fe shows slight enrichment in core than in the inner rim, whereas Mg shows reversal from this trend (Fig.4.30).

Garnet in sillimanite-muscovite and sillimanite-K-feldspar grade rocks show a relaxed zoning pattern (A53/62B, A57/68; Figs. 4.31 and 4.32). Sample A53/62B shows an uniform trend in all the components. Mg, Ca and Mn show very slight reverse zoning only at the rim (Fig. 4.31). This type of relaxed zoning could be due to high rate of volume diffusion and homogenisation at higher temperature, as observed in high temperature terrains by others (Tracy et al., 1976; Woodsworth, 1977). Sample A57/68 shows clearly the reverse zoning with an increase of Mn and Ca content and corresponding decrease in Fe and Mg contents towards rim. This type of reverse zoning may be due to post-growth volume diffusion during cooling after the peak metamorphic temperature (Cygan and Lasaga, 1982). However, growth zoning is observed in the core of garnet in sample MP5 and, while approaching towards the rim, it shows relaxation in the zoning pattern. At the rim of this garnet, reverse zoning for Mg and Mn is observed (Fig. 4.33). As this garnet is sufficiently larger (≈ 2.5 mm diameter), the initial growth zoning has not been fully modified by diffusion at higher temperature (Florence and Spear, 1991). However, the reversal at rim appear to be due to resorption of garnet edge during retrograde process (Grant and Weiblen, 1971; Tracy et al., 1976). This feature of relaxed and homogenised zoning has been observed in most of the garnets examined from sillimanite- muscovite to sillimanite-K-feldspar grade rocks.

The interpretation of zoning relies basically on the assumption that zoning in garnet represents a growth history, type of exchange reaction and condition of metamorphism at which garnet has grown. For example, grossularite content in almandine garnet might be controlled by the presence of calcium-bearing phases like plagioclase, epidote, calcite etc. in the assemblage. Sometimes continuous reaction involving plagioclase and garnet produce an antithetic zoning in the two minerals (Crawford, 1977). This phenomenon of antithetic zoning sometimes observed in a few samples.

The normal growth zoning, observed in garnet to staurolite-kyanite grade rocks can be compared with temperature data (see Tables 5.4 and 5.5). Temperature in these grades increases from garnet core to rim with the corresponding increase in Mg/Fe ratio towards rim, suggesting that this zoning has developed during growth. In higher grades, higher Mg and lower Mn in core is correlatable with the high temperature core data. After considering the reactions 4.7 and 4.8 these data, it is suggested that garnet has grown at high temperature and readjusted during cooling due to post-growth volume diffusion. Fe and Mn increases towards rim and is clearly evidenced from the reduced P-T data. The reverse zoning in garnet rim is generally independent of shape of garnet poikiloblasts and can also be seen as evidence for minor partial resorption of garnet (e.g., sillimanite grade rocks). The decrease in Mg/Fe ratio at the garnet edge indicates decreasing temperature (cooling) and readjustment in composition during post-growth diffusion (Tracy, 1982; St-Onge, 1987). This

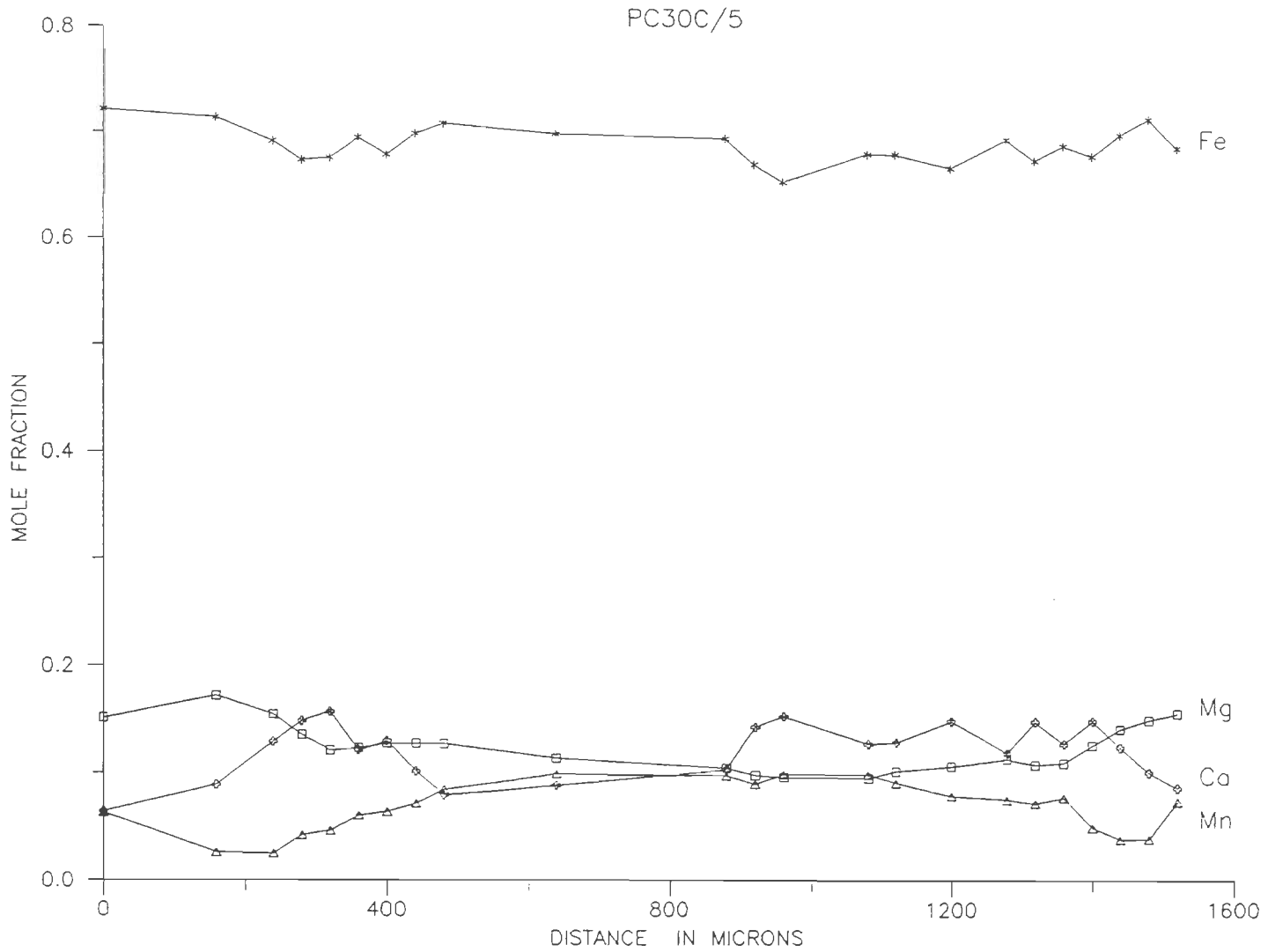


FIGURE 4.30 : Garnet zoning profile (Rim-Core-Rim) for staurolite-kyanite grade, Sample PC30C/5.

A53/62B

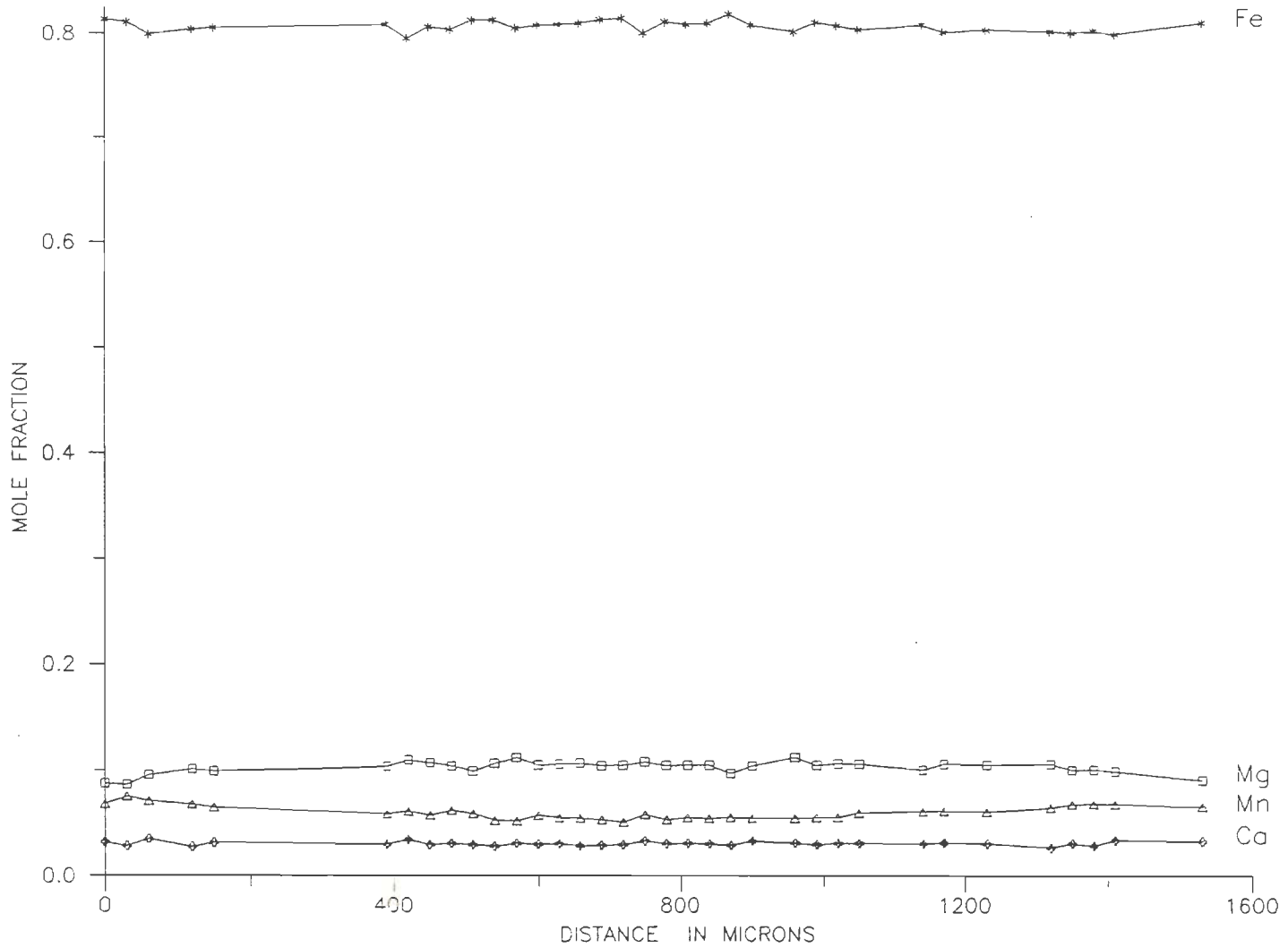


FIGURE 4.31 : Garnet zoning profile (Rim-Core-Rim) for sillimanite-muscovite grade. Sample A53/62B.

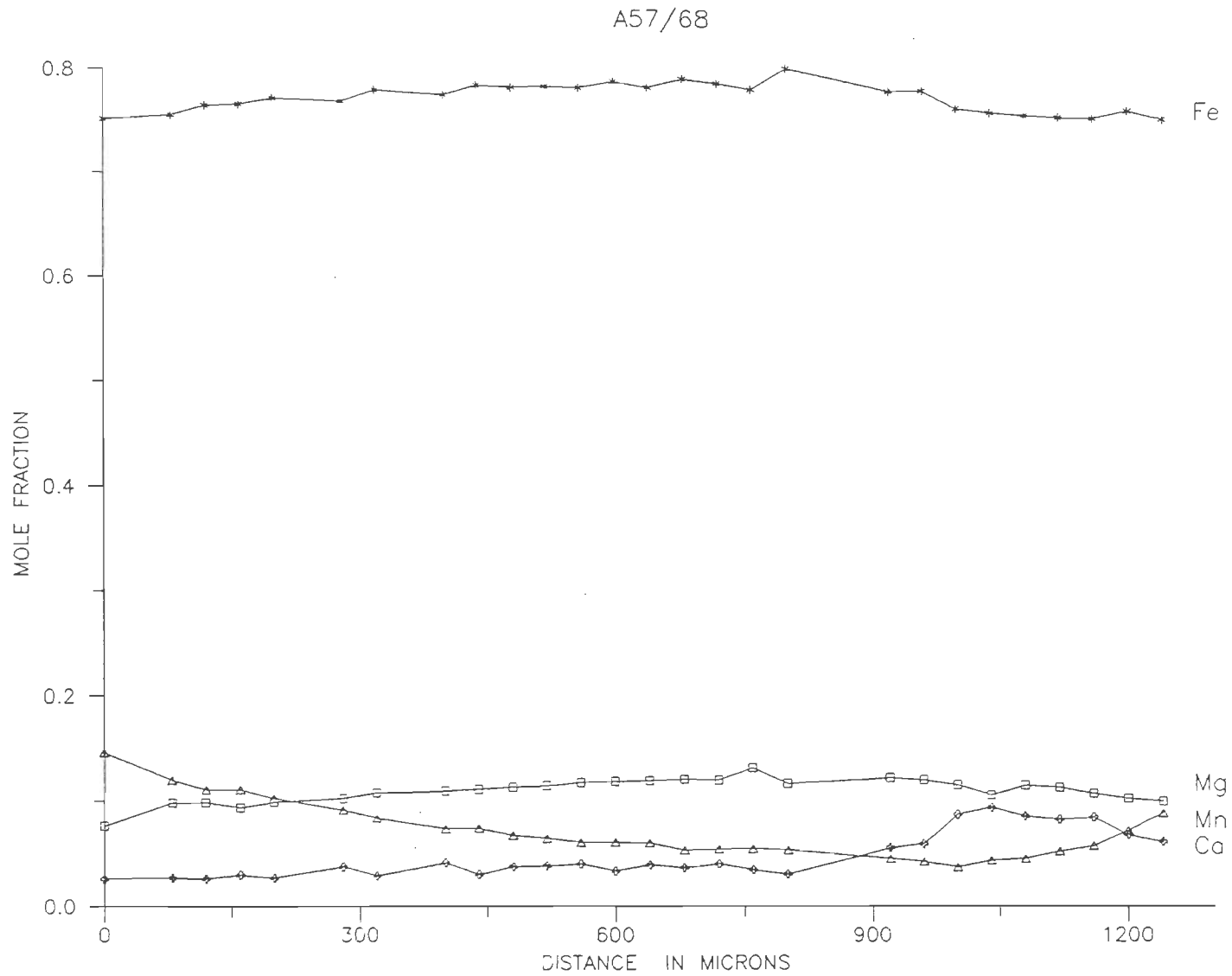


FIGURE 4.32 : Garnet zoning profile (Rim-Core-Rim) for sillimanite-K-feldspar grade. Sample A57/68.

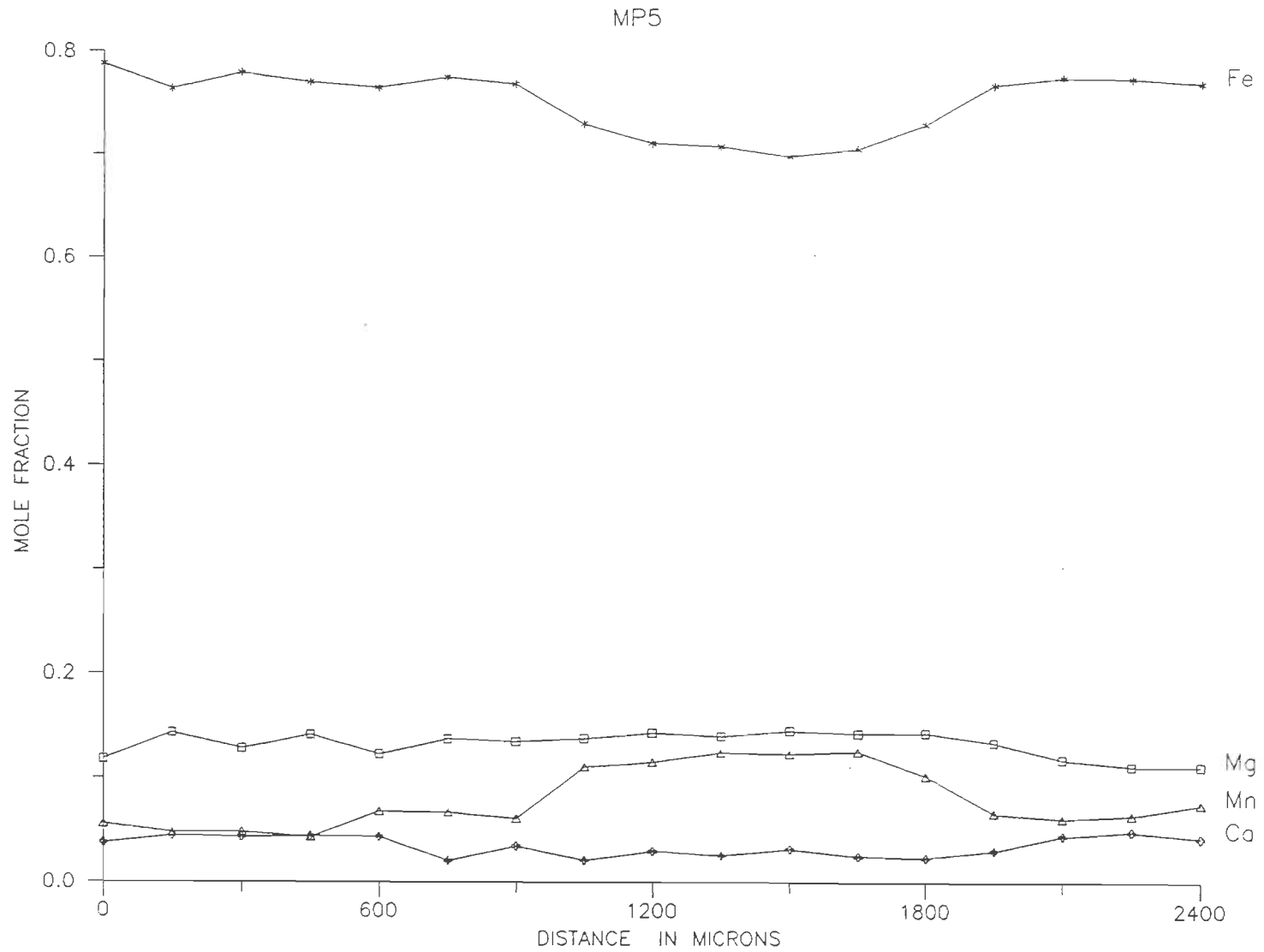


FIGURE 4.33 : Garnet zoning profile (Rim-Core-Rim) for sillimanite-muscovite grade. Sample MP5.

is marked often by the increase in Mn and Fe/Mg ratio towards the edge without much change in Ca. The irregular outline of garnet also indicates a late-stage reaction involving resorption of garnet and the formation of biotite. According to Tracy et al. (1976), growth of biotite is responsible for the selective release of Mg, while retaining Fe and Mn contents in garnet.

4.8 DISCUSSION

Mineral assemblages and reactions, observed in different metamorphic grades, clearly demonstrate that the studied region has undergone Barrovian-type metamorphism. In Chenab-Bhot Nala section, surrounding the Kishtwar Window and just above the MCT, the HHC seem to have been affected by different degrees of metamorphism. On the SW side, the rocks contain primary chlorite, garnet, muscovite and biotite. Presence of primary chlorite, growth of syntectonic garnet and biotite suggest that the latter assemblage has been formed by the Fe-Mg-Mn continuous reaction (4.1; section 4.4.1). The growth of garnet is evidenced by the normal growth zoning in this grade (Fig. 4.28).

Towards NE of the Kishtwar Window and in Suru Valley, rocks contain substantial amount of kyanite and very little staurolite with an increase and decrease in modal biotite and muscovite. Texture, modal assemblage and chemistry of the minerals suggest that staurolite and kyanite have formed by the continuous reactions (4.3) and (4.4). The scanty presence of staurolite in these samples is possibly due to the effect of Mg-rich composition and higher temperature conditions (Pigage and

Greenwood, 1982; Thompson, 1976). The Mg enrichment is envisaged in garnet rim and biotite of this grade (Figs. 4.9 and 4.10). The higher P-T conditions attained by these rocks (see temperature data in Table 5.4) suggest the disappearance of staurolite from this grade (Pigage and Greenwood, 1982).

Further NE towards the centre of the HHC and also along a portion of Parkachik Ringdom section, metamorphism increases to sillimanite - muscovite and sillimanite - K-feldspar grade conditions. However, in Suru Valley only sillimanite - muscovite grade rocks are observed. The increase in metamorphic condition is envisaged by (i) the absence of staurolite, (ii) formation of sillimanite through polymorphic transformation and by continuous/discontinuous reactions such as reaction 4.6, 4.8, 4.9 etc. (section 4.4), (iii) three phase compositional shift with increase in temperature, (iv) prograde P-T path and (v) relaxed garnet zoning with Mg and Mn reversal at garnet edge (Holdaway, 1971; Thompson, 1976; Tracy et al., 1976; Winkler, 1979; Tracy, 1982; St-Onge, 1987; Yardley, 1989). In highest grade, muscovite is completely lacking and indicate the development of higher grade rocks during prograde metamorphism. The P-T data obtained using garnet core (see Chapter-5) confirm the above observations. Biotite shows epitaxial growth of sillimanite and the development of secondary muscovite is observed in a few of the highest grade rocks (Chapter-3). The rim P-T data suggest that fibrolite development and secondary muscovite have probably taken place during this period of cooling and uplift. Further north towards ZSZ, the HHC rocks show decrease in metamorphism to staurolite-

kyanite grade in Mulung Tokpo Section. The mineral assemblages, the reactions and the P-T data are very much similar to those which have been observed on the other side of this section.

Analysis of coexisting garnet-biotite (garnet rim and biotite of matrix) in different metamorphic grades demonstrate the development of mineral assemblages during prograde and in the cooling and uplift stages. It is suggested that Fe/Fe+Mg ratio in garnet and biotite increases with metamorphic grade (Spear, 1989) and is documented in this area. However, the garnet grade samples, particularly of garnet rim and biotite, show more Fe/Fe+Mg ratio than the staurolite-kyanite grade. This could be due to temperature increase, which possibly has taken place by thermal relaxation of higher grade rocks at the time of cooling and uplift.

Syntectonic garnet (garnet-I) shows evidences of both growth and diffusional zoning. Garnet and staurolite-kyanite grades samples reveal bell-shaped Mn and Ca profile with enrichment of Fe and Mg at the rim. This is typical of the normal growth zoning, as has been observed in similar metamorphic grades elsewhere (e.g., Tracy et al., 1976; Banno et al., 1986). However, garnet shows some relaxation in the bell-shaped profile in the higher temperature side of the staurolite-kyanite grade. This relaxation is probably due to modification of growth zoning by volume diffusion at elevated temperature. However, the rim shows reversal in Mn and to a lesser extent in Mg suggesting that the rim has been formed by the breakdown of chlorite (Kretz,

1973). In the higher grades, garnet-I reveals relaxed reverse zoning, having Fe-Mg-rich core and Mn-rich rim. This reversal in the garnet appears to be of post-growth volume diffusion rather than by continuous hydration reaction (Tracy et al., 1976). Decrease in the Mg/Fe ratio towards the rim in these garnets suggests that rim has developed at reduced temperature during the uplift and cooling stages (Tracy, 1982).

CHAPTER - 5

GEO THERMOMETRY AND GEOBAROMETRY

5.1 INTRODUCTION

The regional metamorphic condition is constrained by mineral paragenesis, related metamorphic facies and estimation of pressure-temperature using relevant exchange or discontinuous mineral reactions for which thermochemical and phase equilibria data are available (Robie et al., 1966, 1978; Helgason et al., 1978; Winkler, 1979; Turner, 1981; Ferry, 1982; Berman, 1988). Earlier studies emphasised more on the appearance/disappearance of index minerals and metamorphic facies, where the mineral assemblages are repeated in space and time for rocks of similar chemical composition to characterise metamorphic conditions (cf., Winkler, 1979; Turner, 1981). However, in recent years, P-T condition of metamorphism is evaluated by analysing chemically the equilibrium mineral assemblages. For doing this electron microprobe analysis of individual minerals, availability of thermochemical data on large number of minerals and phase equilibria study of specific mineral systems/reactions are essential.

5.2 THERMOMETRY

The metamorphic temperature is evaluated for the exchange reaction on the basis of intracrystalline distribution of elements between sites of the same phase or intercrystalline distribution of elements between two or more coexisting phases. The exchange reactions which show very little volume change,

large entropy and insensitivity to pressure are ideal thermometers. In such reactions, significant redistribution of elements takes place between the coexisting minerals due to change in temperature (Essene, 1982). Also, the intercrystalline cation distribution does not easily reset during cooling and constitutes a potential geothermometer. Refractory phase such as garnet is less likely to reset during cooling and is best used for exchange thermometer. In the intercrystalline exchange reaction, elements like Ca-Mg-Fe²⁺ between garnet-biotite, garnet-clinopyroxene etc. are considered for temperature calculation. However, the main problem for element like iron is that all the Fe is analysed as Fe²⁺ by microprobe analysis, which may not be true in some phases.

5.3 BAROMETRY

The metamorphic pressure is calculated using mainly the solid-solid reactions, as these reactions are not dependent on the composition or the presence of a fluid phase. Although solid-solid reactions generally are temperature and pressure dependent, most of the reactions are primarily used for pressure calculation, as the temperature is determined by exchange reaction. The selection of suitable reaction for pressure calculation is based on large ΔV and ΔH values. Many of the commonly applied reactions involve minerals like plagioclase, pyroxene, garnet, sillimanite/kyanite, quartz, rutile, ilmenite etc. Since most of the minerals involved in the reactions are complex solid solutions, the pressure calculation is dependent on

standard thermodynamic and well constrained activity-composition data of the participating minerals in a reaction (Essene, 1982).

Expression of mole fraction and activity - composition relationship for geothermobarometry for garnet, biotite, muscovite and plagioclase are given in Tables 5.1 and 5.2 respectively.

5.4 THERMODYNAMIC BASIS

At equilibrium, the overall Gibbs free-energy change (ΔG) of a mineral reaction is expressed as:

$$\Delta G_{(P,T)} = \Delta H_{(1,T)} - T \Delta S_{(1,T)} + \Delta V^{\circ}(P-1) + RT \ln K = 0 \quad \text{--- (5.1)}$$

where

$\Delta H_{(1,T)}$ = Difference in enthalpy between the products and reactants of a reaction at 1 bar and temperature of interest.

$\Delta S_{(1,T)}$ = Difference in entropy between the products and reactants of a reaction at 1 bar and temperature of interest.

ΔV° = Difference in volume between the products and reactants of a reaction at 1 bar, 298°K.

K = Equilibrium constant.

T = Temperature in °K.

P = Pressure in bars.

R = Gas constant (1.987 calories).

If mixing is ideal, then

$$RT \ln K = RT \ln K_D \quad \text{--- (5.2)}$$

i.e., equilibrium constant is equal to distribution coefficient and if the mixing is non-ideal, then

$$RT \ln K = RT \ln K_D \cdot K' \quad \text{---(5.3)}$$

where K' is activity coefficient (γ). The value of γ is obtained from the Margules parameter (W_a) determined experimentally by binary solvus or heat of solution data. Various models have been proposed to derive γ , the simplest one is the regular solution model with symmetrical solvus (e.g. Newton and Haselton, 1981) or subregular solution model with asymmetric solvus (e.g. Hodges and Crowley, 1985).

For geothermobarometry, equation (1) can be rearranged as

$$T = \frac{-\Delta H - (P-1)\Delta V}{R \ln K_D - \Delta S} \quad \text{---(5.4)}$$

$$P = 1 + \frac{T(\Delta S - R \ln K_D) - \Delta H}{\Delta V} \quad \text{---(5.5)}$$

where P is in bars, T in °K, ΔH and ΔS in calories, ΔV in calories/bar and $R = 1.987$ calories.

5.5 APPLICATION OF GEOTHERMOBAROMETRY

As already mentioned, the application of geothermometry and geobarometry is based on the equilibrium mineral assemblages for which well constrained thermodynamic and phase equilibria data are available. In the present area of investigation, the metamorphic rocks are made up of metapelite, metacalcareous and

TABLE 5.1 EXPRESSION OF MOLE FRACTIONS FOR GEOTHERMOBAROMETRY

Minerals	Mole Fractions	
Garnet	X_{Fe}	$= \frac{Fe}{Fe + Mg + Mn + Ca}$
	X_{Mg}	$= \frac{Mg}{Fe + Mg + Mn + Ca}$
	X_{Mn}	$= \frac{Mn}{Fe + Mg + Mn + Ca}$
	X_{Ca}	$= \frac{Ca}{Fe + Mg + Mn + Ca}$
Biotite	X_{Fe}	$= \frac{Fe}{Fe + Mg + Mn + Al^{VI} + Ti}$
	X_{Mg}	$= \frac{Mg}{Fe + Mg + Mn + Al^{VI} + Ti}$
	$X_{Al^{VI}}$	$= \frac{Al^{VI}}{Fe + Mg + Mn + Al^{VI} + Ti}$
	X_{Ti}	$= \frac{Ti}{Fe + Mg + Mn + Al^{VI} + Ti}$
Muscovite	X_{Fe}	$= \frac{Fe}{Fe + Mg + Mn + Al^{VI} + Ti}$
	X_{Mg}	$= \frac{Mg}{Fe + Mg + Mn + Al^{VI} + Ti}$

TABLE 5.1 - continued

$$X_{Al^{VI}} = \frac{Al^{VI}}{Fe + Mg + Mn + Al^{VI} + Ti}$$

$$X_K = \frac{K}{K + Na + Ca}$$

$$X_{Na} = \frac{Na}{K + Na + Ca}$$

$$X_{Mus} = X_K \cdot (X_{Al^{VI}})^2$$

$$X_{Pa} = X_{Na} \cdot (X_{Al^{VI}})^2$$

where Mus - Muscovite; Pa - Paragonite.

Plagioclase

$$X_{An} = \frac{Ca}{K + Na + Ca}$$

where An - Anorthite

TABLE 5.2 EXPRESSION OF ACTIVITY - COMPOSITION RELATIONSHIPS FOR GEOTHERMOBAROMETRY

Minerals	Activity - Composition relationships
Garnet	$a_{Ca} = X_{Ca} \cdot \exp \left[\frac{(3300-1.5T) (X_{Mg}^2 + X_{Fe} \cdot X_{Mg} + X_{Mg} \cdot X_{Mn})}{RT} \right]$ $a_{Fe} = X_{Fe} \cdot \exp \left[\frac{(1.5T-3300) X_{Ca} \cdot X_{Mg}}{RT} \right]$
Biotite	$a_{Fe} = X_{Fe}$
Muscovite	$a_{Mus} = X_{Mus} \cdot \exp \left[\frac{X_{Pa}^2 (W_{Mus} + 2W_{Mus} (W_{Pa} - W_{Mus}))}{RT} \right]$
where	$W_{Pa} = 2923.1 + 0.1590P(\text{bar}) + 0.1698T(^{\circ}\text{K})$ $W_{Mus} = 4650.1 + 0.1090P(\text{bar}) + 0.3954T(^{\circ}\text{K})$
Plagioclase	<p>(a) Newton and Haselton (1981):</p> $a_{Pa} = \frac{X_{An}(1+X_{An})^2}{2} \cdot \exp \left[\frac{(1-X_{An})^2 (2050+9392X_{An})}{RT} \right]$ <p>(b) Hodges and Crowley (1985):</p> $a_{An} = X_{An} \cdot \exp (610.34/T(^{\circ}\text{K}) - 0.3837)$

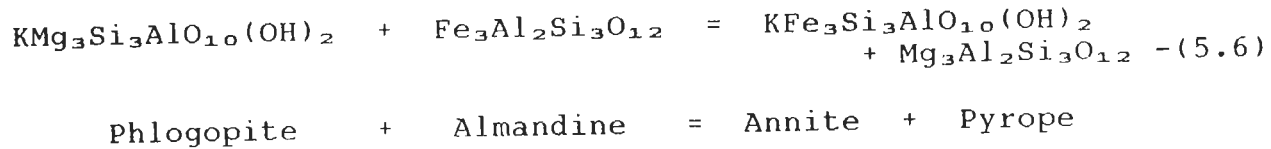
quartzite rocks. However, the metapelite is the predominant rock type in this region and is considered for geothermobarometric work. The common minerals in this rock include biotite, muscovite, garnet, staurolite, sillimanite/kyanite, plagioclase and K-feldspar. Since the condition of metamorphism in the study area is ranging from upper garnet to sillimanite-K-feldspar grades (Chapter-3), it is appropriate to use the assemblages such as garnet-biotite, garnet-plagioclase, plagioclase-muscovite, biotite-muscovite for the geothermometry and garnet-plagioclase-sillimanite/kyanite-quartz, garnet-plagioclase-biotite-muscovite and garnet-rutile-ilmenite-plagioclase-quartz for geobarometry. Among the various geothermometers mentioned, only garnet-biotite thermometer is well constrained (Ferry and Spear, 1978; Ganguly and Saxena, 1984) and is used to calculate temperature. Similarly, first two assemblages are used for pressure calculation, as these are the common assemblages in these rocks. Also, the opaque minerals are present as inclusions in garnet and not in the matrix. Therefore, their usage is very much restricted in the calculation. The geothermobarometric equations, used for P-T estimation, are given in Table 5.3.

5.5.1 Garnet - biotite geothermometer (GB):

The garnet - biotite (GB) geothermometer has been applied widely as this is a common assemblage in pelitic rocks of almost all grades. This geothermometer have been calibrated empirically and through phase equilibria experiments by number of workers such as Thompson (1976), Goldman and Albee (1977), Ferry and

Spear (1978), Pigage and Greenwood (1982), Hodges and Spear (1982), Perchuk and Lavrent'eva (1983), Ganguly and Saxena (1984) and Indares and Martignole (1985).

The intercrystalline exchange reaction is expressed as:

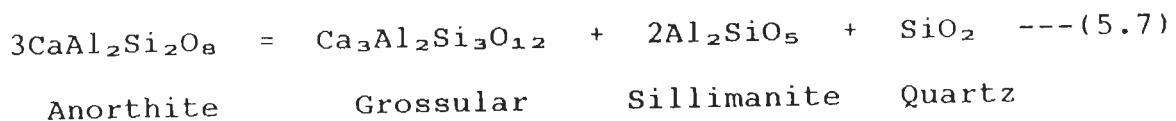


and the $K_D = (\text{Fe}/\text{Mg})^{\text{Bio}} / (\text{Fe}/\text{Mg})^{\text{Qtz}}$.

Among the various calibrations of this geothermometer, temperature is estimated using only the models of Thompson (1976), Ferry and Spear (1978), Hodges and Spear (1982) and Ganguly and Saxena (1984). These calibrations are more suitable with regard to their activities and effects of minor elements on the distribution coefficient and for the range of metamorphic condition observed in this area (Tables 5.1, 5.2 and 5.3).

5.5.2 Geobarometry

5.5.2-i Garnet - plagioclase - Al_2SiO_5 - quartz (GASP): This assemblage is widely used as a barometer due to the common occurrence of these minerals in medium- to high-grade rocks. Ghent (1976) has developed the experimental calibration for the end-member reaction:



The activity of grossular content in garnet is considered to be

TABLE 5.3 GEOTHERMOBAROMETRIC EQUATIONS

GEOTHERMOMETRY

1. Thompson (1976):

$$T = \frac{2740 + 0.0234 (P-1)}{1.560 + \ln K_D}$$

$$\text{where } K_D = (\text{Fe/Mg})^{\text{Gt}} \cdot (\text{Mg/Fe})^{\text{Bio}}$$

2. Ferry and Spear (1978):

$$T = \frac{12454 + 0.057P}{4.662 - 3R \ln K}$$

$$\text{where } K = (\text{Mg/Fe})^{\text{Gt}} / (\text{Mg/Fe})^{\text{Bio}}$$

3. Hodges and Spear (1982):

$$T = \frac{12454 + 0.057P}{4.662 - 3R \ln K}$$

$$\text{where } K = K_D \cdot \exp \left[\frac{(3300 - 1.5T) (X_{\text{Ca}}^2 + X_{\text{Fe}} \cdot X_{\text{Ca}} + X_{\text{Ca}} \cdot X_{\text{Mn}} + X_{\text{Mg}} \cdot X_{\text{Ca}})^{\text{Gt}}}{RT} \right]$$

$$K_D = (\text{Fe/Mg})^{\text{Gt}} \cdot (\text{Mg/Fe})^{\text{Bio}}$$

4. Ganguly and Saxena (1984):

$$T = \frac{W_{\text{FeMg}} ((X_{\text{Fe}}^{\text{Gt}} - X_{\text{Mg}}^{\text{Gt}}) - 0.8) + 1510 (X_{\text{Ca}}^{\text{Gt}} - X_{\text{Mn}}^{\text{Gt}}) + 2089 + 0.00956P}{0.782 + \ln K}$$

$$\text{where } W_{\text{FeMg}} = W^{\text{Fe-Mg}} (\text{Mg}/(\text{Mg}+\text{Fe}))^{\text{Gt}} + W^{\text{Mg-Fe}} (\text{Fe}/(\text{Mg}+\text{Fe}))^{\text{Gt}}$$

$$W^{\text{Fe-Mg}} = 200$$

$$W^{\text{Mg-Fe}} = 2500 \pm 500$$

$$K = (\text{Mg/Fe})^{\text{Gt}} / (\text{Mg/Fe})^{\text{Bio}}$$

TABLE 5.3 - continued

GEOBAROMETRY

1. Newton and Haselton (1981):

For Sillimanite:

$$P = 1 + \frac{T(36.7 + 3R \ln K) - 13339}{1.582}$$

For Kyanite:

$$P = 1 + \frac{T(31.058 + 3R \ln K) - 10005}{1.305}$$

$$\text{where } K = a_{Ca^{Gt}} / a_{An^{Plg}}$$

2. Hodges and Spear (1982):

$$P = \frac{T(30.786 - 3R \ln K) - 9192}{1.3045}$$

$$\text{where } K = a_{An^{Plg}} / a_{Ca^{Gt}}$$

$$a_{An^{Plg}} = X_{An^{Plg}} \cdot X_{An^{Plg}} = 2 \cdot X_{An^{Plg}}$$

3. Ghent and Stout (1984):

$$P = 1 + \frac{T(14.789 - R \ln K) - 4472}{0.7323}$$

$$\text{where } K = \frac{a_{An^{Plg}}}{(a_{Fe^{Gt}})^2 \cdot a_{Ca^{Gt}}}$$

4. Hodges and Crowley (1985):

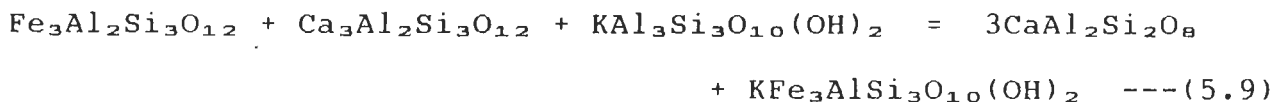
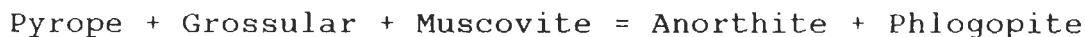
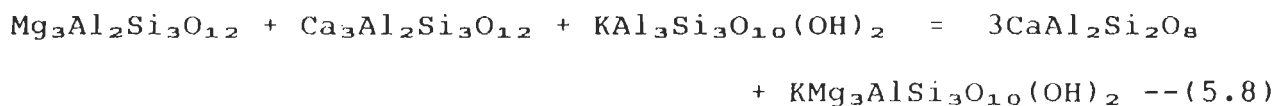
$$P = 1 + \frac{T(12.985 - R \ln K) - 5574}{0.6007 + \left[\frac{(X_{Pa}^{Mu})^{Mu} \cdot (0.109 + 2(X_{Mu}^{Mu})^{Mu} = 0.268)}{3} \right]}$$

$$\text{where } K = \frac{a_{An^{Plg}} \cdot a_{Fe^{Bio}}}{a_{Fe^{Gt}} \cdot a_{Ca^{Gt}} \cdot (a_{Mu}^{0.33})^{Mu}}$$

where T = in °K; P = in bars and R = 1.987 calories

its mole fraction assuming ideal mixing and the activity coefficient of anorthite is taken as 1.276 (Orville 1972) for calculating pressure. However, this model has been modified later by Newton and Haselton (1981), Hodges and Spear (1982) and Koziol and Newton (1988) using different activities for grossular in garnet and anorthite in plagioclase. For the pressure calculation, only Newton and Haselton (1981) and Hodges and Spear (1982) models have been used because of their better activity models (Table 5.2). Though Koziol and Newton (1988) calibration is based on tightly reversed experiments, it gives a higher pressure, which seem to be rather unrealistic for this region.

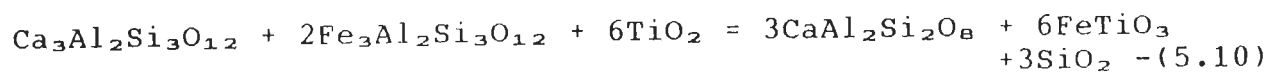
5.5.2-ii Garnet - muscovite - plagioclase - biotite; Ghent and Stout (1981) developed alternative barometers for the medium grade metamorphic condition, using the commonly occurring garnet-plagioclase-biotite-muscovite assemblage of the pelitic rock. The end-member reactions for this assemblage are:



Ghent and Stout (1981) calibrated these equilibria from the K_D data of natural assemblage and using pressure and temperature values derived from GASP (Ghent et al., 1979) and GB (Ferry and

Spear, 1978) equilibria. This model was modified by Hodges and Crowley (1985) by solving the uncertainties through empirical calibration. However, they concluded that much of the uncertainties in P-T estimation stem from uncertainties in enthalpy and entropy rather than by microprobe analysis.

5.5.2-iii Garnet - rutile - plagioclase - ilmenite - quartz: The end member reaction for the above mineral assemblage is



Grossular + Almandine + Rutile = Anorthite + Ilmenite + Quartz

Ghent and Stout (1984) empirically derived this geobarometer, using the pressures obtained from GASP (Ghent et al., 1979) and almandine - rutile - Al_2SiO_5 - ilmenite - quartz equilibria (Bohlen et al., 1983).

Among the various geobarometers mentioned, Newton and Haselton (1981) model has been applied for the rocks, having garnet - plagioclase - sillimanite/kyanite - quartz assemblage. In the absence of aluminosilicate, model for garnet - plagioclase - biotite - muscovite assemblage (Hodges and Crowley, 1985) has been used. However, both the barometers are applied in medium grade rocks, due to the presence of all the required minerals in the assemblage (Table 5.3).

5.6 PROCEDURE FOR GEOTHERMOBAROMETRY

As mentioned earlier, well-calibrated systems were applied for the temperature and pressure calculations. In the study area,

many polished thin sections of all lithologies were examined under transmitted and reflected light to ascertain texturally the equilibrium mineral assemblage for analysis. Altered and retrograde samples were discarded for the analysis. Metamorphic textures were used to distinguish different generations of garnet, mica etc. and the probe analysis was carried out for the minerals of different generations. In each thin section, many grains belong to the same generation of a particular mineral. In each grain, number of points were analysed to check the compositional variation. All the analysed points were checked carefully for the stoichiometry and the points with incorrect analysis were discarded in the P-T calculation. For the zoned minerals like garnet, analysis was carried out both in rim and core and sometimes along two or three lines across the grain. The number of rim and core points were averaged after analysing all the points individually.

5.7 GEOTHERMOBAROMETRIC RESULTS

As described earlier in Chapter-3, both syntectonic (Garnet I; Fig. 3.4) and post-tectonic garnets (Garnet II; Fig. 3.5c) have been analysed for the core and rim compositions with other coexisting phases like biotite, plagioclase, etc. and the data have been utilised to calculate the pressure and temperature. The mineral inclusions, such as biotite, plagioclase, sillimanite / kyanite, quartz etc. commonly present in syntectonic garnet core, are used for the core P-T estimation (e.g., St-Onge, 1987). P-T data using different calibrations for the Chenab - Bhot Nala

section and Suru - Doda Valleys are presented in Tables 5.4 and 5.5. In general, the P-T data obtained for core and rim compositions of syntectonic garnet (Garnet - I) are considerably different in each sample and of all the metamorphic grades, as they developed during D₂ deformation and main M₂ metamorphic event. However, the post-tectonic garnet (Garnet - II), developed during late- to post-D₂ deformation shows more or less similar P-T values. The reasonably acceptable P-T data for each sample, decided on the basis of the assemblage and its effect on the activities of the individual calibrations, are enlightened in Tables 5.4 and 5.5. The garnet core P-T data are used to constrain the prograde metamorphic condition (St-Onge, 1987; Spear, 1989) and the rim data to study the effect of cooling and uplift history.

5.7.1 Chenab - Bhot Nala Section:

1) In this section, the MCT consists mainly of pelites having Ms-Bi-Qz-Chl-Gt-Pl-Op assemblage. Garnet - I shows rim temperature of 550-670°C and pressure of 7.50 and 9.00 kb (A37/43, A41/48, A45/50) (Table 5.4). Garnet - II shows similar P-T values as that of garnet - I rim in this grade.

2) In the SW direction, garnet grade rocks occur very close to the Kishtwar Window and the staurolite-kyanite grade rocks are found, while moving further westward towards Chhatru (Fig. 2.1). Garnet grade assemblage includes Gt-Bi-Ms-Pl-Q-Chl, whereas in staurolite-kyanite grade chlorite disappears completely and contains mainly Gt-Bi-Ms-St-Ky / Sill-Q-Pl assemblage. The

TABLE 5.4 P-T DATA FOR CHENAB - BHOT NALA SAMPLES

S.NO.	SAMPLE NO.	GARNET-I								GARNET-II			
		TEMPERATURE (°C)				PRESSURE (Kbar)				TEMPERATURE (°C)		PRESSURE (Kbar)	
		CORE		RIM		CORE		RIM					
FS	GS	FS	GS	HC	NH	HC	NH	PS	GS	HC	NH		
1	KC21/23	-	-	(461 ±5)	491 ±9	-	-	(10.95 ±.14)	-	-	-	-	
2	KC23/26	-	-	408 ±10	(474 ±13)	-	-	(9.13 ±.59)	-	-	-	-	
3	T3/5	-	-	585 ±18	(601 ±23)	-	-	(6.52 ±.44)	-	-	-	-	
4	KC26/28	-	-	(582 ±16)	576 ±20	-	-	-	-	-	-	-	
5	T4/6	-	-	(582 ±14)	567 ±17	-	-	6.61 ±.21	(6.82 ±.19)	674 ±15	(627 ±22)	(7.68 ±.33)	8.15 ±.39
6	KC6/7	-	-	(578 ±18)	683 ±20	-	-	(8.00 ±.42)	11.19 ±.32	-	-	-	-
7	KC4/5	-	-	(653 ±11)	630 ±8	-	-	(10.12 ±.34)	11.20 ±.44	-	-	-	-
8	KC1/1	-	-	(623 ±17)	624 ±16	-	-	-	(9.84 ±.27)	-	-	-	-
9	T21/28	-	-	(635 ±22)	659 ±25	-	-	5.85 ±.34	(5.84 ±.39)	-	-	-	-
10	T10/16	-	-	(556 ±8)	552 ±9	-	-	-	(7.79 ±19)	-	-	-	-
11	A45/50	-	-	558 ±18	(562 ±17)	-	-	(6.94 ±.18)	7.51 ±.43	-	-	-	-
12	A37/43	-	-	508 ±8	(552 ±9)	-	-	(7.46 ±.14)	8.22 ±.22	496 ±16	(543 ±21)	(6.94 ±.26)	7.64 ±.31
13	A41/48	-	-	671 ±19	(655 ±23)	-	-	(9.25 ±.32)	9.55 ±.53	676 ±19	(678 ±22)	(10.11 ±.30)	11.10 ±.50
14	A46/51	(507 ±5)	490 ±11	(601 ±20)	600 ±19	-	-	(7.57 ±.39)	7.75 ±.44	(619 ±11)	612 ±9	(8.03 ±.19)	8.28 ±.24
15	A47/54	-	-	686 ±15	(651 ±18)	-	-	-	(10.74 ±.38)	750 ±10	(676 ±6)	7.89 ±.33	(10.39 ±.23)

TABLE 5.4 - continued

S.NO.	SAMPLE NO.	GARNET-I								GARNET-II			
		TEMPERATURE (°C)				PRESSURE (Kbar)				TEMPERATURE (°C)		PRESSURE (Kbar)	
		CORE		RIM		CORE		RIM		FS	GS	HC	NH
FS	GS	FS	GS	HC	NH	HC	NH						
16	A47/55	(568 ±11)	550 ±17	679 ±12	(651 ±15)	-	-	(8.74 ±.25)	9.07 ±.58	655 ±14	(631 ±21)	(8.93 ±.47)	9.22 ±.79
17	A47/56	-	-	(591 ±11)	548 ±15	-	-	(7.45 ±.21)	7.39 ±.36	(607 ±19)	550 ±28	(6.23 ±.18)	5.90 ±.47
18	092/110	-	-	(588 ±9)	672 ±9	-	-	(8.55 ±.18)	10.02 ±.55	-	-	-	-
19	093/111A	531 ±7	(556 ±12)	559 ±18	(611 ±17)	-	-	(7.90 ±.42)	8.63 ±.38	-	-	-	-
20	093/111B	-	-	531 ±15	(595 ±11)	-	-	(7.50 ±.23)	8.27 ±.26	-	-	-	-
21	093/111C	-	-	593 ±5	(633 ±7)	-	-	(8.85 ±.11)	9.68 ±.20	-	-	-	-
22	093/112B	-	-	597 ±18	(649 ±19)	-	-	(8.35 ±.26)	11.46 ±.38	-	-	-	-
23	A49/59	-	-	-	-	-	-	-	-	(524 ±15)	507 ±18	4.89 ±.31	(5.02 ±.34)
24	A53/62B	-	-	(639 ±25)	666 ±30	-	-	5.44 ±.17	(5.92 ±.21)	-	-	-	-
25	076/85	-	-	-	-	-	-	-	-	610 ±15	(620 ±21)	5.93 ±.38	(5.84 ±.66)
26	077/90	-	-	-	-	-	-	-	-	606 ±20	(628 ±27)	5.98 ±.31	(5.80 ±.63)
27	086/103	(517 ±12)	544 ±15	(649 ±32)	681 ±44	-	-	5.09 ±.23	(5.44 ±.40)	609 ±21	(639 ±26)	5.43 ±.51	(5.62 ±.37)
28	080/95	-	-	-	-	-	-	-	-	(630 ±8)	684 ±10	6.21 ±.23	(7.03 ±.25)
29	080/96	(702 ±39)	763 ±42	(654 ±27)	715 ±36	-	-	7.20 ±.41	(8.35 ±.23)	-	-	-	-
30	A56/66	-	-	-	-	-	-	-	-	542 ±14	(585 ±19)	4.39 ±.26	(4.50 ±.16)

TABLE 5.4 - continued

S.NO.	SAMPLE NO.	GARNET-I								GARNET-II			
		TEMPERATURE (°C)				PRESSURE (Kbar)				TEMPERATURE (°C)		PRESSURE (Kbar)	
		CORE		RIM		CORE		RIM					
FS	GS	FS	GS	HC	NH	HC	NH	FS	GS	HC	NH		
31	A80/111	-	-	(617 ±20)	602 ±30	-	-	7.99 ±.55	(7.94 ±.63)	656 ±15	(615 ±24)	8.20 ±.44	(8.10 ±.51)
32	A57/68	(736 ±9)	737 ±12	611 ±14	(662 ±16)	7.58 ±.31	(7.97 ±.28)	(7.43 ±.19)	8.16 ±.25	-	-	-	-
33	U64/67	-	-	(643 ±23)	664 ±28	-	-	(5.19 ±.40)	5.04 ±.49	-	-	-	-
34	U67/70	-	-	-	-	-	-	-	-	604 ±20	(658 ±23)	5.12 ±.50	(5.44 ±.55)
35	U60/63	-	-	(665 ±22)	718 ±27	-	-	6.11 ±.17	(6.56 ±.30)	-	-	-	-
36	A65/78	(778 ±31)	770 ±40	(663 ±19)	695 ±22	9.11 ±.42	(9.30 ±.62)	6.41 ±.36	(6.49 ±.37)	-	-	-	-
37	A67/86	837 ±20	(773 ±25)	636 ±19	(651 ±22)	9.30 ±.56	(10.92 ±.45)	(6.51 ±.18)	7.14 ±.27	-	-	-	-
38	U57/60	-	-	-	-	-	-	-	-	650 ±26	(655 ±34)	4.60 ±.13	(5.23 ±.22)
39	U26/28	-	-	-	-	-	-	-	-	608 ±10	(595 ±13)	(4.48 ±.39)	3.53 ±.31
40	U33/35	(734 ±18)	740 ±22	575 ±17	(623 ±20)	-	-	5.15 ±.23	(5.08 ±.43)	-	-	-	-
41	U52/55	(684 ±21)	703 ±21	(601 ±14)	662 ±19	-	-	4.43 ±.46	(4.55 ±.52)	-	-	-	-
42	A74/97	(601 ±35)	611 ±43	-	-	-	-	-	-	672 ±20	(678 ±22)	(4.16 ±.27)	2.89 ±.32
43	U28/30	(758 ±23)	762 ±28	535 ±32	(576 ±38)	-	-	-	-	-	-	-	-
44	U29/31	(659 ±31)	660 ±32	(634 ±2)	675 ±26	-	-	-	(5.63 ±.51)	-	-	-	-
45	U48/51	(688 ±16)	686 ±20	(608 ±18)	654 ±21	-	-	5.75 ±.47	(6.71 ±.38)	-	-	-	-

TABLE 5.4 - continued

S.NO.	SAMPLE NO.	GARNET-I								GARNET-II			
		TEMPERATURE (°C)				PRESSURE (Kbar)				TEMPERATURE (°C)		PRESSURE (Kbar)	
		CORE		RIM		CORE		RIM					
		FS	GS	FS	GS	HC	NH	HC	NH	FS	GS	HC	NH
46	D13/13	(705 ±14)	712 ±18	520 ±27	(581 ±29)	-	-	3.59 ±.32	(3.77 ±.21)	-	-	-	-
47	D43/47	-	-	490 ±44	(553 ±53)	-	-	4.62 ±.25	(4.96 ±.27)	-	-	-	-
48	D4/4	-	-	(694 ±16)	715 ±22	-	-	-	(5.68 ±.38)	-	-	-	-
49	P22/86	-	-	(649 ±6)	697 ±7	-	-	-	(5.81 ±.15)	(652 ±13)	693 ±13	(6.11 ±.17)	5.78 ±.26
50	P12/20	-	-	(676 ±8)	741 ±13	-	-	6.31 ±.40	(7.73 ±.15)	-	-	-	-
51	P9/50	-	-	521 ±17	(561 ±14)	-	-	6.74 ±.36	(6.91 ±.29)	-	-	-	-
52	P9/46	-	-	-	-	-	-	-	-	567 ±13	(599 ±17)	(6.01 ±.32)	6.00 ±.43

NOTE:

- Selected P-T data are given in bracket and highlighted.

(FS - Ferry and Spear, 1978; GS - Ganguly and Saxena, 1984;

HC - Hodges and Crowley, 1985; NH - Newton and Haselton, 1981).

TABLE 5.5 P-T DATA FOR SURU - DODA VALLEYS SAMPLES

S.NO.	SAMPLE NO.	GARNET-I								GARNET-II			
		TEMPERATURE (°C)				PRESSURE (Kbar)				TEMPERATURE (°C)		PRESSURE (Kbar)	
		CORE		RIM		CORE		RIM					
FS	GS	FS	GS	HC	NH	HC	NH	FS	GS	HC	NH		
1	SP20	-	-	(629 ±36)	647 ±43	-	-	(7.74 ±.31)	-	579 ±8	(595 ±17)	(7.42 ±.19)	-
2	SP25	-	-	-	-	-	-	-	-	378 ±26	(458 ±33)	(6.44 ±.36)	-
3	PL19/123	-	-	685 ±17	(671 ±24)	-	-	(11.58 ±.43)	13.61 ±.61	-	-	-	-
4	PL20/125	-	-	(564 ±22)	546 ±16	-	-	(7.54 ±.40)	8.37 ±.49	-	-	-	-
5	PL12/113	-	-	(619 ±20)	590 ±26	-	-	(7.52 ±.43)	8.19 ±.40	-	-	-	-
6	12A/126	-	-	(586 ±18)	571 ±21	-	-	(8.73 ±.21)	9.90 ±.36	-	-	-	-
7	14/103	(602 ±7)	586 ±8	(578 ±18)	573 ±23	-	-	6.80 ±.31	(6.74 ±.27)	-	-	-	-
8	PC15A/1	-	-	(634 ±22)	619 ±15	-	-	7.44 ±.53	(8.09 ±.39)	-	-	-	-
9	PR3/76	-	-	(622 ±9)	677 ±16	-	-	7.29 ±.53	(8.12 ±.30)	-	-	-	-
10	PR6/81	-	-	(615 ±30)	593 ±42	-	-	8.52 ±.41	(9.36 ±.59)	-	-	-	-
11	PR1/73	-	-	(675 ±16)	673 ±25	-	-	(8.72 ±.18)	9.62 ±.30	-	-	-	-
12	PL4/93	-	-	(646 ±8)	662 ±9	-	-	(9.32 ±.27)	9.81 ±.34	-	-	-	-
13	PC15C/22	-	-	(509 ±17)	560 ±39	-	-	(7.64 ±.07)	8.31 ±.26	(525 ±11)	583 ±8	(7.60 ±.49)	8.40 ±.47
14	PC30C/5	(456 ±18)	503 ±22	(633 ±10)	614 ±16	5.36 ±.31	(5.24 ±.36)	8.75 ±.26	(9.03 ±.38)	(651 ±4)	640 ±3	7.53 ±.05	(7.79 ±.06)
15	PC29/24	-	-	(609 ±17)	648 ±17	-	-	(9.07 ±.52)	9.93 ±.55	(635 ±10)	671 ±14	(9.82 ±.41)	10.81 ±.40

TABLE 5.5 - continued

S.NO.	SAMPLE NO.	GARNET-I								GARNET-II			
		TEMPERATURE (°C)				PRESSURE (Kbar)				TEMPERATURE (°C)		PRESSURE (Kbar)	
		CORE		RIM		CORE		RIM					
		FS	GS	FS	GS	HC	NH	HC	NH	FS	GS	HC	NH
16	PC28F/40	-	-	(637 ±20)	626 ±30	-	-	-	-	-	-	-	-
17	PC28D/30	-	-	(650 ±34)	624 ±38	-	-	-	-	-	-	-	-
18	PC28/42	-	-	(611 ±11)	666 ±6	-	-	-	-	-	-	-	-
19	PC24G/61	(648 ±28)	702 ±20	(632 ±18)	695 ±20	-	-	(8.49 ±.50)	10.32 ±.61	(617 ±12)	678 ±21	-	-
20	PC24D/66	-	-	(635 ±14)	649 ±15	-	-	-	-	-	-	-	-
21	BG49	-	-	373 ±11	(450 ±9)	-	-	(5.65 ±.34)	-	-	-	-	-
22	PC16D/83	-	-	(605 ±5)	599 ±12	-	-	8.22 ±.17	(9.75 ±.23)	528 ±23	(531 ±31)	6.37 ±.37	(7.26 ±.50)
23	P30/120	(737 ±23)	738 ±32	(616 ±25)	656 ±23	-	-	(6.83 ±.50)	7.69 ±.46	-	-	-	-
24	MP5	-	-	(668 ±19)	665 ±23	-	-	(7.88 ±.57)	8.75 ±.57	673 ±20	(665 ±23)	(8.42 ±.33)	9.24 ±.60

NOTE:

- Selected P-T data are given in bracket and highlighted.

(FS - Ferry and Spear, 1978; GS - Ganguly and Saxena, 1984;

HC - Hodges and Crowley, 1985; NH - Newton and Haselton, 1981).

garnet-I rim data from staurolite-kyanite grade give temperature of 550- 630°C with pressure of 6.80-7.80 kb (KC26/28, T4/6, T21/28 and T10/16) (Table 5.4).

3) The HHC rocks very close to the MCT and on north eastern side of the Kishtwar Window (Fig. 2.1) has assemblage Bi-Ms-Gt-Pl-Ky-St-Q (Samples A46/51, A47/55, A47/56, U92/110, U92/111, U93/111A, U93/111B, U93/111C, U93/112B). Garnet-I core gives temperature of 500-570°C using biotite inclusions in garnet core region. Garnet - I rim temperature varies from 590°C to 650°C and pressure of about 7.50-8.90 kb respectively. The rim P-T data corresponds with the garnet - II data (Table 5.4).

4) The metamorphism is increased to peak sillimanite-K-feldspar grade in the northeast and towards the higher topographic levels of the HHC. This is clearly observable from Masu to Bhujaz of the Bhot Nala section (Fig. 2.1). Moving along this section pelitic rocks have the assemblage Gt-Bi- Ms-Pl-Sill-Qz about 4 km away from the MCT indicating sillimanite-muscovite grade condition (A49/59, A53/62B, U76/85, U80/96, U86/103) . The garnet - I core and rim temperatures are about 700-735°C and 650°C respectively with rim pressure of about 6.00-8.50 kb. The garnet - II core P-T conditions are similar to garnet - I rim P-T values (Table 5.4).

5) In sillimanite-K-feldspar grade, the gneissic rocks consist of Bi-Sill-Gt-Pl-Kf-Qz assemblage. Using garnet - I, these rocks give temperature of about 780°C for core (A65/78, A67/86, U33/35, U28/30). The maximum core pressure of 11.00 kb is

recorded in sample A67/86 and the other samples record pressure of 8.00-9.50 kb. The rim temperature of these samples varies from 600-665°C with pressure ranging from 5.10-7.50 kb. Other samples (U29/31, U48/51, U52/55, U4/4, U13/13, U43/47, A74/97 and P22/86) in this zone give reduced temperature ranging between 700°C and 600°C for garnet - I core (Table 5.4). However, the rim data using these garnets show a temperature range of 550-650°C and pressure from 3.80 to 6.80 kb (Table 5.4).

6) From the highest structural level and further NE towards Zaskar Shear Zone (Fig 2.1), metamorphism gradually reduces to sillimanite-muscovite (P12/20) and staurolite- kyanite / sillimanite grade (P9/46, P9/50). Garnet - I rim and garnet - II rims give temperature and pressure of about 600-650°C and 6.00-7.00 kb for both the metamorphic grades. This is in agreement with the data obtained for similar metamorphic grade occurring elsewhere in this region (Table 5.4).

5.7.2 Ladakh - Zaskar section:

This section has been broadly divided into two parts namely the Suru and Doda Valleys for the P-T estimation. The metamorphic condition is varying from garnet to sillimanite-muscovite grade in the Suru Valley where pelitic and quartzitic rocks are mainly exposed. It covers an area starting from Sankoo in the north and passes through Parkachik, Ringdom and Pensila in the SE direction. The Doda Valley runs almost parallel to the ZSZ, which separates the HHC from the Tethyan Sedimentary Zone. In this section, emphasis has been given only to the HHC rocks,

close to the ZSZ, where the metamorphism varies from staurolite-kyanite to sillimanite-muscovite grade condition (Fig 2.1). However, in the Suru and Doda Valleys, the rocks are more psammitic and intercalated with quartzite and contain number of granitic intrusive bodies. Therefore, limited number of samples were only available for analysis and P-T estimation.

1) In the Suru Valley, P-T data using garnet - I is available only for staurolite-kyanite grade rocks. The rocks from this grade contain Gt-Bi-Ms-St-Ky-Sill-Pl-Q assemblage (Table 4.1). The garnet core gives a temperature of about 450°C and pressure of about 5.00 kb (PC30C/5). The rim temperature for this grade varies from 560°C to 650°C with a pressure of about 6.70-9.70 kb (PL20/125, PL12/113, 12A/126, 14/103, PC15A/1, PL4/93, PC30C/5, PC29/24, PC28F/40, PC28D/30, PC28/42, PC24G/61, PC24D/66, PC16D/83) (Table 5.5). The rim P-T values are very much similar to the same grade rocks of Bhot Nala section.

2) In the Doda Valley, a few samples were available for the estimation of P-T data in each grade. Staurolite-kyanite grade samples consist of Gt-Bi-Ms-St-Ky/Sill-Q-Pl and record rim temperature of about 560°C and pressure of about 7.00 kb (P9/50; Table 5.4). The maximum core and rim temperatures in sillimanite-muscovite grade (P30/120) near Haptal Tokpo are about 740°C and 620°C-670°C. The rim records a pressure of about 7.70 kb in this grade (Table 5.5).

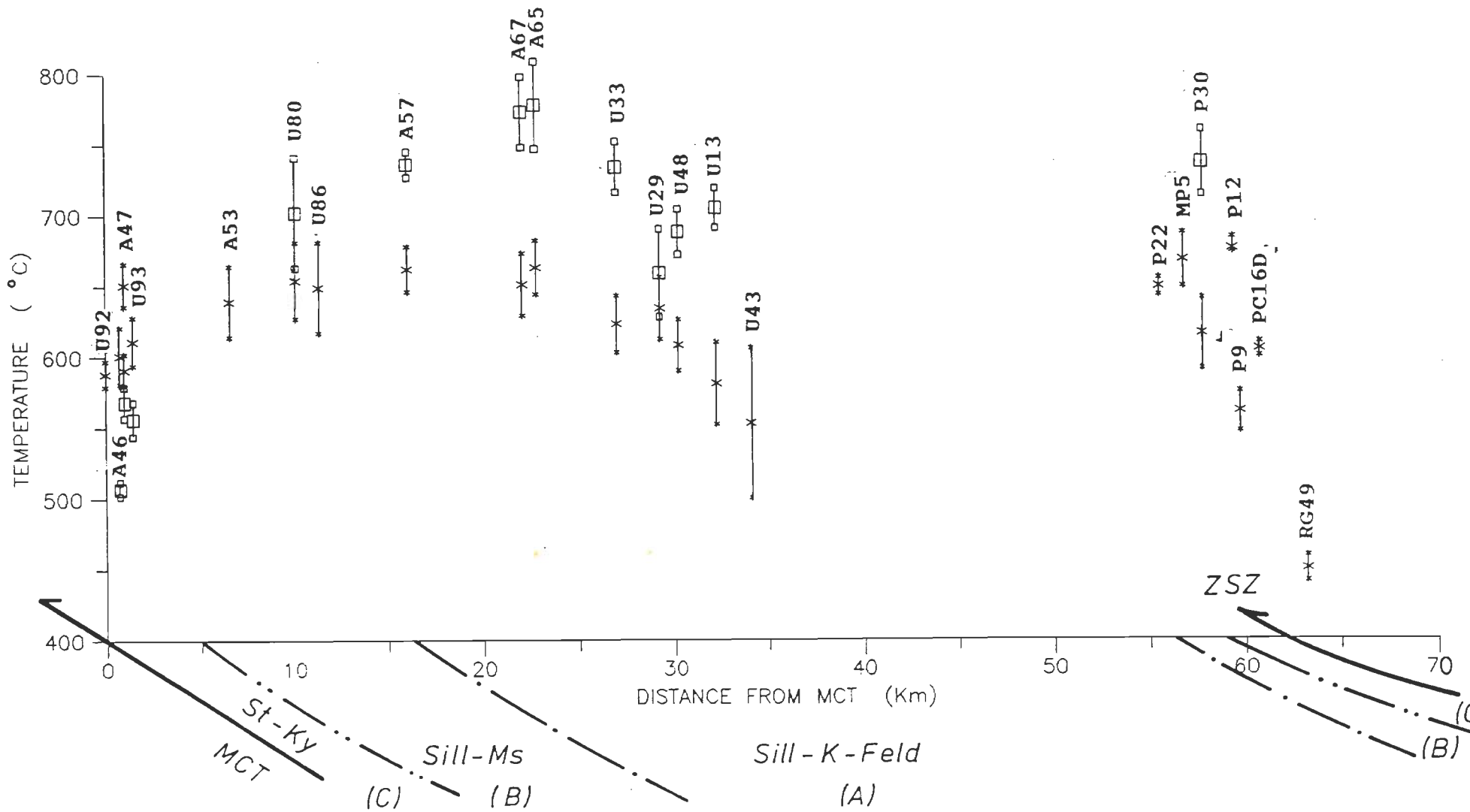
5.8 DISCUSSION

The pressure-temperature data, in conjunction with texture and mineralogy, as discussed in Chapters-3 and 4, suggest that this region have undergone regional metamorphism varying from garnet to sillimanite-K-feldspar grade. To characterise the P-T condition in individual sections, the data have been plotted separately for each section and discussed. Temperature and pressure variations with respect to structural distance from MCT zone in the Chenab-Bhot Nala section are plotted in Figures 5.1 and 5.2 respectively. It is clear from Figures 5.1 and 5.2 that the HHC, occurring on the northeastern side of the Kishtwar Window and within 1 km of MCT, shows temperature and pressure of about 550°C and 8.00-9.00 kb, using inclusion thermobarometry for garnet core. The rim data show an increase of about 50° to 100°C (Fig. 5.1) with no change in pressure (Fig. 5.2). The presence of kyanite (Holdaway, 1971), complete absence of chlorite (Winkler, 1979), increase in Fe/Fe+Mg ratio and reduction in Mn and Ca towards garnet rim (Tracy, 1982) in the assemblage, suggest that the HHC rocks have developed in near isobaric and increased temperature conditions near the MCT. The rarity of staurolite indicates that it became either unstable due to increased temperature (Pigage and Greenwood, 1982) or because of the change in bulk composition due to other metamorphic reactions in the rock.

Moving further northeast, about 10 to 18 km from the MCT, the core temperature increases to about 700°-740°C (Fig. 5.3). The core pressure probably remains constant to that of the

FIGURE 5.3 : Temperature vs distance plot along Bhot Nala cross-section of the HHC.

(Symbols as in Fig. 5.1)



pressure observed near the MCT. The rim temperature and pressure are reduced by about 50°-100°C and 1.00 -2.00 kb respectively (Figs. 5.3 and 5.4). The increase in core temperature is envisaged by the absence of staurolite in the assemblage. However, the absence of kyanite and the epitaxial growth of fibrolite/sillimanite in biotite, muscovite and garnet in the assemblage indicate that this growth possibly has taken place in reduced pressure and at constant or increased temperature condition, considering the Al_2SiO_5 phase diagram of Holdaway (1971). The rim data confirm that fibrolite formation has probably been taken place during exhumation and near isothermal condition. Due to this pressure reduction, prograde kyanite is probably transformed completely to sillimanite/fibrolite in these rocks.

Further northeast, about 18 to 23 km from MCT, the core P-T data have increased to about 780°C and 10.00-11.00 kb (Figs. 5.3 and 5.4). This increase in metamorphism is recorded by the total absence of muscovite and formation of biotite, K-feldspar prismatic sillimanite. The rim data show a decrease in temperature of about 150°C and pressure of about 2.50-3.50 kb (Figs. 5.3 and 5.4). The formation of fibrolite through individual reactions and as epitaxial growth, suggest that these have developed during the cooling stages.

About 23 to 40 km from MCT, the core P-T data show reduction from the peak P-T values that has been observed in sillimanite-K-feldspar gneiss. This reduction is quite variable in this zone

and this feature has also been observed in the rim data (Figs. 5.3 and 5.4). These reduced P-T values are probably due to extensive migmatisation and the formation of leucogranites in this zone. During migmatisation, garnet seems to have undergone resorption, partial reequilibration and grain size reduction, because most of the garnet in these rocks are broken and smaller in size. The grains do not show any evidence of syntectonic growth as observed in other metamorphic grades. Jiang and Lasaga (1990) have suggested that garnet with less than 1 mm size would give erroneous values due to partial homogenisation in higher grades. It is therefore likely that these rocks do not show any evidence of peak metamorphic condition in this zone.

In the Suru Valley, P-T data have been estimated for the area covering Sankoo-Parkachik-Ringdom. However, the data are presented only for a cross-section in dip directions from Panikhar to Ringdom. The grade of metamorphism mostly remain in staurolite- kyanite grade with a small portion exposing sillimanite-muscovite grade rocks near Parkachik. The staurolite-kyanite grade core data indicate a temperature of about 500°C and pressure of about 5.00 kb, whereas the rim data indicate an increase of about 100-150°C in temperature and the 3.00 to 4.00 kb (Figs. 5.5 and 5.6) in pressure. The presence of kyanite and staurolite in the assemblage is conformable with the rim P-T data, which also suggest a prograde growth of these minerals.

In the Pensila-Padam section, the rocks occurring from

FIGURE 5.4 : Pressure vs distance plot along Bhot Nala cross-section of the HHC.

(Symbols as in Fig. 5.1)

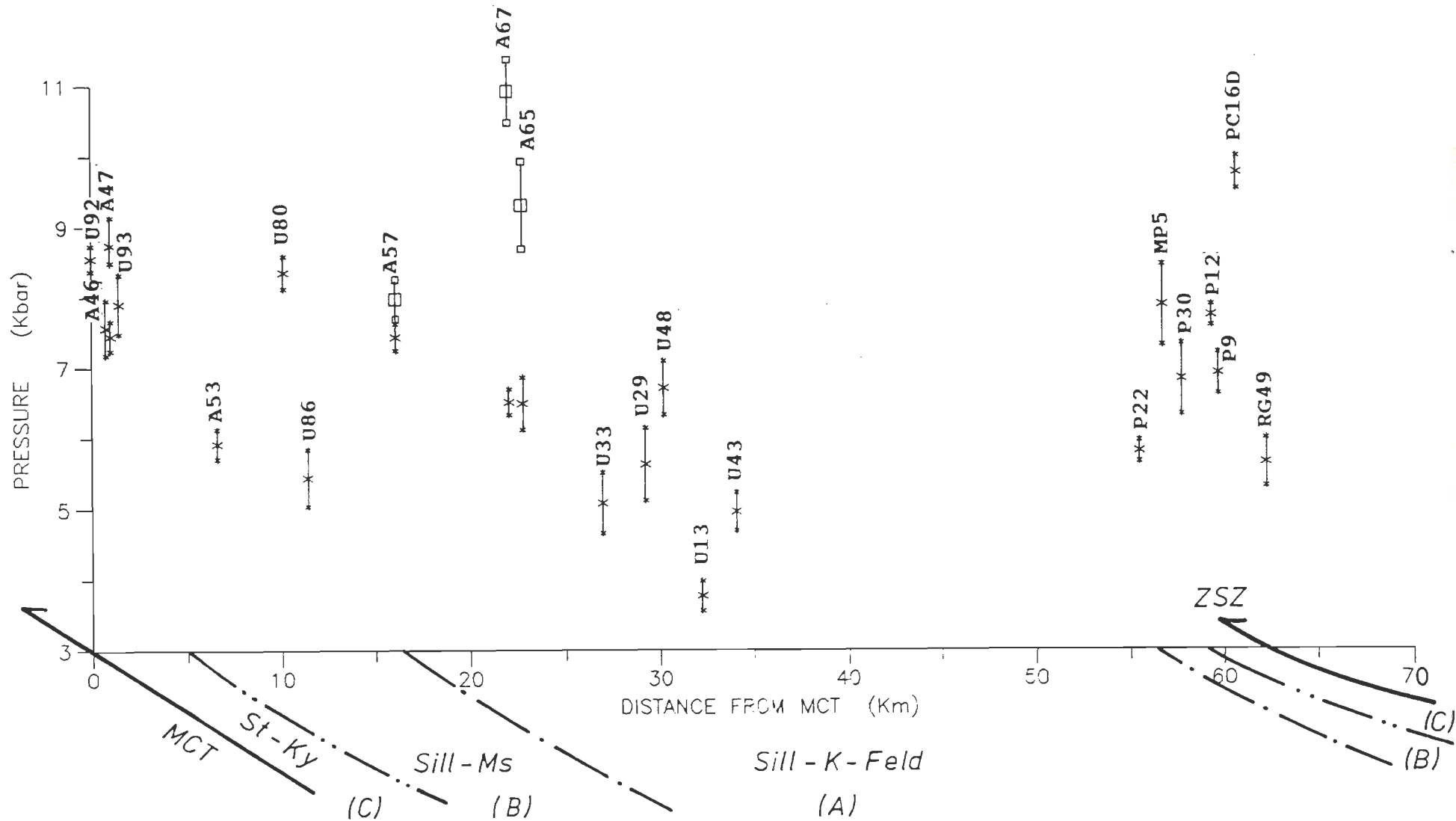


FIGURE 5.5 : Temperature vs distance plot along Suru Valley cross-section of the HHC.
 (Symbols as in Fig. 5.1)

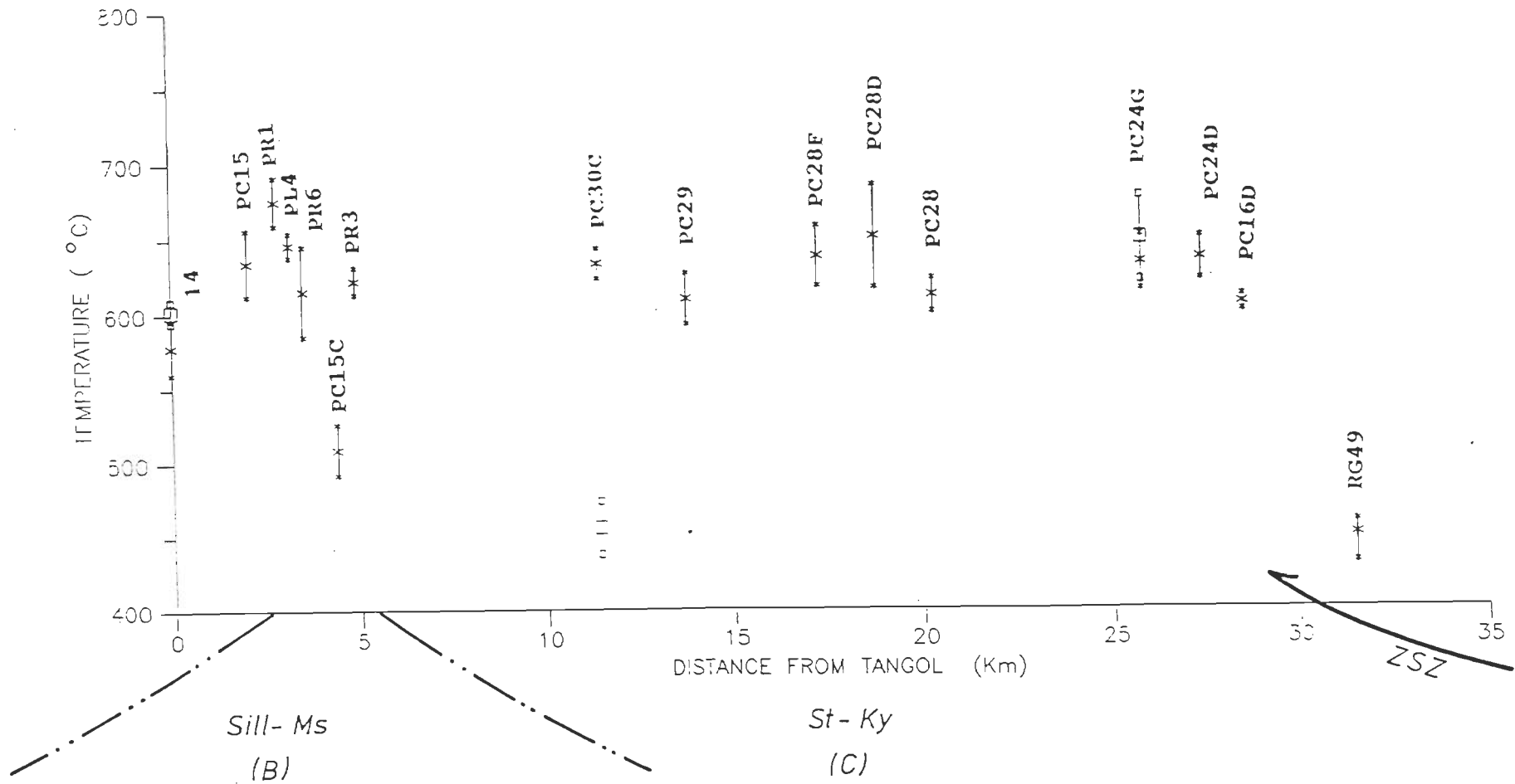
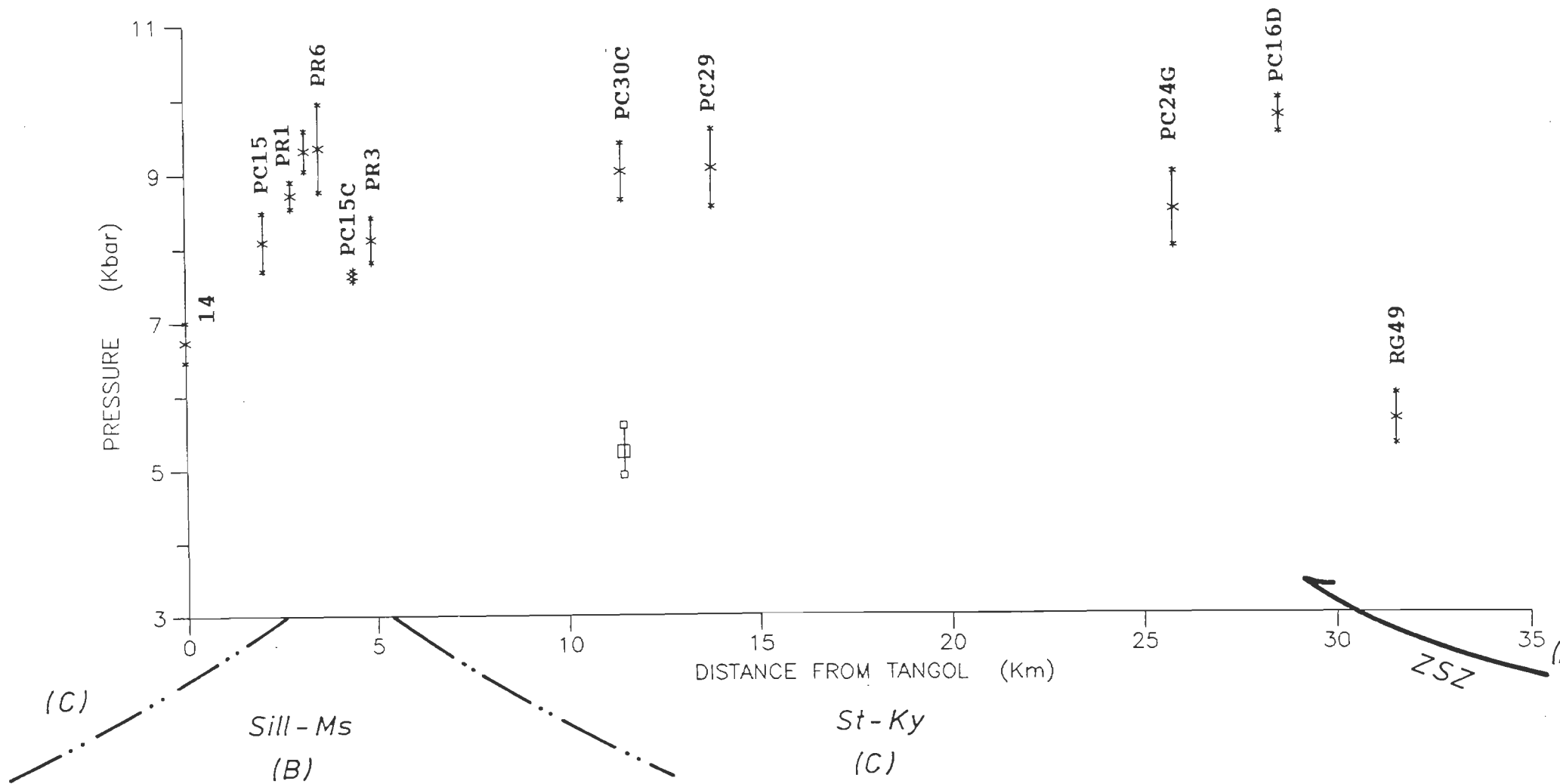


FIGURE 5.6 : Pressure vs distance plot along Suru Valley cross-section of the HHC.
 (Symbols as in Fig. 5.1)



Pensila to Haptal Tokpo show rim temperatures and pressures similar to the rocks that occur both in Parkachik-Ringdom section and also close to MCT zone in Bhot Nala section (Tables 5.4 and 5.5). Moving still further in the southeast direction from Haptal Tokpo towards Mune, the core records a temperature of about 740°C. The rim temperature is reduced by about 100°C and with a pressure of about 7.70 kb. The higher temperature in core is comparable by the absence of staurolite and the presence of sillimanite in these samples. The total absence of kyanite indicates that kyanite, if it was present, has possibly been transformed to sillimanite during cooling due to reduction in pressure .

CHAPTER - 6

SUMMARY AND CONCLUSION

6.1 INTRODUCTION

Recent geodynamic models of the Himalaya envisage the northward movement and subduction of the Indian Plate beneath the Eurasian Plate along the Indus Suture Zone. After the closure of Tethys Ocean, intracontinental crustal shortening and deformation has taken place either along southerly migrating major thrusts such as Main Central Thrust (MCT), Main Boundary Thrust (MBT) or along the large-scale strike-slip faults in Tibet (Dewey and Bird, 1970; Dewey and Burke, 1973; Narain, 1973; Le Fort, 1975; Molnar and Tapponnier, 1975; Valdiya, 1980). It is inferred that the Higher Himalaya rocks have been deformed and metamorphosed during collision and crustal shortening (Le Fort, 1975, 1986; Bouchez and Pecher, 1981; Honeggar et al., 1982; Searle and Rex, 1989). Present work is an attempt in understanding metamorphism and related deformation during Collision Tectonics in parts of Jammu and Kashmir. Results are summarised and discussed here in detail.

6.2 GEOLOGY OF THE AREA

Kishtwar is located along the Chenab River to the southeast of Kashmir valley. Vast metamorphic pile constituting the Higher Himalayan Crystalline (HHC - Salkhala Group) is thrust over the Lesser Himalayan Proterozoic Foreland of the Kishtwar Window along the Main Central Thrust (MCT). Towards southwest and west,

it constitutes a part of Kashmir Nappe, which is overlain by the fossiliferous Paleozoic - Mesozoic succession of Kashmir - Bhadarwah Basin. On the other hand, the Zaskar Shear Zone (ZSZ) separates the overlying Paleozoic-Mesozoic sequence of the Tethyan Sedimentary zone along the northeastern margin of Higher Himalayan Crystalline (HHC - Suru Group) along the Suru - Doda Valleys.

6.3 DEFORMATION AND RELATED METAMORPHISM

The present study envisages at least four phases of deformation along Chenab - Bhot Nala section and Suru-Doda Valleys of the HHC. During first deformation (D_1), isolated, tight and appressed 'flame' folds (F_1) are developed on lithological banding/metamorphic layering (S_0). The axial plane foliation (S_1) of F_1 folds parallels metamorphic layering wherever observed except in the hinge zones. During this deformation, metamorphism (M_1) is weak having quartz-sericite-chlorite-biotite-feldspar-garnet-opaque assemblage of greenschist facies.

The most pervasive second deformational phase (D_2) is manifested by the intense planar fabric S_2 , a prominent NE or SW plunging mineral or stretching lineation (L_2). The F_2 folds are mostly close to isoclinal, reclined to inclined plunging folds on the S_1 foliation and plunge either NE or SW. Stretching/mineral lineation (L_2) parallels the F_2 folds and is characterised by growth of sillimanite, kyanite, staurolite, amphibole, mica and tourmaline.

The growth of moderate to high pressure minerals such as syntectonic garnet (garnet-I), staurolite, kyanite, sillimanite etc., have taken place during D₂ deformation and also along S- and C-surfaces. Therefore, this deformational phase is considered to have taken place during the main M₂ metamorphic event. However, Das (1978, 1987) correlated the prograde M₁ metamorphic event during static phase between D₁ and D₂ deformation. Searle and Rex (1989) and Staubli (1989) considered moderate to high pressure syntectonic M₁ metamorphism related to D₁ deformation. In the present study, growth of post-tectonic garnet (garnet-II) has been interpreted during late to post D₂ deformational phase. Searle and Rex (1989) and Staubli (1989) described growth of staurolite, kyanite and second generation garnet to main M₂ metamorphism during D₂ deformation.

D₃ deformation has produced NW or SE gently plunging isoclinal to tight F_{3a} folds on earlier foliation. Subsequently, F_{3b} folds of open to close and inclined-type are developed on all earlier foliation planes. During this deformation, metamorphism is manifested by synkinematic crystallisation of quartz, muscovite and greenish biotite along axial plane foliation as well as post-tectonic cross-mica growth. Extensive retrograde metamorphism has taken place during the later part of the D₃ deformation in which chlorite has developed at the expense of garnet and biotite. Das (1987) considered that the retrograde metamorphism as M₂ and during the D₂ deformational phase. Searle and Rex (1989) and Staubli (1989) recorded an overall weak retrograde M₃ metamorphism in D₃ deformation.

Kinks, brittle-ductile discrete shear zones and tension gashes are developed during D₄ deformation.

6.4 REGIONAL METAMORPHIC FRAMEWORK

The Lesser Himalayan rocks, exposed in Kishtwar Window, are metamorphosed from chlorite to garnet grade condition. In the HHC rocks occurring along Chenab-Bhot Nala section, the metamorphism varies from garnet to sillimanite-K-feldspar grade. Individual metamorphic grades are envisaged on basis of texture and detailed mineralogy of both Lesser and Higher Himalayan rocks.

The mineralogy of the HHC reveals the presence of staurolite-kyanite grade rocks close to Kishtwar Window on the NE side above MCT. This has been observed by others in this area (Kundig, 1989; Searle and Rex, 1989; Staubli, 1989). However, the observations made above MCT in Kumaon and Nepal Himalaya are different in comparison to this area. In Kumaon Himalaya, kyanite isograd has been mapped above the MCT by Hodges and Silverberg (1988). In Nepal, it has been observed that the kyanite isograd occurs within 5 to 10 km thick MCT zone and the base of MCT is marked by lower grade rocks (Brunel and Kienast, 1986; Hodges et al., 1988; Hubbard, 1989; Mohan et al., 1989; Pecher, 1989).

On the SW side of the window and just above MCT, garnet grade rocks are exposed in HHC, unlike the occurrence of higher grade rocks on the NE side. Moreover, it is observed that the metamorphic isograds do not run parallel to MCT, unlike in Nepal (Le Fort, 1986; Pecher, 1989; Hubbard, 1989) and show cross-cutting relation with MCT (Fig. 2.1). Also, the earlier workers

have mapped the presence of a single metamorphic grade on either side of the window and also interpreted the telescoping of metamorphic isograds above MCT (cf., Searle and Rex, 1989; Staubli, 1989). Das (1987) inferred the presence of chlorite to staurolite grade rocks for this Kishtwar area but it is unclear whether the grades occur above MCT or include the window zone rocks as well.

Moving further NE along Bhot Nala towards higher topographic levels, the metamorphism reaches to sillimanite-K-feldspar grade at the centre of the Great Himalayan Range. When approaching towards ZSZ in Doda Valley from this region, normal metamorphism reaching upto staurolite-kyanite/sillimanite-muscovite grade is observed. It has been suggested that there is telescoping of metamorphic isograds in a 200 meter thick zone due to normal faulting (Herren, 1987; Searle and Rex, 1989; Staubli, 1989). However, petrographic work all along the ZSZ indicates that there is no condensation or telescoping of metamorphic isograds, instead different metamorphic grades are cut obliquely by this shear zone at different places (see Fig. 2.1).

In Suru Valley, the metamorphism ranges from garnet to sillimanite-muscovite grade condition. Garnet grade rocks occur in and around Sankoo and Ringdom, whereas staurolite-kyanite grade rocks are observed in between these places. Sillimanite-muscovite grade rocks are found exposed only in a very small portion of this valley around Parkachik (Fig. 2.1). Along the northern margin, the HHC rocks are separated from Tethyan

Sedimentary Zone by the northwestern extension of the ZSZ. Along this margin, the HHC rocks mostly remain in garnet to staurolite-kyanite grade (Fig. 2.1).

6.5 TEXTURES OF METAMORPHIC ROCKS

Above the MCT, garnet has grown in at least two distinguishable stages, documented by inclusion-rich core (garnet-I) and inclusion-poor rim or inclusion-free idoblastic to subidioblastic garnet (garnet-II). The latter is smaller in size. In higher grades, garnet shows dissolution and corroded margins, where the margins are surrounded by biotite and fibrolite. Syn-tectonic garnet-I shows the S-shaped spiral or rotational Si inclusions of small quartz, mica and opaque minerals. Mostly, internal fabric (Si) and external foliation (Se) maintain their continuity but, in a few cases, this continuity has been disturbed.

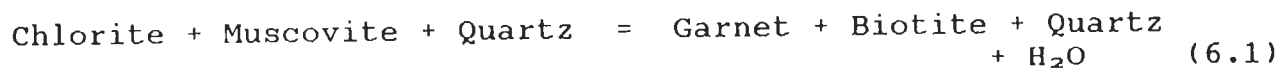
Staurolite crystals commonly contain inclusions of quartz, mica and opaque minerals and a few are inclusion-free subidioblastic grains. Kyanite blades are found mostly with biotite and muscovite. Textural evidences show that kyanite has grown at the expense of staurolite in a static state. Sillimanite occurs as prismatic needles and fibrolite in higher grades. Polymorphic transformation of kyanite to sillimanite has been noticed in high grade rocks. Growth of fibrolite in biotite and sometimes garnet, appear to have been developed during decompressional stage. In sillimanite-k-feldspar grade, primary muscovite is absent. However, development of secondary muscovite

cross-cutting the primary foliation is observed in a few samples, and this possibly have formed during retrograde stage. Feldspars show retrogression and formation of sericite. Retrograde chlorite after garnet and biotite is common in all the grades, but is more pronounced in Doda Valley section.

6.6 METAMORPHIC PARAGENESIS AND MINERAL REACTIONS

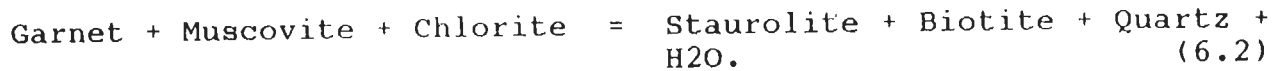
The Lesser Himalayan rocks in Kishtwar Window consist of carbonaceous phyllite, chlorite-sericitic schist, mica schist, garnetiferous schist, quartzite, marble, augen gneiss and granitic gneiss. Above the MCT, the HHC is made up of garnetiferous mica schist, staurolite-kyanite schist, sillimanite-muscovite gneiss/schist, sillimanite-K-feldspar gneiss/schist, amphibolite, calc-silicate and quartzite rocks. As the HHC consists predominantly of pelitic rocks, mineralogy of only this rock is considered for the purpose of metamorphic reactions and chemistry.

Garnet grade consists of primary chlorite, garnet, mica, feldspar and quartz. The formation of garnet in the assemblage is explained by the continuous reaction:

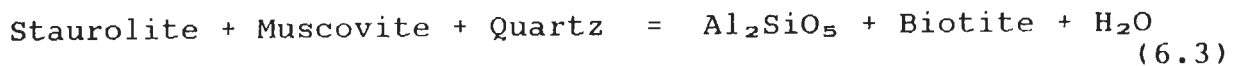


The mineral assemblages found in staurolite-kyanite grade are biotite - muscovite - garnet - kyanite - staurolite - quartz-plagioclase-K-feldspar. Kyanite is present in substantial quantities, whereas staurolite is restricted in occurrence. The increase in modal biotite and the compositional change in

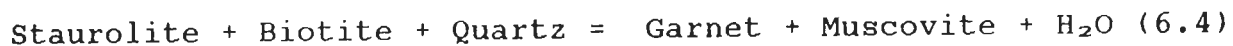
muscovite suggest that the formation of staurolite and biotite is through the continuous reaction:



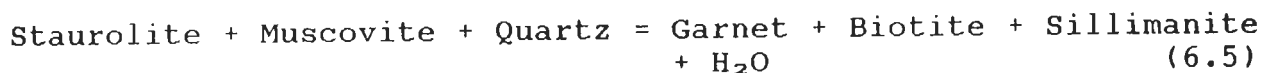
Staurolite is absent in some of the samples and only kyanite is found to occur with other minerals of staurolite-kyanite grade rocks. The absence of staurolite may either because of unsuitable bulk composition or due to the increase in temperature conditions (Winkler, 1979; Pigage and Greenwood, 1982; Yardley, 1989). The disappearance of staurolite and formation of kyanite in the assemblage is possibly by the continuous reaction:



The disappearance of staurolite is evident from the temperature increase of about 50°C from the rocks containing staurolite. In the very same grade, presence of staurolite inclusion in some of the garnet grains suggests that the formation of garnet is by the reaction (Thompson et al., 1977):

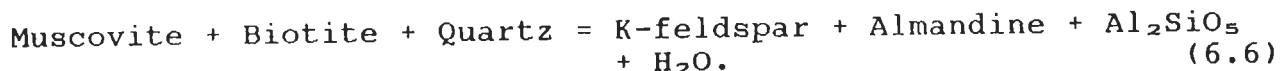


The sillimanite-muscovite grade rocks consist of garnet-biotite - muscovite - sillimanite - plagioclase - K-feldspar - quartz assemblage. Textural study suggests that sillimanite, biotite and garnet have been formed by the discontinuous reaction:



This reaction can take place at higher temperature and moderate to high pressure conditions. Growth of sillimanite in muscovite and quartz and the P-T data obtained (see Tables 5.4 and 5.5) for this grade confirm the above observation.

In sillimanite-K-feldspar grade, muscovite has completely disappeared with increase in K-feldspar in the assemblage. Also, biotite shows epitaxial growth of sillimanite. The disappearance of muscovite suggests the reaction:



In the higher grade schist and gneiss, garnet porphyroblasts are either broken or of subidioblastic character indicating resorption. This garnet resorption may be through the reaction:



Such resorption is evidenced by the reverse zoning where X_{Mg} is reduced with higher X_{Fe} at the garnet edge.

6.7 THERMOBAROMETRIC RESULTS

Temperature is estimated using garnet-biotite exchange thermometer (Ferry and Spear, 1978; Hodges and Spear, 1982; Ganguly and Saxena, 1984; Thompson, 1976). Pressure estimation is made using garnet-plagioclase-sillimanite/kyanite-quartz and garnet-plagioclase-muscovite-biotite discontinuous reactions (Newton and Haselton, 1981; Ghent and Stout, 1984; Hodges and

Crowley, 1985). Error estimation is calculated following the method of Hodges and McKenna (1987). Syntectonic garnet (garnet-I) with inclusions like biotite, plagioclase, quartz etc., are used for evaluating core P-T condition during prograde metamorphism. Matrix minerals in association with inclusion-free rims of garnet-I or subidioblastic garnet-II are used in the calculation of rim P-T data and to decipher the cooling and uplift path of these metamorphic rocks. Garnet-II is homogeneous in composition, as is indicated from the zoning and compositional data. Therefore, core and rim compositions of garnet-II are averaged and used in the calculation of P-T with matrix minerals.

The inferences made from the P-T data along the Chenab - Bhot Nala section and Suru-Doda Valleys are summarised below:

1) In the vicinity of the MCT, rims of garnet-I show temperature of 500-560°C and pressure of 7.00-9.60 kb for garnet grade (Figs. 5.1 and 5.2). The temperature data are in agreement with the data of Staubli (1989). The rocks of the same grade occurring above MCT and within the HHC on the SW side also show more or less the same P-T condition using rim of garnet-I (Table 5.4). Das (1987) reported almost the same temperature with an assumed pressure of 6.00 kb for the garnet grade rocks of the Kishtwar area.

2) Staurolite-kyanite grade rocks of the HHC within 1 km and close to MCT on the NE side of the Kishtwar Window record the core temperature of 500-570°C in garnet-I and a temperature-pressure of 550-650°C and 7.50-9.00 kb in rim (Figs. 5.1 and

5.2). P-T values of garnet-II are exactly similar to the rim data of garnet-I (Table 5.4). Staubli (1989) inferred core and rim temperatures of 520°C and 550-575°C for the same metamorphic grade, which is about 50-75°C less than the present data.

3) Further moving up in the higher structural levels towards NE, garnet-I of sillimanite-muscovite grade gives core temperatures of 700-740°C (Fig. 5.3). P-T estimate from garnet-II or inclusion-free rim on garnet-I is 610-650°C and 6.00-8.50 kb. Sillimanite-K-feldspar grade gives core temperature and pressure of about 780°C and 9.00-11.00 kb. However, the rim P-T shows 600-665°C and 4.50-6.50 kb. A few samples show substantial reduction in core and rim P-T from the above mentioned values, but this is commonly observed in the zone of migmatite (Figs. 5.3 and 5.4).

4) While moving from the highest structural level further NE towards ZSZ in sillimanite-muscovite grade, rims of garnet-I give temperature and pressure of about 675°C and 7.75 kb. Staurolite-kyanite grade rocks show 600°C and 6.00 kb from the rims of garnet-I or from garnet-II (Figs. 5.3 and 5.4)

5) In the Suru Valley along the main cross-section from Panikhar to Ringdom, staurolite-kyanite grade rocks record core P-T of 450°C and 5.25 kb, while rim gives 560-650°C and 6.75-9.75 kb (Figs. 5.5 and 5.6).

P-T data, thus obtained for the HHC rocks from staurolite-kyanite grade on the NE and SW sides of Kishtwar Window, suggest that these rocks have developed initially during prograde

metamorphic condition followed by heating in the later period during uplift of higher grade rocks. The normal growth zoning with an increase in Mg/Fe ratio towards garnet-I rim (Tracy, 1982) and increasing temperature towards garnet rim support the above interpretation. However, Staubli (1989) observed relaxed zoning for the same grade and suggested that growth zoning is modified due to extended period of burial and homogenisation. This may not be valid because intragranular diffusion is very sluggish in medium grade rocks with temperature of about 600° and, therefore, these rocks preserve the growth zoning (Hollister, 1966; Tracy et al., 1976; Tracy, 1982; Frost and Tracy, 1991). Moreover, presence of kyanite, rarity of staurolite and increasing Fe/Fe+Mg ratio towards garnet rim in the Bhot Nala samples indicate that these rocks probably have been formed in near isobaric and increased temperature conditions.

About 10-18 km from the MCT towards higher structural level, garnet-I core temperature is increased by about 170°C with pressure remaining constant from that of staurolite-kyanite grade. On the other hand, the rim temperature remains more or less constant but pressure is reduced by 2.00-3.00 kb from staurolite-kyanite grade. Staubli (1989) recorded temperature of about 575°C for core and 625°C for rim. Still up in the topographic level and upto about 23 km, in sillimanite-K-feldspar grade, garnet-I core records an increase of about 40-80°C from sillimanite-muscovite grade with a slight increase in pressure (Figs. 5.3 and 5.4). For the same grade, P-T condition for garnet-I rim or garnet-II grains are reduced by about 150°C and

2.50-3.50 kb from core. The rim pressure, however, is reduced by another 1.5-2.00 kb than the sillimanite-muscovite grade without much change in rim temperature. Epitaxial growth of fibrolite in biotite and an increase in Fe/Fe+Mg ratio and Mn at garnet rim (Spear et al., 1990; Tracy et al., 1976) suggest their formation during reduced pressure condition. Core P-T data of garnet from both the higher grades demonstrate prograde metamorphism. The mineralogy of these high grade rocks indicate the presence of medium to low pressure minerals such as sillimanite, cordierite etc., and the absence of high pressure minerals like kyanite etc., in the assemblage. However, high Mg/Fe ratio and lower Mn in the garnet core is indicative of prograde metamorphism.

Considering the garnet zoning in higher metamorphic grades (Figs. 4.31 - 4.33), it is evident that garnet has reverse zoning. This growth of garnet at high temperature may either be by reaction (5) or (6). In such growths, intragranular diffusion is fast and the mineral becomes homogeneous revealing no growth zoning (Tracy, 1982). However, after peak metamorphism, compositional readjustment takes place at the rim during cooling, causing Fe and Mn enrichment which finally produces reverse zoning (Kretz, 1973). Another possibility is that garnet of lower grade is overgrown because of increasing temperature at later stage (Thompson et al., 1977; Tracy, 1982; Frost and Tracy, 1991) and become homogenised. However, reverse zoning with higher Mg/Fe and very low Mn in garnet core suggests that these have grown possibly by the first process, which is conformable with P-T data.

At the highest topographic level between 23 and 40 km from window, the rocks are extensively migmatized in the sillimanite-K-feldspar grade. During migmatization, garnet probably has undergone partial reequilibration and grain-size reduction, and therefore, does not give peak metamorphic P-T condition.

The minimum and maximum P-T conditions, obtained for the garnet-I core across the whole of HHC, suggest tectonic subsidence to about 25 to 30 km depth considering the normal thermal gradient for the continental crust. Because of this subsidence, it appears that the HHC rocks have undergone prograde metamorphism M_2 . The prograde path is evident from point A to B in Figure 6.1. In Lahul-Zaskar region, Pognante et al. (1990) opined that stacking and exhumation during intracontinental thrusting has caused this metamorphism. The extra heat for high grade assemblage appears to be the radioactive heat source. However, in Eastern Garhwal, the kyanite grade rocks occurring within 3 km of MCT are described to have been formed at a paleodepth of about 32-34 km during main metamorphism and before thrusting along MCT (Hodges and Silverberg, 1988).

The rim P-T data for the Bhot Nala section show a clear reversal from core data in all metamorphic grades. This change in P-T condition during late M_2 metamorphism has possibly developed at the time of ductile shearing and associated uplift. Temperature reduction in higher grade and, at the same time, increase in staurolite-kyanite grade rocks during late M_2 metamorphism indicates that the lower grade rocks are heated up during thermal relaxation of the higher grade rocks. This

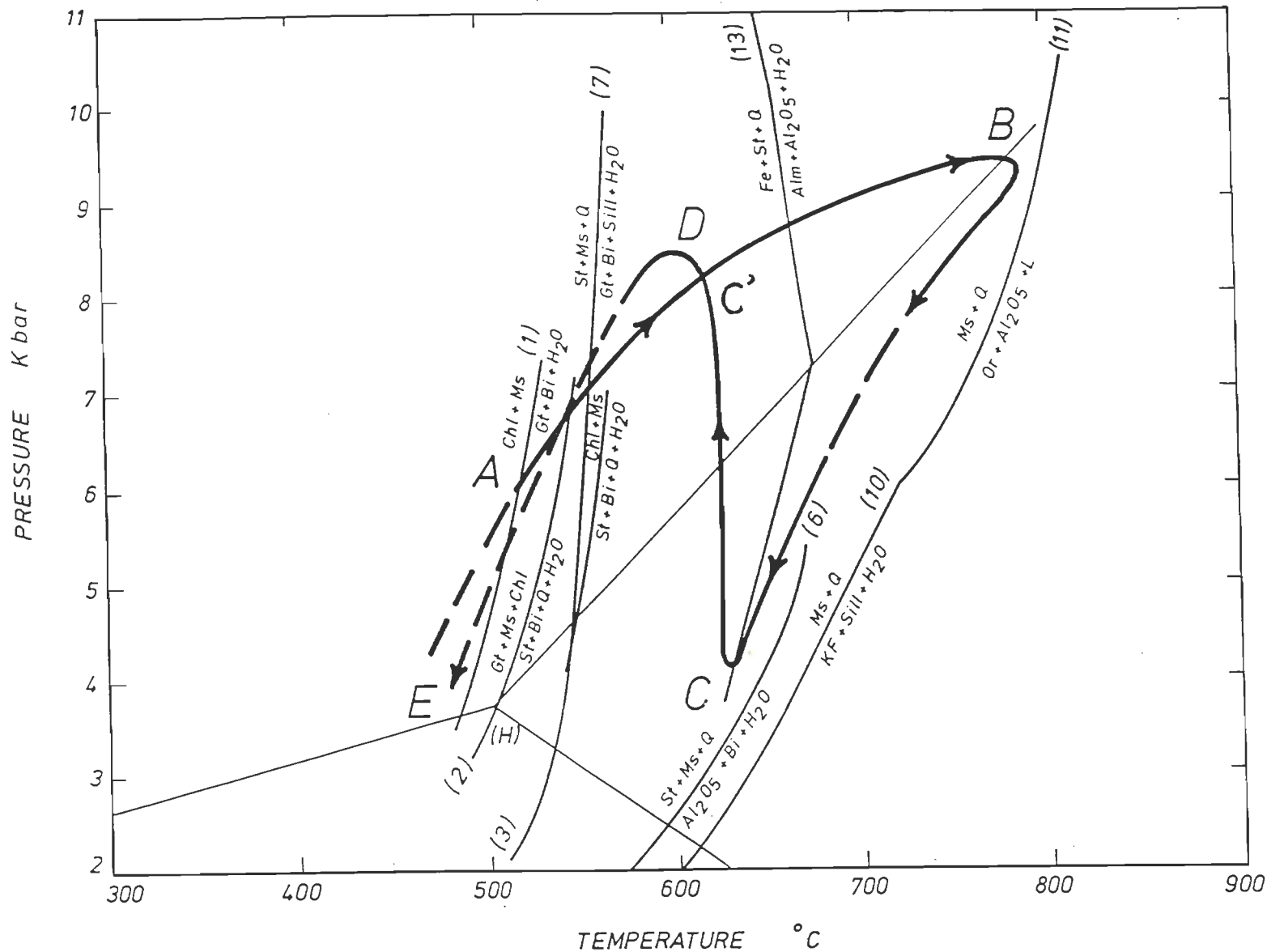


FIGURE 6.1 : P-T diagram showing P-T-t path for the metamorphic rocks from Chenab-Bhot Nala section of the HHC. Selected reactions are represented in the diagram (for details refer text in Chapter 4). Reaction (1) - Hirschberg and Winkler (1968) & Harte (1975); (2) - Froese and Gasparrini (1975); (7) - Carmichael (1978); (3) - Hoschek (1969); (6) - Hoschek (1969); (11) - Storre (1972); (10) - Chatterjee and Johannes (1974); (13) - Yardley (1981); Al_2SiO_5 triple point drawn from Holdaway (1971). Prograde, cooling, uplift and retrograde paths are shown from points A to E. Solid line path is based on P-T data. Dashed line paths are tentatively drawn from mineralogy. For details refer text.

relaxation has probably taken place at the time of exhumation, which is evidenced by reduction in pressure from staurolite-kyanite grade to higher grades (P-T path from point B to C in Fig. 6.1). Moreover, exhumation during ductile shearing at deeper crustal levels and subsequent thrusting along MCT has possibly thickened the crust. This phenomenon has been interpreted from a sharp increase in pressure in near-isothermal conditions (point C to C' in Fig. 6.1). However, higher rim pressure during crustal thickening in staurolite-kyanite grade in contrast to the higher grade rocks (point from C' to D in Fig. 6.1) indicates that the latter rocks exhumed faster than the staurolite-kyanite grade in basal parts of the HHC.

6.8 MODEL FOR INVERTED METAMORPHISM

It is well known that the Higher Himalayan Crystalline (HHC), exposed from Zaskar to Kumaon Himalaya and the Tibetan Slab of Nepal-Sikkim Himalaya exhibit inverted metamorphism (Arita, 1983; Le Fort, 1986; Hodges and Silverberg, 1988; Mohan et al., 1989; Pecher, 1989; Searle and Rex, 1989; Staubli, 1989; Pognante et al., 1990; Thakur et al., 1990). The present study in Zaskar confirms the presence of inverted metamorphism in HHC.

Many models have been proposed to explain inverted metamorphism of the Himalaya. The mineralogy, texture and P-T data obtained in this study has been compared with the above models of inverted metamorphism to understand their applicability for this region.

1. Hot-over-cold recumbent folding:

Le Fort (1975, 1986) proposed that thrusting of the hot Tibetan Slab over cold Lesser Himalaya along the MCT (hot-iron model) resulted in downbuckling of the isotherms along the MCT and produced inverted metamorphism.

2. Hot-over-cold thrusting:

This model is similar to Le Fort's model except that a major dislocation in metamorphic grade across the MCT has been explained by the southward-directed thrusting (e.g., Brunel and Kienast, 1986).

The above models require a rapid uplift and cooling of the HHC (e.g., Thompson and Ridley, 1987) with fast erosion to produce inverted metamorphism (Searle and Rex, 1989). The data from the present study demonstrates a progressive increase in core P-T data from staurolite-kyanite to sillimanite-K-feldspar grade rocks. However, the rim temperature data is more or less uniform in all the metamorphic grades with gradual reduction in pressure from lower to higher grades of the HHC. Consequently, staurolite-kyanite grade shows higher rim temperature than the core. If Le Fort's model is true, it implies that rim temperature in staurolite-kyanite grade should be less than the core temperature, which is expected in cooling stage. Moreover, in such a model, the core is expected to form because of the heat conduction from sillimanite-K-feldspar grade. However, this phenomenon is not observed in Chenab - Bhot Nala traverse and, therefore, this model may not be applicable to explain the inversion.

3. Shear heating along the MCT:

Shearing along MCT has raised the temperature and produced the inverted metamorphism. The thermal effects of shear heating are generally restricted to a narrow zone and remain for a shorter duration (Scholtz, 1980).

In Zaskar, the highest grade metamorphic rocks occur at least 20-30 km away from the MCT and the increase in grade is confirmed from the P-T data. Also, there is no significant change in the rim P-T data of the HHC rocks, which are occurring on both sides of the Kishtwar Window. The uniformity in rim temperature suggests a thermal equilibration of the HHC during uplift. If the metamorphic inversion is due to shear heating, the rim temperature would not show a uniform profile. Moreover, such shear heating would be restricted only to a short distance on either side of the shear zone (Scholtz, 1980; Le Fort, 1986; Vidal et al., 1982; Searle and Fryer, 1986; Searle and Rex, 1989). Therefore, shear heating could not have produced such inversion in this region.

4. Thermal effects of leucogranite magmatism:

The generation of thrust-related Miocene leucogranite at the top of the High Himalayan slab provided the heat source for inverted metamorphism (Le Fort, 1986).

In the present study area, leucogranite occurs as small bodies and to a limited extent at the top of HHC. Thermal effect of such small leucogranite bodies would be restricted to a very limited and, therefore, it would not be possible to produce

metamorphic inversion for such a larger area, unlike it is observed in Nepal (Le Fort, 1986; Pecher, 1989; Searle and Rex, 1989).

5. Syn-to post-metamorphic deformation:

This model implies that a normal upward-decreasing Barrovian metamorphic sequence was deformed by subsequent folding and thrusting (Frank et al., 1977; Searle et al., 1988).

In Himachal Pradesh, metamorphic inversion has been explained due to recumbent folding (Frank et al., 1977; Naha and Ray, 1970). In the present area, the overall metamorphic textures indicate that the minerals in all the metamorphic grades have grown during main D_2 deformation showing syn- to post-tectonic mineral growth. No large folds of D_2 or D_3 deformational phases are observed in this region hence it is unlikely that recumbent folding has caused inverted metamorphism.

6. Thrust Imbrication

Tectonic stacking and imbrication by late thrusts, post-dating peak metamorphism is explained to be the cause for metamorphic inversion (Treloar et al., 1989a, b).

If the inversion is due to thrust imbrication, an abrupt change in metamorphic grade is expected as it is observed in North Pakistan (Treloar et al., 1989a, b). In study area, overall texture and mineral assemblage indicate their development during prograde and main D_2 deformation. Also, the observed metamorphic change is gradual, while moving from grade to grade in the HHC.

Therefore, this model may not be applicable to explain inversion for this region.

Therefore, the known models of inverted metamorphism cannot satisfactorily explain the metamorphic inversion in this part of the HHC. The P-T values indicate that metamorphism was initiated at depth because of subsidence of the Indian Plate during the onset of collision with Eurasian Plate. Further collision has probably caused intense ductile shearing and top-to-southwest overthrust-type movement during peak metamorphism at depth. This seems to have resulted into inverted metamorphism by discrete displacements of higher grade metamorphic rocks over the lower grade, the cooling of the high grade rocks and subsequent heating of the lower grade rocks giving an apparent isothermal uplift. Also, the pressure release during the fast uplift of the higher part compared to the lower or basal part of the HHC, probably equilibrated the whole of HHC with respect to temperature. Therefore, it is possible that the inverted metamorphism observed in this part of the HHC may be due to ductile shearing and related uplift after an initial subsidence.

REFERENCES

- Anand, A., 1986. Deformation and strain pattern of the Central Himalayan metamorphic from North Western Garhwal. Unpublished Ph.D. thesis. University of Roorkee, Roorkee, India.
- Agarwal, N.C. and Kumar, C., 1973. Geology of the Upper Bhagirathi and Yamuna vallys, Uttarkashi District, Kumaon Himalaya. *Him. Geol.*, 3, 1-23.
- Arita, K., 1983. Origin of the inverted metamorphism of the Lower Himalayas, Central Nepal. *Tectonophysics*, 95, 43-60.
- Banno, S., Sakai, C. and Higashino, T., 1986. Pressure-Temperature trajectory of the Sanbagawa metamorphism deduced from garnet zoning. *Lithos*, 19, 51-63.
- Barnicoat, A.C. and Treloar, P.J., 1989. Himalayan metamorphism-an introduction. *J. Meta. Geol.*, 7, 3-8.
- Bell, T.H., 1985. Deformation partitioning and porphyroblast rotation in metamorphic rocks: a radical reinterpretation. *J. Meta. Geol.*, 3, 109-118.
- Bell, T.H., Fleming, R.D. and Rubenach, M.J., 1986. Porphyroblast nucleation, growth and dissolution in regional metamorphic rocks as a function of deformation partitioning during foliation development. *J. Meta. Geol.*, 4, 37-67.
- Bell, T.H. and Rubenach, M.J., 1980. Crenulation cleavage development-evidence for progressive bulk inhomogeneous shortening from millipede microstructures in the Robertson River metamorphics. *Tectonophysics*, 68, T9-T15.
- Bell, T.H. and Rubenach, M.J., 1983. Sequential porphyroblast growth and crenulation cleavage development during progressive deformation. *Tectonophysics*, 92, 171-194.
- Berman, R.G., 1988. Internally consistent thermodynamic data for minerals in the system $\text{Na}_2\text{O}-\text{K}_2\text{O}-\text{CaO}-\text{MgO}-\text{FeO}-\text{Fe}_2\text{O}_3-\text{Al}_2\text{O}_3-\text{SiO}_2-\text{TiO}_2-\text{H}_2\text{O}-\text{CO}_2$. *J. Petrol.*, 29, 445-522.
- Berthe, D. Choukroune, P. and Jegouzo, P., 1979. Orthogenesis, mylonite and non-coaxial deformation of granite: the example of the South Armorician Shear Zone. *J. Struct. Geol.*, 1, 31-42.
- Bhattacharya, D.S. and Das, K.K., 1983. Inversion of metamorphic zones in the lower Himalayas at Gangtok, Sikkim, India. *J. Geol. Soc.*, London, 91, 98-102.

- Bohlen, S.R., Wall, V.J. and Boettcher, A.L., 1983. Experimental investigations and geological applications of equilibria in the system FeO-TiO₂-Al₂O₃-SiO₂-H₂O. *Am. Mineral.*, 68, 1049-1058.
- Bordet, P., 1961. Himalaya du Nepal region de La Makalu (centre Nati, *Rech. Sc. Pans* 225 p), *Recherches geologiques dans Geology.*, 13, 679 - 682.
- Borradaile, G.J., Bayly, M.B. and Powell, cMCA., 1982. Atlas of deformation and metamorphic rock fabrics, Springer-Verlag. Berlin Heidelberg, New York.
- Bouchez, J.L., 1978. Preferred orientation of quartz (a) axes in some tectonics; Kinematics inferences. *Tectonophysics*, 49, 725 - 730.
- Bouchez, J.L. and Pecher, A., 1981. The Himalayan Main Central Crystalline Thrust Pile and its quartz rich tectonites in Central Nepal. *Tectonophysics*, 78, 23 - 50.
- Brunel, M., 1986. Ductile thrusting in the Himalayas: Shear sense criteria and stretching lineations. *Tectonics*, 5, 247-265.
- Brunel, M. and Kienast, J.-R., 1986. Etude petro-structurale des chevauchements ductiles himalayans sur la transversale de l'Everest-Makalu (Nepal oriental). *Cand. J. Earth. Sci.*, 23, 1117-1137.
- Burg, J.P., and Laurent, Ph., 1978. Strain analysis of a shear zone in a granodiorite. *Tectonophysics*, 47, 15-42.
- Caby, R., Pecher, A. and Le Fort, P., 1983. Le grand chevauchement Central Himalaya: nouvelles donnees sur le metamorphisme inverse a la base de la Dalle du Tibet. *Revue Geologique Dynamique Geographic et Physique.*, 24, 89 - 100.
- Carmichael, D.M., 1978. Metamorphic bathozones and bathograds: a measure of the depth of post-metamorphic uplift and erosion on a regional scale. *Am. J. Sci.*, 278, 769-797.
- Chatterjee, N.D. and Johannes, W. 1974. Thermal stability and standard thermodynamic properties of synthetic 2M₁-Muscovite KAl₂(AlSi₃O₁₀(OH)₂). *Contri. Mineral. Petrol.*, 48, 89-114.
- Crawford, A.R., 1974. The Indus Suture line, the Himalaya, Tibet and Gondwana land, *Geol. Mag.*, VIII, 369-383.
- Crawford, M.L., 1977. Calcium zoning in almandine garnet, Wissahickon Formation, Philadelphia, Pennsylvania. *Can. Mineral.*, 15, 243-249.

- Cygan, R.T. and Lasaga, A.C., 1982. Crystal growth and the formation of chemical zoning in garnets. *Contrib. Mineral. Petrol.*, 79, 189-200.
- Das, B.K., 1973. Geology and metamorphism of rocks around Kishtwar, District Doda, Jammu and Kashmir State. *J. India Acad. Geosci.*, 16, 21-39.
- Das, B.K., 1978. Polyphase medium to high pressure regional metamorphism of pelitic rocks around Kishtwar, Jammu and Kashmir State, India. *N. Jb. Miner. Abh.*, 132, 173-190.
- Das, B.K., 1979. Relation between metamorphic crystallisation and deformation: an example from Lower Himalayan Terrain, India. *Geol. Rdsch.*, 68(1), 351-364.
- Das, B.K., 1987. Petrology of Barrovian-Type regional metamorphism in pelitic schists of Kishtwar, Kashmir Himalaya, India. *Proc. Nat. Sem. Tert. Orogeny*, 153-187.
- Dewey, J.F. and Bird, J.M., 1970. Mountain belts and the new global tectonics. *J. Geophys. Res.*, 79(14), 2625 - 2647.
- Dewey, J.F., and Burke, K.C.A., 1973. Tibetan, Variscan and Pre-Cambrian basement reactivation; Products of continental collision. *J. Geol.*, 81(6), 683 - 692.
- Eisbacher, G.H., 1970. Displacement and stress field along part of the oblique fault, Nova Scotia and J. *Earth Sci.* 6, 1095-1104.
- Etchecopar A., 1974. Simulation Par ordinateur de la deformation progressive d' un agregat polycristallin. These zeme cycle, Univ. Nantes, 135p.
- Essene, E., 1982. Geologic thermometry and barometry. In: Ferry, J.M. (ed.) *Characterization of metamorphism through mineral equilibria*, *Reviews in Mineralogy*, Mineral. Soc. Am., 10, 153-206.
- Ferry, J.M., 1982. A comparative geochemical study of pelitic schists and metamorphosed carbonate rocks from south-central Maine, U.S.A.. *Contrib. Mineral. Petrol.*, 80, 59-72.
- Ferry, J.M. and Spear, F.S., 1978. Experimental calibration of the partitioning of Fe and Mg between biotite and garnet. *Contrib. Mineral. Petrol.*, 66, 113-117.
- Florence, F.P. and Spear, F.S., 1991. Effects of diffusional modification of garnet growth zoning on P-T path calculations. *Contrib. Mineral. Petrol.*, 107, 487-500.
- Frank, W., Thoni, M. and Purtscheller, F., 1977. Geology and Petrography of Kulu-South Lahaul area. *Colloques international*, C.N.R.S., 268, 147-172.

- Frost, B.R. and Tracy, R.J., 1991. P-T paths from zoned garnets: some minimum criteria. *Am. J. Sci.*, 291, 917-939.
- Fuchs, G., 1975. Contribution to the geology of the North-Western Himalayas. *Abh. Geol. B.-A.*, 32, 1 - 59.
- Fuchs, G., 1987. The Geology of southern Zaskar (Ladakh) - Evidence for the autochthony of the Tethys Zone of the Himalaya. *Jb. Geol. Bundesanst.*, 130, 465 - 491.
- Ganguly, J. and Saxena, S.K., 1984. Mixing properties of aluminosilicate garnets: constraints from natural and experimental data, and application to geothermobarometry. *Am. Mineral.*, 69, 88-97.
- Ganesan, T.M., Razdan, M.L., Razdan, R.K. and Muthu, V.T., 1981. Stratigraphy, structure and geological history of the Zaskar Basin in the North-Western parts of the Zaskar Mountains, Ladakh, Jammu and Kashmir. *Contem. Geosci. Res. Himalaya*, 1, 177-188.
- Gansser, A., 1964. *Geology of the Himalayas*. Interscience publishers, London., 289 p.
- Ghent, E.D., 1976. Plagioclase-garnet- Al_2SiO_5 -quartz: a potential geobarometer-geothermometer. *Am. Mineral.*, 61, 710-714.
- Ghent, E.D., Robbins, D.B. and Stout, M.Z., 1979. Geothermometry, geobarometry and fluid composition of metamorphosed calc-silicates and pelites, Mica Creek, British Columbia. *Am. Mineral.*, 64, 874-885.
- Ghent, E. D. and Stout, M. Z., 1981. Geobarometry and geothermometry of plagioclase-biotite-garnet-muscovite assemblages. *Contrib. Mineral. Petrol.*, 76, 92-97.
- Ghent, E. D. and Stout, M. Z., 1984. TiO_2 activity in metamorphosed pelitic and basic rocks: Principles and applications to metamorphism in southeastern Canadian Coedillera. *Contrib. Mineral. Petrol.*, 86, 248-255.
- Goldman, D.S. and Albee, A.L., 1977. Correlation of Mg/Fe partitioning between garnet and biotite with O^{18}/O^{16} partitioning between quartz and magnetite. *Am. J. Sci.*, 277, 750-761.
- Grant, J.A. and Weiblen, P.W., 1971. Retrograde zoning near the second sillimanite isograd. *Am. J. Sci.*, 270, 281-296.
- Guidotti, C.V., 1970. The mineralogy and petrology of the transition from the lower and upper sillimanite zone in the Oquossoc area, Maine. *J. Petrol.*, 11, 277-336.

- Harris, R.L., Jr, 1977. Displacement of relict Zircons during growth of feldspathic porphyroblasts. *Bull. Geol. Soc. Am.*, 88, 1828-1830.
- Harte, B., 1975. Determination of a pelitic petrogenetic grid for the Eastern Scottish Dalradian, *Ann. Rept. of the Director, Geophys. Lab., Washington*. 74, 438-446.
- Hatcher, R.D, 1990. *Structural Geology Principles, Concepts and Problems*. Merrill Publishing Company, London., 533 p.
- Hayden, H.H., 1904. The geology of Spiti with parts of Bushahr and Rupshu. *Memo. Geol. Surv. India*, 6, 1 - 121.
- Heim, A. and Gansser, A., 1939. Central Himalayas, geological observations of the Swiss Expedition 1936. *Memo. Soc. Helv. Sci. Nat.*, 73/1, 1-245.
- Helgeson, H.C., Delony, J.M., Nesbitt, H.W. and Bird, D.K., 1978. Summary and critique of the thermodynamic properties of rock forming minerals. *Am. J. Sci.*, 278-A.
- Herren, E., 1987. The Zaskar Shear Zone : Northeast-southwest extension with in the Higher Himalaya (Ladakh, India). *Geology*, 15, 409 - 413.
- Hirschberg, A. and Winkler, H.G.F., 1968. Stabilitätsfelder zwischen chlorit, cordierit und Almandin beider Metamorphose. *Contr. Mineral. Petrol.*, 18, 17-42.
- Hodges, K.V. and Crowley, P.D., 1985. Error estimation and empirical geothermobarometry for pelitic system. *Am. Mineral.*, 70, 702-709.
- Hodges, K.V., Hubbard, M.S. and Silverberg, D.S., 1988. Metamorphic constraints on the thermal evolution of the Central Himalayan Orogen. *Phil. Trans. R. Soc. London*, A326, 257-280.
- Hodges, K.V. and McKenna, L.W., 1987. Realistic propagation of uncertainties in geologic thermometry. *Am. Mineral.*, 72, 671-680.
- Hodges, K.V. and Silverberg, D.S., 1988. Thermal evolution of the greater Himalaya, Garhwal, India. *Tectonics*, 7/3, 583-600.
- Hodges, K.V. and Spear, F.S., 1982. Geothermometry, geobarometry and the Al_2SiO_5 triple point at Mt. Moosilauke, New Hampshire. *Am. Mineral.*, 67, 1118-1134.
- Holdaway, M.J., 1971. Stability of andalusite and aluminosilicate phase diagram. *Am. J. Sci.*, 271, 97-131.

- Honegger, K., Dietrich, V., Frank, W., Gansser, A., Thoni, M. and Trommsdorff, V., 1982. Magmatism and metamorphism in the Ladakh Himalayas (the Indus-Tsangpo Suture Zone). *Earth Planet. Sci. Lett.*, 60, 253 - 292.
- Hollister, L.S., 1966. Garnet zoning : an interpretation based on the Raleigh fractionation model. *Science*, 154.
- Hoschek, G., 1969. The stability of staurolite- and chloritoid and their significance in metamorphism of pelitic rocks. *Contr. Mineral. Petrol.*, 22, 208-232.
- Hubbard, M.S., 1989. Thermobarometric constraints on the thermal history of the Main Central Thrust Zone and Tibetan Slab, eastern Nepal Himalaya. *J. Meta. Geol.*, 7, 19-30.
- Indares, A. and Martignole, J., 1985. Biotite-garnet geothermometry in granulite facies: the influence of Ti and Al in biotite. *Am. Mineral.*, 70, 272-278.
- Jamieson, R.A. and Vernon, R.H., 1987. Timing of porphyroblast growth in the Fleurde Lys super group, Newfoundland. *J. Meta. Geol.*, 5, 273-288.
- Jain, A.K. and Anand, A., 1988. Deformational and strain patterns of an intracontinental collision ductile shear zone - an example from the Higher Garhwal Himalaya. *J. Struct. Geol.*, 10(7), 717 - 734.
- Jain, A.K., Singh, S. and Patel, R.C., 1992. Extensional Tectonics in Orogenic Belts: Comparative structures from the Himalaya and Scandinavian Caledonides. Communicated to *Tectonophysics*.
- Jain, A.K., Thakur, V.C. and Tandon, S.K., 1974. Stratigraphy and Structure of the Siang District, Arunachal (NEFA) Himalaya. *Him. Geol.*, 4, 20-6.
- Jangpangi, B.S., 1972. Some observations on the stratigraphy and reverse metamorphism in Darjeeling hills. *Mineral. Geol.*, 2, 356-370.
- Jangpangi, B.S., 1974. Stratigraphy and tectonics of parts of Eastern Bhutan. *Him. Geol.*, 4, 117 - 136.
- Jhingran, A.G., Thakur, V.C. and Tandon, S.K., 1976. Structure and tectonics of the Himalaya. *Him. Geol. Sem. Sec-IIA.*, 1-36.
- Jiang, J. and Lasaga, A.C., 1990. The effect of post-growth thermal events on growth-zoned garnet: implications for metamorphic P-T history calculations. *Contr. Mineral. and Petrol.*, 105, 454-459.

- Johnson, G.D., Johnson, N.M., Opdyke, N.D. and Tahirkheli, R.A.K., 1979. Magnetic reversal stratigraphy and sedimentary tectonic history of the upper Siwalik group, eastern salt Range and southwestern Kashmir. In: Geodynamics of Pakistan, A. Farah and K.A. De Jong eds., Pak. Geol. Surv., Quetta, 149-165.
- Johnson, M.R.W., 1963. Some time-relations of movement and metamorphism in the Scottish Highlands. *Geologie Mijnb.*, 5, 121.
- Kaul, R., Nikam, P.S. and Narayandas, G.R., 1970. Geology of Precambrian Formation of Kishtwar area, Doda District, Jammu and Kashmir. *Pub. Cent. Adv. Stud. Geol., P.U. Chandigarh*, 10, 45-54.
- Koziol, A.M. and Newton, R.C., 1988. Redetermination of the anorthite breakdown reaction and improvement of the plagioclase-garnet- Al_2SiO_5 -quartz geobarometer. *Am. Mineral.*, 73, 216-223.
- Kretz, R., 1973. Kinematics of the crystallization of garnet at two localities near Yellowknife. *Can. Mineral.*, 12, 1-20.
- Kundig, R., 1989. Domal structures and high-grade metamorphism in the Higher Himalayan Crystalline, Zaskar region, north-west Himalaya, India. *J. Meta. Geol.*, 7, 43 - 55.
- Le Fort, P., 1975. Himalaya: the collided range. Present knowledge of the continental arc. *Am. J. Sci.*, 275 (A), 1 - 44.
- Le Fort, P., 1986. Metamorphism and migmatism during Himalayan collision. In *Collision Tectonics* (eds. Coward, M.P. and Ries A.C.). *Geol. Soc. London, Spec. Pub.*, 19, 159 - 172.
- Lombard, A., 1958. Un itineraire geologique dans l'Est du Nepal (Massif du Mont. Everest). *Denkschr. Schweiz. Naturforsch. Ges.*, 82(1), 107.
- Loomis, T.P., 1983. Compositional zoning of crystals. A record of growth and reaction history. In: *Kinetics and equilibrium in mineral reactions.* (ed. Saxena, S.K.), 1-60, Springer-Verlag, New York.
- Lydekker, R., 1878. Note on the geology of Kashmir, Kishtwar and Pangi. *Rec. Geol. India.*, 11, p.31.
- Mattauer, M., 1986. Intracontinental subduction, crust-mantle decollement and crustal-stacking wedge in the Himalayas and other collision belts. In *Collision Tectonics* (eds. Coward, M.P. and Ries, A.C.), *Geol. Soc. London, Spec. Pub.*, 19, 37 - 50.

- Mehrotra, P.C., 1959-60. Progress report on geological mapping and investigation of mineralisation terrains in the Kishtwar area, Doda District, J & K State. Unpub. report, Geol. Surv. India.
- Mehdi, S.H., Kumar, G. and Prakash, G. 1972. Tectonic evolution of Eastern Kumaon Himalaya : a new approach. *Him. Geol.*, 2, 481-501.
- Middlemiss, C.S., 1910. A revision of Silurian-Trias sequence in Kashmir. *Rec. Geol. Surv. India*, 40(3), 206-260.
- Misch, P., 1971. Porphyroblasts and "Crystallisation force" some textural criteria. *Bull. Geol. Soc. Am.*, 82, 245-251.
- Mohan, A., Windley, B.F. and Searle, M.P., 1989. Geothermobarometry and development of inverted metamorphism in the Drajeeling-Sikkim region of the eastern Himalaya. *J. Met. Geol.*, 7, 95-110.
- Molnar, P., 1984. Structure and tectonics of the Himalaya: constraints and implications of geophysical data. *Ann. Rev. Earth and Planet. Sci.*, 12, 489-518.
- Molnar, P. and Tapponnier, P., 1975. Cenozoic Tectonics of Asia: Effects of a Continental Collision. *Science*, 189, 419 - 426.
- Mukherjee, A., 1979. Inversion of metamorphic zoning in the eastern Himalaya. In: *Meta. Rock Seq. East. Him.*, (eds., Verma, P.K.), 125-138, K.P. Bagchi's Co., Calcutta.
- Naha, K. and Ray, S.K., 1970. Metamorphic history of the Jutogh series in the Simla Klippe, lower Himalayas. *Contrib. Mineral. Petrol.*, 28, 147-164.
- Nanda, M.M., 1959. Progress report on the geological mapping of Kishtwar area, Doda district, J & K State. (Unpub. report G.S.I.F.S. 1959-60).
- Nanda, M.M. and Singh, M.P., 1977. Stratigraphy and sedimentation of Zaskar area, Ladakh and adjoining parts of Lahaul region of Himachal Pradesh. *Him. Geol.*, 6, 365-388.
- Narain, H., 1973. Crustal structure of the Indian subcontinent. *Tectonophysics.*, 20, 249 - 250.
- Newton, R.C. and Haselton, H.T., 1981. Thermodynamics of the Garnet-Plagioclase- Al_2SiO_5 -Quartz geobarometer. In: R.C. Newton et al., Eds., *Thermodynamics of minerals and melts*, 131-147, Springer-Verlag, New York.
- Orville, P.M., 1972. Plagioclase cation exchange equilibria with aqueous chloride solution: results at 700°C and 2000 bars in the presence of quartz. *Am. J. Sci.*, 272, 234-272.

- Parimoo, M.L. and Raina, B.K., 1970. Annual general report. Geol. Surv. India, 101(1), 62-63.
- Patel, R.C., 1991. Structural geometry and strain patterns of the collision zone, Zaskar, NW-Himalaya. Unpubl. Ph.D. thesis, University of Roorkee, Roorkee, India.
- Pati, U.C. and Rao, P.N., 1981. The Main Central Thrust in U.P. Himalaya. Contem. Geosci. Res. Himalaya, eds., A.K. Sinha, Bishen Singh Mahendra Pal Singh, Dehradun, 1981.
- Pecher, A., 1975. The Main Central Thrust of the Nepal Himalaya and the related metamorphism in the Modi - Kholra Cross section (Annapurna Range). Him. Geol., 5, 115 - 132.
- Pecher, A., 1977. Geology of the Nepal Himalaya: Deformation and petrography in the Main Central Thrust zone: Eclog. Geol. Him., 268, 301-318.
- Pecher, A., 1978. Deformations et metamorphisme associes a une zone de cisaillement, exemple du Grand Chevauchement Central himalayan (MCT) transversale des Annapurnas et du Manaslu, Nepal. Unpubl. Ph.D. thesis, Grenoble.
- Pecher, A., 1989. The metamorphism in the Central Himalaya. J. Meta. Geol., 7, 31 - 41.
- Pecher, A. and Le Fort, P., 1986. The metamorphism in Central Himalaya, its relations with the thrust tectonic. Mem. Sci. Terr. (ed Fond. Sci. Geo. et de ses appl.) Nancy., 47, 285-309.
- Perchuk, L.L. and Lavrent'eva IV, 1983. Experimental investigation of exchange equilibria in the system cordierite-garnet-biotite. In: Saxena, S.K. (ed.) Kinetics and equilibrium in mineral reactions. Springer, Berlin Heidelberg, New York, 199-239.
- Pigage, L.C. and Greenwood, H.J., 1982. Internally consistent estimates of pressure and temperature: the staurolite problem. Am. J. Sci., 282, 943-969.
- Pognante, U., Castelli, D., Benna, P., Genovese, G., Oberli, F., Meier, M. and Tonarinz, S., 1990. The crystalline units of the High Himalayas in the Lahaul-Zaskar region (northwest India): metamorphic tectonic history and geochronology of the collided and imbricated Indian plate. Geol. Mag., 127(2), 101 - 116.
- Pognante, U. and Lombardo, B., 1989. Metamorphic evolution of the High Himalayan Crystallines in SE Zaskar, India. J. Meta. Geol., 7, 9 - 17.

- Powell, C. McA. and Conaghan, P.J., 1973. Polyphase deformation in Phanerozoic rocks of the Central Himalaya gneiss, northwest India. *J. Geol.*, 81, 127 - 143.
- Powell, D. and Treagus, J.E., 1967. On the geometry of S-shaped inclusion trails in garnet porphyroblasts. *Mineral. Mag.*, 36, 453.
- Powell, D. and Treagus, J.E., 1970. Rotational fabrics in metamorphic mineral, In: W.S. Pitcher and G.W. Flinn (Eds) *Control of metamorphism*, Wiley; New York, N.Y. 73-102.
- Ramsay, J.G., 1962. The Geometry and Mechanics of formation of similar type folds. *J. Geol.*, 70, 309-327.
- Ramsay, J.G., 1967. *Folding and Fracturing of rocks*. McGraw-Hill, NY., 568 p.
- Ray, S., 1947. Zonal metamorphism in the eastern Himalaya and some aspects of local geology. *Quartly. J. Geol. Mineral. Metall. Soc. India*, 19, 117 - 140.
- Richardson, S.W., 1968. Staurolite stability in a part of the system Fe-Al-Si-O-H. *J. Petrol.*, 9, 467-488.
- Robie, R.A., Hemingway, B.S. and Fisher, J.R., 1978. Thermodynamic properties of minerals and related substances at 298.15°K and 1bar (105 Pascals) pressure and at higher temperature. *U.S. Geol. Surv. Bull.*, 1452, 456pp.
- Robie, R.A., Bethke, P.M., Touimin, M.S. and Edwards, J.L., 1966. X-ray crystallographic data, densities and molar volumes of minerals. In: Clark, S.P.Jr. (ed.) *Handbook of physical constants*. *Geol. Soc. Am. Memo.*, 97, 27-74.
- Sandhu, C.S., 1985. Deformation and Barrovian metamorphism of Kishtwar area- an example from Lower Himalayan terrain, India. In: *Geology of western Himalaya* (ed., Gupta, V.J.), *Contri. Him. Geol.*, 3, 121-149.
- Saxena, M.N., 1971. The crystalline axis of the Himalaya: The Indian Shield and Continental Drift. *Tectonophysics*, 12, 433 - 447.
- Scholtz, C.H., 1980. Shear heating and the state of stress on faults. *J. Geophys. Res.*, 85, 6174-6184.
- Schoneveld, C., 1977. A study of some typical inclusive pattern in strongly paracrystalline rotated garnets. *Tectonophysics*, 39, 453 - 471.
- Searle, M.P., 1983. On the tectonics of the western Himalaya. *Episodes*, 21 - 26.

- Searle, M.P., 1986. Structural evolution and sequence of thrusting in the High Himalayan, Tibetan Tethys and Indus Suture Zone of Zaskar and Ladakh, Western Himalaya. *J. Struct. Geol.*, 8, 923 - 936.
- Searle, M.P., Cooper, D.J.W. and Rex, A.J., 1988. Collision tectonics of the Ladakh - Zaskar Himalaya. *Phill. Trans. R. Soc. London Ser. A.*, 326, 117 - 150.
- Searle, M.P. and Fryer, B.J., 1986. Garnet, tourmaline and muscovite-bearing leucogranites, gneisses and migmatites of the Higher Himalayas from Zaskar, Kulu, Lahoul and Kashmir. In: *Collision Tectonics* (eds., Coward, M.P. and Ries, A.C.), *Geol. Soc. London Spl. Publ.*, 19, 185-201.
- Searle, M.P. and Rex, A.J., 1989. Thermal model for the Zaskar Himalaya. *J. Meta. Geol.*, 7, 127 - 134.
- Shelley, D., 1972. Porphyroblasts and "Crystallisation force". Some textural criteria discussion. *Bull. Geol. Soc. Am.*, 83, 919-920.
- Singh, J., Kanwar, R.C. and Kapila, S.P., 1980. Deformation of the rocks of Kishtwar area, Doda district, Jammu and Kashmir. *Recent Res. Geol.*, 5, 187-201.
- Sinha Roy, S., 1981. Metamorphic facies and inverted metamorphic sequences of the eastern Himalayan crystalline rocks. In: *Met. Geol. Him.* (ed., Saklani, P.S.), 279-302, Today and Tomorrow's Publishers, Delhi.
- Spear, F.S., 1988. Metamorphic fractional crystallization and internal metasomatism by diffusional homogenization of zoned garnets. *Contrib. Mineral. Petrol.*, 99, 507-517.
- Spear, F.S., 1989. Petrologic determination of metamorphic Pressure-Temperature-Time paths. In: *Metamorphic Pressure-Temperature-Time paths* (eds. Spear, F.S. and Peacock, S.M.), *Short course in Geology, Am. Geophysic. Union*, 7, 1-55.
- Spear, F.S., Hicmott, D.D. and Selverstone, J., 1990. The metamorphic consequences of thrust emplacement. Fall Mountain New Hampshire. *Geol. Soc. Am. Bull.*, 102, 1344-1360.
- Spear, F.S. and Selverstone, J., 1983. Quantitative P-T paths from zoned minerals. Theory and tectonic applications. *Contrib. Mineral. Petrol.*, 83, 348-357.
- Spry, A., 1963. The origin and significance of snowball structure in garnet. *J. Petrol.*, 4, 211-222.

- Srikantia, S.V., Ganesan, T.M., Sinha, P.K. and Tirkey, B., 1976. Geology of part of Zaskar Mountains, Ladakh Himalaya, with special reference to Late Caledonian "Kurgiakh Orogeny", Sem. Geology. Mineral Resources and Natural Resources of Power Development of Himalayas with particular reference to Kashmir, (Abstract).
- Srikantia, S.V., Ganesan, T.M., Rao, P.N., Sinha, P.K. and Tirkey B., 1978. Geology of the Zaskar area, Ladakh Himalaya. *Him. Geol.*, 8/2, 1009 - 1033.
- Srivastava, G.S., 1976. Geology of Kishtwar region, Jammu and Kashmir State. *Him. Geol. Sem.*, Sec. IB, 259-271.
- Storre, B., 1972. Dry melting of muscovite and quartz in the range $P_s = 7$ Kbar to $P_s = 20$ Kbar. *Contrib. Mineral. Petrol.*, 37, 87-89.
- Staubli, A., 1986. Inverse metamorphose am Main Central Thrust, NW-Himalaya, Schweizerische Mineralogische und Petrographische Mitteilungen, 66, 485.
- Staubli, A., 1989. Polyphase metamorphism and the development of the Main Central Thrust. *J. Meta. Geol.*, 7/1, 73-93.
- Stocklin, J., 1980. Geology of Nepal and its regional frame. *J. Geol. Soc. London*, 137, 1-34.
- St-Onge, M.R., 1987. Zoned poikiloblastic garnets: P-T path and synmetamorphic uplift through 30 km of structural depth, Wopmay Orogen, Canada. *J. Petrol.*, 28, 1-27.
- Sturt, B.A. and Harris, A.L., 1961. Metamorphic history of the Loch Tummel area, central perthshire, L'pool Manchr. geol, 2, 689.
- Tewari, A.P., 1981. Exotic thrust mass of the Padar area in Kashmir. *Tectonophysics*, 73, 285-294.
- Thakur, V.C., 1977. Divergent isograds of metamorphism in some parts of Higher Himalayan Zone. *Ecol. Geol. l'Himalaya.*, 268, 433 - 441.
- Thakur, V.C., 1980. Tectonics of the Central Crystallines of Western Himalaya. *Tectonophysics*, 62, 141 - 154.
- Thakur, V.C., 1981. Regional framework and geodynamic evolution of the Indus Suture Zone in the Ladakh Himalaya. *Trans. R. Soc. Edinb. Earth Sci.*, 72, 89 - 97.
- Thakur, V.C., 1987. Plate tectonic interpretation of the Western Himalaya. *Tectonophysics*, 134, 91 - 102.

- Thakur, V.C., Rawat, B.S. and Islam, R., 1990. Zanskar Crystallines - some observations on its lithostratigraphy, deformation, metamorphism and regional framework. *J. Him. Geol.* 1 (1), 11 - 25.
- Thompson, J.B.Jr., 1957. The graphical analysis of mineral assemblages in pelitic schist. *Am. Mineral.*, 42, 842-858.
- Thompson, A.B., 1976. Mineral reactions in pelitic rocks (I) Prediction of P-T-X (Fe-Mg) phase relation (II) Calculation of some P-T-X (Fe-Mg) phase relation. *Am. J. Sci.*, 276, 401-454.
- Thompson, A.B., 1982. Dehydration melting of pelitic rocks and the generation of H₂O undersaturated granite liquids. *Am. J. Sci.*, 282, 1567-1595.
- Thompson, A.B. and England, P.C., 1984. Pressure-Temperature-Time paths of regional metamorphism II. Their inference and interpretation using mineral assemblages in metamorphic rocks. *J. Petrol.*, 25 (4), 929-955.
- Thompson, A.B. and Ridley, J.R., 1987. Pressure-Temperature-Time (P-T-t) histories of orogenic belts. *Phill. Trans. R. Soc.*, London, A321, 27-45.
- Thompson, A.B., Tracy, R.J., Lyttle, P.T. and Thompson, J.B.Jr., 1977. Prograde reaction histories deduced from compositional zonation and mineral inclusions in garnet from the Gassetts schist, Vermont. *Am. J. Sci.*, 277, 1152-1167.
- Toksoz, M.N. and Bird, P., 1977. Modelling of temperatures in continental convergence zones. *Tectonophysics*, 41, 181 - 193.
- Tracy, R.J., 1982. Compositional zoning and inclusions in metamorphic minerals. In: J.M. Ferry (ed.), *Characterization of metamorphism through mineral equilibria*. Mineral. Soc. Am., *Rev. Mineral.*, 10, 355-397.
- Tracy, R.J., Robinson, P. and Thompson, A.B., 1976. Garnet composition and zoning in the determination of temperature and pressure of metamorphism, central Massachusetts. *Am. Mineral.*, 61, 762-775.
- Treloar, P.J., Broughton, R.D., Williams, M.P., Coward, M.P. and Windley, B.F., 1989a. Deformation, metamorphism and imbrication of the Indian plate, south of the Main Mantle Thrust, north Pakistan. *J. Meta. Geol.*, 7, 111-125.
- Treloar, P.J., Coward, M.P., Williams, M.P. and Khan, M.A., 1989b. Basement-cover imbrication south of the Main Mantle Thrust, north Pakistan. *Geol. Soc. Am., Spl. Pap.*, 232, 137-152.

- Trzcienski, Jr. W.E., 1977. Garnet zoning-product of a continuous reaction. *Can. Mineral.*, 15, 250-256.
- Turner, F.J., 1981. *Metamorphic petrology - mineralogy, field and tectonic aspects*. 2nd edn., McGraw-Hill, New York.
- Turner, F.J. and Weiss, L.E., 1963. *Structural analysis of metamorphic tectonites*. McGraw Hill, New York, 545 p.
- Valdiya, K.S., 1978. Extension and analogue of the Chail Nappe in Kumaon, *India Jour. Earth Sci.*, 5,1-19.
- Valdiya, K.S., 1980. The two intracrustal boundary thrusts of the Himalaya. *Tectonophysics.*, 66, 323 - 348.
- Valdiya, K.S., 1981. Tectonics of the central sector of the Himalaya. In: *Zagros - Hindu Kush - Himalaya, Geodynamic evolution*, *Geodyn. Ser.*, V-3, (eds., Gupta, H.K. and Delnancy, F.M.), *Am. Geophys. Uni.*, Washington, D.C., 87-110.
- Vernon, R.H., 1978. Porphyroblast Matrix microstructural relationship in deformed metamorphic rocks. *Geol. Rundsch.*, 67 (1), 288-305.
- Vernon, R.H., 1989. Porphyroblast- matrix microstructural relationships : recent approaches and problems. In: *Evolution of metamorphic belts*. (eds Daly, J.S., Cliff. R.A. and Yardley, B.W.D., *Geol. Soc. special publication No. 43*, 83-102.
- Vidal, P., Cocherie, A. and Le Fort, P., 1982. Geochemical investigations of the origin of the Manaslu leucogranite (Himalaya, Nepal). *Geochimica et Cosmochimica Acta*, 64, 2274-2292.
- Vohra, C.P., Jangpangi, B.S., Mehrotra, P.C., Singh, D.P., Puri, V.M.K., Kaul, M.K. and Mehta, P., 1976. *Geology of the Warwan - Nunkun area, J & K State*. *Him. Geol. Sem.*, Sec.IB, 56-63.
- Wadia, D.N., 1931. The syntaxis of the north-west Himalaya, tectonics and orogeny. *Rec. Geol. Surv. India*, 65, 189-220.
- Wakhaloo, S.N. and Dhar, B.L., 1971. On the geology of the area in and around Kishtwar, Doda district, Kashmir Himalaya. *Him. Geol.*, 1, 123-146.
- Ward, C.M., 1984. *Geology of the Dusky Sound area, Fiordland with Emphasis on the Structural metamorphic Development of some porphyroblastic Staurolite pelites*. Unpubl. Ph.D. thesis, University of Otago, Dunedih.
- Willis, I.L., 1984. Interpretation of macroscopic fold structures in the Willyama Supergroup of the Tackaringa Area, Brolcen Hill., *N.S.W.J. Proc. r. Soc. NSW.*, 117, 85 - 97.

- Windley, B.F., 1988. Tectonic framework of the Himalaya, Karokoram and Tibet and problems of their evolution. Phil. Trans. R. Soc. London Ser.A., 326, 3 - 16.
- Winkler, H.G.F., 1979. Petrogenesis of metamorphic rocks. Springer-Verlag, New York Inc., 5th edn., 348.
- Woodsworth, G.S., 1977. Homogenization of zoned garnets from pelitic schists. Can. Mineral., 15, 230-242.
- Yardley, B.W.D., 1989. An introduction to metamorphic petrology. ELBS, Longman Group UK Ltd.
- Yardley, B.W.D., 1981. A note on the composition and stability of Fe-staurolite. Neues Jahrbuch für Mineralogie Monatshefte Jg, 127-132.
- Zwart, H.J., 1963. Metamorphic history of the Central Pyrenees II. Leid. Geol., Meded, 28, 321-376.

APPENDIX -I

MICROPROBE ANALYSIS OF GARNET

ELEMENTS	KC21/23		KC23/26		T3/5		KC26/28				T4/6		KC6/7		KC4/5					
	GARNET		GARNET		GARNET		GARNET-I		GARNET-II		GARNET-I		GARNET-II		GARNET		GARNET-I		GARNET-II	
	RIM	CORE	RIM	CORE	RIM	CORE	RIM	CORE	RIM	CORE	RIM	CORE	CORE	RIM	CORE	RIM	CORE	RIM	CORE	
WEIGHT%																				
OXIDES																				
SiO ₂	37.075	36.597	37.264	38.009	37.023	36.805	37.187	37.099	37.095	37.323	36.794	36.926	36.979	36.889	37.098	37.530	37.436	37.221		
Al ₂ O ₃	21.144	20.602	21.250	21.317	21.173	20.874	21.426	21.130	21.519	21.466	21.108	21.187	21.275	20.975	20.900	21.227	21.077	21.155		
CaO	1.870	7.867	6.365	8.677	2.564	1.915	3.118	3.576	3.073	3.091	1.804	0.773	1.966	2.220	1.959	2.729	2.782	1.549		
FeO	37.000	23.650	30.959	25.607	34.841	32.547	31.095	29.345	31.578	31.272	34.347	34.123	33.833	28.001	29.314	33.755	34.488	34.958		
MgO	1.807	0.637	1.184	0.794	2.472	1.868	3.365	3.315	4.103	4.007	3.316	3.876	4.157	0.830	1.101	3.686	3.683	4.022		
MnO	0.942	10.412	3.589	6.946	1.609	5.428	3.707	4.282	2.465	3.214	1.509	1.642	0.746	11.768	10.341	1.272	0.599	1.072		
Total	99.838	99.764	100.611	101.350	99.682	99.439	100.166	98.748	100.334	100.372	98.878	98.672	98.956	100.683	100.713	100.198	100.066	99.978		
CATION (on the basis of 12 oxygen)																				
Si	3.0066	2.9754	2.9887	3.0108	2.9935	3.0010	2.9718	2.9979	2.9564	2.9708	2.9876	2.9983	2.9821	2.9937	3.0046	2.9961	2.9957	2.9848		
Al	2.0211	1.9743	2.0090	1.9904	2.0179	2.0062	2.0182	2.0126	2.0215	2.0140	2.0202	2.0250	2.0223	2.0064	1.9952	1.9974	1.9880	1.9996		
Ca	0.1625	0.6854	0.5470	0.7365	0.2222	0.1673	0.2671	0.3096	0.2625	0.2637	0.1569	0.0672	0.1699	0.1930	0.1700	0.2333	0.2386	0.1331		
Fe	2.5095	1.6081	2.0767	1.6964	2.3559	2.2195	2.7081	1.9832	2.1048	2.0817	2.3325	2.3174	2.2818	1.9006	1.9856	2.2538	2.3081	2.3443		
Mg	0.2184	0.0772	0.1416	0.0938	0.2980	0.2271	0.4329	0.3993	0.4875	0.4754	0.4013	0.4685	0.4997	0.1004	0.1329	0.4386	0.4394	0.4808		
Mn	0.0648	0.7170	0.2438	0.4661	0.1102	0.3749	0.2509	0.2931	0.2002	0.2167	0.1038	0.1128	0.0510	0.8089	0.7094	0.0860	0.0406	0.0728		
Total	7.9829	8.0374	8.0068	7.9940	7.9976	7.9959	8.0191	7.9958	8.0329	8.0222	8.0023	7.9892	8.0068	8.0031	7.9978	8.0052	8.0103	8.0154		

APPENDIX - I - continued

ELEMENTS	KCl/1		T10/16		T21/28		A37/43		A41/48		A45/50		A46/51					
	GARNET		GARNET		GARNET		GARNET-I		GARNET-II		GARNET-I		GARNET-II		GARNET-I			
	RIM	CORE	RIM	CORE	RIM	CORE	RIM	CORE	RIM	CORE	CORE	RIM	CORE	RIM	CORE	RIM	CORE	
OXIDES																		
WEIGHT%																		
SiO ₂	37.340	36.958	36.673	36.798	36.733	36.552	37.433	37.107	36.976	37.241	36.828	37.228	37.094	37.085	37.036	37.341	37.348	37.664
Al ₂ O ₃	21.458	20.884	21.195	21.160	20.940	20.942	21.299	20.941	20.969	21.058	20.551	21.229	21.056	20.918	20.897	21.080	21.059	21.117
CaO	5.593	4.188	1.001	1.762	1.984	2.086	4.020	8.499	3.558	4.554	6.214	6.174	1.857	5.108	2.155	3.287	3.041	2.986
FeO	30.037	31.306	34.000	32.977	30.994	31.161	34.591	29.542	33.966	31.362	30.177	29.995	36.373	31.865	36.197	36.276	33.415	33.031
MgO	3.479	3.750	3.163	3.013	2.708	2.438	1.853	1.136	1.742	3.789	2.223	3.608	2.682	1.539	2.529	2.001	3.294	3.883
MnO	1.359	1.538	3.733	3.895	5.6955	5.241	2.291	3.363	3.224	1.161	2.465	1.243	0.680	2.494	0.934	0.242	2.530	2.157
Total	99.267	98.623	99.766	99.604	99.049	98.920	101.487	100.589	100.434	99.165	98.458	99.476	99.741	99.009	99.748	100.226	100.686	100.839
CATION (on the basis of 12 oxygen)																		
Si	2.9859	2.9888	2.9693	2.9783	2.9907	2.9788	2.9854	2.9766	2.9865	2.9902	3.0004	2.9758	2.9995	3.0134	2.9996	3.0073	2.9842	2.9911
Al	2.0225	1.9905	2.0227	2.0186	2.0096	2.0117	2.0022	1.9800	1.9963	1.9929	1.9735	2.0002	2.0069	2.0034	1.9949	2.0011	1.9833	1.9767
Ca	0.4789	0.3629	0.0869	0.1528	0.1732	0.1822	0.3436	0.7305	0.3080	0.3919	0.5424	0.5289	0.1609	0.4447	0.1870	0.2837	0.2604	0.2541
Fe	2.0088	2.1171	2.3025	2.2322	2.1104	2.1239	2.3072	1.9820	2.2943	2.1060	2.0562	2.0052	2.4599	2.1654	2.4519	2.4434	2.2328	2.1939
Mg	0.4148	0.4520	0.3818	0.3635	0.3281	0.3569	0.2203	0.1359	0.2097	0.4535	0.2701	0.4299	0.3233	0.1864	0.3054	0.2402	0.3923	0.4596
Mn	0.0920	0.1053	0.2561	0.2670	0.3927	0.3618	0.1547	0.2285	0.2206	0.0790	0.1701	0.0841	0.0466	0.1716	0.0640	0.0165	0.1712	0.1451
Total	8.0029	8.0163	8.0194	8.0124	8.0045	8.0153	8.0135	8.0334	8.0153	8.0134	8.0128	8.0241	7.9970	7.9849	8.0029	7.9921	8.0242	8.0206

APPENDIX - I - continued

ELEMENTS	A46/51		A47/54				A47/55				A47/56				U92/110		U93/111A	
	GARNET-II		GARNET-I		GARNET-II		GARNET-I		GARNET-II		GARNET-I		GARNET-II		GARNET		GARNET	
	RIM	CORE	RIM	CORE	RIM	CORE	RIM	CORE	RIM	CORE	RIM	INNER RIM	CORE	RIM	CORE	RIM	RIM	CORE
WEIGHT%																		
SiO ₂	37.129	37.489	38.486	37.534	38.427	38.277	37.849	37.790	37.808	38.165	37.764	37.845	37.976	37.809	37.975	37.165	36.718	36.626
Al ₂ O ₃	20.982	20.751	21.736	21.101	21.718	21.668	21.106	21.030	21.173	21.077	21.357	21.308	21.580	21.376	21.346	21.029	21.287	21.011
CaO	2.946	2.999	6.921	6.148	4.907	5.051	2.968	3.192	2.713	3.633	2.318	2.567	2.098	2.279	2.221	6.673	4.431	4.172
FeO	33.591	32.439	27.630	28.016	28.002	27.924	32.307	32.851	33.188	32.271	33.959	33.714	32.807	34.009	32.258	29.160	28.484	30.391
MgO	3.059	3.362	5.376	5.993	5.197	6.250	3.966	3.820	3.989	4.048	4.361	4.680	5.017	4.359	4.803	1.334	2.299	2.801
MnO	2.690	2.228	1.407	1.387	2.629	1.529	1.757	1.777	1.996	1.703	0.859	0.920	0.825	0.889	0.848	4.313	7.016	4.364
Total	100.398	99.268	101.556	100.179	100.879	100.699	99.953	100.460	100.868	100.896	100.619	101.035	101.303	100.721	99.452	99.675	100.205	99.364
CATION (on the basis of 12 oxygen)																		
Si	2.9814	3.0211	2.9770	2.9835	2.9962	2.9178	3.0155	3.0059	2.9976	3.0140	2.9932	2.9865	2.9822	2.9938	3.0193	2.9994	2.9580	2.9665
Al	1.9859	1.9711	1.9818	1.9571	1.9959	1.9870	1.9824	1.9721	1.9787	1.9619	1.9953	1.9820	1.9976	1.9950	2.0005	2.0004	2.0184	2.0058
Ca	0.2535	0.2590	0.5736	0.5184	0.4100	0.4211	0.2534	0.2721	0.2305	0.3074	0.1968	0.2171	0.1765	0.1934	0.1892	0.5771	0.3825	0.3620
Fe	2.2558	2.1863	1.7875	1.8437	1.8259	1.8169	2.1526	2.1854	2.2007	2.1314	2.2504	2.2250	2.2204	2.2522	2.1450	1.9682	1.9191	2.0589
Mg	0.3662	0.4039	0.6200	0.7030	0.6039	0.7249	0.4709	0.4528	0.4715	0.4765	0.5153	0.5505	0.5874	0.5146	0.5693	0.1605	0.2760	0.3383
Mn	0.1830	0.1521	0.0922	0.0924	0.1938	0.1008	0.1186	0.1197	0.1340	0.1139	0.0577	0.6151	0.0549	0.5966	0.5710	0.2948	0.4788	0.2993
Total	8.0257	7.9934	8.0321	8.0680	8.0058	8.0285	7.9933	8.0080	8.0130	8.0051	8.0092	8.0225	8.0190	8.0086	7.9804	8.0004	8.0328	8.0306

APPENDIX - I - continued

ELEMENTS	U93/111B		U93/111C		U93/112B		A49/59		A53/62B		U76/85		U80/95		U86/103		A57/68	
	GARNET		GARNET-I	GARNET-II	GARNET		GARNET		GARNET		GARNET		GARNET		GARNET		GARNET	
	RIM	CORE			RIM	CORE	RIM	CORE	RIM	CORE	RIM	CORE	RIM	CORE	RIM	CORE	RIM	CORE
OXIDES																		
WEIGHT%																		
SiO ₂	37.499	37.339	36.867	37.138	37.788	37.426	37.770	37.425	37.665	36.667	36.871	36.377	36.410	36.727	36.447	36.334	36.331	
Al ₂ O ₃	21.196	20.914	20.938	21.221	21.258	21.193	21.222	21.140	21.370	21.045	21.292	21.079	20.876	21.165	20.885	20.781	20.913	
CaO	4.636	4.418	8.828	4.994	9.639	3.258	3.267	0.875	0.925	1.664	1.857	0.837	1.306	1.367	1.143	2.025	1.296	
FeO	27.465	29.478	28.145	29.676	25.497	33.143	32.071	36.310	35.100	32.069	31.060	33.246	33.906	36.283	35.963	32.007	34.634	
MgO	1.891	2.528	2.348	2.611	2.758	3.786	4.613	2.145	2.480	2.743	3.225	1.611	1.751	1.946	2.186	1.956	2.893	
MnO	7.663	5.128	5.263	4.975	2.925	1.658	1.608	2.785	3.395	5.846	6.170	6.859	5.693	3.613	3.760	6.332	2.723	
Total	100.350	99.805	99.389	100.613	99.865	100.465	100.551	100.680	100.935	100.034	100.572	100.011	99.943	101.101	100.384	99.435	98.789	
CATION (on the basis of 12 oxygen)																		
Si	3.0055	3.0040	2.9792	2.9696	2.9950	2.9825	2.9893	3.0122	3.0124	2.9693	2.9629	2.9708	2.9739	2.9650	2.9640	2.9736	2.9737	
Al	2.0024	1.9833	1.9944	2.0000	1.9859	1.9907	1.9797	2.0059	2.0150	2.0085	2.0105	2.0291	2.0098	2.0140	2.0018	2.0046	2.0176	
Ca	0.3982	0.3808	0.5047	0.4279	0.8186	0.2782	0.2771	0.0755	0.0793	0.1443	0.1622	0.0734	0.1143	0.1183	0.0997	0.1776	0.1136	
Fe	1.8411	1.9834	1.9021	1.9846	1.6902	2.2089	2.1227	2.4441	2.3478	2.1722	2.0844	2.2704	2.3161	2.4497	2.4460	2.1908	2.3708	
Mg	0.2259	0.3032	0.2828	0.3112	0.3259	0.4498	0.5444	0.2573	0.2956	0.3311	0.3857	0.1961	0.2132	0.2342	0.2648	0.2386	0.3529	
Mn	0.5202	0.3495	0.3603	0.3369	0.1963	0.1119	0.1077	0.1899	0.2300	0.4010	0.4194	0.4745	0.3939	0.2470	0.2590	0.4390	0.1889	
Total	7.9933	8.0043	8.0235	8.0304	8.0120	8.0221	8.0209	7.9849	7.9801	8.0265	8.0296	8.0146	8.0212	8.0280	8.0352	8.0241	8.0175	

APPENDIX - I - continued

ELEMENTS	077/90		A80/111				080/96		067/70		064/67		A65/78				060/63		057/60	
	GARNET		GARNET-I		GARNET-II		GARNET		GARNET		GARNET		GARNET-I		GARNET-II		GARNET-II		GARNET-I	GARNET-II
	RIM	CORE	RIM	CORE	RIM	CORE	RIM	CORE	RIM	CORE	RIM	CORE	RIM	CORE	RIM	CORE	RIM	CORE		

WEIGHT%

OXIDES

SiO ₂	36.042	36.515	37.369	37.262	37.584	37.645	36.602	36.816	36.641	36.785	36.532	36.906	37.231	36.562	37.294	36.022	37.205	36.628	36.633
Al ₂ O ₃	20.771	20.944	21.361	21.141	21.543	21.520	20.974	21.069	21.065	21.038	20.893	21.213	21.371	21.124	21.635	20.811	21.302	21.082	20.988
CaO	2.793	2.615	3.431	4.353	4.560	3.485	1.772	2.543	0.797	0.956	1.297	1.955	2.243	1.357	1.906	1.297	1.366	1.770	1.680
FeO	36.753	36.009	32.931	34.081	31.863	31.374	33.271	32.882	32.762	34.585	30.992	32.596	33.718	32.128	34.560	33.601	35.510	27.725	28.038
MgO	1.984	2.364	3.649	2.511	3.503	4.434	1.631	1.801	1.329	1.683	2.823	2.480	3.421	2.379	3.658	1.848	3.276	2.805	2.798
MnO	0.690	1.259	1.566	0.831	1.449	1.223	5.589	5.439	8.005	5.951	6.726	5.398	3.055	6.117	2.712	5.987	2.082	9.824	9.855
Total	99.033	99.705	100.305	100.178	100.503	99.682	99.839	100.610	100.599	100.997	99.264	100.549	101.039	99.666	101.766	99.566	100.741	99.844	99.992

CATION (on the basis of 12 oxygen)

Si	2.9607	2.9693	2.9798	2.9908	2.9827	2.9927	2.9843	2.9795	2.9802	2.9773	2.9778	2.9734	2.9679	2.9741	2.9532	2.9575	2.9788	2.9673	2.9674
Al	2.0112	2.0075	2.0077	1.9999	2.0148	2.0164	2.0157	2.0066	2.0195	2.0070	2.0074	2.0145	2.0079	2.0254	2.0194	2.0140	2.0103	2.0131	2.0039
Ca	0.2458	0.2278	0.2932	0.3741	0.3877	0.2969	0.1546	0.2202	0.0694	0.0829	0.1133	0.1688	0.1916	0.1182	0.1618	0.1141	0.1172	0.1536	0.1459
Fe	2.5250	2.4489	2.1962	2.2876	2.1143	2.0855	2.2688	2.2219	2.2285	2.3411	2.1127	2.4312	2.1965	2.2479	2.1856	2.2889	2.3072	2.3777	1.8791
Mg	0.2429	0.2866	0.4336	0.3004	0.4143	0.5253	0.1983	0.2169	0.1611	0.2030	0.3429	0.2979	0.4065	0.2884	0.4318	0.2262	0.3910	0.3388	0.3379
Mn	0.0480	0.0867	0.1058	0.0564	0.0974	0.0824	0.3860	0.3722	0.5514	0.4080	0.4645	0.3683	0.2064	0.4215	0.1819	0.4164	0.1412	0.6742	0.6762
Total	8.0337	8.0261	8.0163	8.0093	8.0106	7.9991	8.0078	8.0173	8.0101	8.0192	8.0185	8.0194	8.0281	8.0132	8.0371	8.0354	8.0161	8.0261	8.0307

APPENDIX - I - continued

ELEMENTS	052/55		048/51		043/47			A67/86					026/28			
	GARNET		GARNET		GARNET			GARNET-I			GARNET-II		GARNET-I		GARNET-II	
	RIM	CORE	RIM	CORE	RIM	INNER RIM	CORE	RIM	INNER RIM	CORE	RIM	CORE	RIM	CORE	RIM	CORE
WEIGHT%																
SiO ₂	36.181	36.559	36.502	36.722	37.422	37.296	36.914	37.198	37.063	37.307	37.047	37.416	36.652	36.732	36.796	
Al ₂ O ₃	20.847	21.071	21.055	21.104	20.798	20.441	20.715	21.356	21.338	21.440	21.191	21.436	21.080	21.142	21.076	
CaO	1.383	1.243	0.882	1.239	1.205	1.195	1.912	2.067	2.069	3.087	1.794	1.876	1.384	1.169	1.300	
FeO	31.638	34.315	31.500	33.611	35.365	34.877	34.811	31.726	32.809	32.342	31.407	33.092	29.173	29.934	29.712	
MgO	1.696	2.605	2.031	3.059	1.088	1.425	1.787	2.982	3.934	4.850	3.225	4.995	3.223	3.384	4.000	
MnO	7.805	4.208	7.264	3.455	4.722	4.853	2.933	5.484	3.240	1.127	5.248	1.316	8.179	7.271	6.729	
Total	99.550	100.000	99.235	99.180	100.600	100.086	99.072	100.814	100.452	100.153	99.912	100.130	99.692	99.633	99.612	
CATION (on the basis of 12 oxygen)																
Si	2.9677	2.9673	2.9859	2.9841	3.0321	3.0360	3.0182	2.9759	2.9628	2.9636	2.9836	2.9739	2.9681	2.9716	2.9682	
Al	2.0155	2.0158	2.0300	2.0214	1.9862	1.9613	1.9964	2.0139	2.0105	2.0075	2.0116	2.0082	2.0121	2.0159	2.0040	
Ca	0.1216	0.1081	0.0772	0.1079	0.1046	0.1042	0.1675	0.1772	0.1771	0.2627	0.1547	0.1597	0.1201	0.1013	0.1123	
Fe	1.8995	2.1703	2.3293	2.1550	2.2843	2.3964	2.3804	2.1228	2.1932	2.1487	2.1154	2.1997	1.9756	2.0252	2.0045	
Mg	0.2074	0.3152	0.2477	0.3705	0.1314	0.1729	0.2178	0.3556	0.4680	0.5743	0.3872	0.5918	0.3890	0.4082	0.4810	
Mn	0.5421	0.2893	0.5033	0.2371	0.3241	0.3346	0.2031	0.3717	0.2203	0.0758	0.3581	0.0887	0.5610	0.4982	0.4598	
Total	8.0246	8.0249	7.9991	8.0052	7.9748	7.9834	7.9835	8.0171	8.0320	8.0327	8.0106	8.0220	8.0259	8.0205	8.0298	

APPENDIX - I - continued

ELEMENTS	U28/30		U29/31				U33/35		A68/91A	A74/97		U4/4	
	GARNET		GARNET-I		GARNET-II		GARNET		GARNET	GARNET		GARNET	
	RIM	CORE	RIM	CORE	RIM	CORE	RIM	CORE		RIM	CORE	RIM	CORE
WEIGHT%													
OXIDES													
SiO ₂	36.787	37.054	36.344	36.743	36.681	36.659	36.575	36.490	37.172	36.431	36.818	36.398	36.655
Al ₂ O ₃	21.132	21.077	20.932	21.191	21.160	21.138	21.059	21.038	21.274	21.164	21.207	20.862	20.984
CaO	1.229	1.596	1.135	1.229	0.881	0.795	1.406	1.172	1.251	0.765	0.895	0.882	1.272
FeO	33.998	34.860	34.483	35.235	33.911	34.874	33.727	34.803	32.421	34.560	35.174	34.607	34.143
MgO	1.853	2.871	2.037	2.996	1.895	2.599	1.786	2.852	1.524	1.858	2.692	2.438	2.575
MnO	4.912	2.525	5.013	3.111	5.368	4.014	5.327	3.196	7.254	5.273	3.553	3.820	3.717
Total	99.911	99.982	99.945	100.505	99.896	100.080	99.880	99.550	100.900	100.051	100.339	99.007	99.345
CATION (on the basis of 12 oxygen)													
Si	2.9906	2.9911	2.9661	2.9623	2.9852	2.9726	2.9802	2.9687	2.9970	2.9692	2.9746	2.9827	2.9858
Al	2.0249	2.0054	2.0136	2.0138	2.0298	2.0204	2.0226	2.0174	2.0221	2.0331	2.0195	2.0150	2.0148
Ca	0.1071	0.1380	0.0992	0.1062	0.0768	0.0691	0.1228	0.1022	0.1081	0.0667	0.0775	0.0775	0.1110
Fe	2.3115	2.3534	2.3538	2.3758	2.3081	2.3651	2.2983	2.3681	2.1861	2.3555	2.3766	2.3717	2.3260
Mg	0.2245	0.3455	0.2478	0.3601	0.2299	0.3142	0.2169	0.3459	0.1831	0.2257	0.3243	0.2977	0.3127
Mn	0.3383	0.1726	0.3466	0.2125	0.3701	0.2757	0.3677	0.2202	0.4957	0.3640	0.2431	0.2653	0.2564
Total	7.9969	8.0061	8.0271	8.0307	7.9999	8.0172	8.0085	8.0226	7.9920	8.0142	8.0156	8.0098	8.0068

APPENDIX - I - continued

ELEMENTS	U13/13			P22/86				P12/20		P9/50				P9/46		P9/43
	GARNET			GARNET-I		GARNET-II		GARNET		GARNET-I		GARNET-II		GARNET		GARNET
	RIM	INNER RIM	CORE	RIM	CORE	RIM	CORE	RIM	CORE	RIM	CORE	RIM	CORE	RIM	CORE	
OXIDES																
WEIGHT%																
SiO ₂	36.754	36.683	36.841	36.603	36.625	36.682	37.048	36.607	36.951	36.938	36.675	36.795	36.439	36.783	35.865	36.843
Al ₂ O ₃	21.072	21.002	21.205	20.971	21.132	21.299	21.330	21.017	21.014	21.039	20.811	21.102	20.560	21.621	21.193	20.859
CaO	0.822	0.832	0.884	0.978	0.892	1.006	0.945	0.840	0.814	3.776	9.343	3.660	3.018	2.793	1.628	3.437
FeO	32.827	32.799	35.047	33.206	35.402	32.092	34.270	33.422	36.047	28.939	24.154	30.313	31.839	30.685	32.179	31.216
MgO	1.442	1.718	2.679	1.902	2.427	1.690	1.981	1.584	2.492	2.137	1.022	2.187	2.391	2.349	2.562	2.586
MnO	7.726	6.589	2.992	6.024	3.395	7.370	4.749	6.816	2.479	6.192	6.639	4.804	4.192	5.508	5.412	3.690
Total	100.643	99.624	99.648	99.984	99.872	100.137	100.323	100.286	99.797	99.020	98.644	98.861	98.438	99.740	98.841	98.631
CATION (on the basis of 12 oxygen)																
Si	2.9842	2.9952	2.9879	2.9872	2.9763	2.9803	2.9946	2.9811	2.9982	2.9999	2.9837	2.9934	2.9908	2.9701	2.9425	3.0008
Al	2.0167	2.0213	2.0272	2.0172	2.0241	2.0397	2.0322	2.0173	2.0098	2.0148	1.9956	2.0236	1.9890	2.0577	2.0495	2.0025
Ca	0.0715	0.0728	0.0768	0.0856	0.0777	0.0875	0.0819	0.0733	0.0708	0.3288	0.8144	0.3190	0.2654	0.2417	0.1432	0.2999
Fe	2.2292	2.2399	2.3770	2.2663	2.4060	2.1806	2.3167	2.2762	2.4462	1.9659	1.6434	2.0625	2.1855	2.0721	2.2080	2.1263
Mg	0.1745	0.2091	0.3239	0.2314	0.2940	0.2046	0.2387	0.1922	0.3014	0.2586	0.1239	0.2652	0.2925	0.2827	0.3134	0.3140
Mn	0.5313	0.4558	0.2057	0.4165	0.2337	0.5072	0.3252	0.4702	0.1704	0.4258	0.4575	0.3310	0.2914	0.3767	0.3761	0.2546
Total	8.0075	7.9941	7.9985	8.0042	8.0117	7.9999	7.9893	8.0103	7.9969	7.9931	8.0185	7.9948	8.0147	8.0010	8.0327	7.9980

APPENDIX - I - continued

ELEMENTS	SP20		SP25		PL19/123		PL20/125			PL12/113			
	GARNET-I		GARNET-II		GARNET		GARNET-I		GARNET-II	GARNET-I		GARNET-II	
	RIM	CORE	RIM	CORE	RIM	CORE	RIM	CORE	INNER RIM	CORE	RIM	CORE	RIM

WEIGHT%

OXIDES

SiO ₂	37.469	37.391	37.043	36.576	37.058	36.908	37.056	37.246	37.308	37.857	37.470	37.158	37.457	37.799	37.550	37.252	37.255	37.741
Al ₂ O ₃	20.856	21.232	21.372	20.740	20.758	20.406	20.803	20.680	20.738	21.506	215294	21.286	21.372	21.492	20.922	20.807	21.083	21.783
CaO	4.118	5.216	6.315	4.516	8.323	8.958	4.129	5.039	4.792	1.747	2.658	2.759	1.278	1.320	1.515	1.575	2.672	2.631
FeO	30.821	30.169	30.857	33.450	28.328	25.620	32.095	30.959	31.343	35.380	34.048	33.210	35.751	35.018	33.228	32.915	32.453	32.853
MgO	2.881	3.324	3.119	2.718	2.478	1.129	3.694	2.746	3.319	3.501	3.530	3.609	3.540	5.2157	3.907	4.563	3.599	4.324
MnO	2.961	2.292	0.653	0.906	1.421	6.391	1.319	2.864	1.750	1.561	2.398	2.891	1.878	0.226	2.795	2.145	2.306	1.313
Total	99.105	99.623	99.360	98.906	98.365	99.411	99.096	99.533	99.250	101.552	101.633	100.913	101.247	101.070	99.917	99.257	99.367	100.146

CATION (on the basis of 12 oxygen)

Si	3.0216	2.9905	2.9704	2.9766	2.9981	2.9922	2.9887	3.0024	3.0034	2.9938	2.9655	2.9626	2.9804	2.9790	3.0100	2.9976	2.9982	2.9999
Al	1.9825	2.0016	2.0200	1.9894	1.9795	1.9500	1.9777	1.9649	1.9678	2.0046	2.0084	2.0004	2.0044	1.9965	1.9768	1.9735	1.9999	1.9941
Ca	0.3558	0.4466	0.5426	0.3938	0.7215	0.7782	0.3569	0.4352	0.4135	0.1480	0.2254	0.2357	0.1090	0.1115	0.1308	0.1351	0.2304	0.2241
Fe	2.0787	2.0185	2.0694	2.2767	1.9167	1.7371	2.1648	2.0871	2.1102	2.3400	2.2537	2.2144	2.3771	2.3081	2.2279	2.2151	2.1843	2.1842
Mg	0.3463	0.3963	0.3729	0.3298	0.2989	0.1364	0.4442	0.3299	0.3983	0.4127	0.4165	0.4290	0.4200	0.6126	0.4669	0.5473	0.4317	0.5124
Mn	0.2022	0.1553	0.0444	0.0624	0.0974	0.4389	0.0901	0.1955	0.1193	0.1045	0.1608	0.1952	0.1265	0.0151	0.1898	0.1462	0.1572	0.0884
Total	7.9871	8.0087	8.0196	8.0287	8.0121	8.0328	8.0224	8.0151	8.0126	8.0038	8.0303	8.0372	8.0174	8.0228	8.0016	8.0156	8.0018	8.0031

APPENDIX - I - continued

ELEMENTS	12A/126		14/103		PC15A/1		PR3/76			PR6/81			PRI/73		PL4/93					
	GARNET-I		GARNET-II		GARNET		GARNET-I		GARNET			GARNET-I			GARNET-II		GARNET		GARNET-I	
	RIM	CORE	RIM	CORE	RIM	CORE	RIM	CORE	RIM	INNER RIM	CORE	RIM	INNER RIM	CORE	RIM	CORE	RIM	CORE	RIM	CORE
WEIGHT%																				
OXIDES																				
SiO ₂	37.469	37.080	36.942	37.410	37.254	37.737	37.526	37.725	36.625	36.904	36.708	37.304	37.529	37.195	37.513	38.038	37.470	37.183	37.668	37.504
Al ₂ O ₃	21.105	20.831	20.877	20.892	21.211	21.048	21.342	21.541	20.361	20.822	20.795	20.967	21.116	20.851	21.067	21.508	21.065	20.909	21.206	20.868
CaO	2.441	3.453	1.563	1.768	2.564	2.743	1.487	1.546	2.808	5.460	2.622	1.776	2.138	5.319	1.833	2.356	2.535	5.497	7.075	6.680
FeO	33.185	32.925	33.895	32.754	31.743	31.679	34.216	34.371	33.104	31.731	33.905	33.315	33.302	28.983	34.320	33.949	31.720	29.936	28.245	27.297
MgO	3.509	3.348	3.692	4.632	3.603	3.942	3.510	4.734	1.781	1.725	2.189	3.794	4.588	1.795	3.903	4.651	3.742	2.197	3.428	3.127
MnO	2.091	1.656	3.045	2.235	4.162	3.616	3.034	1.485	4.710	2.903	3.685	2.947	0.755	6.910	1.932	0.351	3.814	4.467	1.886	3.420
Total	99.801	99.252	100.013	99.691	100.537	100.765	101.115	101.402	99.389	99.605	99.905	100.104	99.427	101.053	100.569	100.855	100.366	100.189	99.505	98.895
CATION (on the basis of 12 oxygen)																				
Si	3.0050	2.9946	2.9772	2.9959	2.9763	2.9978	2.9864	2.9734	2.9982	2.9938	2.9817	2.9923	3.0021	2.9811	2.9932	2.9980	2.9924	2.9882	2.9988	3.0114
Al	1.9951	1.9830	1.9831	1.9721	1.9974	1.9708	2.0018	2.0011	1.9646	1.9878	1.9991	1.9825	1.9910	1.9698	1.9813	1.9981	1.9829	1.9806	1.9896	1.9750
Ca	0.2098	0.2988	0.1349	0.1577	0.2193	0.2335	0.1268	0.1306	0.2463	0.4738	0.2283	0.1526	0.1833	0.4568	0.1567	0.1990	0.2186	0.47331	0.6033	0.5747
Fe	2.2258	2.2273	2.2245	2.1938	2.1210	2.1046	2.2771	2.2658	2.2664	2.1494	2.3032	2.2349	2.2278	1.9427	2.2902	2.2378	2.1186	2.0120	1.8806	1.8350
Mg	0.4195	0.4063	0.4436	0.5530	0.4292	0.4668	0.4162	0.5560	0.2173	0.2082	0.2651	0.4537	0.5470	0.2145	0.4642	0.5465	0.4455	0.2623	0.4068	0.3743
Mn	0.1421	0.1071	0.2379	0.1516	0.2818	0.2433	0.2046	0.0992	0.3266	0.1991	0.2535	0.2005	0.0512	0.4691	0.1306	0.0235	0.2580	0.3041	0.1273	0.2326
Total	7.9974	8.0139	8.0213	8.0180	8.0250	8.0168	8.0128	8.0261	8.0195	8.0122	8.0228	8.0165	8.0024	8.0340	8.0162	8.0029	8.0161	8.0215	8.0064	8.0011

APPENDIX - I - continued

ELEMENTS	PL4/93		PC15C/22		PC30C/5		PC29/24		PC28P/40			PC28D/30							
	GARNET-II		GARNET-I		GARNET-II		GARNET-I		GARNET-II			GARNET-I							
	RIM	CORE	RIM	CORE	RIM	CORE	RIM	CORE	RIM	INNER RIM	CORE	RIM	INNER RIM	CORE					
WEIGHT%																			
SiO ₂	37.116	37.551	36.916	37.140	36.979	37.600	37.313	37.447	36.744	36.778	36.827	36.694	36.936	37.168	37.254	37.336	37.153	37.376	37.432
Al ₂ O ₃	20.955	21.244	20.752	20.842	20.972	21.054	20.880	21.039	20.783	20.539	20.706	20.798	21.009	21.021	20.915	20.900	20.720	20.906	21.268
CaO	3.102	7.069	6.532	7.761	6.719	3.169	5.718	2.134	5.183	5.011	5.472	2.504	1.878	1.240	1.869	2.083	2.149	2.341	0.571
FeO	29.935	29.296	26.017	30.224	29.196	31.971	29.366	31.194	32.281	30.723	31.923	34.012	34.281	34.824	34.832	34.688	34.499	33.774	35.556
MgO	2.958	2.078	2.055	2.277	2.055	3.957	2.212	3.926	2.247	1.880	2.384	3.259	3.520	3.877	2.872	3.426	3.599	3.696	4.490
MnO	5.530	2.827	8.432	1.561	4.695	2.796	5.268	5.329	1.832	4.076	1.512	1.277	1.244	1.228	1.440	1.254	1.139	1.184	1.043
Total	99.597	100.064	100.703	99.716	100.617	100.548	100.756	101.071	99.071	99.007	98.824	98.543	98.869	99.357	99.182	99.687	99.260	99.277	100.360
CATION (on the basis of 12 oxygen)																			
Si	2.9945	2.9995	2.9635	2.9843	2.9643	2.9916	2.9853	2.9792	2.9856	2.9987	2.9929	2.9908	2.9948	2.9979	3.0181	3.0062	3.0038	3.0105	2.9868
Al	1.9928	2.0002	1.9635	1.9739	1.9816	1.9754	1.9690	1.9729	1.9904	1.9737	1.9835	1.9981	2.0078	1.9985	1.9972	1.9835	1.9745	1.9848	2.0003
Ca	0.2681	0.6080	0.5618	0.6605	0.5771	0.2704	0.4903	0.1819	0.4514	0.4377	0.4763	0.2186	0.1632	0.1072	0.1623	0.1797	0.1862	0.2020	0.0489
Fe	2.0199	1.9507	1.7467	2.0311	1.9574	2.1217	1.9649	2.0756	2.1937	2.0949	2.1697	2.3184	2.3246	2.3491	2.3601	2.3359	2.3327	2.2752	2.3727
Mg	0.3557	0.2474	0.2459	0.2728	0.2456	0.4692	0.2631	0.4651	0.2722	0.2285	0.2889	0.3960	0.4254	0.4661	0.3469	0.4112	0.4338	0.4438	0.5340
Mn	0.3780	0.1913	0.5733	0.1063	0.3188	0.1884	0.3570	0.3591	0.1259	0.2815	0.1042	0.0882	0.0855	0.0839	0.0988	0.0855	0.0780	0.0808	0.0704
Total	8.0090	8.0004	8.0542	8.0288	8.0448	8.0212	8.0302	8.0344	8.0192	8.0147	8.0154	8.0102	8.0013	8.0028	7.9833	8.0020	8.0089	7.9971	8.0131

APPENDIX - I - continued

ELEMENTS	PC28D/30		PC28/42		PC24G/61		PC24D/66		RG49		PC16D/83		P30/120		MP5						
	GARNET-II		GARNET		GARNET-I		GARNET-II		GARNET		GARNET-I		GARNET		GARNET-I		GARNET-II				
	RIM	CORE	RIM	CORE	RIM	CORE	RIM	CORE	RIM	CORE	RIM	CORE	RIM	CORE	RIM	INNER RIM	CORE	RIM	CORE		
WEIGHT%																					
SiO ₂	37.167	37.123	36.979	36.575	37.027	36.426	36.671	37.188	37.249	37.204	37.305	37.248	37.275	37.743	36.758	36.866	36.794	36.988	36.965	36.814	36.979
Al ₂ O ₃	20.896	20.777	20.717	20.509	20.644	20.653	20.508	20.921	21.274	20.710	21.250	21.110	21.286	21.476	21.142	20.846	21.069	21.164	21.081	21.046	20.827
CaO	2.309	3.282	3.623	2.329	3.376	1.817	2.660	2.804	2.573	10.133	1.615	1.788	1.182	1.308	1.910	1.658	1.467	0.909	0.812	1.704	1.713
FeO	34.003	33.950	35.846	31.265	30.927	29.735	30.584	33.657	33.404	29.716	34.210	34.820	34.247	33.764	29.484	31.822	35.003	34.751	32.520	34.271	34.632
MgO	3.582	3.050	1.515	1.859	2.052	1.523	1.746	2.762	3.119	0.872	3.175	3.657	2.514	2.932	2.447	3.263	2.953	3.609	3.679	2.700	3.131
MnO	0.961	0.717	1.038	7.727	5.910	10.305	6.422	2.659	2.662	1.223	2.664	2.134	3.684	3.597	7.720	4.798	2.099	2.373	4.827	2.845	2.020
Total	98.919	98.899	99.718	100.265	99.936	100.460	98.590	99.997	100.286	99.857	100.218	100.758	100.187	100.819	99.461	99.253	99.384	99.792	99.884	99.380	99.299
CATION (on the basis of 12 oxygen)																					
Si	3.0065	3.0090	3.0067	2.9782	3.0002	2.9698	3.0126	2.9971	2.9856	2.9949	2.9941	2.9775	3.0028	3.0091	2.9848	2.9910	2.9860	2.9825	2.9802	2.9897	2.9990
Al	1.9924	1.9851	1.9855	1.9684	1.9716	1.9848	1.9858	1.9878	2.0099	1.9651	2.0104	1.9891	2.0212	2.0182	2.0234	1.9935	2.0154	2.0115	2.0033	2.0146	1.9911
Ca	0.2002	0.2850	0.3156	0.2032	0.2931	0.1586	0.2342	0.2420	0.2210	0.8740	0.1389	0.1531	0.1020	0.1117	0.1661	0.1441	0.1275	0.0785	0.0701	0.1482	0.1489
Fe	2.3004	2.3015	2.4396	2.1291	2.0957	2.0277	2.1013	2.2686	2.2395	2.0005	2.2963	2.3279	2.3073	2.2513	2.0021	2.1592	2.3758	2.3436	2.1928	2.3277	2.3492
Mg	0.4320	0.3685	0.1836	0.2256	0.2479	0.1851	0.2138	0.3319	0.3727	0.1041	0.3798	0.4358	0.3019	0.3484	0.2962	0.3946	0.3571	0.4338	0.4422	0.3269	0.3786
Mn	0.0658	0.0492	0.0714	0.5329	0.4056	0.7118	0.4469	0.1815	0.1807	0.0834	0.1811	0.1445	0.2514	0.2429	0.5310	0.3297	0.1444	0.1620	0.3296	0.1957	0.1387
Total	7.9978	7.9984	8.0005	8.0376	8.0141	8.0378	7.9945	8.0090	8.0094	8.0226	8.0007	8.0279	7.9866	7.9818	8.0035	8.0122	8.0063	8.0118	8.0182	8.0029	8.0055

APPENDIX - II

MICROPROBE ANALYSIS OF CHLORITE

ELEMENTS	KC21/23	T3/5
	WEIGHT%	
OXIDES		
SiO ₂	23.475	24.203
Al ₂ O ₃	22.172	22.548
CaO	0.082	0.072
FeO	26.395	25.178
MgO	12.298	15.600
MnO	-	0.167
Cr ₂ O ₃	0.024	-
NiO	-	0.047
F	0.099	0.400
Total	84.505	88.046
	CATION (on the basis of 28 oxygen)	
Si	5.1887	5.1014
Al	5.7767	5.6020
Ca	0.0195	0.0163
Fe	4.8793	4.4383
Mg	4.0523	4.9017
Mn	-	0.0299
Cr	0.0043	-
Ni	-	0.0080
F	0.0693	0.2663
Total	19.9901	20.3639

APPENDIX - III

MICROPROBE ANALYSIS OF BIOTITE

ELEMENTS	KC21/23	KC23/26	T3/5	KC26/28	T4/6	KC6/7	KC4/5	KC1/1	THATRI	T21/28	A37/43	A41/48	A45/50	A46/51	
														MAT.	INC.
WEIGHT%															
OXIDES															
SiO ₂	35.243	35.656	34.973	37.201	36.065	35.418	36.883	36.605	36.770	35.564	35.628	35.522	36.205	36.738	36.915
Al ₂ O ₃	18.855	18.740	17.682	18.930	18.235	16.562	17.466	17.803	19.567	18.638	18.036	17.892	18.043	18.286	18.105
K ₂ O	8.278	8.876	8.181	8.846	7.723	9.066	7.785	8.589	8.631	9.490	8.433	9.067	8.449	8.784	8.231
Na ₂ O	0.266	0.250	0.126	0.212	0.142	0.069	0.129	0.137	0.449	0.090	0.164	0.155	0.113	0.182	0.243
CaO	0.065	0.060	0.138	0.031	0.069	0.101	0.286	0.049	-	-	0.010	0.047	0.026	0.047	0.095
FeO	21.470	21.296	21.376	17.699	18.551	26.772	17.213	18.039	18.379	19.618	21.521	17.334	19.661	18.544	14.819
MgO	8.933	8.723	8.478	11.593	10.015	4.483	8.697	10.438	10.341	8.269	8.179	9.273	8.696	9.703	12.408
MnO	0.090	0.064	0.053	0.069	0.061	0.549	0.041	0.120	0.121	0.302	0.042	0.093	0.045	0.085	0.024
TiO ₂	1.433	1.792	1.507	1.828	1.652	2.236	1.968	1.305	2.046	2.868	2.127	1.990	1.944	2.569	2.008
Cl	0.020	0.031	0.058	0.024	0.104	0.021	0.066	0.101	0.015	0.021	0.032	0.023	0.041	0.061	0.092
Total	94.647	95.482	92.554	96.426	92.594	95.217	90.518	93.163	96.315	94.885	94.167	91.391	93.214	94.985	92.919
CATION (on the basis of 22 oxygen)															
Si	5.4245	5.4483	5.5145	5.5059	5.5685	5.6077	5.7792	5.6291	5.4642	5.4514	5.5152	5.5798	5.6010	5.5531	5.5871
Al	3.4206	3.3752	3.2863	3.3023	3.3184	3.0914	3.2259	3.2270	3.4273	3.3674	3.2909	3.3127	3.2902	3.2581	3.2298
K	1.6255	1.7302	1.6457	1.6708	1.5215	1.8313	1.5565	1.6851	1.6364	1.8559	1.6655	1.8171	1.6677	1.6940	1.5893
Na	0.0794	0.0741	0.0385	0.0607	0.0245	0.0214	0.0391	0.0407	0.1294	0.0269	0.0493	0.0474	0.0339	0.0532	0.0714
Ca	0.0107	0.0098	0.0233	0.0048	0.0114	0.0171	0.0480	0.0081	-	-	0.0016	0.0080	0.0043	0.0076	0.0153
Fe	2.7637	2.7214	2.8189	2.1910	2.3956	3.5314	2.2561	2.3200	2.2843	2.5149	2.7860	2.2772	2.5438	2.3442	1.8758
Mg	2.0496	1.9870	1.9928	2.5574	2.3051	1.0580	2.0314	2.3928	2.2907	1.8894	1.8873	2.1714	2.0054	2.1864	2.7995
Mn	0.0118	0.0083	0.0070	0.0086	0.0080	0.0736	0.0054	0.0156	0.0152	0.0393	0.0055	0.0123	0.0059	0.0109	0.0030
Ti	0.1659	0.2059	0.1787	0.2036	0.1917	0.2664	0.2320	0.1509	0.2287	0.3306	0.2477	0.2351	0.2268	0.2920	0.2285
Cl	0.0052	0.0080	0.0154	0.0060	0.0273	0.0057	0.0175	0.0262	0.0037	0.0056	0.0084	0.0061	0.0107	0.0157	0.0236
Total	15.5569	15.5684	15.5212	15.5111	15.3899	15.5121	15.1911	15.4956	15.4800	15.4813	15.4575	15.4671	15.3892	15.4152	15.4234

APPENDIX - III - continued

ELEMENTS	A47/54	A47/55		A47/56	U92/110	U93/111A		U93/111B	U93/111C	U93/112B	A49/59	A53/62B	U76/85	U80/95	U86/103		A57/68		
		MAT.	INC.			MAT.	INC.								MAT.	INC.	MAT.	INC.	
WEIGHT%																			
OXIDES																			
SiO ₂	37.456	37.189	37.517	37.587	34.694	37.163	37.510	36.170	36.709	36.643	37.540	34.900	36.639	35.620	36.042	35.855	35.487	35.966	
Al ₂ O ₃	18.359	18.487	19.477	18.966	16.909	17.780	19.152	17.421	17.378	17.470	19.026	18.537	19.102	18.697	19.043	19.663	18.917	19.972	
K ₂ O	8.409	9.292	9.376	8.316	9.064	9.236	9.418	9.040	9.252	9.117	8.422	9.547	8.801	9.338	9.042	8.745	9.605	9.195	
Na ₂ O	0.200	0.167	0.281	0.291	0.087	0.154	0.261	0.143	0.154	0.109	0.299	0.203	0.278	0.100	0.273	0.276	0.088	0.174	
CaO	0.062	0.048	0.006	0.051	0.117	0.016	0.013	0.084	0.044	0.033	0.080	0.033	0.010	0.046	0.015	0.096	-	0.017	
FeO	15.598	18.889	15.995	16.915	21.966	19.766	17.231	19.242	19.720	17.978	15.229	23.237	18.901	22.095	22.729	20.208	21.546	22.368	
MgO	12.970	10.053	10.835	11.834	5.524	9.560	10.406	8.682	9.399	10.448	11.684	6.570	10.156	5.594	7.157	8.496	6.786	7.144	
MnO	0.078	0.179	-	-	0.160	0.257	0.058	0.252	0.297	0.160	0.036	0.110	0.180	0.244	0.176	0.061	0.261	0.090	
TiO ₂	1.762	2.476	2.090	1.712	3.304	2.949	2.228	3.156	3.023	2.931	2.303	2.500	2.557	4.274	4.112	2.407	3.304	0.855	
Cl	0.054	0.044	0.047	0.032	0.097	0.039	0.043	0.049	0.049	0.032	0.028	-	0.004	0.047	0.057	0.060	0.139	0.157	
Total	94.935	96.815	95.613	95.698	91.901	96.912	96.311	94.229	96.013	94.923	94.639	95.637	96.627	96.044	98.634	95.855	96.102	95.904	
CATION (on the basis of 22 oxygen)																			
Si	5.5644	5.5333	5.5618	5.5605	5.5716	5.5521	5.5578	5.5594	5.5490	5.5404	5.5760	5.4077	5.4504	5.4475	5.3643	5.4154	5.4232	5.4942	
Al	3.2144	3.2423	3.4033	3.3071	3.2008	3.1310	3.3449	3.1558	3.0961	3.1173	3.3309	3.3862	3.3493	3.3703	3.3408	3.5005	3.4075	3.5961	
K	1.5938	1.7637	1.7733	1.5695	1.8569	1.7605	1.7802	1.7727	1.7841	1.7612	1.5959	1.8873	1.6704	1.8220	1.7169	1.6850	1.8727	1.7920	
Na	0.0577	0.0483	0.0809	0.0836	0.0273	0.0447	0.0749	0.0427	0.0450	0.0321	0.0861	0.0610	0.0802	0.0296	0.0788	0.0807	0.0260	0.0515	
Ca	0.0099	0.0077	0.0010	0.0082	0.0204	0.0026	0.0021	0.0138	0.0072	0.0054	0.0127	0.0055	0.0015	0.0075	0.0024	0.0156	-	0.0028	
Fe	1.9381	2.3501	1.9830	2.0928	2.9512	2.4697	2.1353	2.4738	2.4930	2.2978	1.8920	3.0112	2.3516	2.8260	2.8292	2.5526	2.7538	2.9577	
Mg	2.8722	2.2296	2.3944	2.6098	1.3226	2.1292	2.2984	1.9896	2.1176	2.3583	2.5869	1.5172	2.2521	1.2753	1.5879	1.9129	1.5460	1.6269	
Mn	0.0980	0.0225	-	-	0.0217	0.0325	0.0073	0.0328	0.0380	0.0206	0.0045	0.0144	0.0227	0.0316	0.0222	0.0078	0.0337	0.0116	
Ti	0.1969	0.2770	0.2330	0.1905	0.3988	0.3314	0.2483	0.3649	0.3437	0.3338	0.2572	0.2913	0.2860	0.4916	0.4603	0.2734	0.3797	0.0983	
Cl	0.0136	0.0111	0.0117	0.0080	0.0265	0.0098	0.0109	0.0128	0.0126	0.0082	0.0070	-	0.0010	0.0123	0.0143	0.0154	0.0360	0.0406	
Total	15.4708	15.4856	15.4424	15.4299	15.3979	15.4634	15.4599	15.4183	15.4864	15.4637	15.3493	15.5819	15.4653	15.3138	15.4172	15.4593	15.4787	15.5718	

APPENDIX - III - continued

ELEMENTS	077/90	A80/111	080/96		067/70	064/67	A65/78		060/63	057/60	052/55		048/51		043/47	A67/86	
			MAT.	INC.			MAT.	INC.			MAT.	INC.	MAT.	INC.		MAT.	INC.
WEIGHT%																	
OXIDES																	
SiO ₂	35.898	37.498	35.508	35.882	36.007	36.033	35.392	35.429	35.067	36.229	35.332	34.868	35.611	35.754	35.455	36.171	36.261
Al ₂ O ₃	19.162	19.524	19.106	19.711	19.650	18.536	19.763	20.504	19.255	19.574	19.514	19.847	19.712	19.286	20.846	20.616	20.637
K ₂ O	8.737	8.835	9.473	9.357	9.652	9.613	9.543	8.977	9.132	9.349	9.378	9.219	9.407	9.422	9.365	9.328	9.653
Na ₂ O	0.211	0.321	0.036	0.095	0.095	0.108	0.150	0.132	0.125	0.200	0.149	0.184	0.169	0.211	0.119	0.193	0.189
CaO	0.098	0.073	0.028	0.042	-	0.063	-	0.009	-	0.010	0.042	0.039	-	0.044	0.010	0.006	-
FeO	22.027	18.280	24.506	23.373	23.743	19.216	21.361	20.780	22.524	17.067	22.115	21.771	21.350	20.291	23.053	19.329	18.880
MgO	7.553	10.284	5.543	5.271	6.070	8.294	7.321	7.401	5.558	10.262	6.291	7.118	7.155	7.848	5.373	8.775	8.933
MnO	-	0.133	0.315	0.719	0.169	0.318	0.187	0.169	0.223	0.329	0.359	0.327	0.240	0.112	0.135	0.161	0.105
TiO ₂	2.799	1.938	0.960	1.523	3.447	3.707	3.795	3.096	3.840	2.465	3.395	1.924	3.454	3.559	1.449	2.261	2.695
Cl	0.035	0.001	0.032	0.046	0.057	0.048	0.011	0.009	-	0.009	0.018	0.022	0.071	0.029	0.013	0.163	0.142
Total	96.511	96.887	95.500	96.008	98.876	95.924	97.527	96.504	95.724	95.498	96.589	95.315	97.152	96.549	95.808	96.965	97.462
CATION (on the basis of 22 oxygen)																	
Si	5.4298	5.5297	5.5257	5.5194	5.3800	5.4513	5.3108	5.3314	5.3870	5.4597	5.3747	5.3674	5.3601	5.3881	5.4377	5.3871	5.3684
Al	3.4163	3.3937	3.5045	3.5738	3.4608	3.3052	3.4954	3.6371	3.4865	3.4576	3.4989	3.6011	3.4973	3.4258	3.7685	3.6190	3.6013
K	1.6859	1.6622	1.8807	1.8362	1.8398	1.8554	1.8270	1.7235	1.7898	1.7878	1.8200	1.8105	1.8066	1.8115	1.8325	1.7724	1.8234
Na	0.0618	0.0919	0.0109	0.0285	0.0275	0.0316	0.0437	0.0384	0.0371	0.0580	0.0439	0.0550	0.0493	0.0616	0.0354	0.0557	0.0543
Ca	0.0158	0.0115	0.0046	0.0069	-	0.0103	-	0.0015	-	0.0015	0.0069	0.0065	-	0.0071	0.0016	0.0009	-
Fe	2.7864	2.2545	3.1834	3.0068	2.9670	2.4312	2.6807	2.6154	2.8938	2.1393	2.8136	2.8027	2.6876	2.5574	2.9569	2.4075	2.3377
Mg	1.7031	2.2607	1.2858	1.2058	1.3520	1.8705	1.6389	1.6603	1.2727	2.2927	1.4266	1.6334	1.6055	1.9630	1.2283	1.9481	1.9714
Mn	-	0.0167	0.0416	0.0937	0.0213	0.0407	0.0238	0.0216	0.0290	0.0418	0.0463	0.0427	0.0306	0.0143	0.0175	0.0203	0.0131
Ti	0.3184	0.2149	0.1124	0.1762	0.3874	0.4218	0.4282	0.3504	0.4437	0.2783	0.3884	0.2228	0.3910	0.4034	0.1669	0.2533	0.3001
Cl	0.0090	0.0003	0.0083	0.0121	0.0141	0.0122	0.0029	0.0023	-	0.0022	0.0047	0.0056	0.0180	0.0075	0.0033	0.0411	0.0356
Total	15.4266	15.4359	15.5638	15.4620	15.4500	15.4300	15.4514	15.3825	15.3395	15.4884	15.4240	15.5477	15.4461	15.4397	15.4486	15.5053	15.5053

APPENDIX - III - continued

ELEMENTS	U26/28	U28/30		U29/31		U33/35		A68/91A	A74/97		U4/4	U13/13		P22/86	P12/20	P9/50	P9/46	P9/43	
		MAT.	INC.	MAT.	INC.	MAT.	INC.		MAT.	INC.		MAT.	INC.						
WEIGHT%																			
OXIDES																			
SiO ₂	36.180	35.303	35.275	35.541	35.995	35.071	36.207	33.419	35.543	35.640	35.416	35.292	35.583	35.562	35.345	35.686	35.905	36.148	
Al ₂ O ₃	19.690	19.399	18.878	19.879	18.950	20.096	21.533	19.011	20.276	20.251	19.731	19.979	20.282	19.985	19.266	19.240	20.085	19.969	
K ₂ O	9.591	9.319	9.568	9.554	9.180	9.336	9.300	9.015	9.666	9.276	9.259	9.095	9.038	9.278	9.041	9.225	9.350	9.221	
Na ₂ O	0.165	0.176	0.168	0.120	0.235	0.156	0.132	0.651	0.162	0.211	0.196	0.245	0.217	0.184	0.108	0.186	0.228	0.107	
CaO	0.028	0.027	-	0.019	0.038	0.022	0.036	0.942	0.009	0.012	0.019	0.017	0.039	0.072	0.005	0.077	0.043	-	
FeO	17.178	21.290	22.564	22.179	20.000	21.277	21.886	26.860	21.259	20.250	21.863	22.142	21.809	22.005	25.114	18.890	19.311	18.445	
MgO	9.811	7.517	6.816	6.346	7.739	6.440	6.880	4.605	7.317	8.255	6.448	6.625	6.824	5.890	5.195	9.255	8.560	8.572	
MnO	0.224	0.160	0.032	0.140	0.047	0.161	0.159	0.123	0.116	0.076	0.106	0.219	0.187	0.287	0.382	0.195	0.198	0.237	
TiO ₂	3.405	2.683	3.573	3.907	5.108	2.454	1.097	2.728	2.053	2.116	4.258	2.746	2.515	3.450	2.368	1.684	2.213	2.104	
Cl	0.011	0.020	0.024	0.013	0.020	0.010	0.019	0.413	0.039	0.013	0.019	0.029	0.027	0.038	0.012	0.026	0.015	0.007	
Total	96.283	95.890	96.893	97.694	97.310	95.050	97.241	97.673	96.431	96.548	97.311	96.383	96.515	96.743	96.835	94.457	95.906	94.810	
CATION (on the basis of 22 oxygen)																			
Si	5.3859	5.3850	5.3659	5.3388	5.3648	5.3938	5.4215	5.2003	5.3875	5.3706	5.3284	5.3667	5.3840	5.3864	5.4277	5.4584	5.4116	5.4785	
Al	3.4549	3.4883	3.3848	3.5197	3.3292	3.6431	3.8005	3.4873	3.6226	3.5969	3.4990	3.5811	3.6174	3.5680	3.4872	3.4689	3.5683	3.5673	
K	1.8216	1.8134	1.8568	1.8310	1.7457	1.8379	1.7766	1.7898	1.8693	1.8699	1.7772	1.7645	1.7449	1.7928	1.7713	1.8003	1.7980	1.7829	
Na	0.0476	0.0523	0.0495	0.0348	0.0680	0.0466	0.0384	0.1965	0.0475	0.0616	0.0573	0.0721	0.0638	0.0540	0.0322	0.0551	0.0668	0.0315	
Ca	0.0044	0.0044	-	0.0030	0.0061	0.0037	0.0058	0.1570	0.0015	0.0020	0.0030	0.0027	0.0064	0.0117	0.0009	0.0125	0.0070	-	
Fe	2.1387	2.7156	2.8705	2.7856	2.4930	2.7367	2.7402	3.4956	2.6949	2.5519	2.7511	2.8159	2.7599	2.7872	3.2253	2.4165	2.4342	2.3380	
Mg	2.1772	1.7094	1.5457	1.4210	1.7196	1.4766	1.5356	1.0680	1.6534	1.8543	1.4461	1.5018	1.5391	1.3299	1.1892	2.1102	1.9239	1.9366	
Mn	0.0283	0.0206	0.0042	0.0178	0.0059	0.0209	0.0201	0.0162	0.0149	0.0097	0.0135	0.0282	0.0239	0.0368	0.0497	0.0253	0.0253	0.0305	
Ti	0.3813	0.3074	0.4088	0.4412	0.5726	0.2838	0.1236	0.3194	0.2340	0.2399	0.4818	0.3140	0.2862	0.3931	0.2735	0.1937	0.2508	0.2399	
Cl	0.0029	0.0051	0.0061	0.0033	0.0051	0.0026	0.0049	0.1090	0.0100	0.0032	0.0049	0.0076	0.0070	0.0099	0.0032	0.0068	0.0039	0.0017	
Total	15.4428	15.5014	15.4922	15.3963	15.3100	15.4457	15.4671	15.8391	15.5357	15.5601	15.3624	15.4547	15.4323	15.3698	15.4602	15.5478	15.4898	15.4069	

APPENDIX - III - continued

ELEMENTS	SP20	SP25	PL19/123	PL20/125	PL12/113	12A/126	14/103	PC15A/1	PR3/76	PR6/81	PRI/73	PL4/93	
	MAT.						INC.						
WEIGHT%													
OXIDES													
SiO ₂	35.012	35.204	35.493	36.448	35.581	35.290	35.399	35.854	35.840	34.410	35.552	34.880	35.331
Al ₂ O ₃	17.842	17.887	18.410	19.296	18.760	19.247	19.177	19.659	18.801	18.804	19.067	18.409	18.751
K ₂ O	9.302	9.312	9.458	8.669	8.911	8.555	8.527	8.525	8.586	9.360	9.059	9.456	9.390
Na ₂ O	0.112	0.107	0.133	0.320	0.139	0.331	0.301	0.245	0.294	0.103	0.241	0.150	0.123
CaO	0.004	0.061	0.012	0.014	0.021	0.028	0.111	0.131	0.014	-	0.035	0.037	0.026
FeO	19.273	17.967	19.558	18.210	17.443	17.133	16.825	16.867	19.201	23.692	17.162	18.584	17.700
MgO	8.847	9.685	9.630	10.638	10.362	10.350	10.817	11.164	9.555	6.384	9.977	9.602	10.098
MnO	0.171	0.037	0.131	0.024	0.040	0.026	0.136	0.084	0.073	0.094	0.125	0.311	0.177
TiO ₂	3.092	1.950	1.900	1.934	2.015	1.985	2.089	1.685	2.679	3.149	2.893	2.441	2.371
Cl	0.023	0.021	0.012	0.014	0.021	-	0.008	0.022	0.018	0.069	0.026	0.005	0.021
Total	93.672	92.225	94.734	95.564	93.288	92.629	93.388	94.233	95.057	96.018	94.131	93.875	93.985
CATION (on the basis of 22 oxygen)													
Si	5.4352	5.5097	5.4456	5.4590	5.4637	5.4401	5.4079	5.4161	5.4344	5.3223	5.4110	5.3920	5.4157
Al	3.2647	3.2994	3.3293	3.4068	3.3954	3.4972	3.4531	3.5004	3.3601	3.4282	3.4205	3.3543	3.3879
K	1.8422	1.8594	1.8513	1.6567	1.7457	1.6825	1.6621	1.6430	1.6609	1.8469	1.7593	1.8649	1.8393
Na	0.0336	0.0325	0.0395	0.0930	0.0412	0.0990	0.0891	0.0719	0.0865	0.0308	0.0710	0.0448	0.0367
Ca	0.0006	0.0102	0.0020	0.0023	0.0035	0.0046	0.0181	0.0212	0.0022	-	0.0057	0.0062	0.0043
Fe	2.5022	2.3517	2.5095	2.2811	2.2400	2.2089	2.1497	2.1310	2.4349	3.0647	2.1846	2.4026	2.2690
Mg	2.0475	2.2595	2.2023	2.3751	2.3720	2.3061	2.4633	2.5139	2.1597	1.4719	2.2635	2.2127	2.3075
Mn	0.0225	0.0049	0.0170	0.0030	0.0051	0.0034	0.0176	0.0107	0.0094	0.0123	0.0161	0.0407	0.0230
Ti	0.3609	0.2296	0.2193	0.2178	0.2327	0.2301	0.2400	0.1915	0.3055	0.3627	0.3311	0.2837	0.2732
Cl	0.0060	0.0056	0.0031	0.0036	0.0056	-	0.0021	0.0057	0.0047	0.0181	0.0066	0.0014	0.0054
Total	15.5155	15.5625	15.6190	15.4982	15.5050	15.4719	15.5032	15.5054	15.4584	15.5579	15.4695	15.6034	15.5590

APPENDIX - III - continued

ELEMENTS	PC15C/22	PC29/24	PC30C/5		PC28F/40	PC28D/30	PC28/42	PC24G/61		PC24D/66	RG49	PC16D/83	P30/120		MP5
			MAT.	INC.			MAT.	INC.					MAT.	INC.	
WEIGHT%															
OXIDES															
SiO ₂	35.219	34.819	35.759	35.472	35.027	35.208	34.550	34.892	35.075	35.679	35.040	35.546	35.860	35.078	35.090
Al ₂ O ₃	18.696	18.722	19.229	19.662	18.644	19.186	18.406	18.226	18.379	19.205	16.373	19.529	19.809	18.857	19.279
K ₂ O	9.522	9.244	9.022	8.963	8.272	8.527	9.068	8.761	8.764	8.748	9.546	8.433	8.862	9.013	9.204
Na ₂ O	0.104	0.107	0.306	0.256	0.185	0.237	0.040	0.032	0.111	0.137	0.095	0.288	0.035	0.043	0.217
CaO	0.027	0.027	0.008	0.012	0.081	-	0.080	0.056	0.104	0.056	0.023	0.012	0.038	0.089	-
FeO	18.987	20.864	16.926	16.727	19.206	18.232	23.068	22.239	19.734	20.059	22.452	19.229	20.699	21.018	21.047
MgO	9.518	7.532	10.195	10.964	8.867	9.282	5.031	6.438	6.167	7.962	8.275	9.368	8.740	8.254	7.907
MnO	0.224	0.234	0.088	0.092	0.009	0.053	0.193	0.365	0.324	0.162	0.142	0.092	0.368	0.291	0.076
TiO ₂	2.571	2.640	2.814	1.958	2.850	1.843	3.186	3.198	3.233	2.212	2.724	1.343	1.450	1.282	2.161
Cl	0.017	0.052	0.011	0.008	0.036	0.020	0.041	0.043	0.041	-	0.016	0.014	0.048	0.015	0.032
Total	94.874	94.229	94.424	94.112	93.169	92.584	93.754	94.239	91.923	94.219	94.684	93.850	95.899	93.936	95.006
CATION (on the basis of 22 oxygen)															
Si	5.3827	5.4092	5.4152	5.3804	5.4215	5.4583	5.4527	5.4439	5.5399	5.4811	5.4844	5.4520	5.4296	5.4561	5.3966
Al	3.3113	3.4281	3.4319	3.5153	3.4015	3.5059	3.4237	3.3519	3.4216	3.4229	3.0201	3.5306	3.5345	3.4572	3.4948
K	1.8583	1.8322	1.7567	1.7345	1.6336	1.6864	1.8257	1.7438	1.7661	1.7147	1.9063	1.6502	1.7122	1.7886	1.8059
Na	0.0309	0.0321	0.0849	0.0752	0.0554	0.0712	0.0430	0.0096	0.0339	0.0408	0.0290	0.0858	0.0104	0.0131	0.0647
Ca	0.0044	0.0044	0.0013	0.0019	0.0134	-	0.0136	0.0094	0.0175	0.0093	0.0039	0.0019	0.0061	0.0149	-
Fe	2.4292	2.7108	2.1435	2.1219	2.4862	2.3639	3.0452	2.9017	2.6068	2.5779	2.9392	2.4666	2.6211	2.7341	2.7069
Mg	2.1691	1.7443	2.3014	2.4791	2.0459	2.1451	1.1836	1.4977	1.4520	1.8239	1.9304	2.1419	1.9728	1.9139	1.8127
Mn	0.0290	0.0308	0.0113	0.0118	0.0012	0.0069	0.0258	0.0481	0.0433	0.0250	0.0189	0.0120	0.0472	0.0383	0.0100
Ti	0.2958	0.3085	0.3205	0.2233	0.3317	0.2149	0.3783	0.3754	0.3841	0.2556	0.3206	0.1549	0.1652	0.1500	0.2499
Cl	0.0045	0.0138	0.0028	0.0020	0.0095	0.0052	0.0109	0.0113	0.0111	-	0.0041	0.0036	0.0122	0.0039	0.0083
Total	15.5801	15.5142	15.4745	15.5454	15.3999	15.4578	15.4024	15.3929	15.2763	15.4021	15.6567	15.4994	15.5144	15.5700	15.5497

APPENDIX - IV

MICROPROBE ANALYSIS OF MUSCOVITE

ELEMENTS	KC21/23	KC23/26	T3/5	T4/6	KC6/7	KC4/5	T21/28	A37/43	A41/48	A45/50	A46/51	A47/55	A47/56	U92/110	U93/111A
WEIGHT%															
OXIDES															
SiO ₂	45.109	45.123	45.239	47.029	46.889	45.425	46.479	46.553	45.581	46.546	46.636	47.930	46.497	46.264	48.257
Al ₂ O ₃	35.145	34.336	35.116	35.189	30.298	31.700	33.645	32.528	32.681	32.203	33.585	33.862	33.815	31.392	32.590
K ₂ O	9.125	9.408	8.291	8.520	10.827	8.612	9.728	9.685	9.844	8.863	9.630	9.898	8.920	10.817	10.076
Na ₂ O	1.474	1.161	2.202	1.760	0.269	1.112	0.893	0.907	0.799	1.468	0.995	0.747	1.481	0.290	0.481
CaO	0.026	0.073	0.066	0.079	0.014	0.125	0.021	0.022	0.023	0.020	0.039	0.024	0.044	0.032	0.001
FeO	1.194	1.784	1.665	0.947	3.044	1.289	1.080	1.801	1.471	1.171	1.546	1.496	1.216	2.640	2.020
MgO	0.537	0.755	0.704	0.554	1.223	0.969	0.810	0.962	1.017	0.628	0.865	1.001	0.844	1.021	1.237
MnO	-	0.019	-	0.037	0.112	0.028	0.040	0.021	0.002	0.012	0.023	-	0.012	0.018	0.004
TiO ₂	0.197	0.469	0.479	0.689	0.647	0.902	0.993	0.702	0.923	0.410	0.953	0.921	0.941	0.729	0.890
Cl	-	0.014	0.006	0.027	0.020	0.025	0.014	0.026	0.005	-	0.036	0.008	0.030	0.004	-
Total	92.807	93.140	93.766	94.826	93.389	90.181	93.702	93.201	92.346	93.321	94.300	95.885	93.790	93.208	95.557
CATION (on the basis of 22 oxygen)															
Si	6.1362	6.1468	6.0976	6.2258	6.4470	6.3449	6.2663	6.3333	6.2611	6.2744	6.2644	6.3170	6.2512	6.3577	6.3991
Al	5.6351	5.5132	5.5789	5.4908	4.9109	5.2189	5.3469	5.2158	5.2915	5.4345	5.3157	5.2604	5.3586	5.0850	5.0938
K	1.5836	1.6351	1.4257	1.439	1.9082	1.5346	1.6732	1.6209	1.7251	1.5242	1.6498	1.6643	1.5300	1.8964	1.7016
Na	0.3887	0.3067	0.5755	0.4518	0.0718	0.3011	0.2335	0.2391	0.2129	0.3837	0.2590	0.1909	0.3860	0.0773	0.1237
Ca	0.0038	0.0106	0.0095	0.0112	0.0718	0.0188	0.0030	0.0033	0.0034	0.0029	0.0056	0.0034	0.0055	0.0048	0.0002
Fe	0.1358	0.2032	0.1877	0.1048	0.3501	0.1506	0.1217	0.2050	0.1690	0.1329	0.1736	0.1650	0.1307	0.3034	0.2240
Mg	0.1088	0.1534	0.1415	0.1094	0.2505	0.2019	0.1629	0.1953	0.2082	0.1261	0.1731	0.1967	0.1680	0.2092	0.2446
Mn	-	0.0022	-	0.0041	0.0130	0.0033	0.0046	0.0024	0.0003	0.0014	0.0026	-	0.0014	0.0021	0.0004
Ti	0.0202	0.0481	0.0485	0.0686	0.0669	0.0948	0.1006	0.0718	0.0953	0.0416	0.0963	0.0913	0.0951	0.0754	0.0888
Cl	-	0.0032	0.0013	0.0062	0.0047	0.0058	0.0032	0.0059	0.0011	-	0.0082	0.0017	0.0068	0.0009	-
Total	14.0126	14.0225	14.0663	13.9117	14.0253	13.8745	13.9165	3.9529	13.9680	13.9208	13.9463	13.8907	13.9393	14.0122	13.8793

APPENDIX - IV - continued

ELEMENTS	A65/78	U60/63	U52/55	U48/51	U43/47	U26/28	U33/35	A68/91A	U13/13	P12/20	P9/50	P9/46	P9/43
WEIGHT%													
OXIDES													
SiO ₂	49.983	47.147	46.962	47.078	47.710	48.678	49.772	46.167	47.259	47.419	46.691	50.289	45.660
Al ₂ O ₃	36.434	35.457	35.215	35.137	35.199	34.637	36.465	34.076	35.725	34.836	34.853	36.756	34.627
K ₂ O	9.108	9.673	10.056	9.811	9.254	10.176	8.945	10.673	10.038	10.772	9.645	7.514	9.635
Na ₂ O	0.438	0.449	0.576	0.668	0.501	0.296	0.483	0.608	0.774	0.519	1.091	1.047	1.027
CaO	0.009	0.046	0.023	0.037	0.009	0.009	0.006	0.348	0.010	0.027	0.032	0.132	0.021
FeO	1.119	1.067	1.306	1.020	1.293	1.211	1.154	1.683	1.177	1.645	0.968	0.756	0.732
HgO	0.454	0.367	0.396	0.476	0.578	0.659	0.454	0.710	0.383	0.543	0.578	0.486	0.435
MnO	0.081	0.040	-	-	0.029	0.009	0.007	0.002	0.009	0.018	-	0.007	0.006
TiO ₂	1.566	0.918	0.708	1.173	0.774	0.198	1.110	0.215	0.985	0.528	0.521	0.741	0.633
Cl	-	0.003	-	0.006	0.023	0.004	0.016	0.114	0.012	0.009	0.015	0.011	0.034
Total	99.163	95.167	95.243	95.404	95.362	95.876	98.408	94.596	96.370	96.315	94.391	97.737	92.801
CATION (on the basis of 22 oxygen)													
Si	6.2940	6.2299	6.2264	6.2187	6.2782	6.3865	6.3106	6.2256	6.1927	6.2533	6.2367	6.3584	6.2037
Al	5.4110	5.5225	5.5033	5.4705	5.4596	5.3568	5.4496	5.4163	5.5178	5.4147	5.4874	5.4783	5.5453
K	1.4641	1.6307	1.7009	1.6530	1.5536	1.7030	1.4469	1.8361	1.6781	1.8124	1.6437	1.2121	1.6701
Na	0.1069	0.1151	0.1480	0.1709	0.1279	0.0754	0.1188	0.1590	0.1967	0.1327	0.2827	0.2567	0.2704
Ca	0.0013	0.0065	0.0033	0.0053	0.0013	0.0012	0.0008	0.0503	0.0014	0.0039	0.0045	0.0178	0.0031
Fe	0.1179	0.1180	0.1449	0.1127	0.1423	0.1328	0.1223	0.1898	0.1290	0.1814	0.1080	0.0800	0.0832
Mg	0.0853	0.0722	0.0783	0.0937	0.1135	0.1287	0.0858	0.1428	0.0749	0.1067	0.1151	0.0916	0.0881
Mn	0.0086	0.0045	-	-	0.0033	0.0010	0.0008	0.0003	0.0010	0.0020	-	0.0008	0.0006
Ti	0.1484	0.0912	0.0706	0.1166	0.0766	0.0195	0.1059	0.0218	0.0971	0.0524	0.0524	0.0706	0.0646
Cl	-	0.0008	-	0.0013	0.0052	0.0009	0.0034	0.0260	0.0026	0.0021	0.0038	0.0022	0.0079
Total	13.6376	13.7913	13.8758	13.8427	13.7614	13.8058	13.6449	14.0680	13.8913	13.9616	13.9337	13.5686	13.9372

APPENDIX - IV - continued

ELEMENTS	SP20	SP25	PL19/123	PL20/125	PL12/113	12A/126	14/103	PC15A/1	PR3/76	PR6/81	PR1/73	PL4/93
WEIGHT%												
OXIDES												
SiO ₂	45.031	46.008	45.377	45.935	44.960	45.590	44.852	46.030	45.048	45.451	44.082	45.426
Al ₂ O ₃	33.373	30.823	33.662	35.002	35.006	34.911	34.073	34.576	34.126	34.262	32.926	34.187
K ₂ O	10.169	10.254	9.064	8.532	8.378	8.309	9.146	9.282	10.292	9.229	9.260	10.031
Na ₂ O	0.667	0.051	1.523	1.747	1.819	1.947	1.251	1.432	0.642	1.339	0.920	0.573
CaO	0.015	0.020	0.057	0.024	0.020	0.014	0.050	0.017	0.056	0.037	0.055	0.029
FeO	1.432	1.649	1.939	1.143	0.841	0.793	0.918	1.092	1.336	0.858	3.633	1.128
MgO	0.822	1.539	0.490	0.518	0.500	0.514	0.727	0.585	0.506	0.667	1.628	0.681
MnO	0.020	0.018	0.022	0.031	0.036	0.054	0.060	0.003	-	0.016	0.022	-
TiO ₂	0.834	0.865	0.686	0.601	0.775	0.694	0.821	0.909	0.652	0.731	0.880	0.833
Cl	0.008	0.011	0.003	0.015	0.003	0.018	0.011	0.018	-	0.008	0.016	0.012
Total	92.369	91.691	92.824	93.545	92.338	92.839	91.908	93.417	92.709	92.597	93.920	93.073
CATION (on the basis of 22 oxygen)												
Si	6.1951	6.3828	6.2009	6.1780	6.1213	6.1674	6.1600	6.1870	6.1765	6.1902	6.0475	6.1820
Al	5.4118	5.0410	5.4220	5.5488	5.6177	5.5666	5.5158	5.4779	5.5090	5.5005	5.3242	5.4832
K	1.7850	1.8152	1.5803	1.4640	1.4553	1.4340	1.6026	1.5917	1.7984	1.6037	1.7083	1.7416
Na	0.1779	0.1373	0.4035	0.4556	0.4803	0.5106	0.3331	0.3732	0.1704	0.3537	0.2448	0.1986
Ca	0.0022	0.0029	0.0083	0.0034	0.0030	0.0020	0.0074	0.0025	0.0083	0.0054	0.0081	0.0042
Fe	0.1647	0.1913	0.2216	0.1286	0.0958	0.0897	0.1055	0.1228	0.1531	0.0978	0.4168	0.1986
Mg	0.1686	0.3176	0.0999	0.1038	0.1015	0.1038	0.1488	0.1171	0.1633	0.1354	0.3330	0.1381
Mn	0.0023	0.0021	0.0026	0.0035	0.0041	0.0061	0.0070	0.0004	-	0.0018	0.0026	-
Ti	0.0865	0.0903	0.0705	0.0608	0.0794	0.0707	0.0848	0.0919	0.0677	0.0749	0.0908	0.0852
Cl	0.0018	0.0026	0.0008	0.0033	0.0008	0.0041	0.0025	0.0042	-	0.0018	0.0036	0.0027
Total	13.9959	13.9843	14.0103	13.9499	13.9590	13.9551	13.9676	13.9687	13.9862	13.9652	14.1798	13.9640

APPENDIX - IV - continued

ELEMENTS	PC15C/22	PC29/24	PC30C/5	PC28D/30	PC28/42	PC24G/61	PC24D/66	PC16D/83	P30/120	MP5
WEIGHT%										
OXIDES										
SiO ₂	45.565	44.961	45.201	45.772	45.643	44.980	45.822	45.854	46.955	45.974
Al ₂ O ₃	34.129	33.739	35.126	35.187	32.391	32.746	33.269	34.964	33.901	33.894
K ₂ O	10.208	10.138	9.608	8.406	10.382	10.267	10.274	7.856	9.489	9.283
Na ₂ O	0.734	0.646	1.179	1.865	0.480	0.604	0.628	2.117	0.951	1.113
CaO	0.031	0.040	0.011	0.054	0.047	0.020	0.040	0.024	0.006	0.051
FeO	1.311	1.186	0.981	1.014	2.321	1.765	1.453	0.889	1.326	1.629
MgO	0.705	0.623	0.553	0.582	0.716	0.858	0.929	0.519	0.692	0.623
MnO	0.018	0.065	0.018	0.049	0.038	0.004	0.018	-	0.048	0.065
TiO ₂	0.733	0.900	0.881	0.664	0.840	0.818	0.980	0.519	0.959	1.032
Cl	0.014	0.012	-	0.011	0.022	0.032	-	0.010	0.009	0.035
Total	93.446	92.308	93.557	93.603	92.873	92.089	93.414	92.749	94.339	93.691
CATION (on the basis of 22 oxygen)										
Si	6.1885	6.1804	6.1092	6.1499	6.2760	6.2235	6.2319	6.1922	6.2813	6.2116
Al	5.4629	5.4671	5.5958	5.5724	5.2498	5.3405	5.3332	5.5653	5.3455	5.3978
K	1.7686	1.7779	1.6567	1.4408	1.8213	1.8124	1.7827	1.3534	1.6195	1.6002
Na	0.1932	0.1723	0.3090	0.4858	0.1281	0.1621	0.1655	0.5545	0.2483	0.2915
Ca	0.0044	0.0059	0.0016	0.0078	0.0066	0.0030	0.0059	0.0035	0.0009	0.0074
Fe	0.1489	0.1363	0.1109	0.1140	0.2669	0.2042	0.1655	0.1004	0.1483	0.1841
Mg	0.1426	0.1276	0.1113	0.1166	0.1469	0.1770	0.1884	0.1044	0.1379	0.1255
Mn	0.0021	0.0075	0.0020	0.0056	0.0044	0.0005	0.0021	-	0.0054	0.0075
Ti	0.0749	0.0930	0.0895	0.0671	0.0869	0.0851	0.1003	0.0527	0.0964	0.1048
Cl	0.0032	0.0027	-	0.0026	0.0052	0.0076	-	0.0022	0.0021	0.0079
Total	13.9893	13.9710	13.9862	13.9627	13.9920	14.0160	13.9753	13.9286	13.8856	13.9384

APPENDIX - V

MICROPROBE ANALYSIS OF PLAGIOCLASE

ELEMENTS	KC21/23	KC23/26	T3/5	T4/6	KC6/7	KC4/5	KC1/1	THATRI	T21/28	A37/43	A41/48	A45/50	A46/51	A47/54	A47/55	A47/56	U92/110	U93/111A	
WEIGHT%																			
OXIDES																			
SiO ₂	68.410	67.599	63.352	64.465	68.316	66.079	62.211	67.089	60.807	65.027	61.727	66.533	63.965	62.182	63.833	62.780	64.052	63.230	
Al ₂ O ₃	19.304	20.178	23.151	21.771	20.033	21.125	22.661	19.827	23.698	22.072	23.644	21.110	22.518	23.788	22.463	22.910	22.418	22.955	
K ₂ O	0.044	0.046	0.070	0.093	0.103	0.067	0.091	0.055	0.124	0.149	0.116	0.106	0.094	0.099	0.110	0.080	0.190	0.152	
Na ₂ O	10.960	10.340	8.591	9.540	10.764	9.958	8.496	10.527	8.027	9.479	8.485	10.071	8.905	8.117	9.159	9.380	8.968	8.726	
CaO	0.188	1.210	4.458	3.578	1.329	2.612	5.114	1.532	6.289	3.619	5.734	2.713	4.458	5.696	4.484	3.970	4.270	5.121	
FeO	0.094	0.163	0.089	0.378	0.199	0.024	0.218	0.023	-	0.139	0.181	0.125	0.146	0.210	0.182	-	0.074	0.072	
MgO	0.007	0.015	0.017	0.012	0.022	0.022	0.002	-	0.015	0.013	-	0.053	-	0.069	0.016	-	0.035	0.009	
TiO ₂	-	-	-	0.021	0.016	0.005	0.008	-	-	-	0.022	0.013	-	0.009	-	-	-	-	
Total	99.007	99.557	99.727	99.858	100.782	99.895	98.808	99.052	98.958	100.500	99.909	100.726	100.085	100.168	100.247	99.120	100.068	100.265	
CATION (on the basis of 8 oxygen)																			
Si	3.0087	2.9649	2.8015	2.8504	2.9670	2.9035	2.7888	2.9631	2.7309	2.8524	2.7452	2.9033	2.8220	2.7522	2.8165	2.7987	2.8254	2.7922	
Al	1.0007	1.0432	1.2067	1.1347	1.0255	1.0942	1.1974	1.0322	1.2544	1.1412	1.2394	1.0858	1.1710	1.2410	1.1682	1.2037	1.1689	1.1948	
K	0.0025	0.0026	0.0039	0.0052	0.0057	0.0038	0.0052	0.0031	0.0071	0.0083	0.0066	0.0059	0.0053	0.0056	0.0062	0.0044	0.0107	0.0086	
Na	0.9347	0.8797	0.7366	0.8179	0.9065	0.8484	0.7385	0.9015	0.6988	0.8062	0.7317	0.8521	0.7618	0.6966	0.7836	0.8109	0.7670	0.7472	
Ca	0.0088	0.0569	0.2112	0.1695	0.0618	0.1230	0.2456	0.7259	0.3026	0.1701	0.2732	0.1268	0.2107	0.2701	0.2119	0.1894	0.2019	0.2423	
Fe	0.0035	0.0060	0.0033	0.0140	0.0072	0.0080	0.0082	0.0009	-	0.0051	0.0067	0.0046	0.0054	0.0078	0.0067	-	0.0027	0.0027	
Mg	0.0005	0.0010	0.0011	0.0008	0.0014	0.0014	0.0001	-	0.0010	0.0009	-	0.0035	-	0.0045	0.0011	-	0.0023	0.0006	
Ti	-	-	-	0.0007	0.0005	0.0002	0.0003	-	-	-	0.0007	0.0004	-	0.0003	-	-	-	-	
Total	4.9595	4.9543	4.9643	4.9932	4.9758	4.9753	4.9841	4.9731	4.9949	4.9843	5.0035	4.9824	4.9761	4.9781	4.9943	5.0071	4.9790	4.9883	

APPENDIX - V - Continued

ELEMENTS	U93/111B	U93/111C	A93/112B	A49/59	A53/62B	U76/85	U80/95	U86/103	A57/68	U77/90	A80/111	U80/96	U67/70	U64/67	A65/78	U60/63	U57/60		
	MAT. INCLUSION										MAT. INC.								
WEIGHT%																			
OXIDES																			
SiO ₂	62.998	63.382	61.817	61.905	63.255	63.027	65.709	64.419	64.372	64.273	59.907	63.859	65.064	63.949	62.729	62.902	61.778	63.926	60.205
Al ₂ O ₃	23.416	22.940	23.976	24.478	22.245	23.507	21.599	22.091	22.098	22.411	24.919	23.321	21.769	22.040	23.321	23.913	23.948	22.286	24.353
K ₂ O	0.094	0.096	0.096	0.067	0.120	0.089	0.253	0.115	0.215	0.371	0.076	0.132	0.159	0.310	0.346	0.204	0.254	0.305	0.164
Na ₂ O	8.564	8.733	7.984	7.961	9.820	8.629	9.975	9.208	9.078	9.079	7.262	8.674	9.877	9.287	8.418	8.166	8.121	9.158	7.493
CaO	5.262	4.941	6.031	6.390	3.235	5.512	3.292	4.103	4.015	4.370	7.625	5.347	3.478	4.070	5.505	5.795	5.977	4.200	6.922
FeO	0.147	0.016	0.085	0.077	-	0.199	0.171	0.093	0.255	0.055	0.154	0.066	0.121	0.210	0.121	-	0.090	0.189	0.154
MgO	0.013	0.008	-	0.008	-	-	-	-	0.004	0.013	-	0.015	0.005	0.003	0.004	-	0.001	-	0.012
TiO ₂	0.002	0.001	0.007	-	-	0.013	0.005	-	0.011	0.009	0.015	0.013	-	0.009	0.007	-	0.017	0.013	0.014
Total	100.496	100.169	99.994	100.886	98.675	100.981	101.004	100.030	100.048	100.581	99.958	101.429	100.474	99.878	100.450	100.956	100.186	100.078	99.316
CATION (on the basis of 8 oxygen)																			
Si	2.7761	2.7973	2.7418	2.7245	2.8284	2.7683	2.8707	2.8414	2.8407	2.8256	2.6732	2.7875	2.8579	2.8324	2.7712	2.7596	2.7390	2.8253	2.6995
Al	1.2162	1.1962	1.2534	1.2698	1.1727	1.2170	1.1122	1.1485	1.1494	1.1614	1.3107	1.1999	1.1270	1.1506	1.2144	1.2369	1.2515	1.1611	1.2871
K	0.0053	0.0054	0.0054	0.0037	0.0068	0.0050	0.0141	0.0065	0.0121	0.0208	0.0043	0.0074	0.0089	0.0175	0.0195	0.0114	0.0144	0.0172	0.0094
Na	0.7318	0.7473	0.6866	0.6794	0.8514	0.7349	0.8450	0.7875	0.7768	0.7740	0.6283	0.7342	0.8413	0.7976	0.7210	0.6946	0.6982	0.7848	0.6514
Ca	0.2485	0.2337	0.2866	0.3013	0.1550	0.2597	0.1541	0.1939	0.1898	0.2058	0.3646	0.2501	0.1637	0.1932	0.2606	0.2724	0.2839	0.1989	0.3325
Fe	0.0054	0.0066	0.0032	0.0028	-	0.0073	0.0062	0.0034	0.0094	0.0020	0.0057	0.0024	0.0044	0.0078	0.0044	-	0.0033	0.0070	0.0058
Mg	0.0009	0.0005	-	0.0005	-	-	-	-	0.0002	0.0009	-	0.0010	0.0004	0.0002	0.0003	-	0.0001	-	0.0008
Ti	0.0001	-	0.0002	-	-	0.0004	0.0002	-	0.0004	0.0003	0.0005	0.0004	-	0.0003	0.0002	-	0.0006	0.0004	0.0005
Total	4.9842	4.9810	4.9773	4.9822	5.0143	4.9927	5.0026	4.9813	4.9783	4.9908	4.9873	4.9829	5.0036	4.9996	4.9917	4.9750	4.9909	4.9947	4.9869

APPENDIX - V - continued

ELEMENTS	U52/55	U48/51	U43/47	A67/86	U26/28	U29/31	U33/35	A68/91A	A74/97	U4/4	U13/13	P22/86	P12/20	P9/50	P9/46	P9/43	
	MAT. INC.																
WEIGHT%																	
OXIDES																	
SiO ₂	62.860	66.186	65.496	63.161	62.419	60.643	64.307	63.733	64.129	60.684	64.345	64.221	63.871	66.791	62.999	63.018	63.591
Al ₂ O ₃	22.884	21.140	21.785	23.209	23.270	24.245	22.132	23.215	23.045	23.719	22.627	22.065	21.635	21.314	22.974	23.013	21.904
K ₂ O	0.180	0.238	0.196	0.200	0.246	0.116	0.265	0.292	0.293	0.224	0.237	0.143	0.420	0.195	0.111	0.132	0.219
Na ₂ O	8.598	10.354	9.950	8.689	8.336	7.827	9.219	8.577	9.165	8.120	9.047	9.454	9.331	10.304	8.672	8.250	9.033
CaO	5.091	2.399	3.356	5.003	5.533	6.598	4.022	5.174	3.777	5.960	4.327	3.721	3.728	2.488	5.124	5.085	4.294
FeO	0.101	0.409	0.241	0.125	0.198	0.253	0.191	0.201	0.055	0.288	0.425	0.144	-	0.070	0.236	0.107	0.092
MgO	0.012	-	0.007	0.002	-	-	-	0.003	0.003	-	0.002	0.005	0.032	-	0.017	0.006	0.017
TiO ₂	-	0.001	0.022	0.006	0.005	-	0.009	0.004	-	-	-	-	0.010	0.006	0.002	0.003	0.010
Total	99.726	100.726	101.053	100.395	100.006	99.682	100.143	101.198	100.467	98.996	101.009	99.753	99.025	101.169	100.135	99.615	99.160
CATION (on the basis of 8 oxygen)																	
Si	2.7909	2.8957	2.8613	2.7857	2.7693	2.7088	2.8371	2.7902	2.8162	2.7282	2.8189	2.8412	2.8488	2.9021	2.7874	2.7952	2.8337
Al	1.1975	1.0902	1.1218	1.2065	1.2169	1.2765	1.1508	1.1980	1.1928	1.2569	1.1684	1.1506	1.1374	1.0916	1.1981	1.2032	1.1505
K	0.0102	0.0133	0.0109	0.0112	0.0139	0.0066	0.0149	0.0163	0.0164	0.0129	0.0132	0.0081	0.0239	0.0108	0.0063	0.0075	0.0125
Na	0.7402	0.8784	0.8428	0.7431	0.7171	0.6779	0.7887	0.7281	0.7804	0.7079	0.7685	0.8110	0.8070	0.8681	0.7440	0.7096	0.7805
Ca	0.2422	0.1125	0.1571	0.2364	0.2630	0.3158	0.1901	0.2427	0.1777	0.2871	0.2031	0.1764	0.1782	0.1159	0.2429	0.2417	0.2050
Fe	0.0038	0.0150	0.0088	0.0046	0.0074	0.0095	0.0070	0.0073	0.0020	0.0108	0.0156	0.0053	-	0.0025	0.0087	0.0040	0.0034
Mg	0.0008	-	0.0005	0.0002	-	-	-	0.0002	0.0002	-	0.0001	0.0003	0.0021	-	0.0011	0.0004	0.0011
Ti	-	-	0.0007	0.0002	0.0002	-	0.0003	0.0001	-	-	-	-	0.0003	0.0002	0.0001	0.0001	0.0003
Total	4.9856	5.0050	5.0040	4.9880	4.9877	4.9952	4.9890	4.9829	4.9858	5.0037	4.9878	4.9930	4.9976	4.9913	4.9886	4.9616	4.9872

APPENDIX - V - continued

ELEMENTS	SP20	SP25	PL19/123	PL20/125	PL12/113	12A/126	14/103	PC15A/1	PR3/76	PR6/81	PR1/73	PL4/93
WEIGHT%												
OXIDES												
SiO ₂	60.973	63.404	66.437	67.044	65.696	66.350	63.339	65.805	64.137	66.495	64.617	60.976
Al ₂ O ₃	24.152	22.357	20.723	21.116	21.046	20.706	22.342	21.580	22.398	21.085	22.299	25.256
K ₂ O	0.118	0.076	0.115	0.109	0.097	0.113	0.133	0.110	0.154	0.119	0.069	0.115
Na ₂ O	7.963	9.178	10.266	10.439	10.087	10.559	9.063	9.824	9.1712	10.504	9.418	7.417
CaO	6.707	4.302	2.375	2.163	2.788	2.266	4.539	2.918	4.280	2.384	3.910	7.258
FeO	0.073	0.050	0.033	0.172	0.109	0.025	0.027	0.138	0.092	0.031	0.148	0.067
MgO	0.020	0.004	0.002	0.009	-	-	-	-	-	0.019	0.009	0.021
TiO ₂	0.021	0.021	-	0.021	-	-	0.014	0.007	-	0.005	0.017	0.030
Total	100.028	99.391	99.952	101.073	99.822	100.019	99.457	100.381	100.233	100.642	100.487	101.141
CATION (on the basis of 8 oxygen)												
Si	2.7136	2.8183	2.9184	2.9131	2.8953	2.9154	2.8157	2.8829	2.8266	2.9046	2.8374	2.6835
Al	1.2670	1.1715	1.0730	1.0815	1.0933	1.0724	1.1707	1.1143	1.1635	1.0856	1.1541	1.3101
K	0.0067	0.0044	0.0065	0.0060	0.0054	0.0063	0.0075	0.0061	0.0086	0.0066	0.0038	0.0065
Na	0.6872	0.7909	0.8744	0.8795	0.8620	0.8996	0.7812	0.8345	0.7837	0.8897	0.8019	0.6330
Ca	0.3198	0.2050	0.1118	0.1007	0.1317	0.1067	0.2162	0.1370	0.2021	0.1116	0.1840	0.3422
Fe	0.0027	0.0019	0.0012	0.0063	0.0040	0.0009	0.0010	0.0051	0.0034	0.0011	0.0054	0.0025
Mg	0.0013	0.0003	0.0001	0.0006	-	-	-	-	-	0.0013	0.0006	0.0014
Ti	0.0007	0.0007	-	0.0007	-	-	0.0005	0.0002	-	0.0002	0.0006	0.0010
Total	4.9991	4.9929	4.9855	4.9883	4.9917	5.0014	4.9928	4.9801	4.9879	5.0006	4.9878	4.9801

APPENDIX - V - continued

ELEMENTS	PC15C/22	PC29/24	PC30C/5	PC28D/30	PC28/42	PC24G/61	PC24D/66	RG49	PC16D/83	P30/120	MP5
	MAT. INC.										

WEIGHT%

OXIDES	PC15C/22	PC29/24	PC30C/5	PC28D/30	PC28/42	PC24G/61	PC24D/66	RG49	PC16D/83	P30/120	MP5	
SiO ₂	64.420	64.055	64.543	62.424	67.513	67.145	66.248	67.164	63.045	67.363	65.145	65.653
Al ₂ O ₃	22.298	22.347	22.607	23.187	20.637	20.787	20.748	20.785	23.022	20.942	21.532	21.596
K ₂ O	0.184	0.259	0.117	0.177	0.089	0.118	0.203	0.123	0.152	0.122	0.130	0.089
Na ₂ O	9.263	9.309	9.387	8.397	10.364	10.594	10.300	10.541	8.691	10.799	9.460	10.049
CaO	4.185	4.328	4.297	5.487	1.840	2.267	2.422	1.958	5.139	1.904	3.476	3.051
FeO	0.033	0.053	0.040	0.307	-	0.070	0.154	0.054	0.064	0.143	0.070	0.057
MgO	-	0.018	0.016	0.005	-	-	0.005	-	0.014	-	0.007	0.003
TiO ₂	0.015	0.022	0.027	-	0.005	0.020	0.004	0.024	-	0.015	0.004	0.005
Total	100.400	100.392	101.033	99.983	100.448	100.996	100.084	100.649	100.127	101.289	99.824	100.502

CATION (on the basis of 8 oxygen)

Si	2.8333	2.8225	2.8226	2.7707	2.9419	2.9210	2.9114	2.9273	2.7881	2.9211	2.8728	28761
Al	1.1559	1.1607	1.1653	1.2131	1.0599	1.0651	1.0748	1.0678	1.2000	1.0704	1.1192	1.1151
K	0.0104	0.0146	0.0065	0.0100	0.0049	0.0065	0.0114	0.0069	0.0086	0.0068	0.0073	0.0050
Na	0.7900	0.7954	0.7959	0.7227	0.8756	0.8936	0.8778	0.8908	0.7453	0.9080	0.8089	0.8536
Ca	0.1972	0.2043	0.2013	0.2610	0.0859	0.1057	0.1141	0.0984	0.2435	0.0885	0.1642	0.1432
Fe	0.0012	0.0020	0.0015	0.0114	-	0.0025	0.0057	0.0020	0.0024	0.0052	0.0026	0.0021
Mg	-	0.0012	0.0011	0.0003	-	-	0.0003	-	0.0009	-	0.0005	0.0002
Ti	0.0015	0.0007	0.0009	-	0.0002	0.0006	0.0001	0.0008	-	0.0005	0.0001	0.0002
Total	4.9884	5.0014	4.9951	4.9891	4.9683	4.9956	4.9956	4.9869	4.9888	5.0005	4.9756	4.9954

APPENDIX - VI

MICROPROBE ANALYSIS OF K-FELDSPAR

ELEMENTS	KC6/7	U80/95	U80/96	A57/68	U67/70	U33/35	A74/97	U29/31	U48/51	U43/47	U4/4
WEIGHT%											
OXIDES											
SiO ₂	64.912	64.135	64.685	63.891	63.458	64.451	64.825	64.255	64.174	64.755	65.110
Al ₂ O ₃	18.021	18.283	18.642	18.472	18.619	18.437	18.886	18.611	18.644	18.390	18.903
K ₂ O	16.145	16.255	15.564	15.349	14.518	15.615	15.319	14.449	14.121	15.495	14.474
Na ₂ O	0.702	0.431	0.961	1.192	1.438	0.769	1.225	1.572	1.738	1.032	1.680
FeO	0.034	-	-	0.064	0.082	-	0.079	0.107	-	-	0.003
BaO	0.086	0.320	0.057	0.493	0.403	0.391	0.460	0.455	0.397	0.211	0.445
Total	99.901	99.425	99.910	99.464	98.518	99.753	100.795	99.448	99.074	99.882	100.614
CATION (on the basis of 8 oxygen)											
Si	3.0064	2.9916	2.9875	2.9779	2.9737	2.9925	2.9762	2.9813	2.9820	2.9946	2.9819
Al	0.9838	1.0052	1.0149	1.0150	1.0284	1.0076	1.0220	1.0178	1.0212	1.0024	1.0204
K	0.9540	0.9673	0.9171	0.9127	0.8679	0.9237	0.8973	0.8553	0.8372	0.9142	0.8457
Na	0.0631	0.0390	0.0861	0.1078	0.1307	0.0692	0.1091	0.1414	0.1566	0.0926	0.1492
Fe	0.0013	-	-	0.0025	0.0032	-	0.0030	0.0041	-	-	0.0001
Ba	0.0016	0.0058	0.0010	0.0090	0.0074	0.0071	0.0083	0.0083	0.0072	0.0038	0.0080
Total	5.0102	5.0090	5.0066	5.0248	5.0114	5.0001	5.0160	5.0082	5.0042	5.0076	5.0053

APPENDIX - VII

MICROPROBE ANALYSIS OF STAUROLITE

ELEMENTS	KC26/28		T4/6		P9/43		P9/46		PC15A/1		PC16D/83	
	RIM	CORE	RIM	CORE	RIM	CORE	RIM	CORE	RIM	CORE	RIM	CORE
WEIGHT%												
OXIDES												
SiO ₂	27.544	27.893	27.198	27.811	27.386	27.916	27.182	26.167	27.033	27.341	27.077	27.114
Al ₂ O ₃	52.600	52.566	51.756	52.314	51.794	51.933	52.015	51.595	52.585	52.449	53.643	53.502
FeO	11.543	12.214	12.601	12.643	11.198	11.066	11.616	11.614	13.042	13.699	13.602	14.183
MgO	1.533	1.685	1.359	1.344	1.332	1.361	1.329	1.318	1.640	1.752	1.355	1.568
MnO	0.360	0.323	0.077	0.147	0.398	0.380	0.239	0.331	0.173	0.239	0.309	0.256
CaO	-	-	-	-	-	0.037	0.018	0.087	0.007	-	-	-
TiO ₂	0.934	0.840	0.872	0.819	0.741	0.676	0.729	0.754	0.760	0.887	0.741	0.746
ZnO	0.934	0.840	0.930	0.816	0.376	0.311	0.740	0.857	1.261	1.161	0.161	0.176
Total	95.351	96.199	94.794	95.895	93.224	93.679	93.869	92.722	96.500	97.527	96.887	97.545
CATION (on the basis of 48 oxygen)												
Si	8.1470	8.1955	8.1674	8.2377	8.2597	8.3585	8.1883	8.0133	8.0252	8.0504	7.9362	7.9184
Al	18.3386	18.2047	18.3191	18.2649	18.4131	18.3281	18.4688	18.6238	18.4006	18.2031	18.5320	18.4169
Fe	2.8555	3.0012	3.1646	3.1320	2.8245	2.7710	2.9263	2.9745	3.2380	3.3734	3.3341	3.4169
Mg	0.6758	0.7380	0.6085	0.5933	0.5989	0.6074	0.5967	0.6015	0.7257	0.7690	0.5922	0.6827
Mn	0.0902	0.0804	0.0196	0.0369	0.1016	0.0963	0.0611	0.0857	0.0434	0.0595	0.0766	0.0632
Ca	-	-	-	-	-	0.0118	0.0059	0.0287	0.0023	-	-	-
Ti	0.1862	0.1498	0.1969	0.1825	0.1680	0.1521	0.1652	0.1736	0.1697	0.1963	0.1633	0.1639
Zn	0.2040	0.1822	0.2568	0.2223	0.1043	0.0856	0.2049	0.2411	0.3441	0.3142	0.0433	0.0472
Total	30.4973	30.5518	30.7329	30.6696	30.4701	30.4109	30.6171	30.7423	30.9489	30.9659	30.6778	30.7564
Fe/Fe+Mg	0.809	0.803	0.839	0.841	0.825	0.820	0.831	0.832	0.817	0.814	0.849	0.833

APPENDIX - VIII

MICROPROBE ANALYSIS OF ILMENITE

ELEMENTS	KC26/28	THATRI	A45/50	A37/43	A41/48	A80/111	U86/103	A67/86	U29/31	U48/51	U13/13	U4/4	P12/20
WEIGHT%													
OXIDES													
FeO	46.187	45.950	46.553	45.644	45.621	47.768	45.780	46.871	47.190	47.215	45.718	47.361	47.351
TiO ₂	53.157	53.753	52.793	54.121	53.994	54.104	53.858	54.330	52.741	53.281	53.630	53.765	53.242
V ₂ O ₃	0.294	0.288	0.296	0.295	0.295	0.291	0.291	0.300	0.293	0.298	0.291	0.278	0.295
Al ₂ O ₃	0.025	-	-	0.015	0.019	0.057	0.020	0.006	0.010	0.030	0.013	0.032	0.018
Cr ₂ O ₃	-	-	0.072	0.026	-	0.004	-	-	0.032	0.006	0.013	-	0.032
Total	99.663	99.991	99.714	100.101	99.929	102.224	99.950	101.507	100.266	100.830	99.666	101.436	100.938
CATION (on the basis of 6 oxygen)													
Fe	1.9480	1.9275	1.9666	1.9088	1.9116	1.9682	1.9194	1.9391	1.9865	1.9736	1.9231	1.9662	1.9783
Ti	2.0160	2.0276	2.0055	2.0353	2.0345	2.0046	2.0306	2.0212	1.9965	2.0028	2.0287	2.0072	2.0003
V	0.0118	0.0116	0.0120	0.0118	0.0119	0.0114	0.0117	0.0119	0.0118	0.0119	0.0117	0.0111	0.0118
Al	0.0116	-	-	0.0009	0.0011	0.0032	0.0012	0.0004	0.0006	0.0018	0.0008	0.0020	0.0011
Cr	-	-	0.0029	0.0010	-	0.0002	-	-	0.0013	0.0003	0.0005	-	0.0013
Total	3.9774	3.9666	3.9870	3.9579	3.9590	3.9876	3.9629	3.9726	3.9927	3.9903	3.9648	3.9865	3.9927

APPENDIX - VIII - continued

ELEMENTS	SP20	PL19/123	PL12/113	14/103	PC15A/1	PL4/93	PL4/93	PC15C/22	PC29/24	PC28F/40	PC24G/61	PC16D/83	MP5
WEIGHT%													
OXIDES													
FeO	46.834	49.672	45.537	43.386	46.893	35.565	45.024	47.344	45.943	46.622	47.058	47.334	45.670
TiO ₂	52.844	50.996	54.788	53.778	53.421	64.205	54.433	53.164	53.275	52.665	52.869	54.123	53.951
V ₂ O ₃	0.289	0.272	0.305	0.292	0.292	0.355	0.298	0.295	0.281	0.292	0.284	0.300	0.300
Al ₂ O ₃	0.011	-	0.033	0.020	0.015	0.048	0.020	0.028	0.003	0.153	0.010	-	0.025
Cr ₂ O ₃	0.034	0.008	-	0.043	0.068	-	-	-	-	-	-	-	-
Total	100.012	100.949	100.663	97.519	100.689	100.172	98.780	100.830	99.501	99.732	100.263	101.757	100.066
CATION (on the basis of 6 oxygen)													
Fe	1.9739	2.1019	1.8897	1.8511	1.9604	1.4071	1.8839	1.9803	1.9390	1.9688	1.9795	1.9572	1.9115
Ti	2.0028	1.9405	2.0446	2.0633	2.0083	2.2843	2.0481	1.9997	2.0219	1.9999	1.9999	2.0125	2.0306
V	0.0117	0.0110	0.0121	0.0119	0.0117	0.0135	0.0120	0.0118	0.0114	0.0118	0.0115	0.0119	0.0120
Al	0.0007	-	0.0019	0.0012	0.0009	0.0027	0.0012	0.0016	0.0002	0.0091	0.0006	-	0.0015
Cr	0.0014	0.0003	-	0.0017	0.0027	-	-	-	-	-	-	-	-
Total	3.9904	4.0538	3.9484	3.9293	3.9840	3.7076	3.9453	3.9935	3.9724	3.9896	3.9932	3.9816	3.9603

APPENDIX - IX

MICROPROBE ANALYSIS OF RUTILE

ELEMENTS	A47/56	PL12/113	14/103	12A/126	PR6/81	PC30C/5	PC29/24
WT%							
OXIDES							
SiO ₂	0.545	0.305	0.931	0.803	0.572	0.722	0.444
TiO ₂	99.582	100.581	99.741	99.816	100.361	99.182	99.684
V ₂ O ₃	0.561	0.571	0.572	0.564	0.573	0.561	0.549
Al ₂ O ₃	-	0.078	0.021	0.045	0.065	0.067	0.051
Cr ₂ O ₃	0.179	0.061	0.070	0.094	-	0.052	-
Total	100.866	101.072	101.336	101.321	101.571	100.582	100.727
CATION (on the basis of 2 oxygen)							
Fe	0.0060	0.0034	0.0103	0.0089	0.0063	0.0080	0.0049
Ti	0.9911	0.9924	0.9895	0.9898	0.9916	0.9903	0.9926
V	0.0059	0.0060	0.0060	0.0060	0.0060	0.0060	0.0058
Al	-	0.0012	0.0003	0.0007	0.0010	0.0010	0.0008
Cr	0.0019	0.0003	0.0007	0.0010	-	0.0005	-
Total	1.0049	1.0033	1.0068	1.0064	1.0049	1.0058	1.0041